STRAIN SOFTENING FOR MICROPILES UNDER TENSILE LOADING

A study on the softening behaviour of Dutch Pleistocene sand

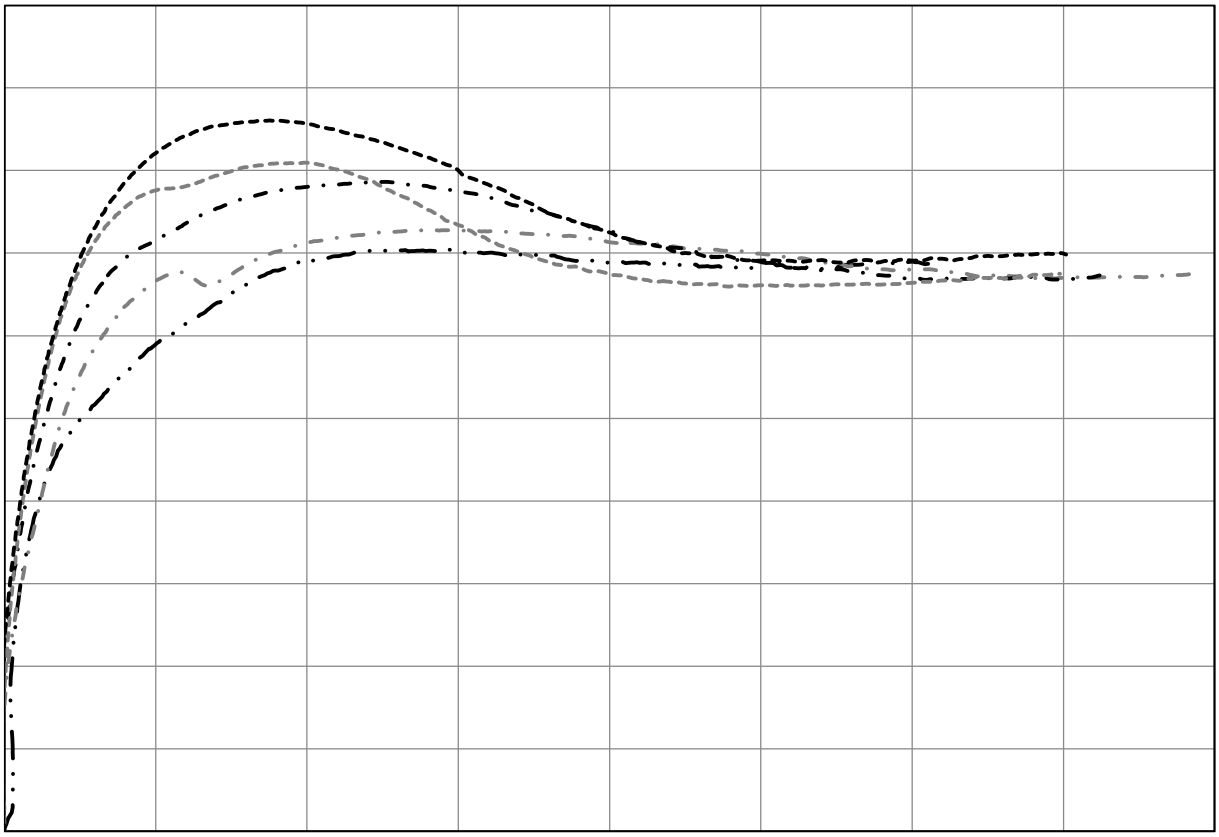

T.G.M. Laumen

Faculty of Civil Engineering and Geosciences
Section of Geo-Engineering
Delft university of Technology

bam infra

TU Delft

VolkerInfra

STRAIN SOFTENING FOR MICROPILES UNDER TENSILE LOADING

A study on the softening behaviour of Dutch Pleistocene sand

By

T.G.M. Laumen

in partial fulfilment of the requirements for the degree of

Master of Science

in Civil Engineering

at the Delft University of Technology,

to be defended publicly on Monday October 16, 2017 at 14:00 AM.

Thesis committee:	Prof. dr. K.G. Gavin	TU Delft
	Ing. H.J. Everts	TU Delft
	Dr. Ir. R.B.J. Brinkgreve	TU Delft
	Ir. K.J. Reinders	TU Delft
	J. Salazar Rivera M.Sc.	BAM Infraconsult
	Ing. J. Cromwijk	Volker Infra

PREFACE

This M.Sc. thesis has been performed in combination with BAM Infraconsult and Volker Infra, as a last part to fulfil my degree of Geo-Engineering at the Delft University of Technology. The recent of the CUR 236 addendum on the axial stiffness of micropiles initiated a better understanding was needed concerning the softening behaviour for micropiles under tensile loading.

An attempt is made to gain a better understanding into the softening concept at micropiles. With the help of large scale tests on micropiles, numerical modelling, as well as small scale tests, this investigated. A large number of factors influencing the behaviour of a micropile, The limited control concerning the installation of the piles but large influence on its behaviour in combination with the complex critical state soil mechanics describing the softening behaviour and the limited insight in the geomechanical behaviour in the conventional testing method made a seemingly manageable subject, very complex. Multiple methods were therefor used to get the most complete picture. Not all of these aspects succeeded though a firm basis is made for further research into this challenging subject.

This thesis would have never succeeded without the help of numerous people. First, I would like to thank Bart van Paassen and Aissa Yahyaoui for their confidence in my abilities, giving me the opportunity to do this thesis at both companies. Second, I would like to my thesis committee: Prof. dr. K.G. Gavin, Ing. H.J. Everts, Dr. R.B.J. Brinkgreve and Ir. K. Reinders for the time and efforts they put into the thesis. However, in specific, I would like to thank Jaap Cromwijk of Volker Infra and Javier Salazar Rivera of BAM Infraconsult for their input into the research and knowledge on the subject. In case of questions or problems, they were always willing to help, despite their busy schedules. Third, I would like to thank Arno Mulder of the Geotechnical Laboratory of the TU Delft. His experience into element testing as well as his technical knowledge about the testing equipment was invaluable. Fourth, I would like to thank Herman Krijgsman, the wisdom he shared during the long nights of testing and his willingness to understand the importance of some aspects of testing, even if they meant doing an additional effort. Fifth, I would like to thank my fellow Geo-Engineering students for their support especially the ‘micropile team’. Last, my family and friends and Wieske deserve a thanks for their understanding. For a large part of the thesis I devoted less attention to them I should have. When ideas did not work out, which happened during a significant part of the thesis, their support was crucial to keep me motivated.

T.G.M. Laumen

October 2017

“Success is the ability to go from failure to failure without losing your enthusiasm.”

- Unknown

CONTENT

Preface IV
List of Figures X
List of Tables XII
Nomenclature XIV
Summary XVIII
1. Introduction 1
1.1. Formulation of the research questions 1
1.2. Methodology 1
1.2.1. Literature study 2
1.2.2. Strain softening modelling 2
1.2.3. Model validation 2
1.2.4. Conclusion and recommendation 2
1.3. Readers manual 3
2. Literature study 4
2.1. introduction 4
2.2. Conceptual model: tensile bearing capacity micropile 4
2.3. Current design guidelines micropiles: CUR 236 5
2.3.1. Tensile design capacity piles; CUR 236 5
2.3.2. Strain softening behaviour shear strength; CUR 236 addendum 6
2.3.3. Conclusion 7
2.4. Strain softening behaviour sand 8
2.4.1. Shear behaviour sand 8
2.4.2. Dilatancy 9
2.4.3. Shear band development 10
2.4.4. Critical state soil mechanics 12
2.4.5. Conclusion 13
2.5. Soil structure interaction 15
2.5.1. Interface friction 15
2.5.2. Interface area 18
2.5.3. Horizontal pressure 18
2.5.4. Shear band development in interface 20
2.5.5. Conclusion 23
2.6. Modelling of softening: Hypoplasticity 24
2.6.1. Constitutive model 24
3. Numerical modelling 26

3.1. Parameter determination 26
3.1.1. Parameters testing 26
3.1.2. Results parameters 27
3.2. Numerical modelling: hypoplasticity 28
3.2.1. Numerical model 28
3.2.2. Expected and required results 30
3.2.3. Results conceptual model 31
3.2.4. Conclusion numerical model 34
4. Small scale physical modelling 35
4.1. Set-up and testing procedure 36
4.2. Influence relative density 37
4.2.1. Peak and residual shear stress 37
4.2.2. Softening mobilisation $\Delta u_{softening}$ 39
4.3. influence confining pressure 39
4.3.1. Peak and residual shear stress 39
4.3.2. Softening mobilisation $\Delta u_{softening}$ 41
4.4. Influence sand characteristics 41
4.5. conclusion 43
5. Large scale testing 44
5.1. Current testing procedure: CUR 236 44
5.2. Large deformation testing 45
5.2.1. Testing procedure 46
5.2.2. Results 47
5.2.3. Conclusion 47
6. Implementation into design code & recommendations 49
6.1. Shortcomings current design guideline 49
6.2. Subdivision based on installation effect 49
6.3. Implementation and recommendations current design guideline 51
6.3.1. SLS 51
6.3.2. ULS 54
6.4. Recommendation in situ testing methods 54
6.5. Future research 55
7. Conclusion 56
7.1. Conclusions sub questions 56
8. Limitations of research 59
9. Bibliography 61
A. Parameter determination Hypoplasticity 69

B. Numerical modelling results 97
C. Small sclae physical modelling results 107
D. Large scale testing.....115

LIST OF FIGURES

FIGURE 1: PARAMETERS OF INFLUENCE ON STRAIN SOFTENING 3
FIGURE 2: DISCRETISATION OF TRANSFER SHEAR STRESSES ALONG MICROPILE 4
FIGURE 3: MOBILISED SHEAR STRESS – DISPLACEMENT BEHAVIOUR (CUR 236 ADDENDUM, 2016) 6
FIGURE 4: COMPARISON STRESS – STRAIN BEHAVIOUR IN TRIAXIAL TEST FOR DIFFERENT D_R AND I_1/I_{SS} FOR DILATIVE (A) AND CONTRACTIVE (B) BEHAVIOUR (BEEN AND JEFFERIES, 1985) 8
FIGURE 5: GRAPHICAL REPRESENTATION OF SPHERICITY AND ROUNDNESS (CHO ET AL., 2006) 9
FIGURE 6: RELATION MAXIMUM FRICTION ANGLE – DILATANCY ANGLE (SOLID LINE) CALCULATED WITH EQUATION 7 AND ROWE'S STRESS – DILATANCY RELATION (DASHED LINE) (BOLTON, 1986) 10
FIGURE 7: SHEARING BEHAVIOUR IDEALISED AS TWO SLIDING BLOCKS (NEWLAND & ALLELY, 1957) 11
FIGURE 8: SHEAR BAND FORMATION PLANE STRAIN TEST: A = TOYOURA SAND, B = TICINO SAND (ODA & KAZAMA, 1998) 11
FIGURE 9: STATE PARAMETER REPRESENTATION IN VOID RATIO – STRESS SPACE 12
FIGURE 10: GRAPHICAL REPRESENTATION OF FACETS INFLUENCING BEARING CAPACITY AT LOCAL LEVEL 15
FIGURE 11: GRAPHICAL REPRESENTATION OF ROUGHNESS R_T AND RELATIVE ROUGHNESS R_N (FIOVARANTE, 2002) 16
FIGURE 12: PHYSICAL MODELLING OF PARTICLE MOVEMENT ALONG A SMOOTH INTERFACE (A,LEFT) AND ROUGH INTERFACE (B,RIGHT) (UESUGI ET AL., 1988) 16
FIGURE 13: MOBILIZED SHEAR STRESS AND VOLUMETRIC STRAIN PLOT AGAINST TOTAL DISPLACEMENT FOR A SMOOTH INTERFACE (LEFT) AND ROUGH INTERFACE (RIGHT) (UESUGI ET AL., 1988) 17
FIGURE 14: COMPARISON SHEAR STRESS DEVELOPMENT, MODEL PILE – DS-CNS FOR HIGH RELATIVE DENSITY AND DIFFERENT ROUGHNESS (UPPER:0.01, LOWER: 1.08) (FIORAVANTE, 2002) 18
FIGURE 15: SCHEMATISATION OF THE SHEARING BEHAVIOUR IN INTERFACE SYSTEM (DEJONG ET AL., 2006) 20
FIGURE 16: SHEAR STRESS (A), VERTICAL DISPLACEMENT (B) AND PIV DATA (C) OF CNS TEST FOR DIFFERENT INTERFACE DISPLACEMENTS (DEJONG ET AL., 2003) 21
FIGURE 17: SHEAR STRAINS IN PILE INTERFACE, VARYING ROUGHNESS (R_N) AND RELATIVE DENSITY (D_R) (TEHRANI ET AL., 2016) 22
FIGURE 18: SHEAR BAND SIZE NORMALISED TO GRAIN SIZE (D_{50}) FOR DENSE SAMPLE ($D_R \approx$ 90%) AND ROUGH INTERFACE (R_N>0.1) (TEHRANI ET AL., 2016) 22
FIGURE 19: GRAINSIZE DISTRIBUTION TESTED SAMPLES 27
FIGURE 20: PLAXIS MODEL: SOIL IN GREEN, MICROPILE IN GREY AND LINE LOAD IN BLUE 29
FIGURE 21: LOAD DISTRIBUTION ALONG AT MICROPILE (BARLEY ET AL., 2003) 31
FIGURE 22: PLAXIS MODEL: PRESSURISATION PHASE, SIG'$_{XX}$ 31
FIGURE 23: PLAXIS MODEL: FINE MESH, LOADING 120%, $T_{MOBILISED}$ 32
FIGURE 24: PLAXIS MODEL: LOADING 40%, $T_{MOBILISED}$, CLOSE-UP 33
FIGURE 25: PLAXIS MODEL: LOADING 120%, $T_{MOBILISED}$, CLOSE-UP 33
FIGURE 26: GRAPHICAL REPRESENTATION T_{PEAK}, $T_{RESIDUAL}$, U_{PEAK} AND $U_{RESIDUAL}$ IN CUR 236 ADDENDUM MODEL 35
FIGURE 27: SCHEMATIC REPRESENTATION OF DS APPARATUS 36
FIGURE 28: MOBILISED SHEAR STRESS DEVELOPMENT FOR DIFFERENT D_R WITH P'=64 KPA .37
FIGURE 29: T_{PEAK} (=■) AND $T_{RESIDUAL}$(=●) WITH VARYING D_R, P' = 64 KPA 38

FIGURE 30: RATIO BETWEEN T_{PEAK} AND $T_{RESIDUAL}$, P'= 64 KPA.....38
FIGURE 31: DISPLACEMENT FROM T_{PEAK} TO $T_{RESIDUAL}$ WITH P'=64 KPA 39
FIGURE 32: MOBILISED SHEAR STRESS DEVELOPMENT FOR DIFFERENT D_R WITH P'=306 KPA40
FIGURE 33: RATIO BETWEEN T_{PEAK} AND $T_{RESIDUAL}$ WITH P'=64 KPA (■) AND P'=306 KPA (♦) 41
FIGURE 34: DISPLACEMENTS FROM T_{PEAK} TO $T_{RESIDUAL}$ WITH P' = 64 KPA (■) AND P' = 306 KPA (♦) 41
FIGURE 35: GRAIN SIZE DISTRIBUTION TESTED SOIL SAMPLE: FORMATION OF DRENTE.....42
FIGURE 36: MICROSCOPIC PHOTOGRAPH OF THE SAND GRAINS (SCALE = 0.500 MM (TOP LEFT)) 43
FIGURE 37: SCHEMATIC OVERVIEW PILE TESTING SET-UP 44
FIGURE 38: LOADING SCHEME FAILURE TEST (CUR 236, 2011) 45
FIGURE 39: FORCE IN JACK (■) DURING SOFTENING TEST PILE 2 WITH EXPONENTIAL FIT (—) 47
FIGURE 40: SUBDIVISION MICROPILE TYPES BASED ON SIG'_H AND D_R 50
FIGURE 41: PROPOSED ADAPTATION CURRENT CUR236 ADDENDUM MODEL 53
FIGURE 42: SHEAR STRAIN DEVELOPMENT IN SHEAR BAND 53
FIGURE 43: DISPLACEMENTS FROM T_{PEAK} TO $T_{RESIDUAL}$ WITH P' = 64 KPA (■) AND P' = 306 KPA (♦) 57
FIGURE 44: RATIO BETWEEN T_{PEAK} AND $T_{RESIDUAL}$ WITH WITH P' = 64 KPA (■) AND P' = 306 KPA (♦) 58

LIST OF TABLES

TABLE 1: MICROPILE TYPES (CUR 236) 5
TABLE 2: BEARING CAPACITY DIFFERENT MICROPILE TYPES (CUR 236, 2011) 6
TABLE 3: HYPOPLASTIC PARAMETERS FORMATION OF *DR*ENTE AND STERKSEL 27
TABLE 4: BENTONITE MIXED MATERIAL (MOHR-COULOMB MODEL, *DR*AINED) 28
TABLE 5: MICROPILE MATERIAL (LINEAR ELASTIC, NON-POROUS) 28
TABLE 6: INTERFACE PARAMETERS 30
TABLE 7: RELATIVE DENSITIES AND VOID RATIOS 37
TABLE 8: PEAK FRICTION ANGLES FOR VARYING D_R AND *P'* 40

NOMENCLATURE

ABBREVIATIONS

A	Linear soil behaviour hypoplastic constitutive model
B	Non – linear soil behaviour hypoplastic constitutive model
CNS	Constant normal stiffness
CPT	Cone Penetration Test
CSL	Critical State Line
CUR	Civieltechnisch Centrum Uitvoering, Research en Regelgeving
DIC	Digital Image Correlation
DIN	Deutches Institut für Normung
DS	Direct Shear
DS-CNS	Direct Shear test – Constant Normal Stiffness
LVDT	Linear Variable Differential Transformer
NEN	National Eurocode
OCR	Overconsolidation ratio
PIV	Particle image velocimetry
SLS	Serviceability Limit State
ULS	Ultimate Limit State

SYMBOLS

α	Pycnotropy exponent governing peak friction angle [-]
$\alpha_{t,expected}$	Expected tensile bearing capacity factor in accordance with CUR 236 [-]
$\alpha_{t,max}$	Maximum tensile bearing capacity factor in accordance with CUR 236 [-]
β	Pycnotropy exponent governing stiffness [-]
β'	Friction factor [-]
γ_{sat}	Saturated volumetric weight [kN/m^3]
γ_{unsat}	Unsaturated volumetric weight [kN/m^3]
γ_{sand}	Shear strain sand [-]
δ	Interface friction [^{o}]
ε_1	Vertical strains [-]
ε_3	Horizontal strains [-]

ε_v	Volumerical strains [-]
v'	Poisson's ratio [-]
σ'	Effective soil stress [kPa]
σ'_1	Vertical effective stress element test [kPa]
σ'_3	Horizontal effective stress element test [kPa]
σ'_a	Axial effective stress [kPa]
σ'_h	Horizontal effective stress general [kPa]
σ'_r	Radial effective stress [kPa]
σ'_v	Vertical effective stress general [kPa]
τ	Mobilised shear stress [kPa]
τ_{mob}	Mobilised shear 'strength' [kPa]
τ_{peak}	Peak shear stress [kPa]
$\tau_{residual}$	Residual shear stress [kPa]
φ	Friction angle [^{o}]
$\varphi_{average}$	Average friction angle along micropile [^{o}]
φ_c	Angle of repose [^{o}]
φ_{cv}	Constant volume friction angle [^{o}]
φ_p	Peak friction angle [^{o}]
ψ	Dilatancy angle [^{o}]
Ψ	State parameter [-]
a	Dimensionless constant describing critical stress surface [-]
c	Constant exponential fit softening test [kN]
c'	Cohesion [kPa]
C_u	Coefficient of uniformity [-]
D	Stretching tensor [kPa]
D_{50}	Average particle size [mm]
$D_{micropile}$	Diameter micropile [m]
D_R	Relative density [%]
E'	Young's modulus [kPa]
e_{c0}	Critical state void ratio at reference state (zero pressure) [-]
e_{d0}	Minimum void ratio at reference state (zero pressure) [-]
e_{i0}	Maximum void ratio at reference state (zero pressure) [-]

e_{max}	Maximum void ratio [-]
e_{min}	Minimum void ratio [-]
E_{oed}	Oedometer modulus [kPa]
e_{ss}	Steady state void ratio [-]
f_1	Densification factor [-]
f_2	Group effect [-]
f_3	Length effect [-]
f_b	Barotropy (stress) factor [-]
f_d	Pycnotropy factor related to material state [-]
f_e	Pycnotropy (density) factor [-]
F_p	Design load failure test pile [kN]
f_s	Stiffness factor [-]
$f_{softening}$	Softening factor [-]
h_s	Granular hardness [GPa]
I_1	Average pressure triaxial test [kPa]
I_{ss}	Average pressure triaxial test in steady state [kPa]
K	Coefficient of horizontal pressure [-]
K'	Installation factor [-]
K_0	Coefficient of neutral lateral earth pressure [-]
K_1	Cavity expansion factor [-]
K_2	Horizontal pressure factor [-]
K_a	Coefficient of active lateral earth pressure [-]
$K_{average}$	Average coefficient of lateral earth pressure [-]
K_p	Coefficient of passive lateral earth pressure [-]
k_s	Creep criterion [mm]
n	Exponent of compression law [-]
$O_{p,average}$	Average circumference micropile [m]
p'	Average confining pressure [kPa]
q	Deviatoric stress [kPa]
q_c	Cone resistance CPT [MPa]
R	Sand grain roundness [-]
R_n	Relative interface roughness [-]

R_t	Structure roughness [mm]
$R_{t,d}$	Tensile design bearing capacity [kN]
$R_{t,failure\ test}$	Tensile bearing capacity failure test [kN]
$R_{t,residual}$	Residual tensile bearing capacity softening test [kN]
S	Sand grain sphericity [-]
t	Time [min]
t_s	Shear band thickness [mm]
T_s	Cauchy granulate stress tensor [kPa]
$\dot{\mathrm{T}}_s$	Objective stress rate tensor [kPa]
$\hat{T}_s$	Stress ratio tensor [kPa]
$\hat{T}_s^*$	Deviatoric stress tensor [kPa]
$\Delta u_{softening}$	Differential displacement between τ_{peak} and $\tau_{residual}$ [mm]
$u_{failure}$	Displacement of reinforcing steel micropile at failure [mm]
u_i	Displacement discretisation ‘i’ [mm]
u_{peak}	Displacement to τ_{peak} in performed DS tests [mm]
$u_{peak,CUR236}$	Displacement to τ_{peak} in accordance with CUR 236 addendum [mm]
$u_{residual}$	Displacement to $\tau_{residual}$ in performed DS tests [mm]

SUMMARY

In March 2016, an addendum to the Dutch design guideline for micropiles, CUR 236, was published. This addendum elaborated on the 'axial stiffness of micropiles'. The softening behaviour was here first mentioned as an aspect relevant for the axial stiffness of the micropiles. Due to the slender geometry of the micropiles, this further translates into axial capacity. Up to this moment very little research was done into this phenomenon and to be conservative a 'best guess' of 50% of the peak shear stress was made.

The goal of this thesis is to have a more profound understanding about this (strain) softening behaviour, leading to the main research question: *"How does strain softening manifest for micropiles under tensile loading?".* This strain softening behaviour can be further subdivided into the mobilisation from peak to residual shear stress and the reduction of the residual shear stress relative to the peak. Furthermore, the installation effects play a big role in the bearing capacity. Also, some thought is given to the large scale measurements of the behaviour.

Three different paths are chosen to research the strain softening behaviour. Numerical modelling, small scale tests on sand and large scale pile tests are performed. In case of the numerical modelling, the large scale situation is simulated in the numerical software Plaxis, using an axisymmetric model and the hypoplastic constitutive model. Direct shear tests are assumed to represent a small part of the micropile, simulating the local softening behaviour. Numerous tests are performed varying relative density and top pressure to assess the local strain softening behaviour. Last, a method is developed to quantify the occurring ratio between peak and residual shear stress in-situ, extending on the current prescribed testing procedure (CUR 236, 2011).

The only constitutive model available that describes the critical state soil behaviour for sand is the hypoplastic sand model. However, the combination of the tensile loading, softening implementation into the hypoplastic sand model in Plaxis and the deformations, induce considerable inaccuracies and physically impossible behaviour. This rejects further elaboration with this approach. The direct shear tests are performed on only sand, based on the results of Uesugi & Kishida (1987), assuming a rough surface. In summary, a clear dependency on relative density and average confining pressure is observed. Varying from a reduction of approximately 30% for samples with the maximum possible density to 0% for a sand with a medium dense packing. Furthermore, the displacements necessary to mobilise from peak to residual shear stress show a uniform trend, independent of relative density or pressure. Quantitatively, the displacement ranges between 2 and 3 mm. In the large scale tests, due to unexpected, structural failure, the majority of the test results, unfortunately, were unusable. The pile test that did produce workable results, behaved as expected. It could be deduced that the used methodology works.

The use of the hypoplastic constitutive model in Plaxis, does not give the expected results. It can thus be concluded that a fully coupled stress – strain analysis of the problem is unfortunately impossible. Concluding on the direct shear tests performed, the implementation in the CUR 236 addendum is too simplistic. In terms of ratio between peak and residual shear stress, a dependency based on relative density and average confining pressure should be included. In terms of displacement, the found displacement is larger. It should however be noted that the direct shear tests are only a simplification, approximating the actual situation. The performed large scale tests do show results in line with expectations and could be used in the future to assess the softening behaviour in-situ.

1. INTRODUCTION

In this addendum on the existing CUR 236 a new approach is introduced to determine better predict the deformation behaviour of micropiles loaded in tension. This approach discretises the micropile into small elements, defining the shear stress mobilisation in based on the displacement occurring and cone resistance present (q_c). To take possible strain softening into account, a number of 'best guesses' is implemented into the new model to calculate shear stress mobilisation. The residual shear stress is assumed 50% of the peak shear stress and a displacement of 1 mm is needed to mobilise from peak to residual shear stress. Furthermore, this model is implicitly used in the bearing capacity due to the flexibility of the micropiles. The lacking fundamental substantiation is the basis for this M.Sc. thesis.

1.1. FORMULATION OF THE RESEARCH QUESTIONS

With the very limited research done on softening behaviour for micropiles in sandy soils, in this M.Sc. thesis, an attempt is made to gain a better understanding. The main research question is formulated as following.

"How does strain softening manifest for micropiles under tensile loading?"

This main research question can be subdivided into:

1. *"What variables influence strain softening behaviour?"*
2. *"Does the installation method influence the strain softening behaviour?"*
3. *"How can this strain softening behaviour be modelled for the soil-structure interaction of the micropile-soil interface?"*
4. *"How do the sand parameters influence this strain softening mobilisation?"*
5. *"How do the sand parameters influence the residual shear strength?"*
6. *"How can strain softening be measured with tests on the micropiles?"*
7. *"Does the strain softening model results match the physical data?"*

1.2. METHODOLOGY

The main research question stipulates that the strain softening behaviour of micropiles loaded in tension will be investigated in this thesis. The research is broken down into multiple research questions, giving the outline. The built-up of the thesis is as following:

- Literature study for theoretical background on strain softening
- Modelling of strain softening behaviour
- Assessment of strain softening model through physical data

Crudely summing up all parts, first a literature study will be done to gain more insight in the background of the softening behaviour. Then, the soil behaviour needs to be modelled in

accordance with the theory. Last, the model will be validated with physical data to assess its correctness and limitations.

Furthermore, this entire thesis needs to be thorough enough to be as complete as possible, but also fit the limited period of eight months. Bearing this in mind, the following elaboration on the earlier on mentioned sub questions is made.

1.2.1. Literature study

The first two research questions concern factors of influence on the strain softening behaviour of the soil. A lot of is already known about strain softening of sandy soils hence the required knowledge can be gathered through literature study. The focus here will be on what parameters do influence the softening behaviour of the shear strength. A subdivision is made between sand parameters and installation effects.

1.2.2. Strain softening modelling

With insight gained in the basis of the material behaviour, the soil structure interaction can be modelled to accurately assess the softening behaviour of the shear stress around the micropile. This is done with a numerical model, using the hypoplasticity constitutive model in Plaxis. Hypoplasticity is the only constitutive framework able to behave according to critical state soil mechanics when sand behaviour is modelled. Furthermore, an adaptation of the current 'CUR 236 addendum' – model is made based on small scale physical tests.

1.2.3. Model validation

Within the modelling, a better expression is given for the softening behaviour. This behaviour should be validated in large scale pile tests. Validation is of importance due to the large number of aspects influencing the strain softening at micropiles, best tested in actual pile tests. Please refer to Figure 1.

However, the current testing framework of the CUR 236 only tests the global behaviour of a micropile and the softening behaviour is taken into account implicitly. Therefor a new testing methodology is developed to measure the post peak decrease in bearing capacity. This is again done by measuring the global micropile behaviour but with the certainty that the sand along the entire micropile is mobilised towards its residual shear stress. Unfortunately, no method is found to accurately test the local displacement necessary towards the residual shear stress. Furthermore, in hindsight, the numbers of tests could be performed is too limited to validate the results from the models.

1.2.4. Conclusion and recommendation

To conclude the thesis, the found results from the modelling used to give a recommendation. The main focus is on how the current implementation of the softening behaviour in the CUR 236 can be improved. Furthermore, a final answer on the proposed research questions is given and the limitations of the thesis are discussed.

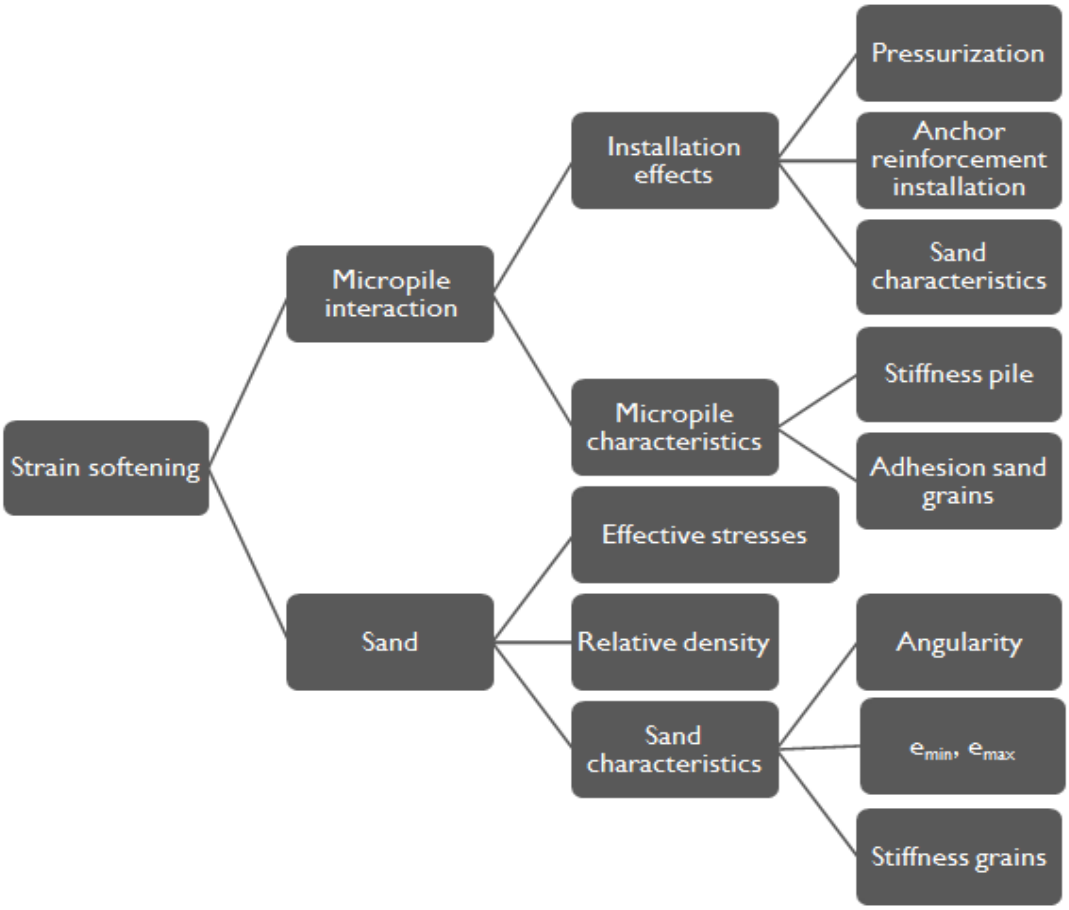

FIGURE 1: PARAMETERS OF INFLUENCE ON STRAIN SOFTENING

1.3. READERS MANUAL

This thesis is subdivided into eight chapters. After this first chapter, the introduction, the subdivision is made into four main components. Chapter 2, all literature concerning micropiles and strain softening is summarised. Chapter 3 and 4, the strain softening modelling is discussed, both numerical (chapter 3) and physical modelling (chapter 4). The model validation is considered in chapter 5, large scale pile testing. Last, the conclusion and recommendation are combination of chapter 6, 7 and 8, respectively covering the implementation of the obtained results into the current design code, the conclusion of the thesis and the limitations to the performed research.

2. LITERATURE STUDY

2.1. INTRODUCTION

For the investigation of the strain softening behaviour around micropiles, multiple aspects should be emphasised. Softening is the term used to describe the decrease in shear strength with increasing strain, after the peak shear strength is mobilised. The two aspects denoting the shear strength of a micropile are the mechanical behaviour of the sand and the interaction between the micropile and the surrounding sand. On these subjects, literature is investigated to obtain a better understanding of the theory behind them. Furthermore, literature on micropiles and their current design guidelines are discussed.

2.2. CONCEPTUAL MODEL: TENSILE BEARING CAPACITY MICROPILE

The total tensile capacity of a micropile is the result of the summation of all tensile stresses along the length of the pile. Graphically, this can be modelled by a grout element inside the soil, discretized by a certain number of elements transferring the tensile forces to the soil via springs and sliders. Please refer to Figure 2. The micropile is discretised by an arbitrary number of five springs.

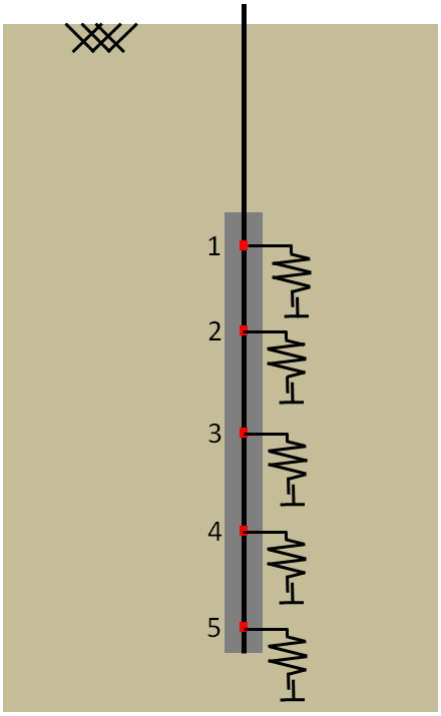

FIGURE 2: DISCRETISATION OF TRANSFER SHEAR STRESSES ALONG MICROPILE

The spring – slider system represent the shear behaviour of the soil. This behaviour, in turn, depends on the stress state, density and displacement of the individual elements. Soil state and construction of the micropile influence the shear characteristics of the soil. The total tensile capacity of the micropile in Figure 2 is equal to the summation of the shear stresses of each individual discretisation. In the actual case, the micropile is discretised with an infinite number of elements. The tensile capacity of the micropile, $R_{t,d}$, would be given by equation 1.

$$R_{t,d} = \int_{head}^{tip} \tau(\sigma', e, u)\, dL \quad (1)$$

The tensile bearing capacity of the micropile depends on the length of the micropile, *L,* the stress state *σ'*, void ratio *e* and displacement of the individual elements *u*.

As equation 1 stipulates, the bearing capacity of the micropile is equal to the summation of all shear stress along the micropile. Softening behaviour is the decrease in shear stress of the sand occurring past the peak shear stress mobilised by the loading of the micropile. The manor and size of the decrease are the main objective of this thesis.

2.3. CURRENT DESIGN GUIDELINES MICROPILES: CUR 236

In the Netherlands, the construction of deep excavations is usually accompanied with large uplift forces due to the high groundwater table. On a regular basis, micropiles are used in structures prone to large uplift forces. This uplift generates a force directed upwards. To have vertical equilibrium at the bottom of the building pit, micropiles are installed to counteract this force. This happens through shear forces along the pile interface conveyed to the subsoil under the floor. This soil-micropile interaction is described in the Dutch design guideline CUR 236.

Micropiles are in-situ constructed piles. In the Dutch design guideline, differentiation is made between five different types. These five different categories are denoted in Table 1.

TABLE 1: MICROPILE TYPES (CUR 236)

Pile categories	Installation method	Pile type (example)
A	Double bore pipe internally flushed	GEWI-pile
B	Single bore pipe externally flushed	GEWI-pile
C	Self-boring	Groutinjection pile
D	Screwed	Fundex pile
E	High frequency vibrated	GEWI-pile

2.3.1. Tensile design capacity piles; CUR 236

Micropiles are designed to counteract the uplift forces, this means that each micropile has to transfer the tensile load to the subsoil. This load is transferred from pile shaft through shear stresses onto the subsoil. The level of shear stresses that can be transferred to the soil is, as common for soils, strain dependent. In other words, a certain pile displacement is necessary to mobilize the maximum tensile capacity. The CUR 236 gives a design philosophy through which the total geomechanical tensile capacity can be determined. This geomechanical pull-out resistance depends on:

- α_t: pile class factor for tension, depending on soil type, pile type and installation method
- $O_{p,average}$: circumference of the anchoring body
- f_1 = 1.0: densification factor
- $f_2 \leq 1.0$: group effect factor
- $f_3 \leq 1.0$: length effect factor

These factors are used to calculate the design tensile capacity, $R_{t;d}$. $R_{t;d}$ is calculated using equation 1.

$$R_{t;d} = \int_0^L f_1 \, f_2 \, f_3 \, \alpha_t \, q_{c,z,excavation} \, O_{p,average} \, dz \qquad (2)$$

The group effect factor f_2 discounts of overlapping shear zones when the piles are relatively close to each other. The factor f_3 discounts the length effect. This reduction is the result of softening behaviour along the micropile.

How the micropiles are installed significantly influences the bearing capacity of the micropile. In the Dutch design guidelines, the influence of the installation effects on the bearing capacity is linked to the cone resistance with a factor α_t. Please refer to equation 2 (CUR 236, 2011). Depending on the micropile type and pressurisation, this varies between 0,006 and 0,025 and the cone resistance limited to 20 MPa and 15 MPa, shown in Table 2.

TABLE 2: BEARING CAPACITY DIFFERENT MICROPILE TYPES (CUR 236, 2011)

Type [-]	Cut-off value q_c [MPa]	$\alpha_{t,\,expected}$ / $\alpha_{t,\,max}$ [-]
A	20	0.017 / 0.025
B	20	0.017 / 0.025
C	20	0.012 / 0.025
D	15	0.012 / 0.025
E	15	- / 0.025

The magnitude of the mobilized shear stress is limited to the effective weight of the soil surrounding a pile group also called the “kluitcriterium”.

2.3.2. Strain softening behaviour shear strength; CUR 236 addendum

Soils are often characterized by a highly non-linear stress-strain behaviour. In the CUR 236 addendum, this stress-strain behaviour is described by the following curve.

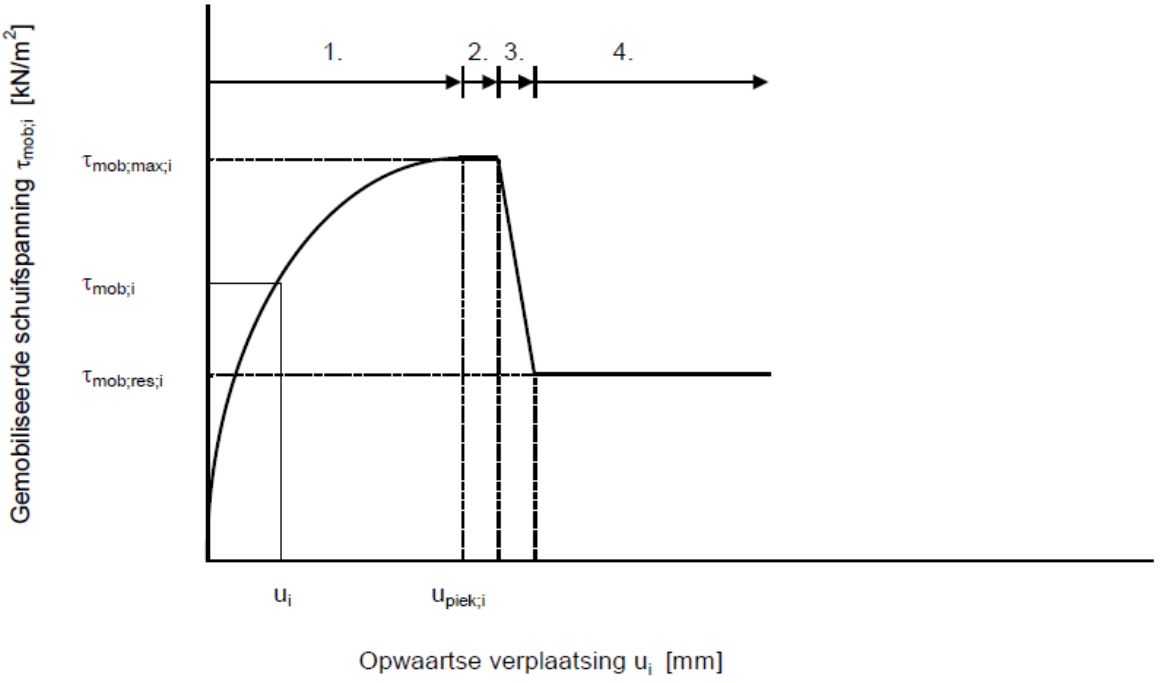

FIGURE 3: MOBILISED SHEAR STRESS – DISPLACEMENT BEHAVIOUR (CUR 236 ADDENDUM, 2016)

Figure 2 shows the stress-displacement behaviour of soil around micropiles according to CUR 236 (addendum). The graph is subdivided into four sections, that can be described as follows:

1. Describes the shear stress mobilization until the maximum shear stress $\tau_{mob;max;I}$, in accordance with Figure 7.0 from NEN 9997-1+C1. Depending on the pile type, the micropile displacement is 10 mm or 25 mm
2. A small interval assumed to have a constant maximum mobilized shear stress, for an arbitrarily chosen 1 mm displacement.
3. Decreasing mobilized shear stress through further mobilization of the anchoring body, for an arbitrarily chosen displacement of 1 mm. This interval is only used for the stiffness calculation, in case of strength calculations it is neglected.
4. After the decrease, a constant mobilized shear stress is reached, the residual shear stress $\tau_{mob;res;i}$. This residual shear stress is determined by a 'best guess' at 50% of the maximum shear stress.

2.3.3. Conclusion

The behaviour for the increasing mobilized shear stress, section 1, is well defined. Concerning the softening behaviour, 'best guesses' are used to make a conservative estimate. Please refer to Figure 3. This behaviour, which can be described as strain softening behaviour, is, at this moment in time, still not well defined.

Moreover, the expected bearing capacity based on the CUR 236 is significantly affected by the installation method used.

2.4. STRAIN SOFTENING BEHAVIOUR SAND

Strain softening denotes the decrease of shear strength observed after the peak shear strength in stress – strain behaviour of sandy soil. At large displacements, the shear strength of densely packed sands tends to drop from a peak to a residual shear strength. This behaviour is described by critical state soil mechanics. Furthermore, literature that researched the occurrence of the stress – strain behaviour in shear bands is discussed.

2.4.1. Shear behaviour sand

Been and Jefferies (1985) did triaxial tests on sands with varying densities, confining pressures. Please refer to Figure 4. These showed that sands with same void ratios but different confining pressures behaved differently, Figure 4A. Furthermore, it was observed that sands with different void ratios and confining pressures could show similar normalized stress – strain behaviour, Figure 4B. This was in contrast with previous believe that the relative density determined the shear strength.

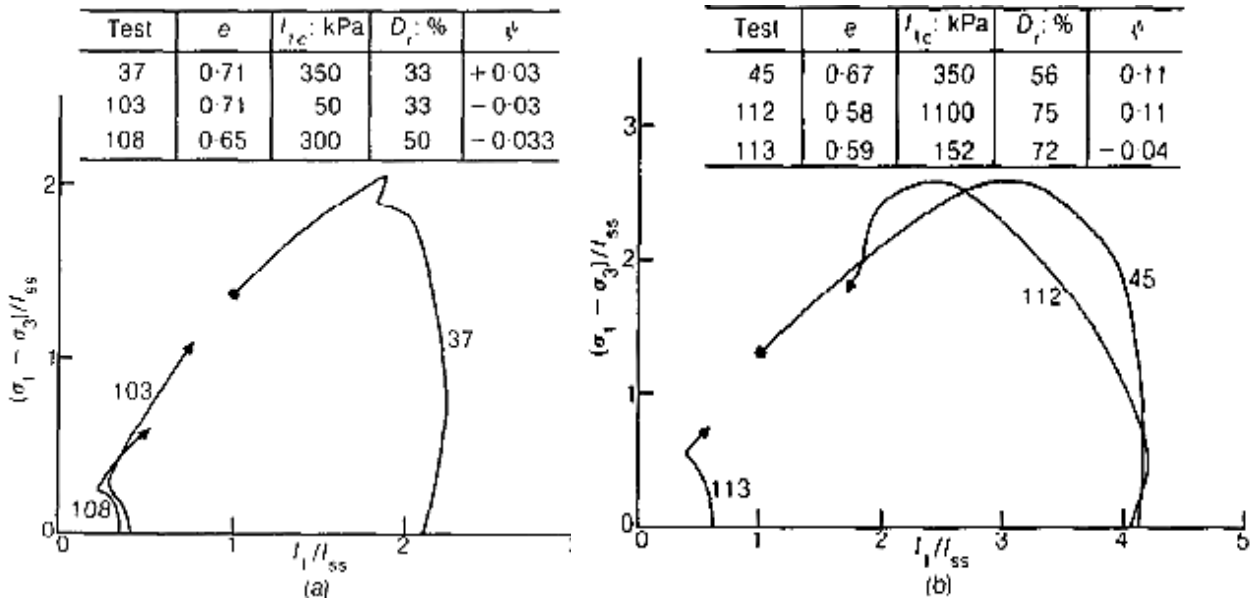

FIGURE 4: COMPARISON STRESS – STRAIN BEHAVIOUR IN TRIAXIAL TEST FOR DIFFERENT D_R AND I_1/I_{SS} FOR DILATIVE (A) AND CONTRACTIVE (B) BEHAVIOUR (BEEN AND JEFFERIES, 1985)

Figure 4 displays the results of triaxial tests performed at different confining pressures and void ratios, with the average pressure $p' = \frac{\sigma'_1+\sigma'_2+\sigma'_3}{3}$ (I_1 in Figure 4) normalized to a reference state. If the different tests are compared for both dilative and contractive behaviour, the kernel concept is confirmed (Been and Jefferies, 1985). In Figure 4A, test 37 and 103 both have a relative density of 33% though the former clearly shows dilative and the latter contractive behaviour. The tests with different relative density and confining pressure, test 103 and 108 show the same normalized stress strain behaviour. Analogously this occurs for the contractive behaviour in Figure 4B.

Furthermore, the influence of the particle shape plays a big role in the shear strength development of sand. The particle shape characteristics can be subdivided into the effect of roundness, sphericity and smoothness of the particles. Furthermore, the mineralogy of the sand and size of the grains play a role. These characteristics have both direct and indirect effects. Direct on the angle of internal friction, rough and angular grains give a higher friction.

Indirect, the sand characteristics influence the critical state behaviour in numerous ways: the packing (e_{min}, e_{max}), stiffness and the critical state.

All aforementioned parameters can be expressed through dimensionless constant and have the following physical representation (Cho et al., 2006):

1. The sphericity (S) (or eccentricity) of a particle denotes the deviation a sand grain has from a perfect sphere. This parameter is described by the quotient of the maximum inner curvature radius and the minimum radius to include the entire grain. Please refer to Figure 5 for a graphical representation.
2. Roundness (R) is a measure for the angularity of a particle, a perfectly round particle can be described by a summation of one circle while an angular particle will have sharp edges. The angularity is described by the quotient of the average curvature radius and the minimum radius within the particle. Please refer to Figure 5.
3. The smoothness describes the particle surface texture.

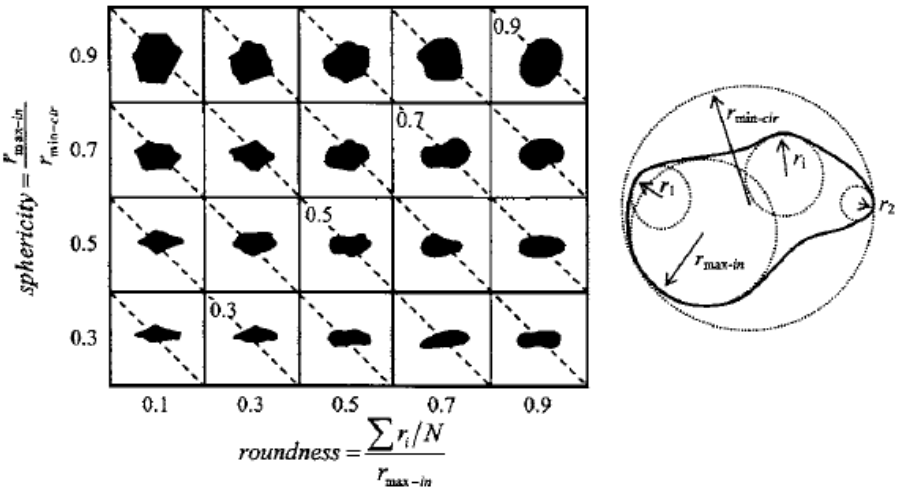

FIGURE 5: GRAPHICAL REPRESENTATION OF SPHERICITY AND ROUNDNESS (CHO ET AL., 2006)

The research of Cho et al. (2006) shows the dependency of e_{min} and e_{max} on the roughness R, sphericity S. Also, the uniformity of the grain distribution also has an influence on the range of void ratios of a sand (Youd, 1973). An increase in this range increases the dilatancy occurring during shearing, increasing the peak behaviour thus the softening occurring. Since the dilatancy is suppressed by higher confining pressure, the stress dependency will increase (Cho et al., 2006).

Furthermore, the grain characteristics directly influence the shear characteristics of a sand. The angularity positively, and roundness negatively, influences the constant volume friction angle of a sand φ_{cv}. Please refer to equation 3 (Cho et al., 2006).

$$\varphi_{cv} = 42 - 17R \tag{3}$$

2.4.2. Dilatancy

Bolton (1986) broadly elaborated on the dilatancy of sands. In this paper, the difference between the peak friction angle φ_{peak} and constant volume friction angle φ_{cv} is related to the dilatancy of a sand. This is first described theoretically in Rowe's stress – dilatancy relation for plane strain, equation 4.

$$\frac{\sigma'_1}{\sigma'_3} = \left(\frac{\sigma'_1}{\sigma'_3}\right)_{crit} \left(1 - \frac{d\varepsilon_v}{d\varepsilon_1}\right) \tag{4}$$

With Mohr-Coulomb stress theory, the angle of internal friction φ and the dilatancy angle ψ can be deduced, please refer to equation 5 and 6. Equation 6 denotes the influence of volumetric behaviour on the shear strength through dilatancy.

$$\sin\varphi_{peak} = \frac{\left(\frac{\sigma'_1}{\sigma'_3}\right)_{max} - 1}{\left(\frac{\sigma'_1}{\sigma'_3}\right)_{max} + 1} \tag{5}$$

$$\sin\psi_{max} = \frac{\left(\frac{d\varepsilon_1}{d\varepsilon_3}\right)_{max} + 1}{\left(\frac{d\varepsilon_1}{d\varepsilon_3}\right)_{max} - 1} \tag{6}$$

When combining equations 4, 5 and 6, an expression for difference in friction angle based on relating the difference between peak and residual strength to the dilatancy. Bolton (1986) expressed this in terms of the maximum dilatancy angle ψ_{max}, please refer to equation 7 and Figure 6.

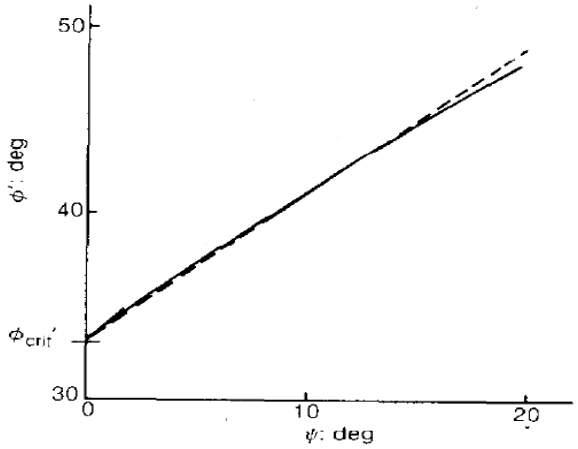

FIGURE 6: RELATION MAXIMUM FRICTION ANGLE – DILATANCY ANGLE (SOLID LINE) CALCULATED WITH EQUATION 7 AND ROWE'S STRESS – DILATANCY RELATION (DASHED LINE) (BOLTON, 1986)

$$\varphi_p \approx \varphi_{cv} + 0.8\,\psi_{max} \tag{7}$$

Figure 6 shows the theoretical relation of the peak friction angle (φ' in Figure 6), based on the stress state and volumetric behaviour of a sandy soil (solid line). Furthermore, it shows the volumetric behaviour expressed in terms of the maximum dilatancy angle (dashed line). As demonstrated in the graph, they almost completely coincide with each other, concluding the dilatancy describes the peak behaviour well. In other words, the softening is described by the dilatancy angle of a sandy soil.

2.4.3. Shear band development

When loading granular material, stresses are the result of the interaction of the individual grains. In shear, this interaction is associated with volumetric changes, depending on the original state of the material compaction and/or dilatancy. Newland & Allely (1957) proposed the analogy of the two sliding blocks, shown in Figure 7. On the sliding plane, the shear stresses concentrate and the granular material dilates. Numerous studies have done both

theoretically and experimentally research in to the shear band development, amongst other: Mühlhaus & Vardoulakis, 1987; Tatsuoka et al., 1990; Oda & Kazama, 1998; Nematt-Nasser & Okada, 2001; Röchter et al., 2010.

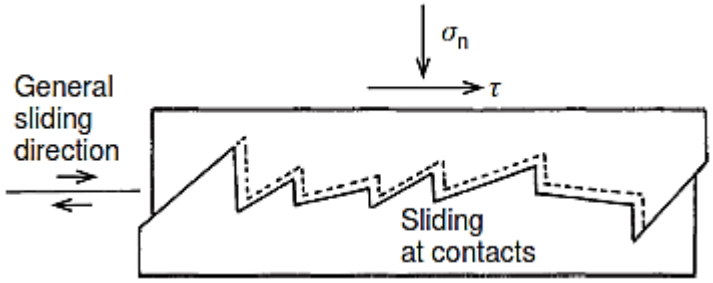

FIGURE 7: SHEARING BEHAVIOUR IDEALISED AS TWO SLIDING BLOCKS (NEWLAND & ALLELY, 1957)

Oda & Kazama (1998) took X-ray photographs of plain strain tests on Toyoura and Ticino sand. Figure 8 clearly shows the concentration of shear in a narrow band across the tested specimen. In specific the shear band thickness t_s is interesting for this thesis. This is often linked to the particle size D_{50}. For this specific study a t_s/D_{50} ratio of 7 to 8 was found. Other research found similar ratios with a maximum range of between 7 and 20 times D_{50} (Yoshida, 1994). Furthermore, it was shown that the shear band formation starts around the peak shear stress and the non-recoverable strains concentrate within this band.

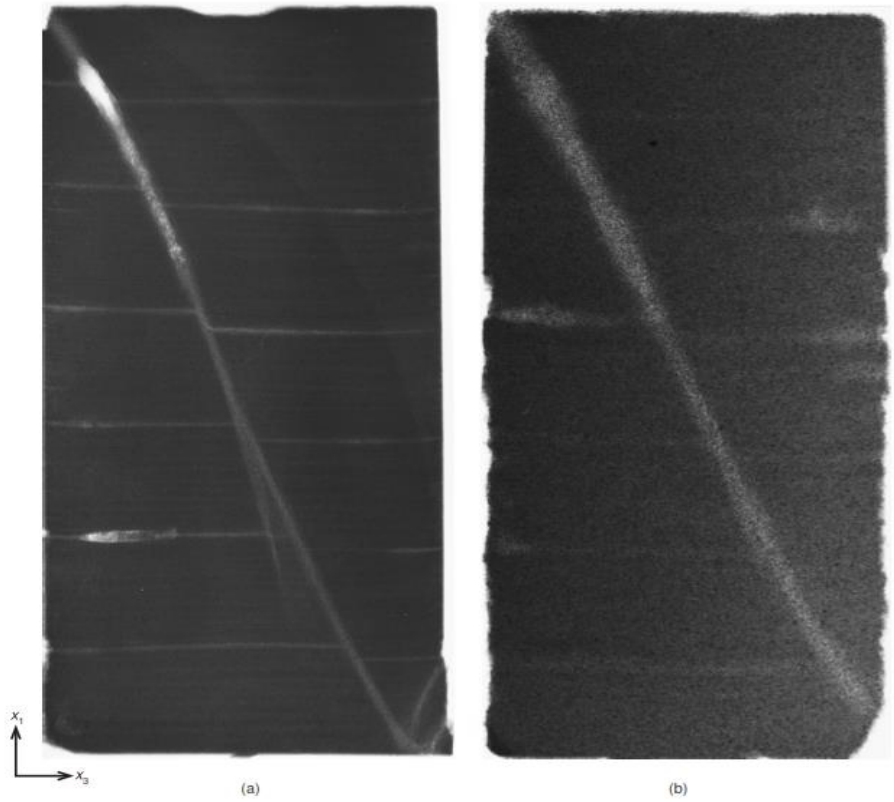

FIGURE 8: SHEAR BAND FORMATION PLANE STRAIN TEST: A = TOYOURA SAND, B = TICINO SAND (ODA & KAZAMA, 1998)

Oda and Kazama (1998) also showed that the shear band orientated parallel to the major principal stress direction, with small anomalies caused by the present microstructure of the sand matrix.

2.4.4. Critical state soil mechanics

Critical state soil mechanics governs the difference in behaviour for soil with different volumetric and pycnometric states. Hence, a sand with a different relative density and/or a different confining pressure, behaves differently. This behaviour is volumetrically controlled as described in Rowe's stress – dilatancy relationship, equation 4.

The contractive – dilative behaviour causes the typical hardening and softening behaviour. The $q - \varepsilon_1$ graphs of a triaxial test typically shows this behaviour. The link between the relative density and volumetric behaviour was first recognized by Casagrande (1938). Later on, it was proved that the role of the confining pressure of the sand could not be neglected (Lade 1972). These demonstrated that even with high relative densities, sands under high confining pressures behaves similarly to loose sands.

The combination of these concepts is represented by the state parameter Ψ (Been and Jefferies, 1985). This parameter substantiated that the behaviour of a sand is determined by the distance a certain sand is from its critical state line (CSL). The CSL is based on the kernel concept: a sand has a reference state and the distance from this reference state in void ratio – stress space characterises the behaviour of sand. At first, this was called the 'steady state'. Please refer to Figure 9 for a graphical representation of this concept.

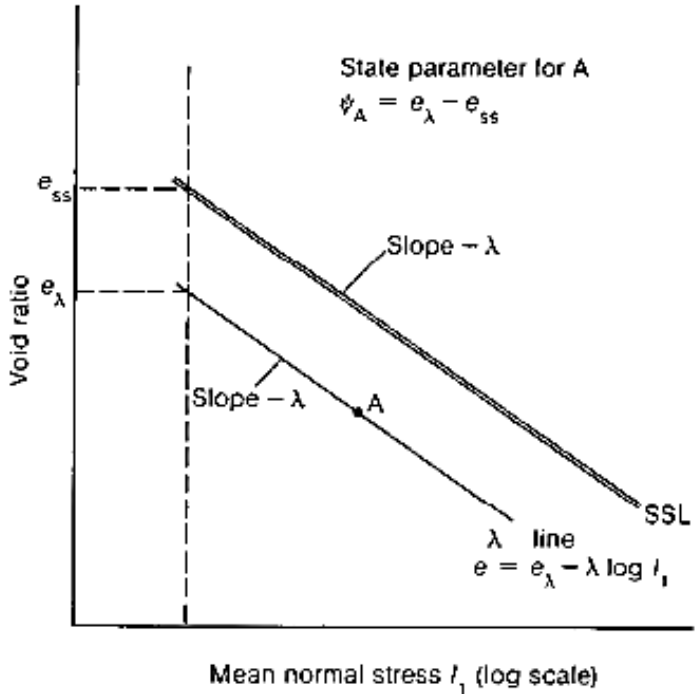

FIGURE 9: STATE PARAMETER REPRESENTATION IN VOID RATIO – STRESS SPACE

Been and Jefferies (1985) further showed that sands with same void ratios and different pressures behaved differently and that sands with different void ratios and confining pressures behaved similarly when they had the same state relative to the reference state, the CSL. This relation is expressed in terms of Ψ, as stipulated in equation 8 and shown in Figure 5.

$$\Psi = e - e_{ss} \tag{8}$$

The state parameter Ψ governs the peak behaviour, as does the dilantancy angle. This results into the following equation (Been & Jefferies, 2006).

$$\varphi_p \approx \varphi_{cv} + 46\,\Psi \tag{9}$$

Moreover, depending in the sand, it will behave in a certain manner. This is governed by the sand characteristics and will determine the course of the critical state (line).

The packing of the sand can be expressed by e_{min} , e_{max} and the difference between the two, $\Delta e_{min\text{-max}}$. With a higher roundness and sphericity, the range of void ratio's decreases. In other words, e_{min}, e_{max} and the difference between the two gets smaller. Irregularity of the grains prevents them from attaining denser packing. The stiffness is also directly correlated to the irregularity of the particles. The higher the irregularity, the lower the stiffness. This is caused by small scale effects, e.g. higher contant deformation, and on inter-granular scale, e.g., contact breakage (Coop, 2005). The critical state is also affected by the particle shape. With low densities, the interparticle contact is low and particle shape is of minor importance. At high densities, it plays a large role in the dilative behaviour of a sand. The prevention of dilatancy by irregularity of grains gravely increases the effort needed to dilate the soil. This phenomenon is mainly governed by the angularity. The influence of the grain shape parameters on mechanical behaviour of sand was summarized in Cho et al. (2006).

As discussed in Bolton (1986) the mineralogy influences the critical state behaviour of the sand. This is mainly caused by the influence of the characteristics of the minerals on the particle shape characteristics. In case of quartz, the sliding frictional resistance is lower in comparison with other minerals like feldspars due to differences in roughness (Horn and Deere, 1962).

The grain size also influences the shear strength. Through the shear zone thickness, the shear strength is impacted. Small shear zones are build up out of less particles hence a shorter chain. Since the strength of the chain is governed by the weakest link, a smaller number of particles means a smaller change on a potential point of failure. In case of a larger grain size less particles will make up the failure zone hence a higher shear strength (Anthony and Marone, 2005).

2.4.5. Conclusion

The drop in shear strength, denoted as the softening behaviour, depends on state of the sand and grain characteristics. The state of the sand is a combination of pressures acting on the sand and the density. This behaviour is described by critical state soil mechanics, linking the packing or void ratio to a 'critical state'. This critical state is denoted by the minimum void ratio at certain confining pressure that still shows dilative behaviour. When a sand has a denser packing than the critical state, the shear strength of the sand increases as a result of dilatancy (Bolton, 1986). This creates the strain softening of sandy soils upon shearing. The denser the packing, the higher the drop from peak and residual shear strength. In other words, more softening behaviour will occur. Higher pressures mean better confinement of the sand matrix hence more energy is needed for dilation to occur (Been and Jefferies, 1985). A higher confining pressure thus suppresses this dilatancy mechanism, again restricting the softening behaviour.

Furthermore, it is demonstrated that the shearing of sand occurs in thin zones within the sand matrix. This mechanism is comparable to two blocks sliding over each other and the shearing and volumetric behaviour concentrates in the zone between the blocks (Newland & Allelly, 1952). The thickness of this zone, t_s, mainly depends on the grain size, D_{50}, with a ratio of between 7 and 20 times D_{50}. This mechanism starts developing close to the peak shear stress and is oriented parallel to the major stress direction.

Sand characteristics can also marginally influence the softening. Both by influencing the relative density and the mechanical behaviour. Eccentricity and angularity of the grains

increases the e_{min}, e_{max} and $\Delta e_{min\text{-}max}$ affecting critical state behaviour. Furthermore, angularity, eccentricity and roughness increase the friction between grains. Differences in mineral content mainly influence roughness of the particles. Last, diameter mainly influences the number of grains in the shear zone, a lower number of particles means a lower chance on a weak link (Anthony and Marone, 2005).

2.5. SOIL STRUCTURE INTERACTION

The mechanical behaviour of the sand is an important aspect in the softening behaviour of micropiles, however the interface between micropile and soil will always be governing in the maximum shear force conveyed to the soil. In other words, no more softening can occur than the interface can transfer load to the soil. Hence, it is of vital importance to have a thorough understanding of the interaction to quantify the decrease in shear strength.

The interaction can be expressed through equations 10 and 12, encapsulating both pressures and frictional resistance.

$$\tau = \beta' \sigma'_v \tag{10}$$

$$\beta' = K \tan \delta \tag{11}$$

$$K = K_1 K_2 \tag{12}$$

The shaft friction between micropile and sand, τ, is controlled by the cavity expansion factor K_1, the coefficient of horizontal pressure K_2 and interface friction angle δ. These phenomena are combined into the friction factor β' (Juran et al., 1999). When equation 10, 11 and 12 are combined the shear strength of the interface is given by equation 13. The individual aspects are graphically represented in Figure 10.

$$\tau = K_1 K_2 \sigma'_v \tan \delta \tag{13}$$

In this chapter, these aspects are further discussed.

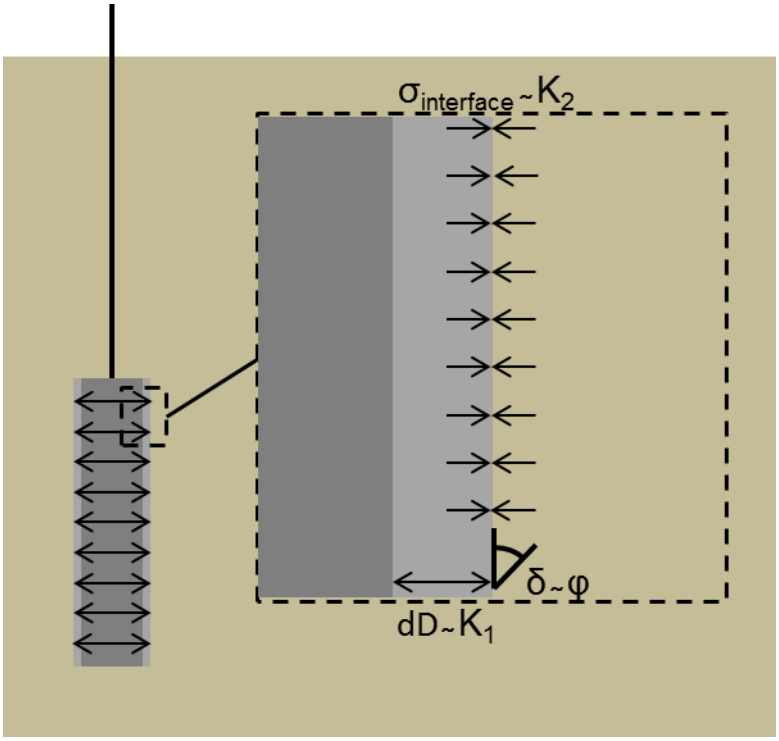

FIGURE 10: GRAPHICAL REPRESENTATION OF FACETS INFLUENCING BEARING CAPACITY AT LOCAL LEVEL

2.5.1. Interface friction

The ultimate shear stress transferred through the interface between sand and micropile depends on the relative roughness of the interface, R_n (Kishida and Uesugi, 1986). The

relative roughness is governed by the roughness of the structure R_t and the diameter of the sand particles, denoted by D_{50}, $R_n = R_t/D_{50}$. Please refer to Figure 11 for a graphical representation.

- R_n<0.02, smooth interface, $\tau_{interface,max} < \tau_{soil,max}$ hence $\delta < \varphi$
- R_n>0.1, rough interface, $\tau_{interface,max}=\tau_{soil,max}$ hence $\delta = \varphi$

The difference in $\tau_{interface}$, the shear stress on the interface and τ_{soil}, the shear stress in the soil depends on the mobilization of the dilatancy of the sand. In case of a smooth interface, the friction force will not be high enough to dilate the sand matrix. This means the shear stresses on the interface cannot reach the maximum shear stress in the sand. In case of a rough interface, this is possible.

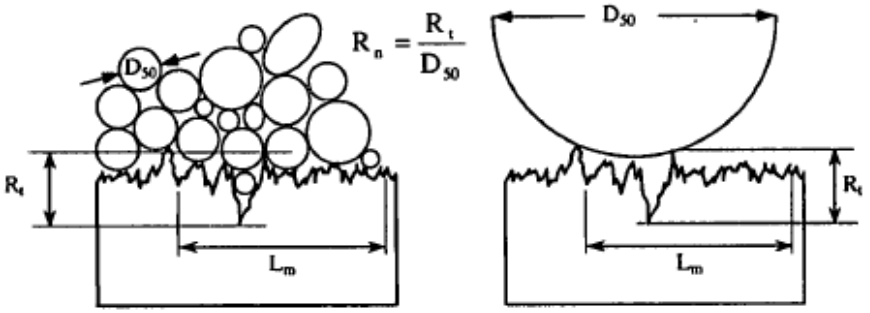

FIGURE 11: GRAPHICAL REPRESENTATION OF ROUGHNESS R_T AND RELATIVE ROUGHNESS R_N (FIOVARANTE, 2002)

This is further demonstrated by Uesugi et al. (1988). In this research simple shear test are performed on top of a smooth and rough steel plate. The measured force required as well as the vertical strain are measured. In case of a simple shear, the vertical strain is equal to the volumetric strain, since the horizontal strain is restricted. This means the vertical strain is equal to the volumetric strain. In case of positive volumetric strain, dilation occurs, hence the surface is able to mobilize the maximum shear stress of the sand. Furthermore, the sand grain movement was tracked to see the relative movement of the sand.

Figure 12a, shows the particle movement of the sand grains with the shearing of the smooth plate. The movement of the sand particles is very limited compared to the movement of the steel plate, in other words sliding of the particles over the steel plate occurs. Figure 12b, the particle movement of sand particles with the rough interface. The particles clearly are dragged along with the steel plate.

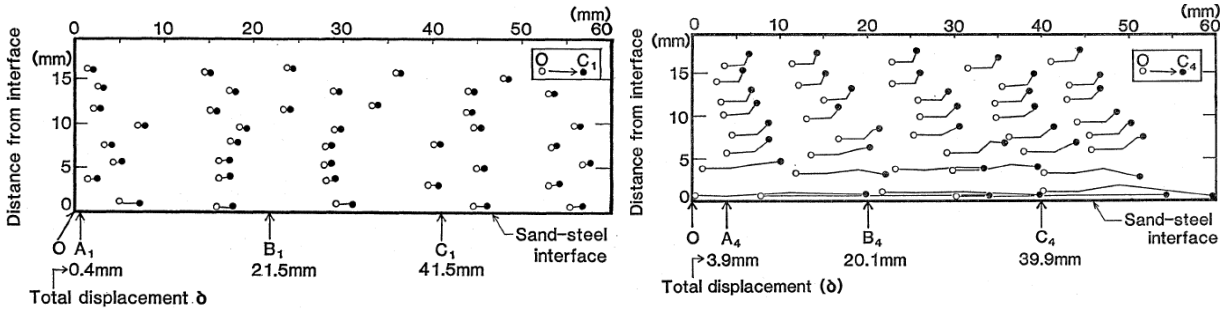

FIGURE 12: PHYSICAL MODELLING OF PARTICLE MOVEMENT ALONG A SMOOTH INTERFACE (A,LEFT) AND ROUGH INTERFACE (B,RIGHT) (UESUGI ET AL., 1988)

When comparing the volumetric strains, the theory of the mobilization of dilatancy (Yoshimi and Kishida, 1981; Kishida and Uesugi, 1987) is clearly confirmed.

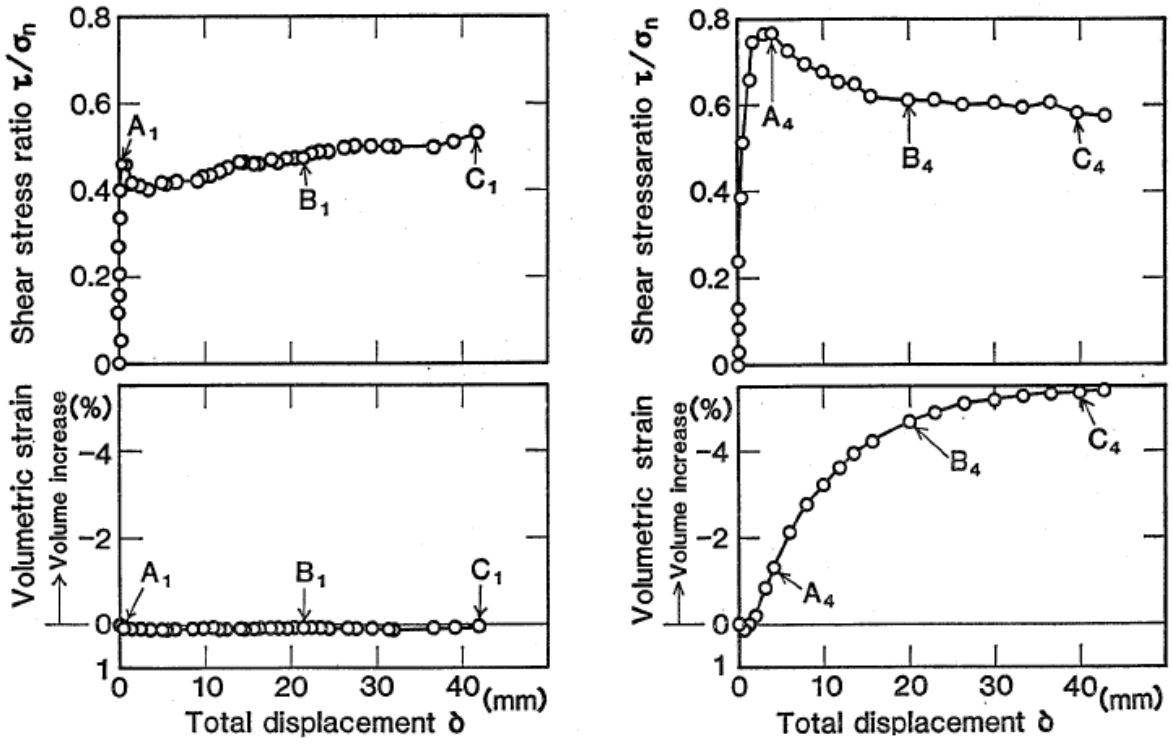

FIGURE 13: MOBILIZED SHEAR STRESS AND VOLUMETRIC STRAIN PLOT AGAINST TOTAL DISPLACEMENT FOR A SMOOTH INTERFACE (LEFT) AND ROUGH INTERFACE (RIGHT) (UESUGI ET AL., 1988)

Figure 13, the volumetric strains and shear stress are shown for the different interfaces. In case of the smooth interface, left in Figure 13, the volumetric strain is negligible, hence the slipping of the grains along the interface meant frictional forces were insufficient to dilate the sand matrix. For the rough interface, volumetric strains clearly develop with increasing shear displacements, as is a peak in the shear stress. This shows the importance of sufficient roughness of the interface. In case of a micropile, the roughness of the interface, R_t, can be approximated by $D_{50}/2$, in other words, $R_n = \frac{D_{50}/2}{D_{50}} = \frac{1}{2}$. The interface can thus be considered rough.

Fioravante (2002) compared Interface Direct Shear tests with Constant Normal Stiffness (DS-CNS) with shear stress development along a model pile in a geotechnical centrifuge. Different interface roughness are used in combination with a high relative density of the sand. Figure 14 shows these results. The upper graph shows the peak shear stresses for a smooth interface. The 'X', '+' and '-' represent the DS-CNS tests results, the model pile results are represented by the square and rhombus. The lower graph shows the peak shear stresses for a rough surface. This can be assumed for micropiles. On different stress levels, the peak shear stresses of coincide. The peak shear stress in case of shaft friction can thus be modelled well with the use of a direct shear test.

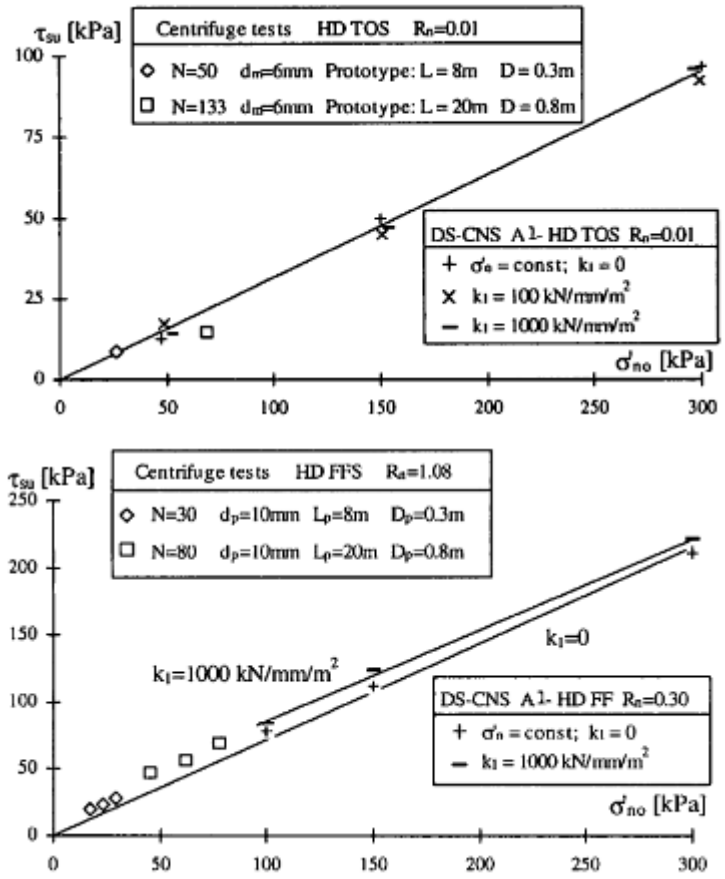

FIGURE 14: COMPARISON SHEAR STRESS DEVELOPMENT, MODEL PILE – DS-CNS FOR HIGH RELATIVE DENSITY AND DIFFERENT ROUGHNESS (UPPER:0.01, LOWER: 1.08) (FIORAVANTE, 2002)

2.5.2. Interface area

Additionally, the interface surface can increase through pressurization due to expansion of the cavity, this effect increases the bearing capacity of the micropile. The positive influence of cavity expansion is expressed by the factor K_1. According to the Littlejohn (1970), the increase in shaft size is a factor 1.4 to 1.7. In accordance with CUR236, an increase of around 20% is taken into account depending on the pile diameter.

2.5.3. Horizontal pressure

The horizontal pressure can be expressed by the coefficient of horizontal pressure K. This coefficient ultimately ranges from active soil pressure, K_a, and passive soil pressure, K_p. When in rest, the horizontal pressure is governed by the neutral soil pressure K_0. These pressure coefficients can be expressed by equations 14 to 16 (Rankine, 1857; Jaky,1944).

$$K_a = \frac{1 - \sin\varphi}{1 + \sin\varphi} \tag{14}$$

$$K_p = \frac{1 + \sin\varphi}{1 - \sin\varphi} \tag{15}$$

$$K_0 = 1 - \sin\varphi \tag{16}$$

Depending on the installation method, the horizontal pressure on the interface varies somewhere between the neutral pressure and the passive earth pressure.

Construction of grout body

The construction of the grout body represents the part of the installation in which the grout is placed and a grout body is formed in the soil. Depending on the pile type the construction of the grout body is done by cased boring (internal flushing or external flushing), self-boring piles, screwing of a steel casing or by high frequency vibrating of a casing.

In case of type A micropiles, the two casings are installed tip level of the micropile. The outside casing is to prevent the borehole from collapsing. The soil inside the outer casing is then flushed in between the outer and inner casing. When both casings reach tip level, the inner casing is removed and the anchor steel is installed. The outer casing prevents relaxation of surrounding soil.

In contrast to type A, type B flushes the soil outside the casing. With this micropile type, only one casing is bored into the soil up to tip level. Soil inside the casing is removed through flushing, reaching the surface along the outside of the casing. Transporting soil along the outside of the casing can result into some relaxation of the surrounding soil through transport of sand particles present near the exterior of the casing.

In case of type C, a drill head is installed onto the tip of the reinforcing steel and drilled into the soil. With nozzles, the grout is pumped into the soil and the rotating motion of the drill head mixes it with grout and soil. Pressurisation at the end can be performed, the effect is however limited (CUR 236, 2011). Type D is similar, in this case however an auger tip is used and the mixing can be executed better due to a fixed tip. In both case, some relaxation of the surrounding soil can occur.

High frequency vibrating is another possibility for installing the casing. With the use of high frequencies vibrations. In some cases, nozzles injecting water are installed at tip level to aid installation. On the tip of the casing, a peak is fixed to prevent soil from entering the inside of the casing. Due to the vibrations, the state of the sand can change to a looser state. Also, horizontal effective stresses can decrease.

Pressurization

Pressurization of the micropile is done during the installation to increase the horizontal pressure of the micropile onto the surrounding soil. Depending on the installation method of the casing, multiple scenarios can occur.

In case of no pressurization, only the hydrostatic pressure of the grout will act on the soil. Horizontal pressure coefficient K can thus be approximated with K_0 (Juran et al., 1999). When the grout is pressurized, the final horizontal pressure in the interface depends on the quantity of the pressure and the method used for casing installation. Furthermore, as a result of the pressurization, the soil cavity will expand. In case of high pressures, this could mean a significant difference in interface area, which is discussed in the section 3.5.3. Due to cavity expansion the soil moves into a passive state thus the horizontal pressure will be in between K_0 and K_p. Though full mobilization of the passive earth pressure will be hard to reach, the earth pressure will be close to K_p when construction happened properly. This pressurization is expressed by the factor K_2

Load history

When the soil previously experienced significantly higher effective vertical stresses over a long period, the horizontal pressure can exceed the value of 1 – sin φ. This phenomenon is called overconsolidation. If this is the case, in addition to earlier statements, the neutral horizontal pressure can be approximated by equation 17 (Kulhawy and Mayne, 1982).

$$K_{0,OCR} \approx (1 - \sin\varphi) OCR^{\sin\varphi} \quad (17)$$

The overconsolidation ratio, *OCR* $\left(= \frac{\sigma'_{v,OC}}{\sigma'_{v,NC}}\right)$, is the ratio between the maximum effective vertical stress in situ ever reached, and the current vertical effective stress.

2.5.4. Shear band development in interface

It is broadly investigated how shear bands occur within soil. What is however as important is the coupling with the interface. The interface will provoke a certain shear band.

This was, amongst many others, found by DeJong et al. (2006). In Figure 15, the shear behaviour of granular materials is represented. The deformations concentrate within a thin interface shear band, as a rule taken at several times D_{50}, next to the interface. This zone is shown in Figure 15 by the parallelogram and dashed square. The spring represents radial stiffness of the soil resulting in stress increases or decreases depending on the volumetric behaviour.

DeJong et al. (2003) investigated the interface load transfer in an interface shear box with a Constant Normal Stiffness (CNS). With the help of Particle Image Velocimetry (PIV) the particle movement is tracked. An interface shear box of 60 mm x 100 mm is used with a

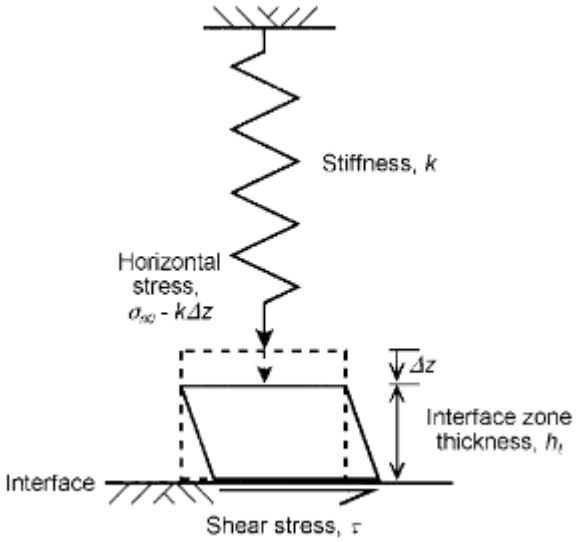

FIGURE 15: SCHEMATISATION OF THE SHEARING BEHAVIOUR IN INTERFACE SYSTEM (DEJONG ET AL., 2006)

height of 20 mm. It should be noted that the focus of the PIV data was on the middle 1/3th of the shear box to minimise boundary effects caused by the rigid edges. A rough interface is used.

Figure 16 shows the shear stress development, vertical displacement and PIV data of a CNS test on a silica sand. The PIV data display the particle movement and clearly distinguishes two zones, a zone without significant displacements and a zone with significant gradient of horizontal displacement, the shear zone. Within this zone, the displacement gradient occur uniformly, parallel (horizontal) and perpendicular (vertical) to the interface (DeJong et al., 2003). This translates into the linear increase of horizontal displacements within the shear zone. The height of the zone only slightly varies from 3.5 mm at 1 mm to 5.3 mm at 12 mm interface displacement, corresponding with between 5 and 8 times D_{50}.

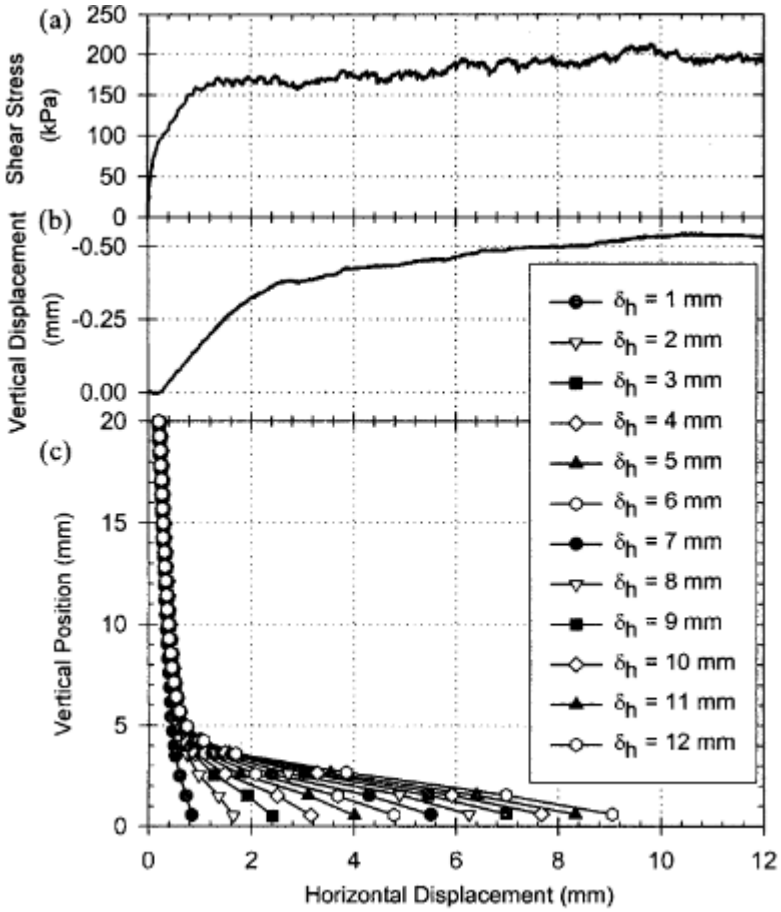

FIGURE 16: SHEAR STRESS (A), VERTICAL DISPLACEMENT (B) AND PIV DATA (C) OF CNS TEST FOR DIFFERENT INTERFACE DISPLACEMENTS (DEJONG ET AL., 2003)

This mechanism is also monitored in small scale pile tests Tehrani et al. (2016). The effect of surface roughness and soil density on the shearing behaviour was investigated with the help of PIV and Digital Image Correlation (DIC). A model pile with a diameter of 490 mm (B) and a embedment length of 490 mm in an Ohio Gold Frac Sand is investigated. With PIV and DIC, displacements of the sand particles are tracked. Figure 17 shows shear strains around the pile for different relative densities and roughness. In agreement with Uesugi & Kishida (1988), the rough interfaces (dashed lines) show a shear strains mobilisation while the smooth interfaces (straight lines) only slip. Furthermore, a small difference is observed between the densities.

A further elaboration is made on the shear band formation. This is done with the help of a digital portable microscope instrumented with an accurate virtual grid (0.2 D_{50} x 0.2D_{50}) focussed onto an area 300 mm in the soil body. To assess the shear band formation, the movement of grains is calculated with the help of the DIC technique. When an element of the grid only has 10% of the vertical displacement of the adjacent grid, it is assumed to be the border of the shear band (Tehrani et al., 2016).

Figure 18 demonstrates the shear band size for a dense sand with a rough interface. Also for the model piles, the average shear band is 3.2 D_{50} and 4.2 D_{50} for respectively dense and medium-dense sands.

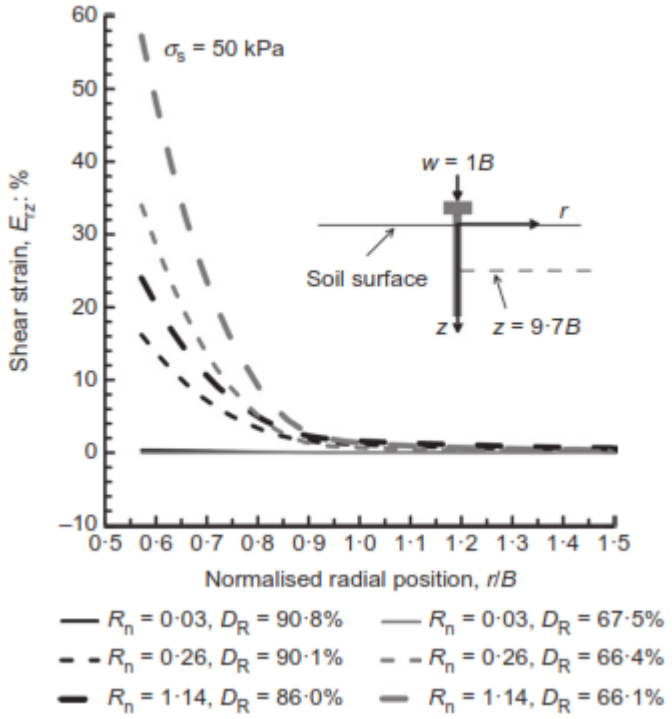

FIGURE 17: SHEAR STRAINS IN PILE INTERFACE, VARYING ROUGHNESS (R_N) AND RELATIVE DENSITY (D_R) (TEHRANI ET AL., 2016)

When comparing both the shear band formation in the interface shear box and the model pile test, shown in Figures 16 and 18, a very similar behaviour is shown in terms of size and displacement behaviour. It can be observed that practically all displacements take place inside the small shear band adjacent to the interface.

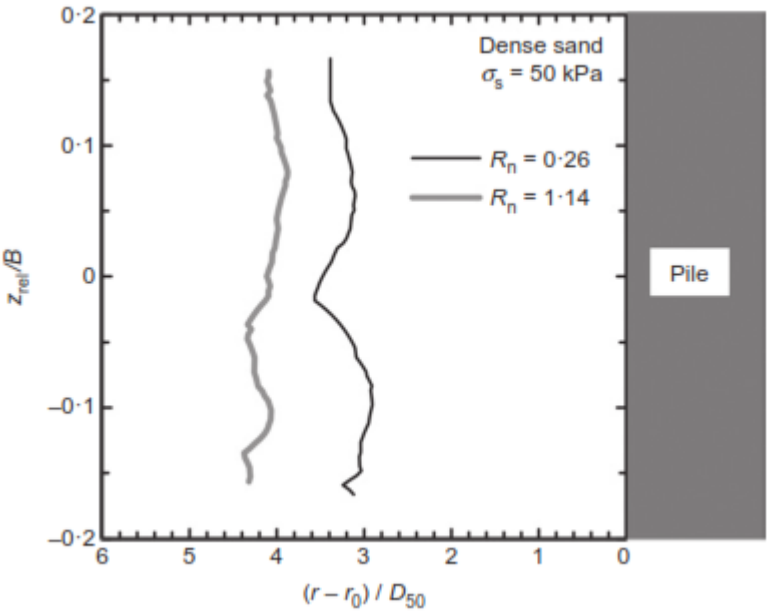

FIGURE 18: SHEAR BAND SIZE NORMALISED TO GRAIN SIZE (D_{50}) FOR DENSE SAMPLE ($D_R \approx 90\%$) AND ROUGH INTERFACE (R_N>0.1) (TEHRANI ET AL., 2016)

2.5.5. Conclusion

The soil – structure interaction can be expressed by equations 6 and 7. The interaction is affected by the pressures in the interface and the frictional capacity of the interface. This chapter further elaborated on this.

Pressures on the interface depend on the installation method of the casing and the pressurization, expressed by the factor K_2. Furthermore, the expansion of the cavity due to pressurization increases the surface area of the interface. This effect is indicated by the factor K_1. Combined, these effects give the factor K' (Juran et al., 1999).

Friction of the interface is governed by the relative roughness of the interface. In case the roughness of the micropile is larger than 0.1 times the D_{50}, the interface is rough. It can be assumed that the interface is as strong as the soil itself. For micropiles, the sand grains construct the interface. It is thus safe to assume that in each frictional resistance of the soil is equal to that of the sand. In other words $\delta = \varphi$ (Uesugi & Kishida, 1987).

All phenomena combined give equation 15, encapsulating the interaction (Juran et al., 1999).

The majority of the deformation behaviour takes place in a small zone adjacent to the interface. This is causes by shear band formation. A interface shear box (DeJong et al., 2003), and small scale test piles (Tehrani et al., 2016) show similar shear band formation. As investigated intensively for sands, also with the presence of an interface, the shear band is in the order of 3 to 8 times the average particle diameter D_{50}.

2.6. MODELLING OF SOFTENING: HYPOPLASTICITY

Within numerical modelling there are numerous constitutive models available, both experimental and commercial. Plaxis is a frequently used finite element program. To assess the constitutive model is suitable for numerical simulations of the softening behaviour within the presented modelling situation, a small elaboration is made on hypoplasticity.

2.6.1. Constitutive model

The concept of hypoplasticity originates from a paper by Kolymbas (1985). The soil behaviour was described as in-elastic material with the use of a single nonlinear tensorial function of rate type. Based on this formulation, numerous aspects of the mechanical behaviour of granular soils have been investigated. An important aspect is the incorporation of the critical state behaviour (Wu and Bauer, 1993). This demonstrated the barotropic (pressure) and pyknotropic (density) dependency of the mechanical behaviour of a specific soil. In other words, the same soil behaves differently with different stresses and densities.

The state of the material can be fully subscribed by the void ratio *e*, the Cauchy granulate stress tensor T_s and the velocity of the grain skeleton v_s. Within this formulation, macro-pores and other complex soil grain structures are not taken into account as is cementation. Parameter T_s can also be described as the inter-granular or effective stress tensor.

$$\mathring{T}_s = F(T_s, e, D) \tag{18}$$

Equation 15 denotes the notation of $\mathring{T}_s$, the objective stress rate tensor, as a function of T_s,*e* and *D*. This is the basis of the hypoplastic constitutive formulation by Gudehus (1996) and later Bauer (1996). *D* is the stretching tensor of the granular skeleton, expressed as symmetric part of the deformation gradients *L*, the change rate of the velocity vector v_s throughout the soil continuum. Bauer (1996) proposed the division of the hypoplastic formulation into a linear and a nonlinear part, denoted by equation 19.

$$\mathring{T}_s = A(T_s, e, D) + B(e, T_s)\|D\| \tag{19}$$

The variable *A* describes a linear soil behaviour in *D* where the soil behaviour is hypoelastic. The parameter *B* describes the nonlinear part of *D*. For a more usable and transparent formulation of the constitutive model, the parameters *A* and *B* are factorised in a more suitable way, equation 20 and 21.

$$A(T_s, e, D) = f_e L(T_s, D) \tag{20}$$
$$B(e, T_s) = f_e f_d N(T_s) \tag{21}$$

With the factors f_e and f_d representing the density dependency relative to the critical state. Furthermore, an additional constant f_b is introduced. This barotropy factor is used to calculate the stiffness factor $f_s = f_b f_e$. This resulted into the formulation of the objective stress rate tensor, equation 22.

$$\mathring{T}_s = f_e f_b\left(L\left(\hat{T}_s, D\right) + f_d N(\hat{T}_s)\|D\|\right) \tag{22}$$

The expression is built up out of the tensors *L* and *N*||*D*||. These depend on the stretching tensor *D* and the stress ratio tensor $\hat{T}_s = \frac{T_s}{tr\, T_s}$. This equation is rewritten by Von Wolffersdorff (1996) into equation 23.

$$\dot{T}_s = f_e f_b \frac{1}{tr\,\hat{T}_s^2}\left(F^2 D + a^2 tr\left(\hat{T}_s D\right)\hat{T}_s + f_d a F(\,\hat{T}_s + \hat{T}_s^*)\|D\|\right) \tag{23}$$

With $\hat{T}_s^* = \hat{T}_s - \frac{1}{3}I$, the deviatoric stress tensor. Equation 23 is the result of the implementation of the Matsuoka/Nakai failure criterion, equation 24 into equation 22. This failure criterion is governed by the parameters *a* and *F*, respectively describing the influence of the critical state surface in stress space and the stress tensor, please refer to equations 24 to 26. The stress space, a and F are mostly governed by the lode angle θ and the dilatancy angle ψ

$$a = \sqrt{\frac{3}{8}}\frac{(3 - \sin\varphi_c)}{sin\varphi_c} \tag{24}$$

$$F = \sqrt{\frac{1}{8}tan^2\psi + \frac{(2 + tan^2\psi)}{2 + \sqrt{2}\tan\psi\cos 3\theta}} - \frac{1}{2\sqrt{2}}\tan\psi \tag{25}$$

$$\tan\psi = \sqrt{3}\left\|\hat{T}_s^*\right\|, \cos 3\theta = -\sqrt{6}\frac{tr\hat{T}_s^{*3}}{(tr\hat{T}_s^{*2})^{\frac{3}{2}}} \tag{26}$$

For further elaboration on the structuring of the constitutive modelling of hypoplasticity, please refer to the papers written by Gudehus (1996), Bauer (1996) and Von Wolffersdorff (1996).

3. NUMERICAL MODELLING

3.1. PARAMETER DETERMINATION

In this section, a description of the tested soil is given. Furthermore, the results of the parameter determination are presented. For an elaboration of the parameters determination, please refer to Appendix A.

3.1.1. Parameters testing

The Hypoplastic (HP) model in PLAXIS uses complex and sensitive parameters. Therefore, it is important to determine the input parameters for the HP model with the use of laboratory tests. No proper empirical correlations exist for this model. The input parameters for the HP model are:

- e_{c0} (maximum void ratio) (Herle and Gudehus, 1999)
- e_{d0} (minimum void ratio)
- e_i (ultimate maximum void ratio, 1.15*e_{max} (Herle and Gudehus, 1999)
- h_s (granular hardness)
- n (pressure sensitivity of the grain skeleton)
- φ_c (critical friction angle)
- α (determined using φ_p, ψ_p and φ_c (peak friction and dilatancy angle))
- β (1 for natural non-cohesive soils) (Herle and Gudehus,1999)

To be able to determine these parameters, several element tests have to be performed. Based on these tests the input parameters are determined. The following tests will be carried out:

- Angle of repose test (JGS)
- Void ratios test (JGS)
- Oedometer test
- Direct shear test

Two different non-cohesive soils are used from the same borehole; one from the formation of Drente (B320-13) and one from the formation of Sterksel (B320-16). Both are Pleistocene soils. They can be characterized as coarse, well graded sands, respectively glaciofluvial and fluvial. The grain size distributions of both soils can be found in Figure 19. It can be denoted sample B320-16, in contrast to B320-13, contains a small gravel fraction.

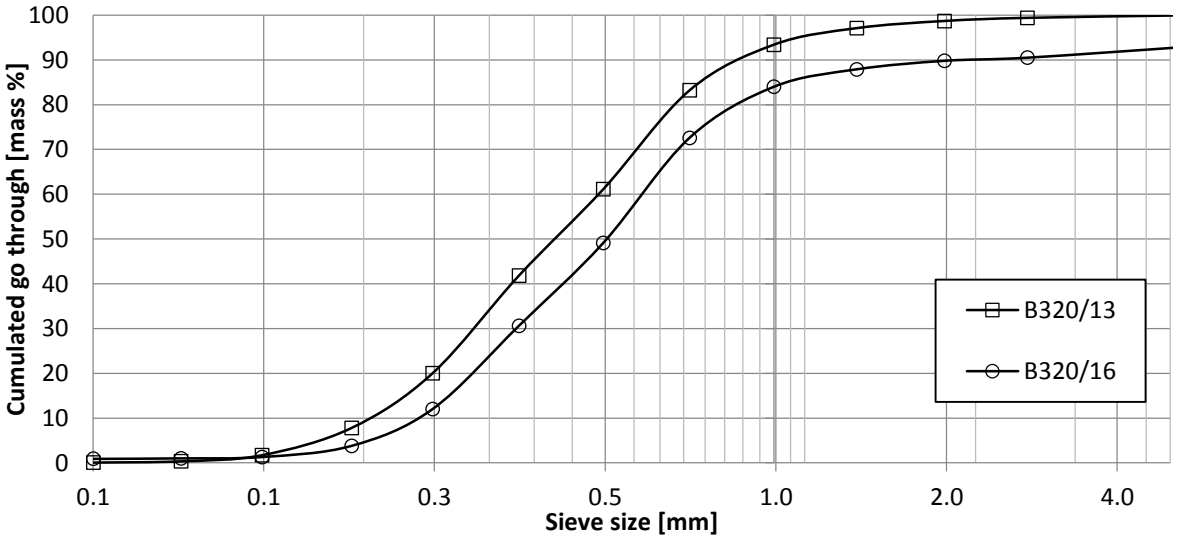

FIGURE 19: GRAINSIZE DISTRIBUTION TESTED SAMPLES

3.1.2. Results parameters

All tests performed on the two soil samples give the parameters presented in Table 3. It shows similar HP parameters for both geologic formations. Furthermore, the order of magnitude of the parameters is similar to earlier research (Herle and Gudehus, 1999).

TABLE 3: HYPOPLASTIC PARAMETERS FORMATION OF DRENTE AND STERKSEL

Formatie	ϕ_c [°]	h_s [GPa]	n [-]	e_{d0} [-]	e_{c0} [-]	e_{i0} [-]	α [-]	β [-]
Drente	31.1	13	0.27	0.51	0.74	0.86	0.151	1
Sterksel	32.8	10	0.26	0.51	0.74	0.85	0.157	1

Last, it is important to notice β is set to 1. This can actually vary (Herle and Gudehus, 1999), but as the influence of this parameter is small it is not calculated it is simply chosen to be 1.

3.2. NUMERICAL MODELLING: HYPOPLASTICITY

To gain a better understanding in the shear stress development along the micropile, the micropile is modelled as similar as possible to the actual installation process within an axisymmetric geometry. Furthermore, the load – displacement curve of the head of the micropile from the model is tried to fit to the actual results. Relative density of the sand surrounding the pile is extrapolated from CPT data. Interface pressure is an unknown and is fit via the load displacement curves.

First, the built-up of the numerical model is explained thoroughly. Then, the expected outcome from the model is discussed. By first describing an expected outcome, results of the numerical model can be assessed for correctness as well as usefulness. Last, the results are presented and discussed.

3.2.1. Numerical model

The model is built-up out of three major volume elements:

- Surrounding soil
- Bentonite mixed soil above micropile
- Micropile

The material behaviour of the present sandy soil is described by the hypoplastic model. This material is initially modelled as with the parameters of the soil of the Drente formation, see Table 3. For the initial void ratio, *e* is chosen at 0.6. In practice, the bentonite mixed material is made to not contribute to the tensile bearing capacity of the micropile. This behaviour is modelled with the Mohr-Coulomb constitutive model. The model parameters are given in Table 4. It should be noted that these values are initially chosen arbitrarily since the influence of this material should be minimal.

TABLE 4: BENTONITE MIXED MATERIAL (MOHR-COULOMB MODEL, DRAINED)

γ_{unsat} [kN/m^3]	γ_{sat} [kN/m^3]	φ [-]	c' [kPa]	E' [kPa]	ν' [-]	tension cut-off
15	17	20	5	2000	0.33	yes

The micropile is modelled with a linear elastic material, see Table 5. The volumetric weight of the micropile is assumed to the same as concrete. For the stiffness, an equivalent stiffness is used. At relatively low loads, the grout body will crack under the tensile load (CUR 236, 2011). The steel reinforcement of the micropile then governs the stiffness. Since the micropile transfers the tensile load through the grout body, this volume needs to be modelled, an equivalent stiffness is used to correctly model both the circumference and the stiffness of the micropile. The equivalent stiffness E' is calculated with equation 27.

$$E' = E_{steel}\frac{A_{steel}}{A_{micropile}} = 20 * 10^6 kN/m^2 \quad (27)$$

The stiffness of the steel E_{steel} is taken at GEWI stiffness, 195 *10^6 kN/m^2 (CUR Addendum, 2016). The diameter of the steel and micropile are respectively 63.5 mm and 200 mm.

TABLE 5: MICROPILE MATERIAL (LINEAR ELASTIC, NON-POROUS)

γ_{unsat} [kN/m3]	γ_{sat} [kN/m3]	E' [kPa]	ν' [-]
24	24	20*10^6	0.1

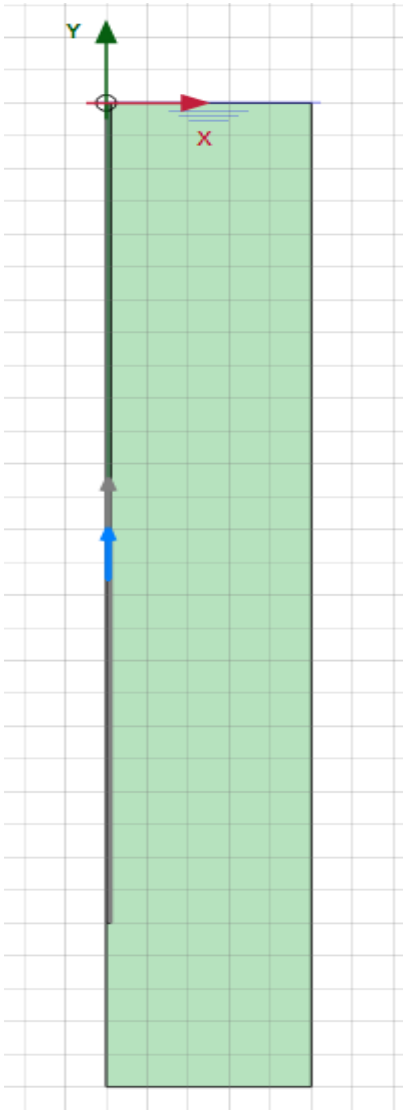

FIGURE 20: PLAXIS MODEL: SOIL IN GREEN, MICROPILE IN GREY AND LINE LOAD IN BLUE

The numerical modelling is done with the following phases:

1. Initial phase
2. Pressurisation
3. 10% F_p
4. 40% F_p
5. 70% F_p
6. 90% F_p
7. 120% F_p

A distributed load in the radial direction simulates pressurisation. Loading, a percent of the maximum capacity F_p, on the micropile is also done with a distributed load on the head of the micropile, in the axial direction. This differs from the 'actual' tests where the micropile is loaded at ground level with a 'point load'. Numerically, this can however be problematic in combination with the axissymetric geometry. Furthermore, the connection between the very slender, stiff reinforcement steel to the relatively flexible micropile volume element gives impossible stress concentration and thus deformations. To prevent these inaccuracies from occurring, it was chosen to model the load as a representative distributed load. Please refer to Figure 20.

Element size is varied between large and very small, respectively 1.5 and 0.1 m. The effect local mesh refinement is also assessed. Furthermore, the soil structure interface is modelled in three different manners.

- No interface
- Interface without activation
- Interface

The interface strength is kept equal to the soil strength (Kishida and Uesugi, 1986). To make sure that significant strains occur in the sand, first the micropile – sand interface is modelled rigid without interface. To investigate numerical stability, an interface is also tried in two ways. First, it is tried to put the interface in the model without activating it. Moreover, a model is used with an active, very stiff interface. The high stiffness and strength parameters are used to minimise interface influence. Table 6 shows the interface parameters.

TABLE 6: INTERFACE PARAMETERS

φ [°]	ψ [°]	E_{oed} [kPa]
42	11	60000

Last, the stiffness of the grout body is decreased to see how the redistribution of mobilisaed shear stresses in the soil body changes. The stiffness is reduced to $20*10^5$ kN/m^2. It is assumed that an infinitely stiff micropile mobilises a constant shear stress along the micropile. The opposite is expected with a flexible micropile. The mobilisation of shear stresses constantly redistributes further into the micropile with an increasing tensile load.

3.2.2. Expected and required results

The behaviour of the numerical model should be similar to the large scale tests. Since the micropile behaviour for tested micropiles normally is only known at a global scale, assumptions are made of what behaviour is expected from the sand tests. When the global numerical results coincide with the expectations, it can be argued that the local behaviour displayed by the numerical model approximates the ‘actual’ sand behaviour.

In the model, three aspects are of paramount importance for accurate modelling:

1. Pressurisation
2. Distribution of shear stresses
3. Accurate shear stresses

The pressurisation phase should show an increase of the radial effective stress approximately equal to the distributed load, decreasing radially from the micropile.

Shear stresses transferred from the micropile onto the sand should continuously redistribute along the micropile shaft. A higher load on the micropile should results into higher strains in the micropile and the adjacent soil. This interaction is influenced by the mobilised shear stress, however, the shear stress is also a function of the strain of the micropile. At relatively small loads, the maximum shear stress is mobilized at the top of the micropile. Increasing the load, strains will increase and it is expected stresses will mobilise to a residual value. Please refer to Figure 21 for a graphical representation of this mechanism.

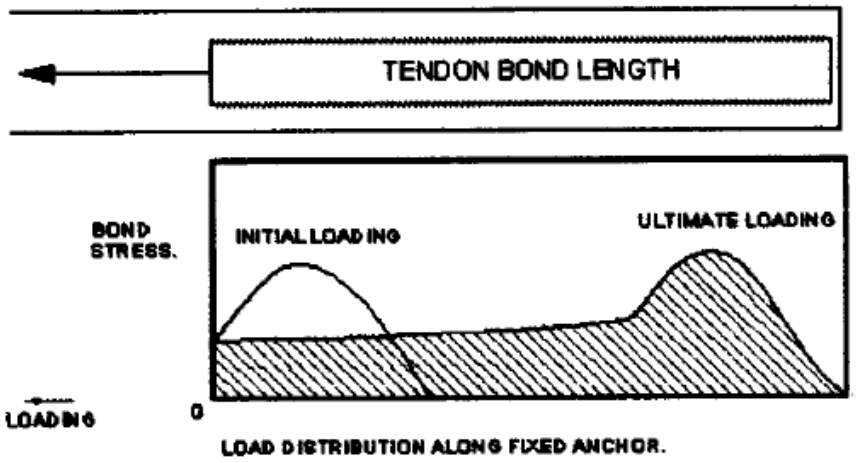

FIGURE 21: LOAD DISTRIBUTION ALONG AT MICROPILE (BARLEY ET AL., 2003)

Last, the shear stresses along the micropile should develop smoothly without fluctuations/oscillations. This insures local differences do not induce uncertainties into the mobilised stress of the sand around the micropile. High accuracy is of paramount importance for accurately deducing the softening behaviour from the numerical model.

3.2.3. Results conceptual model

The assessment of the results is based on the aforementioned criteria. Multiple observations can be made with respect to the expected soil behaviour.

The results of the pressurisation stage are in line with the expectations. Horizontal effective stresses increase up to the distributed load, representing pressurisation. Furthermore, this horizontal stress increase decreases radially from the micropile interface. This is shown in Figure 22 for a pressurisation of 500 kPa.

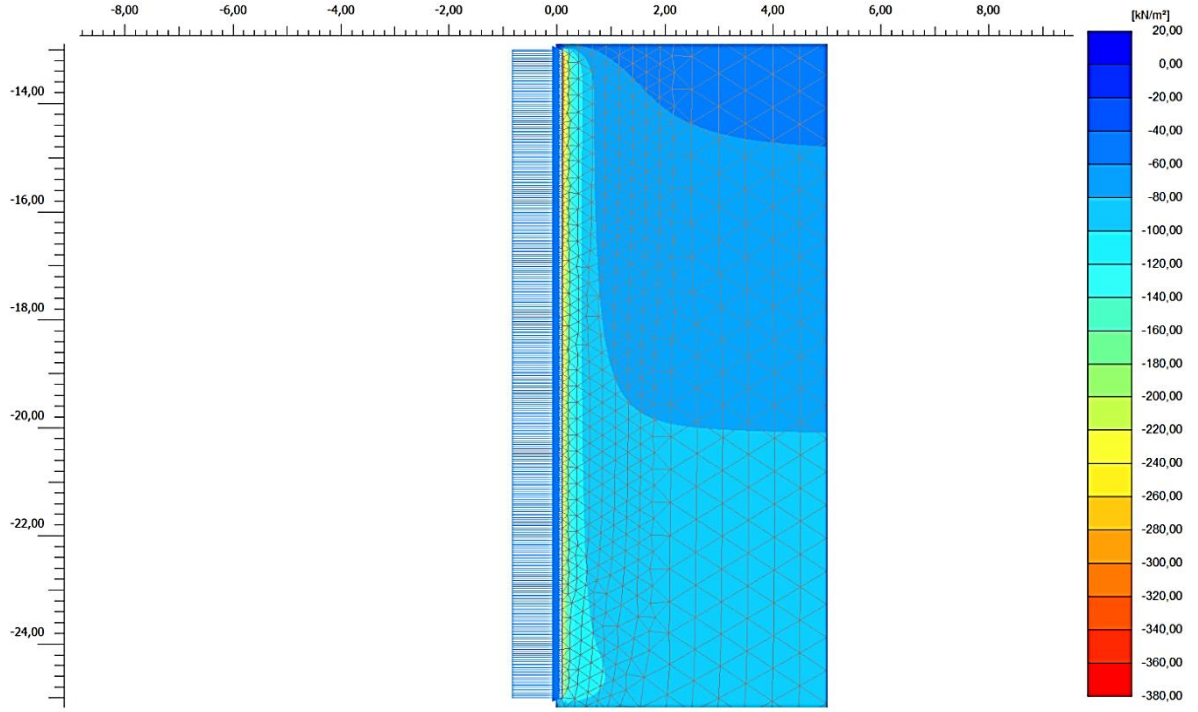

FIGURE 22: PLAXIS MODEL: PRESSURISATION PHASE, SIG'$_{XX}$

After this phase, the micropile is loaded axially. At low loads the principal stresses accurately follow the direction of loading and giving a nice homogeneous stress distribution. Please refer to Appendix B.

The principal stresses and mobilised shear stress distribution along the micropile do not coincide with the expectations. Instead of initially showing an increase in shear stress and with increasing strains mobilising to a residual strength, it continuously increases. This is in contradiction with the actual behaviour of the sand and the single stress point behaviour in the soil testing facility of Plaxis. Here, a decrease of the mobilised shear stress after the peak shear stress is clearly shown. Please refer to Figure 21.

Moreover, when inspecting the numerical results up close, stress inaccuracies are observed. In Figures 23 to 25, the development of the stress inaccuracies can be seen clearly from 40% to 120% F_p.

Mesh size influences the model behaviour. When the element size is reduced, stress concentrations tend to get smaller in size however also more abundant. Large stress differences occur in stress points adjacent to the micropile. This demonstrates the redistribution of shear stresses does not occur properly. When increasing loads, some stress points take up too much stress and others are unloaded which amplifies each other at the following load step, in the end giving big differences in mobilised shear stresses. In short, the redistributing of shear stresses in combination with the loading in tension introduces accuracy problem within the numerical model.

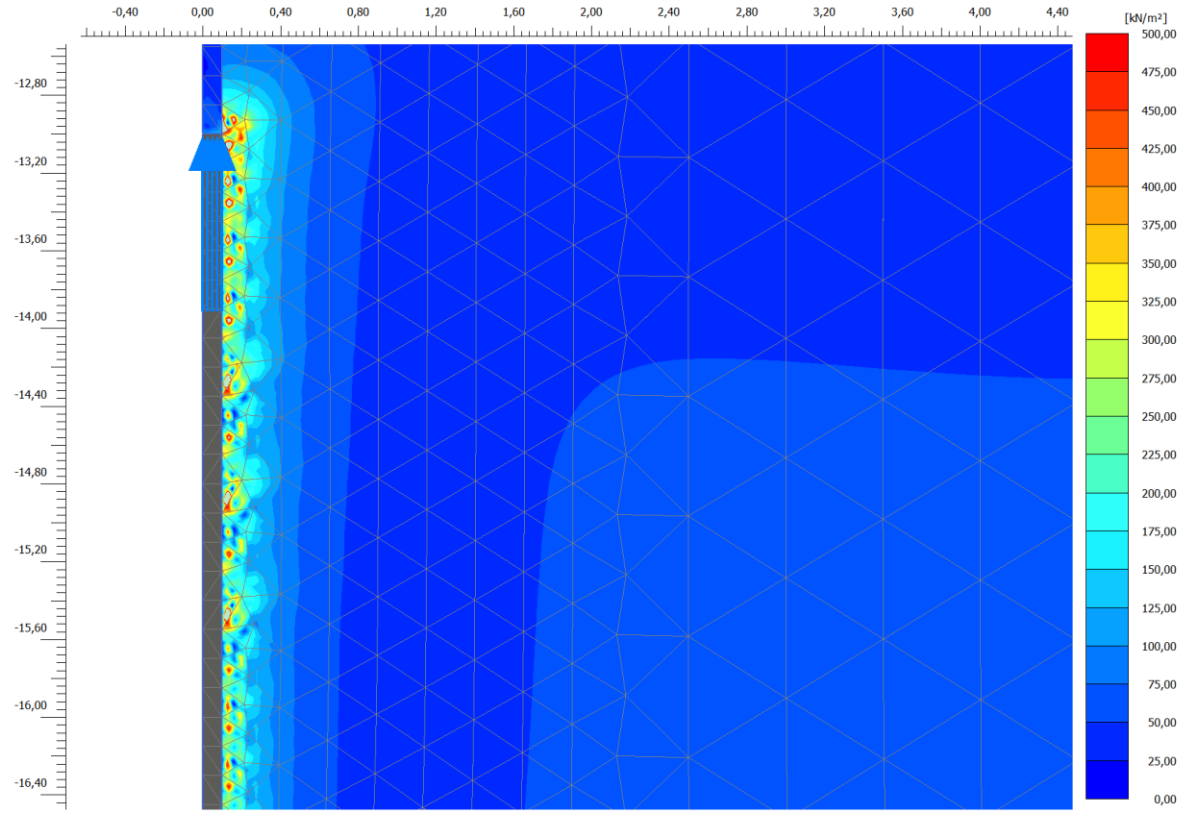

FIGURE 23: PLAXIS MODEL: FINE MESH, LOADING 120%, $T_{MOBILISED}$

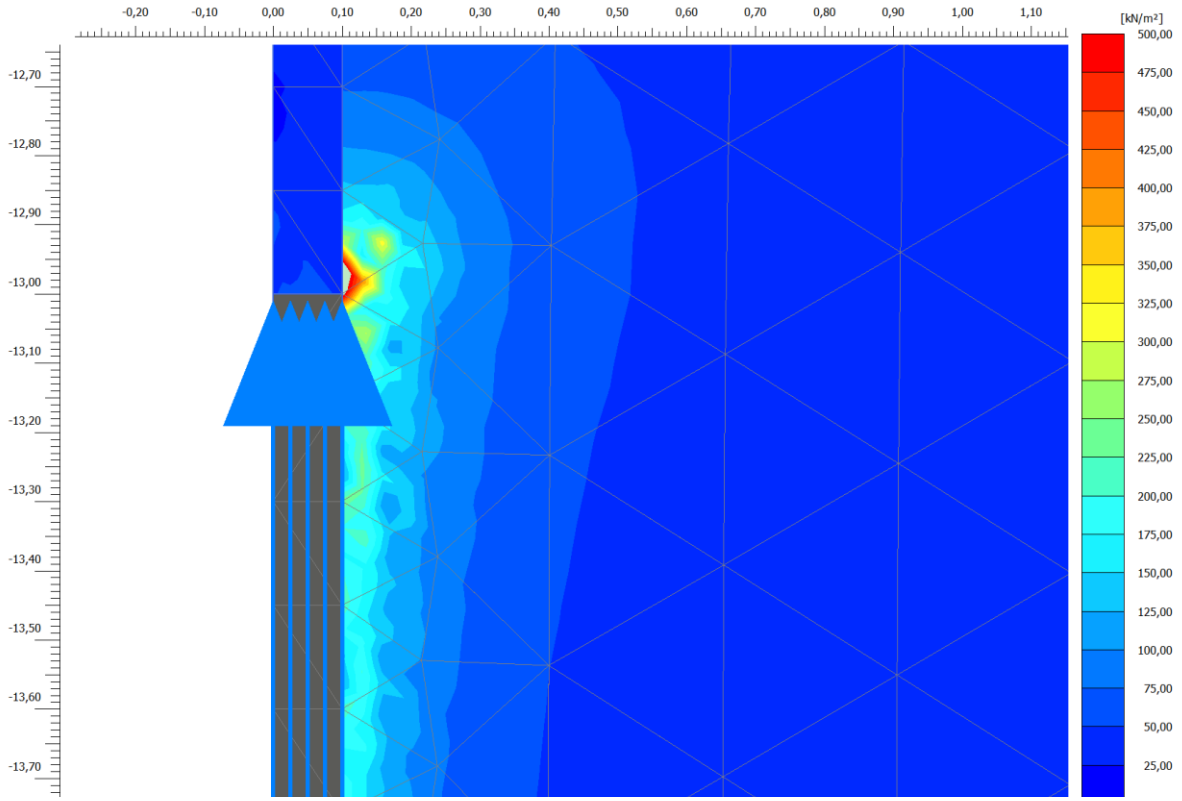

FIGURE 24: PLAXIS MODEL: LOADING 40%, $T_{MOBILISED}$, CLOSE-UP

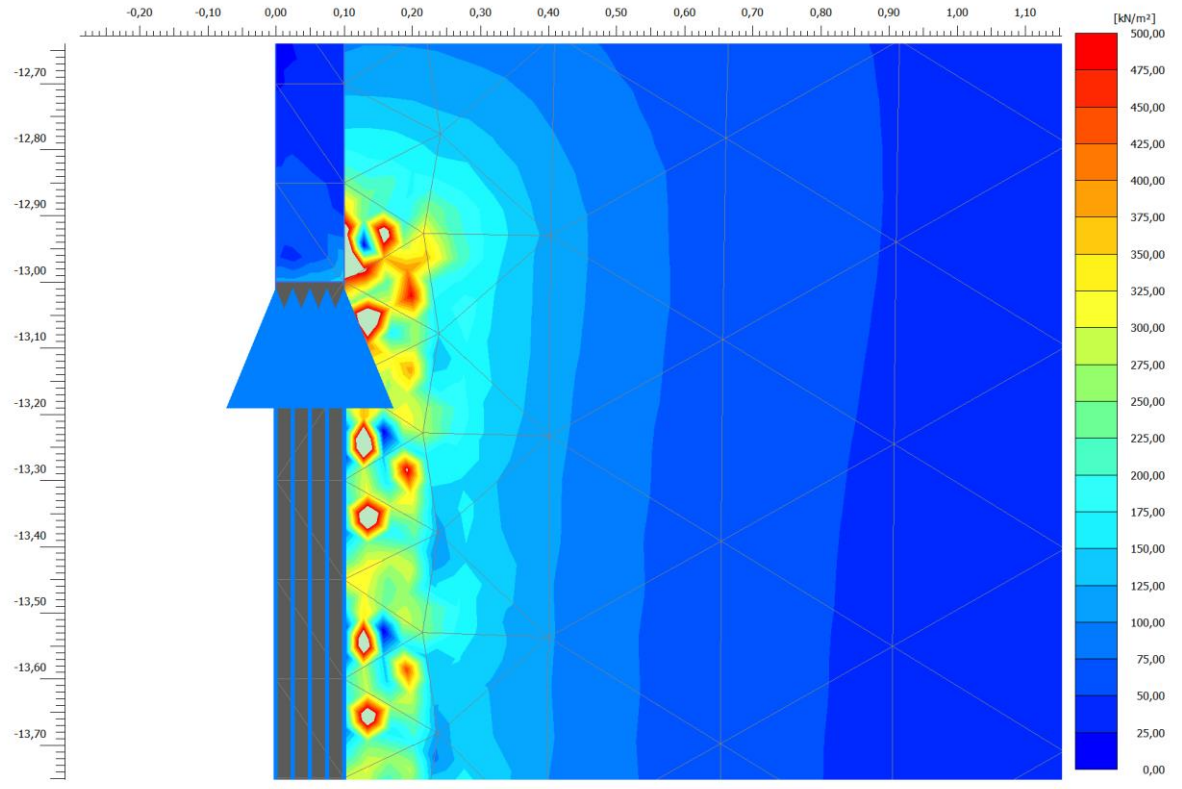

FIGURE 25: PLAXIS MODEL: LOADING 120%, $T_{MOBILISED}$, CLOSE-UP

Introducing an interface does not have an influence on the stress introduction into the hypoplastic material. Furthermore, adaptation of the numerical control parameters (Gudehus, et al., 2008) does not solve the inaccuracy issues. The arc-length control is both used and not used. In addition, the maximum step size is lowered to decrease the step size up a minimum of 10000 steps. The desired minimum and maximum number of iterations is decreased to respectively 3 and 5, based on the soilmodels.info research (Gudehus et al., 2008). The thought is to reduce or remove inaccuracies with the smaller step size and reduce unnecessary iterations. Please refer to Appendix B for the numerical results.

When a micropile with a decreased stiffness is modelled, the inaccuracies occur at lower loads. This substantiates the fact that the issue occurs due to the redistribution of shear stresses since a more flexible pile redistributes the shear stresses more at lower loads. The numerical results are shown in Appendix B.

As denoted by Brinkgreve (1994), the classical approach of local softening plasticity induces problems. The results from the numerical calculations tend to be mesh dependent. Additionally, the local softening implementation could lead to convergence problems inducing inaccuracies.

Though the advised numerical control parameters are used, the combination of the non-linear behaviour of the hypoplasticity model, the local implementation of the softening behaviour and the tensile loading, cause considerable inaccuracies.

3.2.4. Conclusion numerical model

The pressurisation of the micropile on the hypoplastic material can be modelled well. Figure 22 shows the stresses in the expected direction (horizontal) and with the expected magnitude. Furthermore, a radial decrease occurs.

Axial loading of the micropile becomes problematic. The local shear stresses arbitrarily fluctuate. Moreover, the redistribution of shear stresses does not occur as expected in accordance with Barley et al. (2003). What is expected in the model is a peak behaviour at high relative densities. Though the constitutive model shows the peak behaviour on a single stress point level, within the finite element mesh, this behaviour is not displayed.

Both results are most likely caused by the highly non-linear behaviour of the softening in combination with the local softening plasticity implementation into the finite element mesh (Brinkgreve, 1994). A combination of this and the loading of the micropile in tension induce stress inaccuracies. Combined, the results are unsatisfactory for their purpose in this thesis.

Since a high accuracy and correct distribution of shear stresses is of paramount importance for a correct assessment on the softening behaviour at the micropile, it can be concluded that the hypoplastic model unfortunately cannot be used to gain a better understanding of the softening behaviour.

4. SMALL SCALE PHYSICAL MODELLING

The softening behaviour can be modelled on a small scale based on Direct Shear (DS) tests. By assuming the DS box is a small section of the micropile, the local stress – strain behaviour can be assessed. This assumption is often made to simplify the testing and maximise control over the state the tested sample is in (e.g. homogeneity of sample). In research, DS tests are performed in multiple different settings. This is done by, amongst many others: Boulon & Foray (1986), Uesugi & Kishida (1987), Uesugi et al. (1988), Lehane (1992), Jardine et al. (1993) and Tabucanon et al. (1995).

The main goal of the DS testing in this thesis is to express the influence of relative density and stress level on the softening behaviour of Dutch Pleistocene sand, in specific the Drente formation, in a loading mechanism similar to shaft friction mobilisation. As formulated by Bolton (1986), the softening behaviour is a volumetrically controlled phenomenon. This causes the shear stress development from the peak to the residual value. The main characteristics for this softening behaviour are the peak shear stress τ_{peak}, residual shear stress $\tau_{residual}$ and displacement at which the residual shear stress occurs $u_{resdiual}$. Please refer to Figure 26 for a graphical representation.

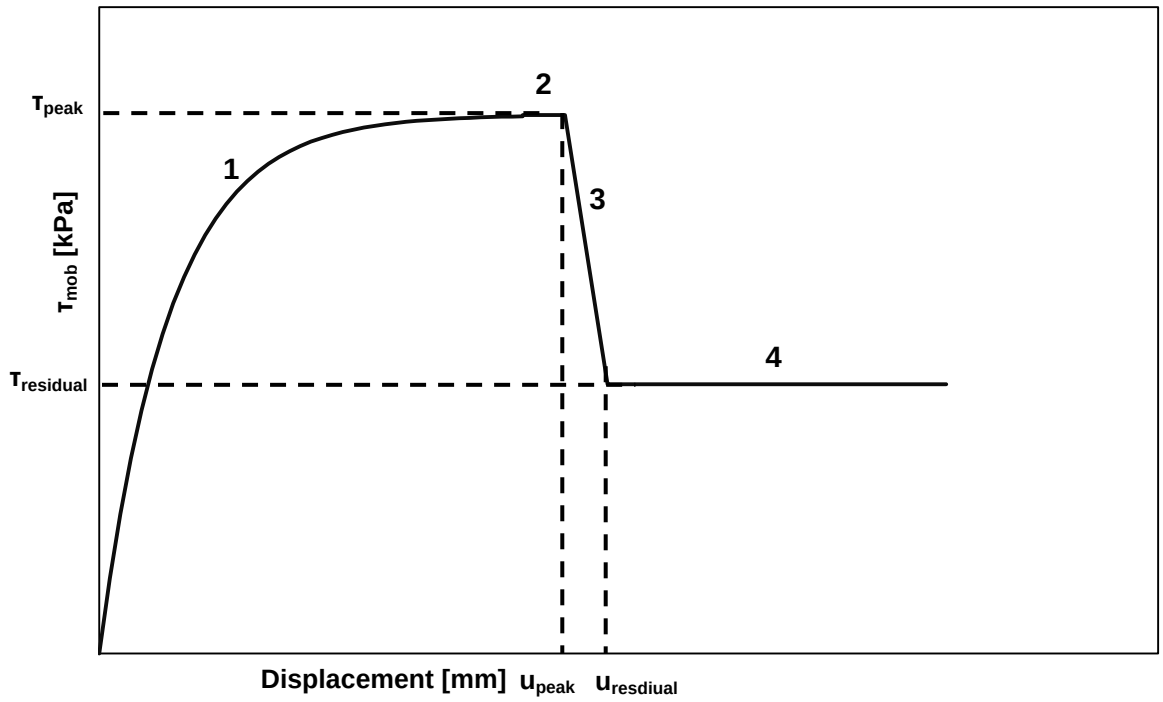

FIGURE 26: GRAPHICAL REPRESENTATION T_{PEAK}, $T_{RESIDUAL}$, U_{PEAK} AND $U_{RESIDUAL}$ IN CUR 236 ADDENDUM MODEL

The influence of relative density and stress level on the softening behaviour of the sand in this thesis is researched by doing DS tests with sand in both boxes. The assumption of a rough interface is made (Uesugi and Kishida, 1987). The relative density is varied between 50% and 100% with steps of 10%.

The normal stress is chosen at 100 and 500 kPa. Been and Jefferies (1985) linked the volumetric behaviour occurring to the average confining pressure *p'*. Assuming K_0 = 0.4, *p'* is respectively equal to 64 kPa and 306 kPa for top pressures 100 kPa and 500 kPa. This

corresponds with stress levels in reality, taking into account a significant increase in horizontal effective stress as a result of pressurisation.

Per relative density and stress level, three DS tests are performed to average effects of heterogeneity of the sample.

4.1. SET-UP AND TESTING PROCEDURE

For the DS tests, a square box is used with dimensions (LxWxH): 100 mm x 100 mm x 30.7 mm. The top load is applied on the DS box via an arm. With the arm, with a multiplication factor of 10.28, the loading process is simplified. A load of 10 kg translates to a top pressure 100 kPa. A shearing speed of 0.5 mm/min is used. The used sand is oven dried making the influence of the shearing speed negligible. Figure 27 displays a schematisation of the DS apparatus.

In Figure 27, the numbers represent the following parts of the DS apparatus:

1. Frame
2. Actuator
3. Direct shear box
4. LVDT (Linear Variable Differential Transformer)
5. Load cel
6. Load arm
7. Top weight

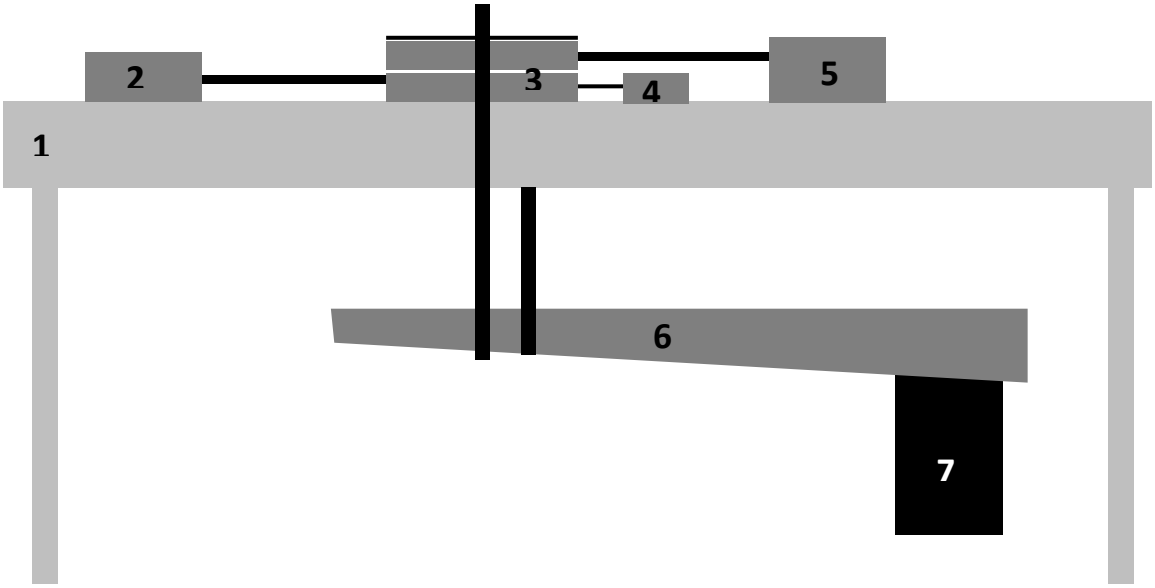

FIGURE 27: SCHEMATIC REPRESENTATION OF DS APPARATUS

The actuator (2) is the instrument pushing the bottom DS box at a constant speed. The LVDT (4) and load cell (5) respectively record the load needed to shear and the displacement occurring during shearing.

$$D_R = \frac{e_{max} - e}{e_{max} - e_{min}} * 100 \quad (28)$$

To assess the influence of the relative density on the softening behaviour, DS tests are performed at the relative densities (or void ratios) displayed in Table 7. Please refer to equation 28 for the formulation of D_R. To build up a sample with a homogeneous relative

density, a vibratory table is used in order to densify the sand matrix. After densification, D_R is back-calculated by weighting the DS box .

TABLE 7: RELATIVE DENSITIES AND VOID RATIOS

D_R [%]	e [-]
50	0.63
60	0.61
70	0.58
80	0.56
90	0.54
100	0.51

4.2. INFLUENCE RELATIVE DENSITY

The average confining pressure *p'* on the sample is first chosen at 64 kPa. Per relative density, three tests are performed. The influence of D_R on the softening behaviour is discussed in this section.

4.2.1. Peak and residual shear stress

Figure 28 displays the mobilised shear stress for each relative density. The relative density is positively correlated with the peak behaviour of the sand as shown by Bolton (1986). It should be noted that for each different relative density, one test is arbitrarily chosen to display in the figure. Other results can be found in Appendix C. Furthermore, it can be observed that the shear stress is globally mobilised to a residual value, $u_{residual}$, around 3.5 mm. The exception to this is D_R = 90% where $u_{residual} \approx$ 4.5mm.

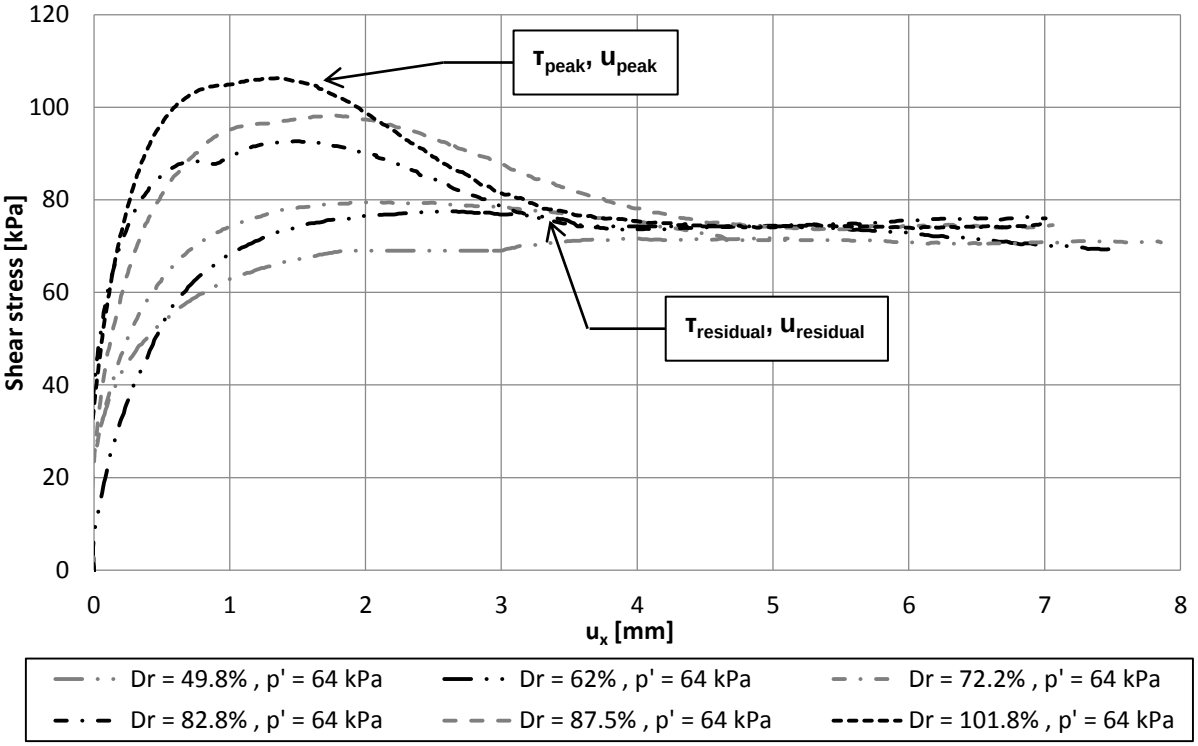

FIGURE 28: MOBILISED SHEAR STRESS DEVELOPMENT FOR DIFFERENT D_R WITH P'=64 KPA

Peak and residual shear stresses of all performed tests are plotted against D_R in Figure 29. The accuracy of the D_R is a few percent due to practical implications. This causes the small

spread. The overall picture shows a distinct trend upwards in the peak shear stress while the residual shear stress remains constant with increasing relative density.

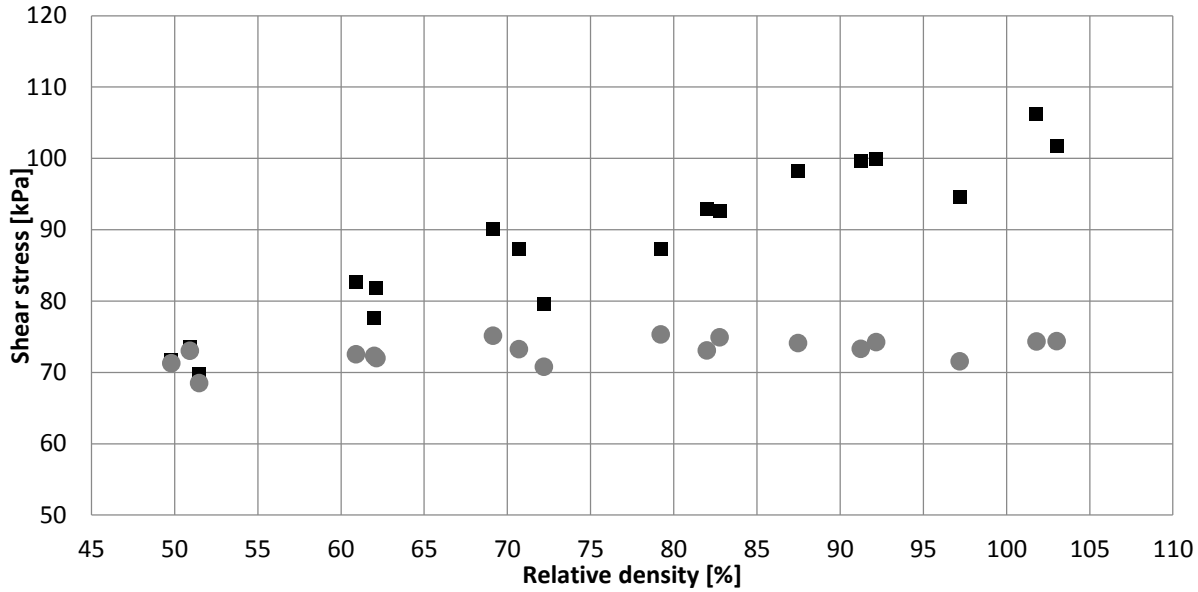

FIGURE 29: T_{PEAK} (=■) AND $T_{RESIDUAL}$(=●) WITH VARYING D_R, P' = 64 KPA

To quantify the softening behaviour, the ratio between τ_{peak} and $\tau_{residual}$, $f_{softening}$, is calculated. For the peak and residual value, the average of the three performed tests per density is used. With the average used, the heterogeneity of the tested sample is minimised.

Figure 30 shows the ratio between peak and residual shear stress. The squares represent the average ratio, the crosses all individual tests. The ratio shows a clear inverse correlation with respect to D_R as expected with respect to the dilatancy theory of Bolton (1986). The range of reduction from τ_{peak} to $\tau_{residual}$ ranges from approximately 0.7 for a very dense packing of the sand ($D_R \approx 100\%$) to 1 for a medium dense packing ($D_R \approx 50\%$). For $D_R < 50\%$, only compactive behaviour will occur thus no peak behaviour. This translates in a ratio of unity.

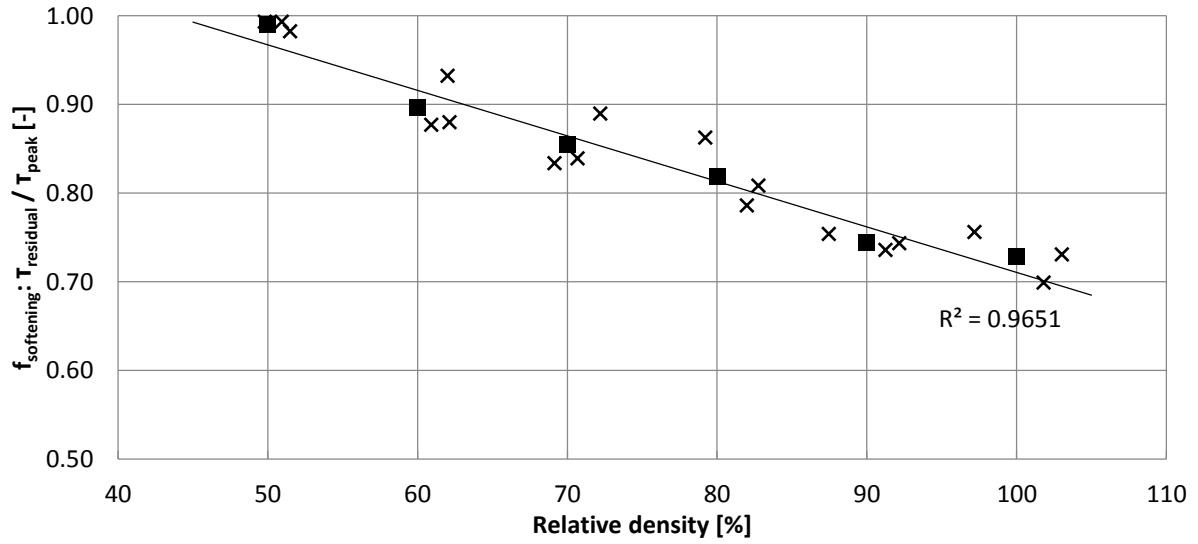

FIGURE 30: RATIO BETWEEN T_{PEAK} AND $T_{RESIDUAL}$, P'= 64 KPA

The average ratio with respect to D_R can be estimated accurately (R^2 = 0,965).

4.2.2. Softening mobilisation $\Delta u_{softening}$

Another important aspect of the softening behaviour is the mobilisation from peak to residual shear stress. From the DS tests, the displacement at which τ_{peak} mobilises (u_{peak}) to $\tau_{residual}$ is obtained. For the displacement where full mobilisation has occurred, $\tau_{residual}$ ($u_{residual}$), the same is done. Please refer to Figure 28, u_{peak} and $u_{residual}$ are indicated with arrows. The displacements u_{peak} and $u_{residual}$ are subtracted to get $\Delta u_{softening}$, which represents the displacement needed to mobilise from τ_{peak} to $\tau_{residual}$. This data is displayed in Figure 31, varying D_R for an average confining pressure of 64 kPa.

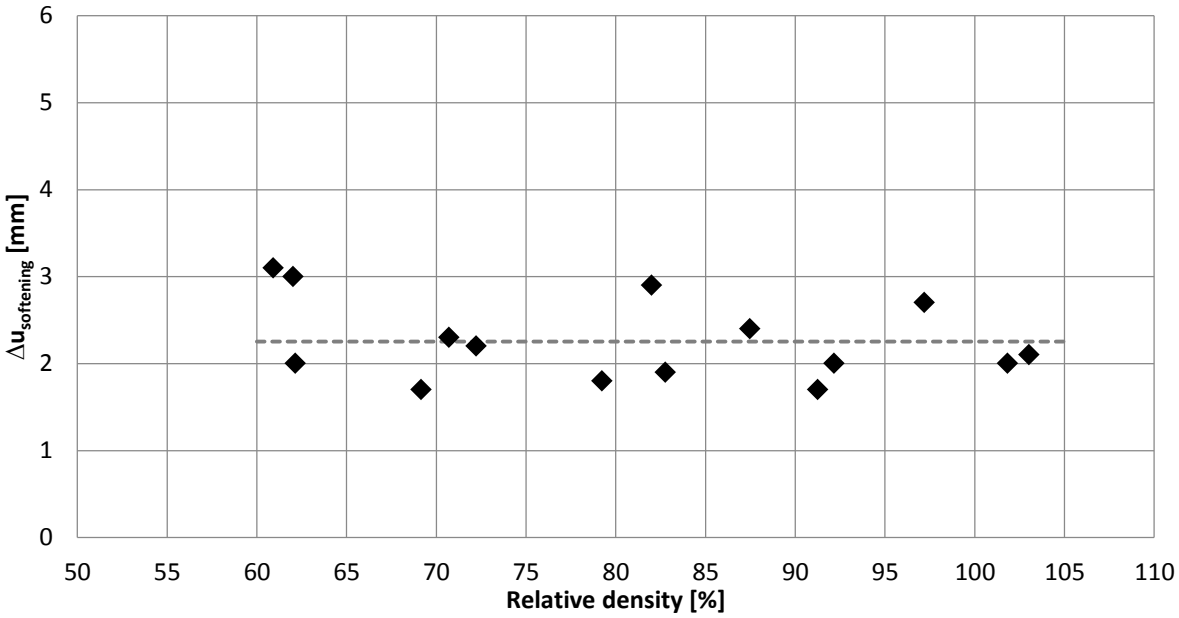

FIGURE 31: DISPLACEMENT FROM T_{PEAK} TO $T_{RESIDUAL}$ WITH P'=64 KPA

The average difference in displacement is equal to 2.3 mm and represented by the grey dashed line in Figure 31. A relatively small spread in the results can be observed. For this specific sand, with *p'* of 64 kPa , the displacements from τ_{peak} to $\tau_{residual}$ lie between 2 or 3 mm. Moreover, no trend in terms of D_R is observed. This can also be observed qualitatively from the shear stress mobilisation in Figure 28.

4.3. INFLUENCE CONFINING PRESSURE

Been and Jefferies (1985) showed the stress – strain behaviour of a granular soil is governed by the state of the soil. This means both the relative density and the average confining pressure are of influence. Therefore, the tests for the earlier mentioned D_R are also performed at higher top pressures. Again, the mobilisation of shear stresses to a residual value is investigated.

4.3.1. Peak and residual shear stress

Figure 32 shows the shear stress development for top pressure of approximately 500 kPa or *p'* = 306 kPa. Again, a peak behaviour is observed, thus softening does occur. The relative difference between τ_{peak} and $\tau_{residual}$ however appears to be smaller compared to the tests at a lower *p'*, shown in Figure 28 and 32.

No peak behaviour is observed with the D_R = 50% tests at 100 kPa top pressure, hence performing the tests at higher top pressures is redundant and not done.

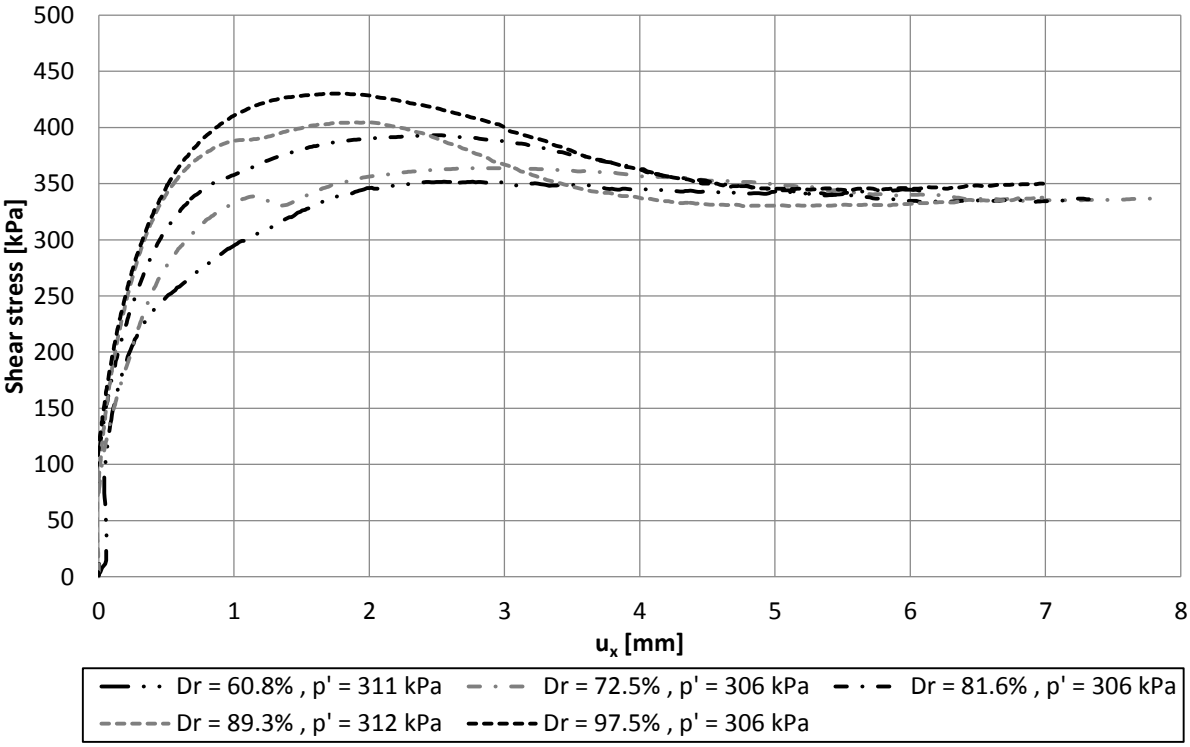

FIGURE 32: MOBILISED SHEAR STRESS DEVELOPMENT FOR DIFFERENT D_R WITH P'=306 KPA

When the shear stress is normalised to the top pressure and expressed in terms of peak friction angle, a distinct difference between the different top pressures is shown. Please refer to Table 8. The peak friction angles are dependent on dilatancy (Bolton, 1986) and are lower at a higher average confining pressure. This is the results of the suppression of the dilatant behaviour. This is in line with the theory on the state parameter, a sand with the same density has a higher state parameter and exhibits less dilatant behaviour (Been and Jefferies, 1985).

TABLE 8: PEAK FRICTION ANGLES FOR VARYING D_R AND P'

D_R [%]	φ_{peak} [°]	
	***p'* = 60 kPa**	***p'* = 300 kPa**
50	33.8	-
60	37.0	33.8
70	38.7	35.1
80	40.4	37.5
90	42.9	38.7
100	43.3	40.0

From the DS tests, the peak and residual shear stresses are obtained. With this data, the softening ratio is again determined. Please refer to Appendix C for all results. Fundamentally, the residual friction angle approximates the constant volume friction angle φ_{cv}. The constant volume friction angle is also pressure independent. Since a higher confining pressure suppresses dilatancy, a higher softening ratio should occur. Please refer to equation 7.

Figure 33 confirms this hypothesis. The ratios for the DS tests at a higher average confining, are higher. In other words, under higher confining pressures less softening behaviour occurs.

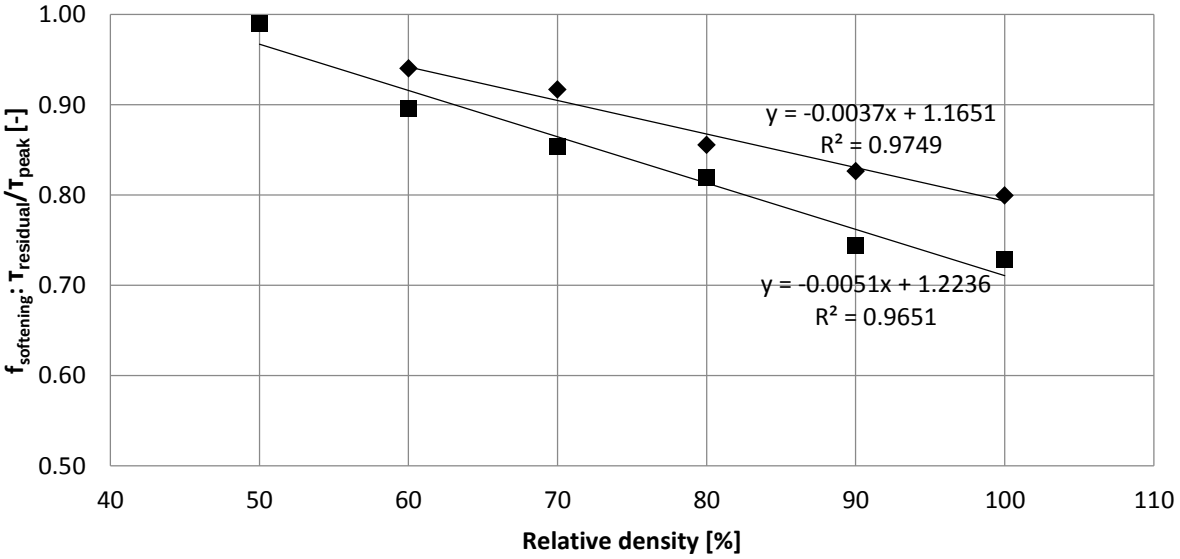

FIGURE 33: RATIO BETWEEN T_{PEAK} AND $T_{RESIDUAL}$ WITH P'=64 KPA (■) AND P'=306 KPA (♦)

4.3.2. Softening mobilisation $\Delta u_{softening}$

When the differences between u_{peak} and $u_{residual}$ are obtained at the higher average confining pressure, results are comparable to the earlier shown results. Please refer to Figure 34. The average displacement at a higher confining pressure hardly differs from that at a lower pressure. It can thus be concluded that the softening mobilisation displacement $\Delta u_{softening}$ is independent of average confining pressure within the practically occurring stress levels.

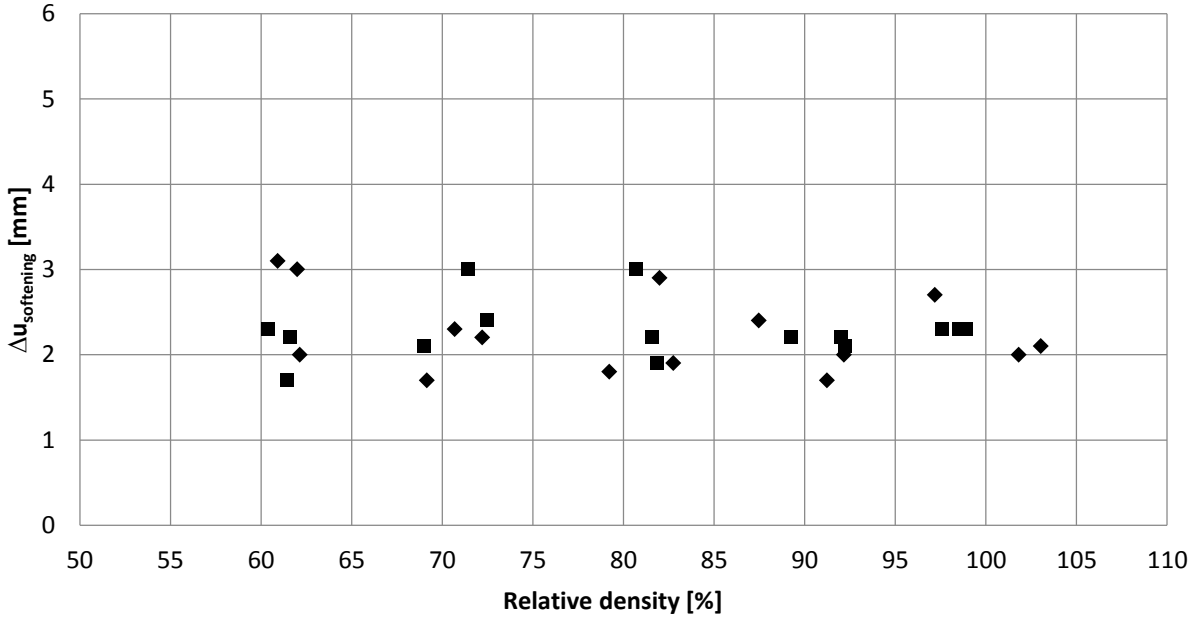

FIGURE 34: DISPLACEMENTS FROM T_{PEAK} TO $T_{RESIDUAL}$ WITH P' = 64 KPA (■) AND P' = 306 KPA (♦)

4.4. INFLUENCE SAND CHARACTERISTICS

The tested sand is from the Pleistocene age, more specific the Drente formation. There are however multiple sand formations from the Pleistocene age. Furthermore, micropiles are occasionally also founded on Holocene sand layers. Different formation or even geological age translates into differences of the origin of the material, manner of deposit and loading history. Combined these factors influence the sand grain characteristics, which in term have

an influence on the material behaviour of the sand. Though it is assumed the influence is only minor, they are discussed to be thorough.

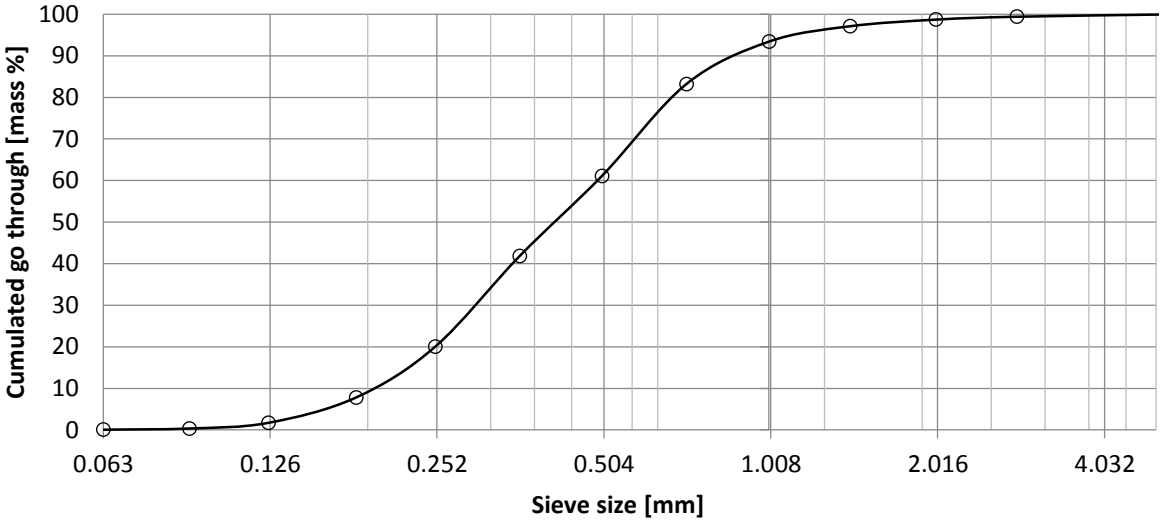

FIGURE 35: GRAIN SIZE DISTRIBUTION TESTED SOIL SAMPLE: FORMATION OF DRENTE

The volumetric characteristics are mainly influenced by:

- Gradation
- Grain shape

The sand used can be described as a well-graded, fine to coarse, sub-angular, quartz sand. Figure 35 shows the grain size distribution of the tested sand. The particle size gradually increases from very fine to coarse particle size, with a D_{50} of 0.411 mm and a uniformity index C_u of 2.49.

The sand particles are photographed under a microscope, displayed in Figure 36. The majority of the particles is transparent, indicating quartz minerals. Considering the roundness of the grains, a relatively large spread in grain shapes can be observed. In the microscopic image, grain characteristics vary between round, angular, spherical and eccentric. When using the chart given in Figure 5 (Cho et al., 2006), sphericity and roundness on average are respectively 0.9 and 0.5.

In case of this sand from the Drente formation, the coefficient of uniformity is relatively large, slightly decreasing the range of void ratios. The roundness is sub-angular, resulting in an average of minimum and maximum void ratio and the sphericity is high, causing a low minimum and maximum void ratio. Furthermore, the grains are sub-angular for this sand thus between round and angular, the residual strength, approximated by φ_{cv}, can thus be considered average (Cho et al., 2006).

How large the differences are for Dutch sands is not considered in this thesis. Since the influences are however limited, it is assumed that this sand is a relatively accurate representation of sandy soils encountered in engineering practice in the Netherlands.

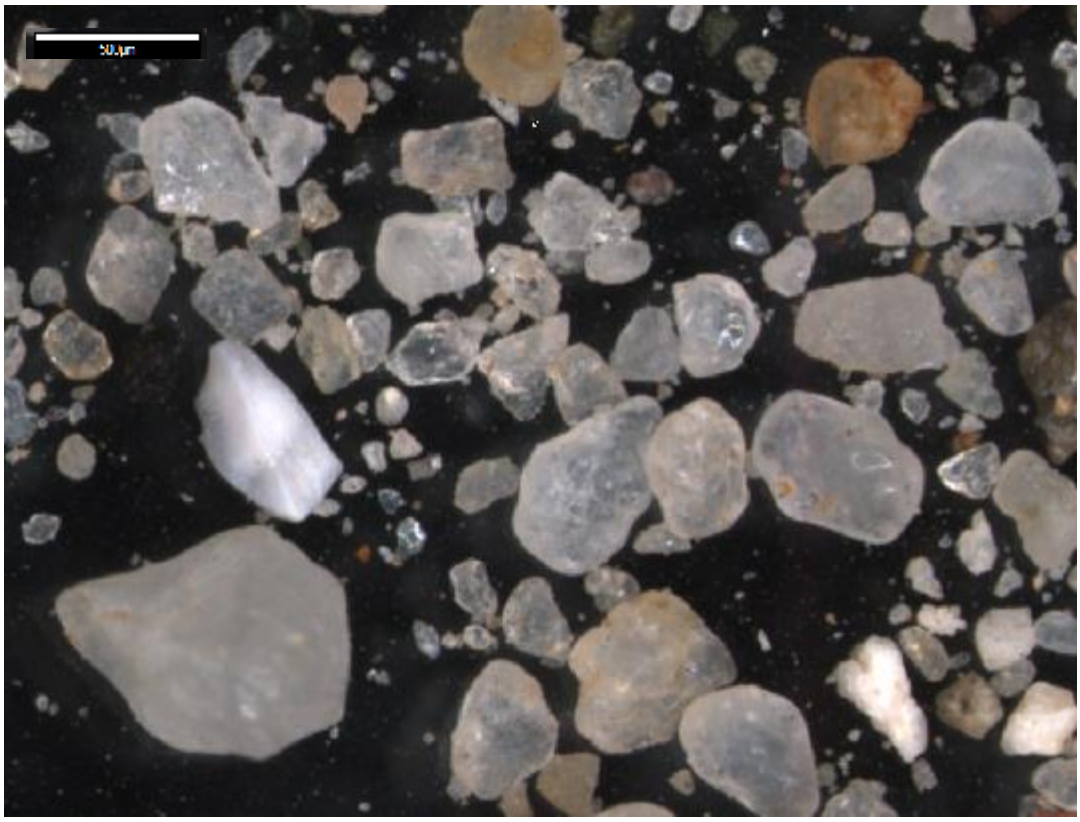

FIGURE 36: MICROSCOPIC PHOTOGRAPH OF THE SAND GRAINS (SCALE = 0.500 MM (TOP LEFT))

4.5. CONCLUSION

From the performed DS tests, multiple aspect concerning the softening can be concluded for this particular Dutch Pleistocene sand.

In contradiction to what is used in the CUR 236, the residual shear stress is not 50% of the peak value. Rather, this reduction is related to the volumetric behaviour occurring during shearing (Bolton, 1986). In agreement with this theory, the tests show a reduction from τ_{peak} to $\tau_{residual}$ dependent on relative density and average confining pressure (Been and Jefferies, 1985). Vice versa, the occurrence of peak behaviour in the mobilised shear stress depends on the relative density and average confining pressure. Plotting the ratio in terms of relative density, a well-fitting relationship can be found. This is shown in Figure 33.

Additionally, the mobilisation from peak towards the residual shear stress displays a relatively uniform image. All tests mobilise towards $\tau_{residual}$ between 2 and 3 mm with an average of 2.3 mm. Furthermore, the results exhibit only a small deviation from the average. No relationship with respect to relative density or pressure is found. Please refer to Figure 34.

For the tests, a well graded, sub-angular, fine to coarse grained sand is used from the formation of Drente. A more uniform grading will result in a smaller range of e and both roundness and sphericity are positively correlated with a lower e_{min} and e_{max}. The influence of these parameters is however limited. The angularity (or roundness) does influence the absolute value of the residual shear stress (Cho et al., 2006). Please refer to equation 3. This however, does not influence the difference between the peak and residual value (Bolton, 1986).

5. LARGE SCALE TESTING

Additionally, a part of this thesis was devoted to the large scale testing of softening behaviour. The testing method is explained and an attempt is made to interpret the softening behaviour with this testing method.

5.1. CURRENT TESTING PROCEDURE: CUR 236

The design guidelines considering micropiles, the CUR 236, is set up that a project require very conservative design values for the bearing capacity. Higher design values are only allowed in case of on-site testing. This is done on piles made with the same construction method and similar dimensions. To optimise the bearing capacity design, it is standard to perform on-site tests.

Testing the piles occurs with a test set-up shown in Figure 37. Please note that this is a schematic overview. In Appendix D, photographs of the actual used set-up can be found.

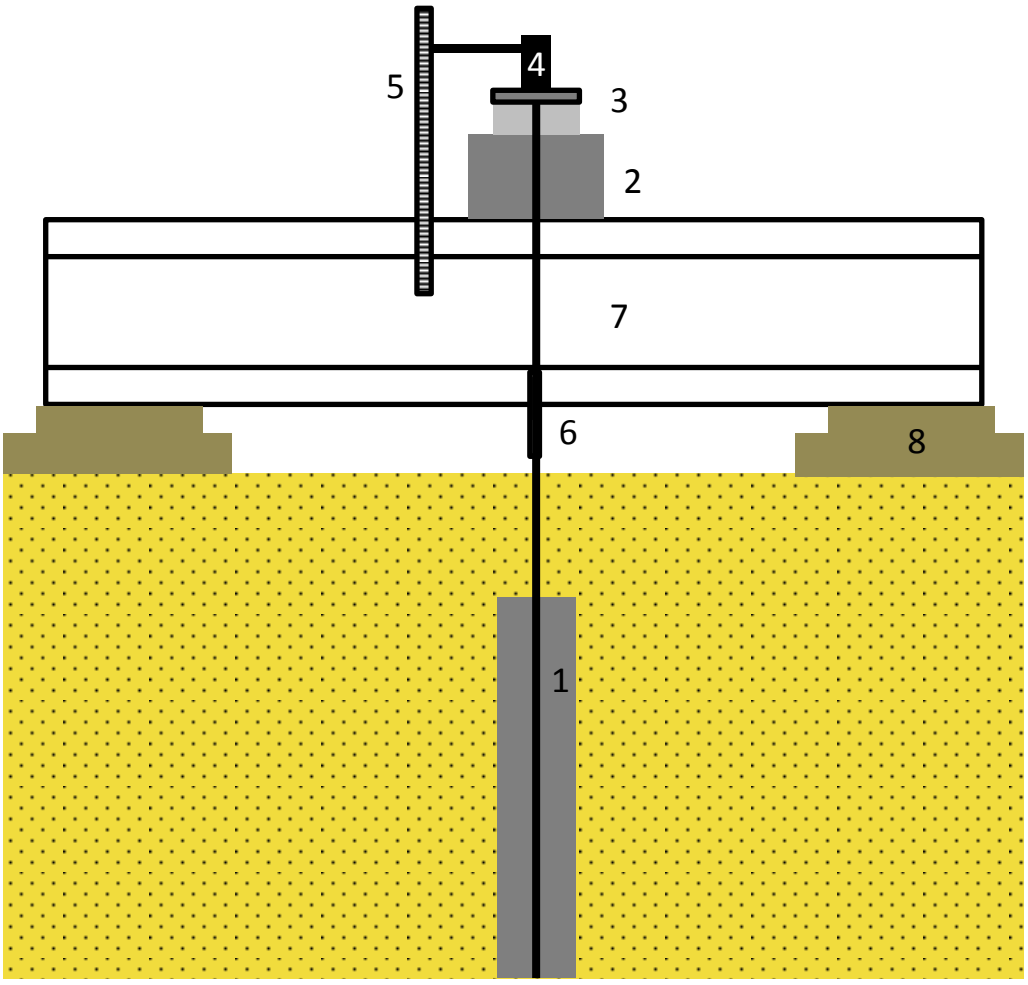

FIGURE 37: SCHEMATIC OVERVIEW PILE TESTING SET-UP

The numbers in Figure 37 depict the following parts of the set-up:

1. Micropile
2. Jack
3. Load cel

4. End bolt
5. Measurement rod
6. connector bolt: micropile – loading bar
7. Loading frame
8. Wooden plates

The jack is controlled hydraulically in accordance with the loading scheme given by the CUR236. Please refer to Figure 38. With steps of 15% and further 10% the load is increased. In between the load increments, the pile load is reduced to the arbitrary low value of approximately 10% expected bearing capacity F_p. Then, the load is increased again to a higher test load. This is all done stepwise. When the new (higher) test load is reached, the deformations are checked with the creep criterion k_s.

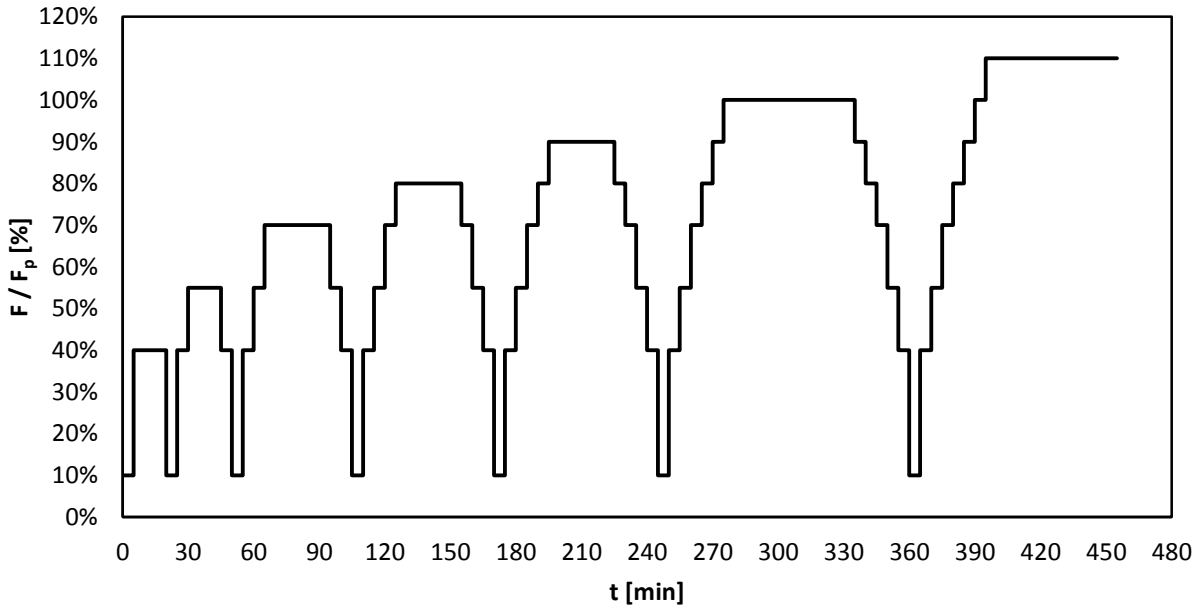

FIGURE 38: LOADING SCHEME FAILURE TEST (CUR 236, 2011)

The creep criterion originates from the DIN. The assumption is that in case of a constant load, sand will show very limited displacements occurring immediately at the instance of loading. When time dependent displacements do occur, it is assumed the maximum tensile capacity of the micropile is reached. Please refer to equation 29.

$$k_s = \frac{u_2 - u_1}{\log \frac{t_2}{t_1}} \leq 2\ mm \tag{29}$$

Geomechanical failure occurs when the maximum bearing capacity is reached. At this moment, the summation of all shear stresses around the micropile has reached its maximum, shown in equation 1. In case of a relatively short, stiff micropile, the shear stresses along the pile approximate τ_{peak}.

5.2. LARGE DEFORMATION TESTING

The ratio of dimensions of the piles tested often differ from the production piles. It is customary to use short piles for pile testing due to economical and practical reasons. The same reinforcement steel is used as in the production piles. Since the bearing capacity of the test micropile however is lower, it will behave more stiff. The combination of both the shorter length and higher stiffness with respect to the bearing capacity will drastically decrease the effect of differential strain in the sand around the micropile thus the softening behaviour.

In the case of an infinitely stiff pile, its ultimate bearing capacity $R_{t,failure\ test}$ is independent of the pile stiffness. The displacements are in this case constant over the micropile thus is the shear stress along the shaft. Because of the large area of reinforcement steel and short length, the assumption is made that the test piles are 'infinitely stiff'. It can be argued that the peak shear stress is reached along the entire pile. This does however also mean that if the pile loaded beyond $R_{t,failure\ test}$ at a certain displacement, it will mobilise the sand from τ_{peak}, if present, to $\tau_{residual}$. With a residual bearing capacity $R_{t,residual}$. The softening factor $f_{softening}$ can now be approximated with the following equation 30.

$$f_{softening} \approx \frac{R_{t,residual}}{R_{t,failure\ test}} \tag{30}$$

This is the basis for the performed large scale tests executed for this thesis.

5.2.1. Testing procedure

Due to limited time for the testing within the project, 30 minutes per pile, making uses of the creep criterion is unfortunately impossible. Another possibility is to let the jack and sum of shear stress along the micropile find equilibrium. This procedure is chosen.

Before this procedure, the micropile first needs to be displaced until the all sand is mobilised to $\tau_{residual}$. Therefore, a force marginally higher than the bearing capacity is put onto the micropile. After 'sufficient' displacement, the hydraulic circuit is closed and the current volume under a certain pressure in the jack will find equilibrium with the shear stresses along the pile. This happens as a results of continuous increase of the size of the pressure chamber in the jack. The increase of the pressure chamber in the jack, lowers the pressure thus resulting in a lower load on the micropile. Equilibrium will be found when the extension of the jack results in a decrease of load on the pile equal to the resisting force by the soil.

The 'sufficient' displacement is roughly based on the current design guideline. To be certain the entire micropile has displaced enough to mobilise all sand around the shaft into the $\tau_{residual}$, the pile is displaced two times $u_{peak,CUR236}$. This value is chosen arbitrarily at twice the displacement needed since the sections after peak mobilisation in the code can be considered doubtful. In case the tip of the micropile still has not mobilised any shear stresses at failure, this displacement is considered adequate. Smaller displacements could suffice, but since the actual shear stress development along the micropile is not measured, a conservative estimate is assumed best.

When the pile is displaced up to the desired displacement, the circuit is closed and the displacement and load decrease is monitored. The total procedure can be summarised by the following steps:

1. Micropile fails in accordance with CUR 236 test procedure
2. Increase pressure in jack slightly for continuous displacement pile 'after failure'
3. Displace pile up to $u_{failure} + 2*u_{peak,CUR236}$
4. Close the hydraulic circuit of jack
5. Measuring forces on pile and displacements pile head

In total eight piles, high frequency vibrated (type E), are tested. Half of the piles are pressurised (pile 1 – 4), other half is constructed under hydrostatic pressure (pile 5 – 8).

The piles are approximately 13 m long, with pile head GL – 12 m and pile tip at GL – 25 m. The diameter of the piles is 200 mm.

5.2.2. Results

When the procedure from the previous section is followed, the jack forces are displayed in Figure 39. All measured results from this test can be found in Appendix 4. Unfortunately, only one pile could be tested. This is a result of structural failure of the other piles, making it impossible to further assess the geomechanical behaviour.

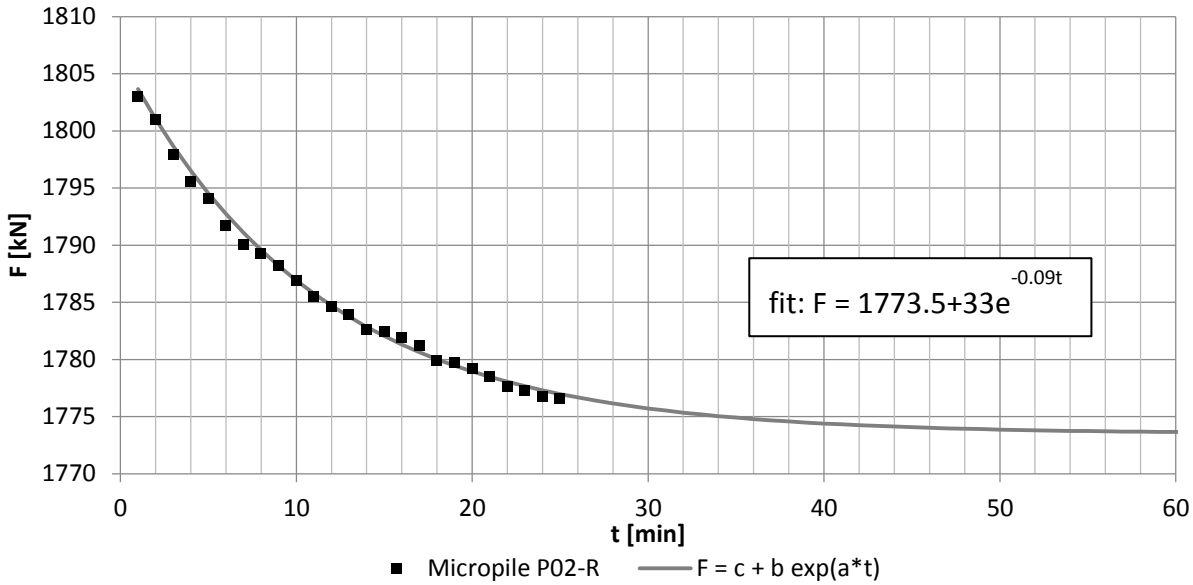

FIGURE 39: FORCE IN JACK (■) DURING SOFTENING TEST PILE 2 WITH EXPONENTIAL FIT (▬)

Figure 39 displays the measured force of the jack on the micropile during the 'softening test'. The fit is made with an exponential function of the form given in equation 31.

$$F = c + a * e^{-b*t} \tag{31}$$

The function consists out of 3 factors that can be varied to fit the theoretical decrease. Factor *c* determines the final value, in other words $R_{t,residual}$, factor *a* determines the increase from *c* at t=0 and factor *b* determines the rate of decrease. Combined, a unique combination of the three factors will results into a fit, finding $R_{t,residual}$ (= *c*). For pile 7, factor *c* is equal to 1773.5 kN. The total bearing capacity of this pile, resulting from the failure tests, is equal to 1760 kN Please refer to Appendix D. This results into a softening factor $f_{softening} = \frac{R_{t,residual}}{R_{t,failure\ test}} = \frac{1773.5}{1760} \approx 1$. The slightly higher value of $R_{t,residual}$ is caused by measuring inaccuracies within the current testing method.

A decrease or increase of the displacements is not observed. This is most likely the result of an increasing displacement of the micropile in combination with decreasing axial stresses.

5.2.3. Conclusion

The number of succeeded tests is unfortunately too limited to base hard conclusions concerning the softening behaviour. On the used method, some preliminary conclusions can be made.

It is practically feasible to continuously displace the micropile after geomechanical failure. When carefully steering the jack, this procedure can be performed in a controlled manner. Closing the hydraulic circuit, the upward force put on the micropile shows a continuous decrease over time. With an exponential function, the data can be fitted. With the fit of the

measured tensile loads on the micropile, the factor *c* can be found, approximating the residual strength of the micropile $R_{t,residual}$. Please refer to equation 31.

This whole procedure, finally resulting in $R_{t,residual}$ contributes to a better understanding of the residual shear stress with respect to the peak shear stress. The entire procedure used can easily be integrated into the current framework of failure tests, providing a simple, practically based method of approximating the residual shear stress.

6. IMPLEMENTATION INTO DESIGN CODE & RECOMMENDATIONS

First, the shortcomings of the implementation of softening implementation into the current design guideline are discussed. An alternative subdivision is proposed, differentiating between the effect of different micropile types on D_R and p'.

An attempt is made to implement aforementioned results concerning strain softening into the current design guidelines. The emphasis will be on the SLS design though the ULS design is also discussed.

6.1. SHORTCOMINGS CURRENT DESIGN GUIDELINE

As stipulated in the research questions and further elaborated in the literature study, the current design guideline CUR 236 addendum is mainly based on arbitrary 'best guesses' when concerning the strain softening behaviour.

The softening model in the CUR 236 addendum is displayed in Figure 3. Section 3 and 4 of this model show the bilinear development modelling the strain softening. Section 3 represents the mobilisation from τ_{peak} to $\tau_{residual}$ in a displacement of 1 mm. This is followed by section 4, with a constant $\tau_{residual}$ of 0.5*τ_{peak}.

Theory however describes a more complex behaviour based on relative density and average confining pressure characterised with the state parameter (Been and Jefferies, 1985). This parameter describes a compactive or dilative behaviour based on the void ratio relative to a reference state, the CSL, in stress – density space. The lower the void ratio of a sand is, the more dilative behaviour it contemplates. Dilative behaviour in its part is the volumetric behaviour causing an increase in the mobilised shear stress (Bolton, 1986). This governs the peak behaviour hence the strain softening.

A simple reduction without a dependency on relative density or pressures, is a too crude approximation. Moreover, the reduction to 50% of τ_{peak} does not have any fundamental basis.

Furthermore, the softening behaviour does not only have an influence to the SLS behaviour. Due to the length effect (Ostermayer and Scheele, 1977), the ULS capacity is also influenced by the softening behaviour. This is translated into a reduction factor for the length effect, f_3.

6.2. SUBDIVISION BASED ON INSTALLATION EFFECT

The installation method influences the bearing capacity of the micropile and thus the state of the sand. A theoretical approach is chosen to elaborate on the effect of the construction of the pile on the softening behaviour. An attempt is made to qualitatively discuss the different aspects of micropile construction have on the effect on D_R and p' of the surrounding sand. Subsequently, an estimation of the magnitude of softening behaviour can be made. The different aspects of micropile construction are divided based on pile type, in accordance with CUR 236, and pressurisation of the grout body.

The subdivision in bearing capacity due to packing of the sand or a higher interface pressure is the basis for this chapter. In earlier research, Juran et al. (1999), Reese and O'neill (1988), Lehane (1992) separated both variables. With a firm qualitative basis made in this chapter, a

good judgement can be made concerning the influence of the installation method on the softening behaviour.

Based on the installation method both D_R and σ'_h can differ (Juran et al., 1999). With available literature, all micropile types in the CUR236 can be subdivided into four categories. This is shown in Figure 40.

The first division is made based on pile installation. Research on the shaft bearing capacity of bored or auger piles assumes a coefficient of horizontal effective stress, close to the neutral case K_0 (Reese and O'neill (1988), Juran et al. (1999)). In case of pressurisation, the horizontal effective stress can be mobilised up to K_p. This does however depend on the construction of the micropiles. From failure tests, the actual capacity and thus K can be estimated. For further elaboration of this, please refer to section 6.3.1.

In case of the type E, the installation effects can have a considerable influence on the soil bearing capacity. In some cases, the high frequency vibratory installation significantly negatively influences the cone resistance around the piles taken after construction (personal communication P. Langhorst, BAM, 25-8-2017). A combination of D_R and σ'_h however determines both the bearing capacity and the cone resistance. This makes the results ambiguous and unclear what parameter is influenced. The only certainty is that σ'_h increases after pressurisation. How much is again uncertain.

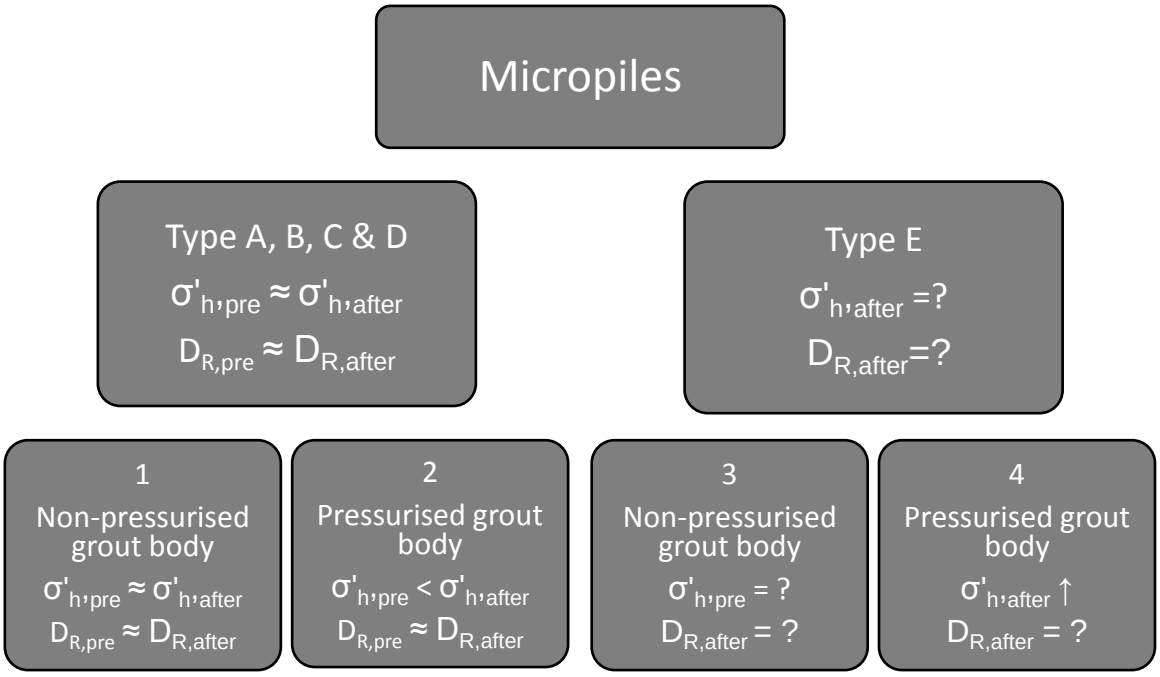

FIGURE 40: SUBDIVISION MICROPILE TYPES BASED ON SIG'$_H$ AND D_R

6.3. IMPLEMENTATION AND RECOMMENDATIONS CURRENT DESIGN GUIDELINE

As stipulated in the section 6.1, the dependency of the strain softening on D_R and p' are currently not taken into account. With the DS tests performed, the stress and density dependency of the softening behaviour is approximated. If in design practice an accurate assessment of the present stress state and density can be made, the strain softening behaviour taken into account more accurately in the future.

6.3.1. SLS

A better implementation of the softening behaviour would be a significant improvement of the current CUR 236 addendum model. Failure tests assess the bearing capacity of the micropile, taking into account the installation effects. These results are currently extrapolated to the production piles through α_t. For D_R and p', this should also be done to gain a better understanding of the softening behaviour. Furthermore, the piles should be discretised in elements representative for the present soil profile based on D_R and p'.

Improved design approach

The adapted implementation based on the findings of this thesis can be summarised by the following procedure.

1. Perform CPT
2. Discretise soil profile into small elements
3. Determine D_R from CPT for all discretisations with formula Lunne
4. Perform failure test
5. Approximate $K_{average}$ from test failure test
6. Determine p' for all discretisations
7. Determine $f_{softening}$ for all discretisations based on Figure 33

The installation method undeniably influences the tensile bearing capacity of the micropiles. This influence is separated into two different influences: micropile installation and grout pressurisation. As discussed in section 6.2 and displayed in Figure 40.

In the design guideline, it is accustomed to base τ_{peak} on failure tests on short, large scale micropiles. The residual strength then is calculated relative to the peak value. This is reversed with respect to what is commonplace in literature (Bolton, 1986). Equation 32 describes the reduction.

$$\tau_{residual} = f_{softening}(D_R, p') * \tau_{peak} \quad (32)$$

This reduction depends relative density and average confining pressure. To gain a better understanding of the softening behaviour occurring, it is of paramount importance to correctly estimate these parameters.

In the current design methodology, the bearing capacity is based on the cone resistance present near a micropile. Multiple empirical relationships are available to link the cone resistance to the relative density and is thus advised to use to determine D_R. The NEN 9997-1 prescribes the empirical correlation of Lunne (1983) and is thus also for this case recommended.

For *p'* only a rough estimation can be made within the current testing framework. Since the influence is less significant, this is still useful. The stresses are considered axissymetric. The average confining pressure is now given by equation 33.

$$p' = \frac{\sigma'_a + 2 * \sigma'_r}{3} \tag{33}$$

In this case, the axial effective stress is equal to the vertical effective stress: $\sigma'_a = \sigma'_v$. This can be calculated from borehole data or deduced from CPT data. The radial effective stress is equal to the horizontal effective stress: $\sigma'_r = \sigma'_h$. This results into equation 34.

$$p' = \frac{\sigma'_v + 2 * \sigma'_h}{3} \tag{34}$$

The horizontal effective stress is largely influenced by the installation method. In case of pressurisation of the grout, the horizontal pressure cannot be approximated by $\sigma'_v * K_0$. The coefficient of horizontal pressure K will, depending on the level of pressurisation, increase towards K_p. To be able to assess the increase in σ'_h, the formulation proposed by Juran et al. (1999) is used. From the failure tests performed, $R_{t,failure\ test}$ is measured. This means the global tensile bearing capacity of the micropile is known. Adopting the formulation by Juran et al. (1999) slightly to base the circumference $O_{p,average}$ on the CUR236, the average horizontal effective pressure can be calculated. Please refer to equation 35. The horizontal effective stress level is limited by the vertical effective stress level (Rankine, 1857). It can thus be argued that an average coefficient of horizontal effect stress is more appropriate. This is given in equation 36.

$$\sigma'_{h,average} = \frac{R_{t,failure\ test}}{O_{p,average} \tan \varphi_{average}} \tag{35}$$

$$K_{average} = \frac{\sigma'_{h,average}}{\sigma'_{v,average}} \tag{36}$$

Short testing piles should be used to substantiate the use of an average friction angle $\varphi_{average}$.

With the average coefficient of horizontal pressure and the vertical effective stress known, the average confining pressure can be estimated with equation 37.

$$p' = \sigma'_v \frac{1 + 2 * K_{average}}{3} \tag{37}$$

Adaptation CUR 236 addendum model: $\tau_{residual}$

With a good estimation of the relative density and average confining pressure, an expression for the softening factor $f_{softening}$ can be given. Please refer to Figure 33. The residual shear stress in Figure 41, denoted by section 4, is a combination of the linear relationship found in Figure 33 and equation 32. As an example $f_{softening}$ is chosen for $p' = 64$ kPa. The figure futher shows the current CUR model significantly overestimating the softening reduction.

In contrary to the current model, $\tau_{residual}$ is dependent on the relative density and average confining pressure in the improved model. The difference in residual shear stress is denoted by the different dashes in Figure 41. In case the average confining pressure is closer to 306 kPa, this $f_{softening}$ relationship should be used. The effect on the softening ratio is however small.

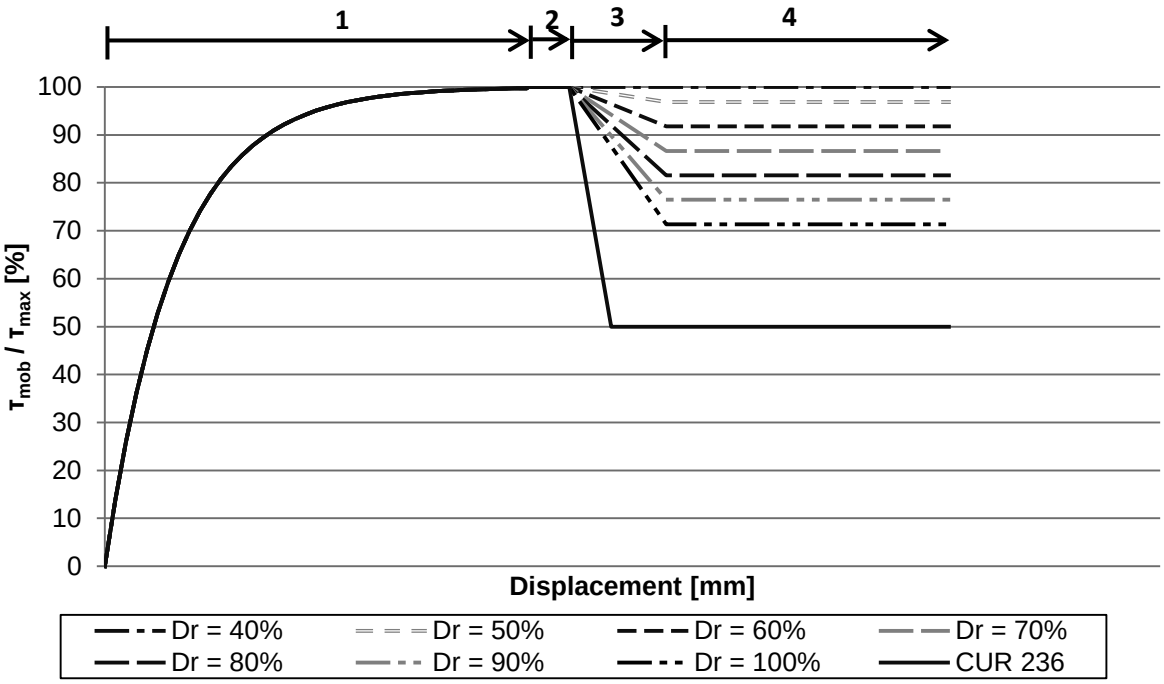

FIGURE 41: PROPOSED ADAPTATION CURRENT CUR236 ADDENDUM MODEL

Adaptation CUR 236 addendum model: $\Delta u_{softening}$

For the softening mobilisation, the linear development from the CUR 236 addendum model, in Figure 41 this is denoted as section 3, is used. The residual shear stress $\tau_{residual}$ and the displacement necessary to mobilise towards $\tau_{residual}$, $\Delta u_{softening}$ are different. Equation 38 presents the proposed shear stress development based on $f_{softening}$.

$$\tau_{mob} = \tau_{peak} * \left(1 + \frac{(f_{softening} - 1)(u - u_{peak})}{\Delta u_{softening}}\right) \quad (38)$$

The displacement towards $\tau_{residual}$, $\Delta u_{softening}$ is chosen at 2.3 mm This is in line with the average of the DS test results. Results of $\Delta u_{softening}$ lie between 2 mm and 3 mm. Please refer to Figure 34.

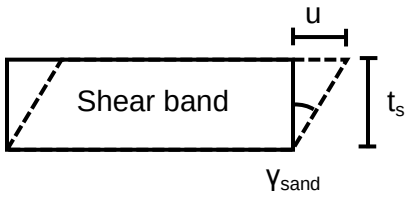

FIGURE 42: SHEAR STRAIN DEVELOPMENT IN SHEAR BAND

A direct link with the large scale pile can be made through equation 39. The shear stress mobilisation is in the current design guideline dependent on the displacement while the behaviour of the soil is actually governed by shear strains, γ_{sand}. However, the shear stress development can be expressed in terms of displacements. In this case, the shear band thickness t_s is assumed to be constant. Based on literature, it is a valid to assume a shear band occurs around the peak shear stress. Please refer to Figure 42 for a graphical representation.

$$\gamma_{sand} = \frac{u}{t_s} \tag{39}$$

As further shown in DeJong et al. (2003) and Tehrani et al. (2016), the thickness of the shear band in the DS test and a tested model pile have a similar size, order of magnitude 3 to 8 times D_{50} . This substantiates the assumption that the displacement to mobilise from τ_{peak} to $\tau_{residual}$ can be approximated by the DS test results.

6.3.2. ULS

For the ultimate limit state capacity design, the softening behaviour of the micropile is included in the f_3 factor. This factor is used to account for the length effect. This length effect. is the result of differential deformations along the length of the micropile. The ULS capacity of the micropile is influenced by this phenomenon.

The f_3 reduction is based on calculations performed with the CUR 236 addendum model. These calculations are essentially done by varying the length of the micropile and the stiffness of the micropile. For different a length and stiffness of the micropile, a different bearing capacity is found. The ratio between the bearing capacity of a 4.0 m long reference pile, and longer piles, is the f_3 factor.

In the previous paragraph, it is recommended to expand the CUR 236 addendum model with respect to the softening behaviour. Since this model is also used for the f_3 factor in the ULS calculations, also the length effect reduction factor should be based on the extent of reduction towards the residual shear stress. Next to micropile length and stiffness, the f_3 factor should also be based on the relative density of the present soil. Moreover, the minor influence of the average confining pressure could be taken into account.

The f_3 factor is based on a that the soil body that is considered homogeneous. When long piles are constructed or heterogeneous soil conditions occur, this is a very limited assumption. In these cases, a more advanced calculation based on the SLS model in combination with the present soil conditions is advised.

Since the SLS model is input for the ULS calculations, the similar uncertainty concerning the type E micropiles is present.

6.4. RECOMMENDATION IN SITU TESTING METHODS

From the testing of the micropiles, a lot of tests were unfortunately unusable. Hard conclusions on the geomechanical behaviour cannot be made from the tests. Some recommendations are made with respect to the implementation of the testing methodology. This could be a valuable improvement to the current testing framework. The in situ softening behaviour can be tested with a test pile, extending the current testing framework of CUR 236.

The proposed testing method is based on the fact that sufficient displacement, ensures enough strain to mobilise all sand along the micropile into the residual shear stress. Furthermore, it uses the pressure – volume relationship within the hydraulic pressure chamber of the jack to make equilibrium with this residual shear stress. The recommended testing procedure is:

1. Micropile fails in accordance with CUR 236 test procedure
2. Increase pressure in jack slightly for continuous displacement pile ‘after failure’
3. Displace pile up to $u_{failure} + 2*u_{peak,CUR236}$
4. Close the hydraulic circuit of jack

5. Measuring forces on pile and displacements pile head

During slow decay of the pressure in the jack, forces on the micropile converge towards the equilibrium i.e. the total residual strength of the micropile. In this research, per test, 25 minutes were available to monitor the force on the micropile. To find the total residual strength of the micropile, the force decay is fitted with an exponential function. Please refer to equation 40.

$$F = c + a * e^{-b*t} \tag{40}$$

The constant *c* represents $R_{t,residual}$. Since the maximum capacity $R_{t,failure\ test}$ is also tested in the failure test, preceding this test, the softening factor can be approximated with equation 41.

$$f_{softening} \approx \frac{R_{t,residual}}{R_{t.failure\ test}} \tag{41}$$

An important condition for this approach to work is a high stiffness the testing pile. The high stiffness can be obtained with the use of a large diameter reinforcing steel. Also, a small length is recommended, preferably the minimal 5.0 m prescribed by CUR 236. This minimises the influence of the length effect on the tensile bearing capacity (Ostermayer and Scheele, 1978).

6.5. FUTURE RESEARCH

For future research, the main recommendation is extensive testing of shear stress mobilisation and horizontal effective stresses along actual micropiles. This ensures the effects of the installation effects on the softening behaviour are correctly taken into account. The influence of the installation effects is in this thesis approached from a theoretical point of view. Undeniably, the influence of pressurisation on horizontal effective pressure of the adjacent sand should be confirmed. Also, the assumption of the negligible influence of the pressurisation on the relative density should be validated. In part, this influences $f_{softening}$. Furthermore, the displacements from peak to residual shear stress $\Delta u_{softening}$ should be confirmed, validating the assumption that the shear band formation next to the large scale pile is similar to that in the DS test.

The number of succeeded large scale pile 'softening tests' were very limited. Though the softening testing procedure behave in accordance with expectations, the unexpected pile failures did limit the number of tests analysed. More tests should be performed to verify the outcomes of the testing procedure are useful in a quantitative manner.

Micropile type E installation effects diffusely causes significant reduction of cone resistance adjacent to piles. Whether the often occurring reduction is a result of a decrease in D_R or σ'_h is unknown. This does however mean correctly estimating the softening behaviour is impossible. Future research should be done to have a more profound understanding of the influence of this pile type.

Probably, the upper limit of the average confining pressure is not reached in this thesis. To gain better insight into the softening behaviour at higher pressures, this should be performed.

The influence of the sand grain characteristics on the softening behaviour, though proved small based on literature, should be validated.

7. CONCLUSION

With the addendum on the CUR 236, the axial stiffness of micropiles is extended from a single spring to a discretisation of soil elements. Each soil element has a peak and residual mobilised shear stress and combined, the stiffness of the micropile can be calculated. The residual value, which is a new aspect in the mobilised shear stress of the discretised elements, is however chosen arbitrarily on 50% of the peak shear stress. This gave rise to the following research question:

How does strain softening manifest for micropiles under tensile loading?

This main research question is subdivided into multiple research questions. For the softening behaviour, this MSc. thesis differentiates between residual shear stress and shear stress mobilisation (from τ_{peak} to $\tau_{residual}$). To gain a better understanding lab tests, large scale physical tests are performed as well as numerical modelling.

7.1. CONCLUSIONS SUB QUESTIONS

What variables influence strain softening behaviour?

Strain softening is the decrease of peak shear stress to residual shear stress. The peak is, in contrary to how it is framed in the CUR 236, varying and not the residual shear stress. Bolton (1986) showed the shear stress mobilisation is volumetrically controlled. A densely packed sand dilates during shearing, creating a peak value in the mobilised shear stress. A loosely packed sand however compacts. Been and Jefferies (1985) further linked this to the state parameter Ψ. This related the state a sand is in, with a certain void ratio at a certain average confining pressure, to a reference state, the critical state line. The lower a void ratio in void ratio – stress space with respect to the critical state line, the more dilative behaviour can be observed. Vice versa applies for contractive behaviour. This concept covers the main variables influencing the softening behaviour namely: the density of a sand and the present average confining pressure. Moreover, these characteristics can vary with different sand grain characteristics (Cho et al., 2006).

Considering the deformations, the post peak mobilisation of the shear stress and thus the softening behaviour is concentrated within a shear band (Newland and Allely, 1957). This shear band will form in the critical zone where the highest shear stress is present. In this thesis, this is assumed to be in the pile – sand interface.

Does the installation method influence the strain softening behaviour?

The main influence of the installation method on the micropiles originates from two aspects:

- Pile construction: bored casing, self-boring, screwed or vibratory casing
- Pressurisation: additional pressure on grout after installation

For the influence on the strain softening, the differentiation should be made between the effect on D_R and on p'. Concerning the pile construction, influence is assumed to be small or negligible for type A, B, C and D. For type E however, a clear reduction in shear strength of the sand can be observed (personal communication P. Langhorst, BAM, 25-8-2017). The cause of this reduction is however uncertain. Further research should give more clarity about this mechanism. The pressurisation on the other hand has a clear influence on the horizontal effective pressure thus on p' (Juran et al., 1999).

How can this strain softening behaviour be modelled for the soil-structure interaction of the micropile-soil interface?

Modelling of the strain softening behaviour is tried with a finite element program, more specific Plaxis. This would lead to a coupled stress strain model most advantageous for modelling the installation effects as well as the strain softening behaviour. The only constitutive model able to simulate the critical state behaviour of sand, is the hypoplastic model. Though the element size and numerical control parameters are varied within all possible limits, the results are continuously not in accordance with physical behaviour and show large inaccuracies at relatively high strains. This is the result of a combination of the high non-linearity of the model (peak behaviour of stress – strain relationship), the non-local implementation of the softening behaviour and the relatively large strains in tensile loading.

In a further attempt to model the strain softening behaviour, the current CUR 236 addendum model is used a basis. The assumption of the bilinear progression is preserved, the course is however adapted to approximate the actual stress – strain mobilisation. This stress – strain relationship is obtained from DS tests on sand, modelling an individual discretisation.

How do the soil variables/parameters influence this strain softening mobilisation?

The strain softening mobilisation denotes the required displacement for the development from τ_{peak} to $\tau_{residual}$, named $\Delta u_{softening}$. Figure 43 displays these displacements from the DS tests.

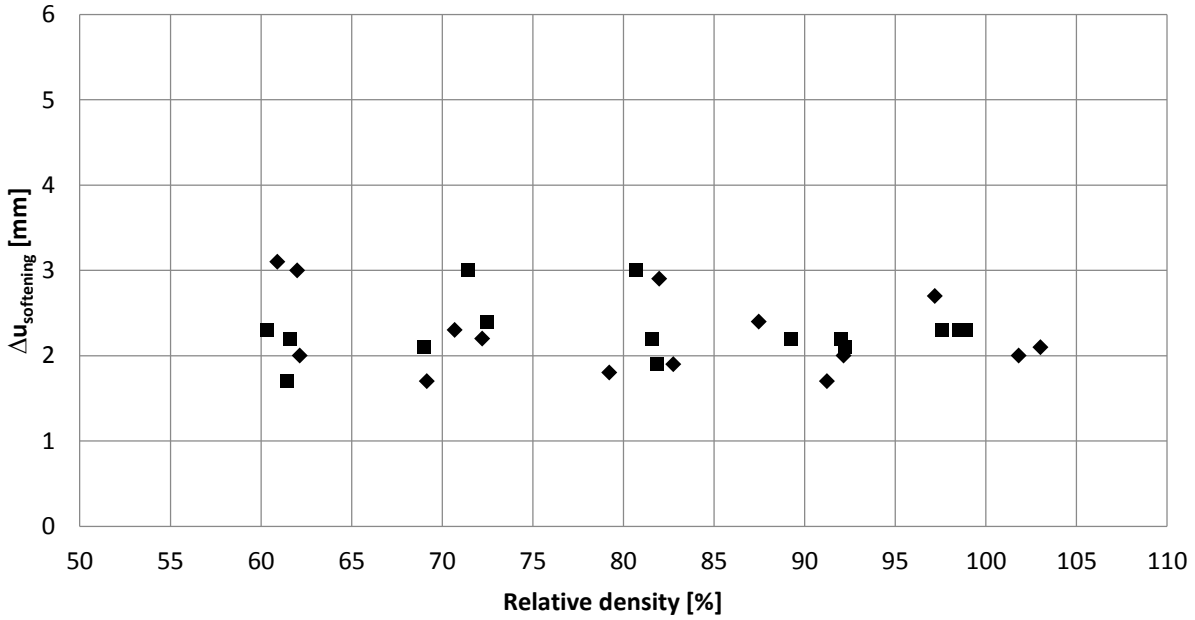

FIGURE 43: DISPLACEMENTS FROM T_{PEAK} TO $T_{RESIDUAL}$ WITH P' = 64 KPA (■) AND P' = 306 KPA (♦)

It can be observed that no correlation is present between D_R or p' and the occurred displacement. Practically all results lay within a narrow band between 2 and 3 mm displacements. The average displacement found needed for the mobilisation is 2.3 mm. It should be noted that these results are obtained from a DS test with sand in both boxes. In literature, it is however found that the shear band size in a DS test is comparable to a model pile (Tehrani et al., 2016) (DeJong et al., 2003). The displacements are thus a relatively good approximation of the large scale situation.

How do the soil variables/parameters influence the residual shear strength?

For all DS tests, the ratio between τ_{peak} and $\tau_{residual}$ i.e. $f_{softening}$, is calculated. The relative densities are arbitrarily chosen at 50%, 60%, 70%, 80%, 90% and 100%. The top pressure is arbitrarily chosen at approximately 100 kPa and 500 kPa, or a *p'* of 64 kPa and 306 kPa The average of the ratios of three tests performed per D_R and *p'* is taken, to account for heterogeneity of the built up sample. This gives a relationship between $f_{softening}$ and D_R for multiple *p'* as shown in Figure 44.

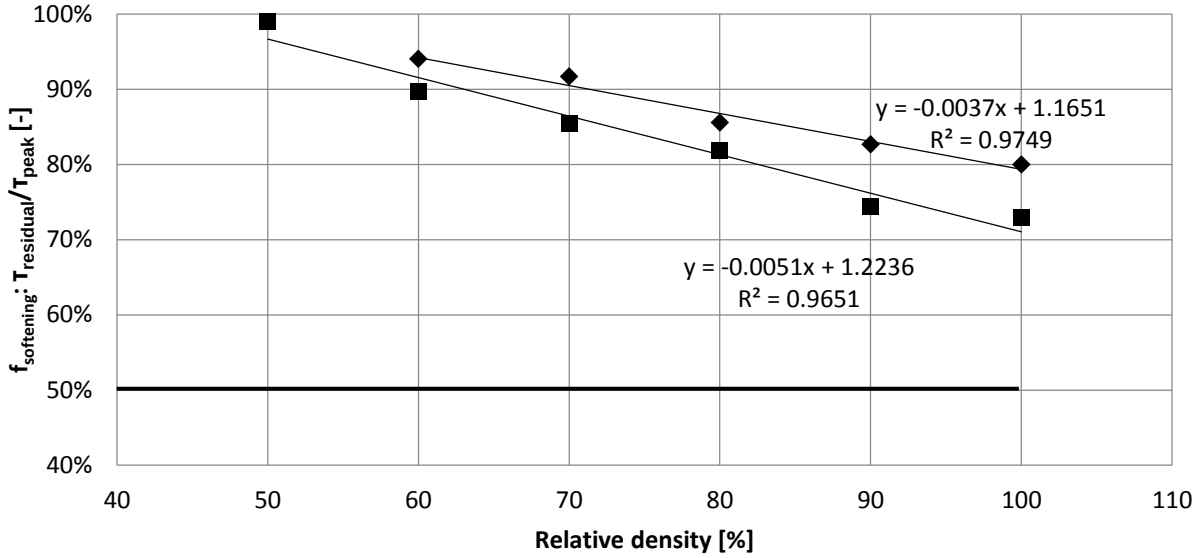

FIGURE 44: RATIO BETWEEN T_{PEAK} AND $T_{RESIDUAL}$ WITH WITH P' = 64 KPA (■) AND P' = 306 KPA (♦)

A clear difference with the CUR 236 addendum approach is shown (constant black line at 50%). With decreasing D_R, the ratio between peak and residual shear stress increases. This is in accordance with theory. Furthermore, the relationship between $f_{softening}$ and D_R can be accurately approximated with a linear trend line. Moreover, a higher average confining pressure suppresses dilatancy, increasing $f_{softening}$. Also for higher *p'*, a linear relationship approximates $f_{softening}$ accurately.

How can the strain softening (model) be assessed with tests on the micropiles?

In this thesis, the choice is made to assess the strain softening occurring at a micropile within the already existing testing framework of CUR 236. With this approach, the shear stress reduction can be assessed very efficient and the influence of local heterogeneity does not blur the measured results. The used approach makes use of the fact that a continuous large displacement of the micropile will lead to a mobilisation towards the residual shear stress along the entire micropile. The assumption is made that this is definitely the case with a head displacement is chosen at arbitrarily very large at $u_{failure}$+2*$u_{peak,CUR236}$. The force needed for continuous displacement is marginally higher than the 'residual' tensile bearing capacity of the micropile. When the displacement is reached, the hydraulic circuit is closed and the jack will autonomously find equilibrium with the residual bearing capacity of the micropile. The ratio between $R_{t,residual}$ and $R_{t,failure\ test}$ approximates $f_{softening}$ in case of a short pile.

Does the strain softening model results match the physical data?

Due to a large number of unexpected failures in the test piles, a too limited set of data is present to link the DS test results to the large scale pile tests.

8. LIMITATIONS OF RESEARCH

Numerous assumptions and simplification are used in this MSc. thesis. To be thorough, these are therefore mentioned or discussed in short in this chapter.

An important simplification is the use of the DS test, representing a small sand body, adjacent to the micropile. In this case, the interface is assumed rough, i.e. to be equally strong as the sand (Uesugi and Kishida, 1986). Additionally, the boundary effects caused by the rigid DS box are neglected. The choice to base the research on DS tests, is for the modelling of the shaft friction mobilisation on a small scale, the best choice. This does however not mean that the stress state is entirely accurate. In case of pressurised micropiles, the stress state is approximated well. Please refer to equation 42 and 43. For non-pressurised micropiles, the stress state in the minor principle stress direction differs significantly. Please refer to equation 44.

$$\sigma'_{h,pile,pressurised} \approx K * \sigma'_v \approx 2 \; to \; 4 * \sigma'_v \tag{42}$$

$$\sigma'_{h,pile,non-pressurised} \approx K_0 * \sigma'_v \approx 0.3 \; to \; 0.4 * \sigma'_v \tag{43}$$

$$\sigma'_{h,DS\,test} \approx \frac{\sigma'_y}{K_0} \approx 2 \; to \; 3 * \sigma'_v \tag{44}$$

Furthermore, the sand used for the DS tests is a sub-angular, well graded quartz sand from the Pleistocene age. Though this is by far the most common layer to found piles on in the Netherlands, the results of a specific formation, the formation of Drente, are extrapolated to a general case. Different geological history and grain characteristics can marginally influence the stress – strain behaviour of the sand (Cho et al., 2006). Last, the effective stress increase as a result of the volumetric changes are taken into account in the DS test (Lehane et al., 1993)

The pile construction is another simplification used in the recommendation for the implementation of the softening behaviour. In case of micropile type A, B, C and D, the assumption is made that the pile installation does not influence the stress state around the micropile. The influence of the pressurisation of the grout on the D_R is neglected. Micropile type E, can have a large influence on the surrounding soil. The influence of this installation method shows a diffuse image. Due to very limited research until this moment, the actual influence of the installation method is unfortunately unknown.

Another limitation is the approximation of the state the sand has. Numerous empirical correlations are present for the relation between q_c and D_R. However, the accuracy of these correlations is limited. Further densification caused by the pressurisation is assumed negligible.

The average confining pressure can only be roughly estimated. A reasonably accurate estimation of σ'_v can be made. For σ'_h, the maximum accuracy is the average along the micropile, based on failure tests. The influence of p' is limited thus the effect is most likely insignificant.

The geological history of the sand is also not taken into account in the recommendation. Possible overconsolidation can result into a different stress state than expected, though not

taking an extra horizontal effective pressure into account can only lead to a conservative estimate of the softening behaviour.

9. BIBLIOGRAPHY

Anaraki, K., Delft Univeristy of Technology, MSc. Thesis, *Hypoplasticity Investigated Parameter Determination and Numerical Simulation*, June 2008, Delft

Anthony, Jennifer L., and Marone, C., *Influence of particle characteristics on granular friction*, Journal of Geophysical Research: Solid Earth 110.B8, 2005, Wiley Online Library

Barley, A., Bruce, D., Bruce, M., Lang, J., Aschenbroich, H., *High capacity and fully removable soil anchors,* 27th Annual Conference on Deep Foundations, 2003

Bauer, E., *Calibration of a comprehensive hypoplastic model for granular material,* Soils and Foundations 36.1, Japanese Geotechnical Society, 1996, p. 13-26

Been, K., Jefferies, M.G., *A state parameter for sands,* 1985, Géotechnique No. 2, p. 99-112

Bolton, M. D, *The strength and dilatancy of sands*, Géotechnique 36.1, 1986, 65-78

Boulon, M., Foray, P., *Physical and numerical simulation of lateral shaft friction along offshore piles in sand,* Proceedings of the 3rd International Conference on Numerical methods in Offshore piling, Nantes, France, 1986, p. 127-147.

Brinkgreve, R., Delft University of Technology, Lecture notes Behaviour of Soils and Rocks CIE4361 *Hypoplasticity*, January 2015, Delft

Brinkgreve, R., Delft University of Technology, *Geomaterial Models and Numerical Analysis of Softening*, PhD. thesis, May 1994, Delft, p. 104

Casagrande, A., *The shearing resistance of soils and its relation to the stability of earth dams*, Proceedings of the Soils and Foundation Conference of the US Engineer Department, 1938

Consoli, N., Casagrande, M., Coop, M., *Effect of fiber reinforcement on the isotropic compression behavior of a sand*, Journal of geotechnical and geoenvironmental engineering, 2005, 131.11: 1434-1436

Cho, G., Dodds, J., Santamarina, J. Carlos, *Particle shape effects on packing density, stiffness, and strength: natural and crushed sands*, Journal of geotechnical and geoenvironmental engineering, 2006, 132.5: 591-602

DeJong, J.T., Randolph, M.F., White, D.J., *Interface load transfer degradation during cyclic loading: a microscale investigation*, Soils and Foundations 43.4, Japanese Geotechnical Society, August 2003, 81-93

DeJong, J.T., White, D.J., Randolph, M.F., *Microscale observation and modelling of soil-structure interface behaviour using particle image velocimetry*, Soil and Foundations 46.1, Japanese Geotechnical Society, Febuary 2006, 15-28

Fioravante, V., *On the shaft friction modelling of non-displacement piles in sand*, Soils and Foundations 42.2, Japansese Geotechnical society, April 2002, 23-33

Gudehus, G., *A comprehensive constitutive equation for granular materials*, Soils and foundations 36.1, 1996, p. 1-12

Gudehus, G., Amorosi, A., Gens, A., Herle, I., Kolymbas, D., Maˇs´ın, D., Muir Wood, D., Nova, R., Niemunis, A., Pastor, M., Tamagnini, C., and Viggiani, G.. *The soilmodels.info project*, International Journal for Numerical and Analytical Methods in Geomechanics, 32(12):1571-1572, 2008

Gudehus, G., Herle, I., *Determination of parameters of a hypoplastic constitutive model,* Mechanics of Cohesive-Frictional Materials 4, 1999, p. 461-486

Horn, H. M., Deere, D. U., *Frictional characteristics of minerals*, Geotechnique, 1962, 12.4: 319-335

Jaky, J., *The coefficient of earth pressure at rest*, Journal of the Society of Hungarian Architects and Engineers, 1944, 78.22: 355-358

Jardine, R. J., Lehane, B. M., and Everton, S. J., *Friction coefficients for piles in sands and silts*, Offshore site investigation and foundation behaviour, Springer Netherlands, 1993, 661-677.

Juran, I., et al., *Micropiles: the state of practice. Part II: design of single micropiles and groups and networks of micropiles*, Proceedings of the Institution of Civil Engineers-Ground Improvement, 1999, 3.3: 89-110

Kolymbas D. *A generalized hypoplastic constitutive law*, Proceed. 11th Int. Conf. Soil Mech. Found. Eng.,1985, San Francisco, p. 2626

Lade, P. Vestergaard, *The stress-strain and strength characteristics of cohesionless soils*, University of California, Berkeley, 1972

Lehane, B., *Experimental investigations of pile behaviour using instrumented field piles*, PhD thesis, Imperial College London, University of London, 1992

Lehane, B., Jardine, R.J., Bond, A.J., Frank, R., *Mechanisms of shaft friction in sand from instrumented pile tests*, Journal of Geotechnical Engineering 119.1, 1993, p.19-35

Lunne, T., Christoffersen. H.P., *Interpretation of cone penetrometer data for offshore sands*, Offshore Technology Conference, Offshore Technology Conference, 1983, p. 181 – 188

Lupea, C., Delft University of Technology, MSc. Thesis, *Long Term Effects of Cyclic Loading on Suction Caisson Foundations,* August 2013, Delft

Mayne, P.W., Kulhawy, F.H., K_0 - *OCR Relationships in Soil*, Journal of the Soil Mechanics and Foundations Division 108.6, 1982, p. 851-872.

Mühlhaus, H.B., Vardoulakis, I., *The thickness of shear bands in granular materials,* Géotechnique 37.3, 1987, p. 271-283

Nematt-Nasser, S., Okada, N., *Radiographic and microscopic observation of shear bands in granular materials,* Géotechnique 51.9, 2001, p. 753 – 765

NEN 9997-1:2016 nl, *Geotechnisch ontwerp van constructies – Deel 1: Algemene regels*,2016

Newland, P., Allely, B., *Volume changes in drained triaxial tests on granular material,* Geotechnique 7, 1957, p. 17-34

Oda, M., Kazama, H., *Microstructure of shear bands and its relation to the mechanisms of dilatancy and failure of dense granular soils,* Géotechnique 48.4, 1998, p. 465-481

Ostermayer, H., Scheele, F., *Research on ground anchors in non-cohesive soils*, Proceedings of the 9th International Conference on Soil Mechanics and Foundation Engineering. Vol. 97. Tokyo: The Japanese Society of Soil Mechanics and Foundation Engineering, 1977

Rankine, W., *On the stability of loose earth*, Philosophical Transactions of the Royal Society of Londen, Vol 147, 1857

Reese, L.C., O'Neill, M.W., *Drilled shafts: Construction procedures and design methods*, Pub. No. FHWA-HI-88-042, U.S. Dept. of Transportation, Washington D.C., 564-565

Röchter L., König, D., Schanz, T., Triantafyllidis, T., *Shear band and strain softening in plane strain extension: physical modelling*, Granular Matter 12, 2010, p. 287-301

Stichting SBRCURnet, *SBRCUR-rapport 236 Ankerpalen*, november 2011, Gouda

Stichting SBRCURnet, *Addendum bij SBRCUR-rapport 236 Ankerpalen – Axiale veerstijfheid*, maart 2016, Delft

Tabucanon, J.T., Airey, D.W. and Poulos, H.G., *Pile skin friction in sands from constant normal stiffness tests*, Geotechnical Testing Journal (GTJODJ) 18.3, September 1995, p. 350-364

Tatsuoka, F., Nakamura, S., Huang, C.-C., Tani, K., *Strength anisotropy and shear band direction in plane strain tests of sand,* Japanese Society of Soil Mechanics and Foundation Engineering, march 1990, Vol. 30 no. 1, p. 35-54

Tehrani, F.S., Han, F., Salgado, R., Prezzi, M., Tovar, R.D., Castro, A.G., *Effect of roughness on the shaft resistance of non-displacement piles embedded in sand,* Géotechnique 66.5, 2016, 386-400, http://dx.doi.org/10.1680/jgeot.15.P.007

Uesugi, M., Kishida, H., *Influential factors of friction between steel and dry sands*, Soils and foundations 26.2, 1986, 33-46.

Uesugi, M., Kishida, H., Tsubakihara, Y., *Behavior of sand particles in sand-steel friction,* Soils and foundations 28.1, March 1988, 107-118

Verruijt, A., Broere, W., *Grondmechanica*, TU Delft, 2011

Von Wolffersdorff, P-A., *A hypoplastic relation for granular materials with a predefined limit state surface*, Mechanics of Cohesive-frictional Materials 1.3, 1996, p. 251-271

Wu, W. and Bauer, E., Proc. of the Int. Workshop on Modern Approaches to Plasticity, *A Hypoplastic model for barotropy and pyknotropy of granular soils,* 1993, Elsevier

Yoshida, T., *Strain localization and shear banding during failure of sands,* University of Tokyo, PhD thesis

Youd, T.L., *Factors controlling maximum and minimum densities of sands*, ASTM Spec. Tech. Public., 523, 1973, 98-112

LIST OF FIGURES APPENDICES

FIGURE A-1: SAMPLE DRENTE FORMATION (B320 – M13), CLOSE TOGETHER 69
FIGURE A-2: SAMPLE DRENTE FORMATION (B320 – 13), GRAINS SEPARATED 69
FIGURE A-3: SAMPLE STERKSEL FORMATION (B320 – M13), CLOSE TOGETHER 70
FIGURE A-4: SAMPLE STERKSEL FORMATION (B320 – M13), GRAINS SEPARATED.....70
FIGURE A-5: ROUNDNESS AND SPHERICITY OF TESTED SANDS, IN ACCORDANCE WITH CHO ET AL. (2006).....71
FIGURE A-6: ANGLE OF REPOSE MEASUREMENT 72
FIGURE A-7: GRAPHICAL REPRESENTATION ANGLE OF REPOSE.....72
FIGURE A-8: ANGLE OF REPOSE MEASUREMENT OF HEIGHT 73
FIGURE A-9: FILLED TESTING MOLD JAPANESE STANDARD TEST 74
FIGURE A-10: TESTING EQUIPMENT MINIMUM AND MAXIMUM VOID RATIO JAPANESE STANDARD ...74
FIGURE A-11: E_{MIN} (♦) AND E_{MAX} (■) OF DRENTE FORMATION SAND, AVERAGE AS DASHED LINE 75
FIGURE A-12: E_{MIN} (♦) AND E_{MAX} (■) OF STERKSEL FORMATION SAND, AVERAGE AS DASHED LINE...75
FIGURE A-13: OEDOMETER SET-UP.....76
FIGURE A-14: CLOSE UP INSTALLED OEDOMETER MOULD 77
FIGURE A-15: OEDOMETER TESTS ON DRENTE FORMATION SAND FOR DENSE (E_0=0.47), MEDIUM DENSE (E_0=0.58) AND LOOSE (E=0.7) PACKING 77
FIGURE A-16: OEDOMETER TESTS ON STERKSEL FORMATION SAND FOR DENSE (E_0=0.47), MEDIUM DENSE (E_0=0.58) AND LOOSE (E=0.7) PACKING 78
FIGURE A-17: OEDOMETRIC RESPONSE DRENTE IN ACCORDANCE WITH HERLE AND GUDEHUS (1999) AND FIT.....78
FIGURE A-18: OEDOMETRIC RESPONSE STERKSEL IN ACCORDANCE WITH HERLE AND GUDEHUS (1999) AND FIT.....79
FIGURE A-19: OEDOMETRIC RESPONSE SAMPLE DRENTE , E = 0.47 80
FIGURE A-20: OEDOMETRIC RESPONSE SAMPLE DRENTE, E=0.58 80
FIGURE A-21: OEDOMETRIC RESPONSE SAMPLE DRENTE, E=0.71 81
FIGURE A-22: OEDOMETRIC RESPONSE SAMPLE STERKSEL, E=0.45 81
FIGURE A-23: OEDOMETRIC RESPONSE SAMPLE STERKSEL, E=0.57 82
FIGURE A-24: OEDOMETRIC RESPONSE SAMPLE STERKSEL, E=0.72 82
FIGURE A-25: PHOTOGRAPH DIRECT SHEAR APPARATUS, SIDE VIEW 84
FIGURE A-26: PHOTOGRAPH DIRECT SHEAR APPARATUS, TOP VIEW 84
FIGURE A-27: TOP CAP TILTING DURING LOADING.....85
FIGURE A-28: SHEAR STRESS, SAMPLE DRENTE: D_R=80%, Σ_{YY} =100, 200 & 300 KPA.....86
FIGURE A-29: DISPLACEMENTS, SAMPLE DRENTE: D_R=80%, Σ_{YY} =100, 200 & 300 KPA.....86
FIGURE A-30: SHEAR STRESS, SAMPLE DRENTE: D_R=90%, Σ_{YY} =100, 200 & 300 KPA.....87
FIGURE A-31: DISPLACEMENTS, SAMPLE DRENTE: D_R=90%, Σ_{YY} =100, 200 & 300 KPA.....87
FIGURE A-32: SHEAR STRESS, SAMPLE STERKSEL: D_R=80%, Σ_{YY} =100, 200 & 300 KPA.....88
FIGURE A-33: DISPLACEMENTS, SAMPLE STERKSEL: D_R=80%, Σ_{YY} =100, 200 & 300 KPA.....88
FIGURE A-34: SHEAR STRESS, SAMPLE STERKSEL: D_R=90%, Σ_{YY} =100, 200 & 300 KPA.....89
FIGURE A-35: DISPLACEMENTS, SAMPLE STERKSEL: D_R=90%, Σ_{YY} =100, 200 & 300 KPA.....89
FIGURE A-36: COMPARISON STF – DS TEST: DRENTE D_R=80%, Σ_{YY}=100 KPA 90
FIGURE A-37: COMPARISON STF – DS TEST: DRENTE, D_R=80%, Σ_{YY}=200 KPA 91
FIGURE A-38: COMPARISON STF – DS TEST: DRENTE, D_R=80%, Σ_{YY}=300 KPA 91
FIGURE A-39: COMPARISON STF – DS TEST: DRENTE, D_R=90%, Σ_{YY}=100 KPA 92
FIGURE A-40: COMPARISON STF – DS TEST: DRENTE, D_R=90%, Σ_{YY}=200 KPA 92
FIGURE A-41: COMPARISON STF – DS TEST: DRENTE, D_R=90%, Σ_{YY}=300 KPA 93
FIGURE A-42: COMPARISON STF – DS TEST: STERKSEL, D_R=80%, Σ_{YY}=100 KPA 93
FIGURE A-43: COMPARISON STF – DS TEST: STERKSEL, D_R=80%, Σ_{YY}=200 KPA 94

FIGURE A-44: COMPARISON STF – DS TEST: STERKSEL, D_R=80%, Σ_{YY}=300 KPA 94
FIGURE A-45: COMPARISON STF – DS TEST: STERKSEL, D_R=90%, Σ_{YY}=100 KPA 95
FIGURE A-46: COMPARISON STF – DS TEST: STERKSEL, D_R=90%, Σ_{YY}=200 KPA 95
FIGURE A-47: COMPARISON STF – DS TEST: STERKSEL, D_R=90%, Σ_{YY}=300 KPA 96
FIGURE B-1: PRINCIPAL STRESS DIRECTIONS: PRESSURISATION 500 KPA 97
FIGURE B-2: PRINCIPAL STRESS DIRECTIONS: 10% F_P 98
FIGURE B-3: PRINCIPAL STRESS DIRECTIONS: 40% F_P 98
FIGURE B-4: PRINCIPAL STRESS DIRECTIONS: 70% F_P 99
FIGURE B-5: PRINCIPAL STRESS DIRECTIONS: 90% F_P 99
FIGURE B-6: PRINCIPAL STRESS DIRECTIONS: 120% F_P 100
FIGURE B-7: MOBILISED SHEAR STRESS: 10% F_P 101
FIGURE B-8: MOBILISED SHEAR STRESS: 40% F_P 101
FIGURE B-9: MOBILISED SHEAR STRESS: 70% F_P 102
FIGURE B-10: MOBILISED SHEAR STRESS: 90% F_P 102
FIGURE B-11: MOBILISED SHEAR STRESS: 120% F_P 103
FIGURE B-12: INACCURACIES MOBILISED SHEAR STRESS, MODEL WITH INTERFACE (NOT ACTIVATED), 120% F_P 104
FIGURE B-13: INACCURACIES MOBILISED SHEAR STRESS, MODEL WITH INTERFACE (ACTIVATED), 120% F_P 105
FIGURE B-14: INACCURACIES MOBILISED SHEAR STRESS, REDUCED STIFFNESS MICROPILE, 40% F_P 106
FIGURE C-1: MOBILISED SHEAR STRESS D_R≈50%, P'=64KPA 107
FIGURE C-2: MOBILISED SHEAR STRESS D_R≈60%, P'=64 KPA 107
FIGURE C-3: : MOBILISED SHEAR STRESS D_R≈70%, P'=64 KPA 108
FIGURE C-4: MOBILISED SHEAR STRESS D_R≈80%, P'=64 KPA 108
FIGURE C-5: MOBILISED SHEAR STRESS D_R≈90%, P'=64 KPA 109
FIGURE C-6: MOBILISED SHEAR STRESS D_R≈100%, P'=64 KPA 109
FIGURE C-7: MOBILISED SHEAR STRESS D_R≈60%, P'=306 KPA 110
FIGURE C-8: MOBILISED SHEAR STRESS D_R≈70%, P'=306 KPA 110
FIGURE C-9: MOBILISED SHEAR STRESS D_R≈80%, P'=306 KPA 111
FIGURE C-10: MOBILISED SHEAR STRESS D_R≈90%, P'=306 KPA 111
FIGURE C-11: MOBILISED SHEAR STRESS D_R≈100%, P'=306 KPA 112
FIGURE C-12: T_{PEAK} (=■) AND $T_{RESIDUAL}$ (=●) WITH VARYING D_R, P'= 306 KPA 113
FIGURE C-13 RATIO BETWEEN T_{PEAK} AND $T_{RESIDUAL}$, P'=107 KPA (AVERAGE=■, TEST=X) & P'=306 KPA (AVERAGE=♦, TEST=+) 113
FIGURE C-14: DISPLACEMENT TO T_{PEAK} (□) AND $T_{RESIDUAL}$(○) AND THE DIFFERENCE OF BOTH, DU (♦) AT P'=306 KPA 114
FIGURE C-15: DISPLACEMENT TO T_{PEAK} (□) AND $T_{RESIDUAL}$(○) AND THE DIFFERENCE OF BOTH, DU (♦) AT P'=306 KPA 114
FIGURE D-1: LARGE SCALE TEST SET-UP, FRONT VIEW 115
FIGURE D-2: LARGE SCALE SET-UP, SIDE VIEW 116
FIGURE D-3: FAILURE TEST ON PILE 2 IN ACCORDANCE WITH CUR236 117
FIGURE D-4: CREEP CRITERION DURING FAILURE TEST PILE 2 118

LIST OF TABLES APPENDICES

TABLE A-1: TESTS RESULTS ANGLE OF REPOSE 73
TABLE A-2: E_{MIN}, E_{MAX} AND E_I OF DRENTE FORMATION SAND 75
TABLE A-3: E_{MIN}, E_{MAX} AND E_I OF STERKSEL FORMATION SAND 75
TABLE A-4: LOADING SCHEME OEDOMETER TESTS 76
TABLE A-5: STIFFNESS PARAMETERS H_S AND N BASED ON FIT 79
TABLE A-6: COMPARISON H_S: PLAXIS STF AND THEORY 83
TABLE A-7: COMPARISON N: PLAXIS STF AND THEORY 83
TABLE A-8: CHOSEN H_S AND N 83
TABLE A-9: CALCULATION A PARAMETER DRENTE 90
TABLE A-10: CALCULATION A PARAMETER STERKSEL 90
TABLE A-11: HYPOPLASTIC PARAMETERS FORMATION DRENTE & STERKSEL 96
TABLE D-1: SOFTENING TEST PILE 2 119

A. PARAMETER DETERMINATION HYPOPLASTICITY

A.1. MICROSCOPIC ANALYSIS SAND

Microscopic photographs show both samples are, on average, sub-angular and relatively spherical, please refer to Figure A-1 to A-4. A relatively large spread in angularity and sphericity is however observed. Using Figure A-5, the angularity and sphericity can be approximated.

FIGURE A-1: SAMPLE DRENTE FORMATION (B320 – M13), CLOSE TOGETHER

FIGURE A-2: SAMPLE DRENTE FORMATION (B320 – 13), GRAINS SEPARATED

Figure A-3: SAMPLE STERKSEL FORMATION (B320 – M13), CLOSE TOGETHER

FIGURE A-4: SAMPLE STERKSEL FORMATION (B320 – M13), GRAINS SEPARATED

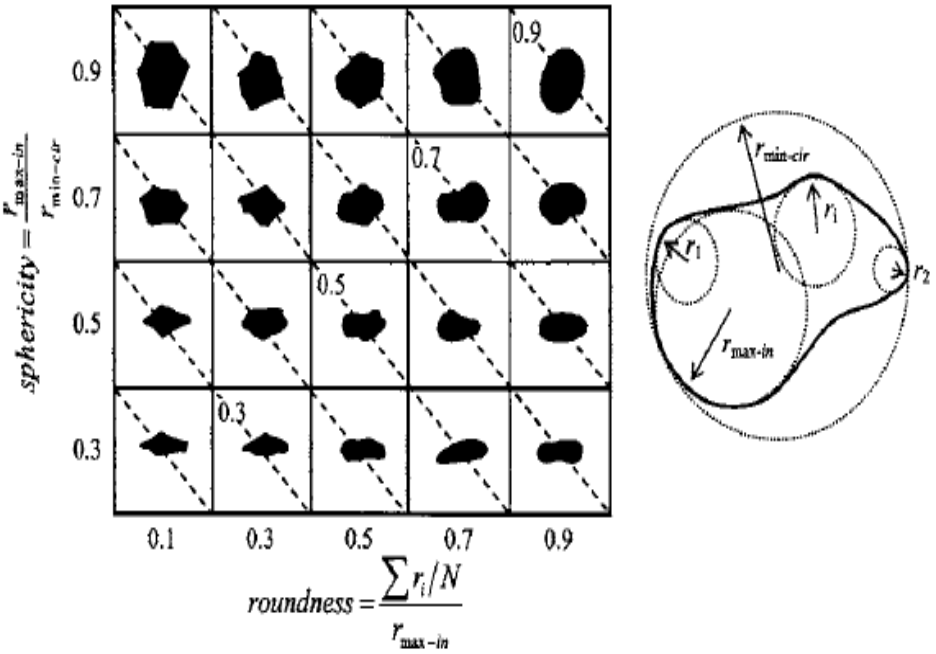

FIGURE A-5: ROUNDNESS AND SPHERICITY OF TESTED SANDS, IN ACCORDANCE WITH CHO ET AL. (2006)

A.2. ANGLE OF REPOSE

The constant volume angle φ_{cv} can be approximated by the angle of repose φ_c. The test, based on the JGS, is describe in the next subsection.

I.ii.i. Test procedure

φ_c or in this case, the angle of repose, can be determined using a 12 mm funnel (JGS). By very slowly and gradually lifting the funnel opening away from a surface, a conically shaped mass of sand, in its loosest state is obtained. By measuring the angle of the slope φ_c is determined, please refer to Figures A-6 to A-8. The measuring technique is shown in figure.

By measuring the height (h) and the width (w) of the conically shaped sand mass, φ_c can be determined using the following equation:

$$\varphi_c = tan^{-1}\left(\frac{h}{\frac{1}{2}w}\right) \tag{45}$$

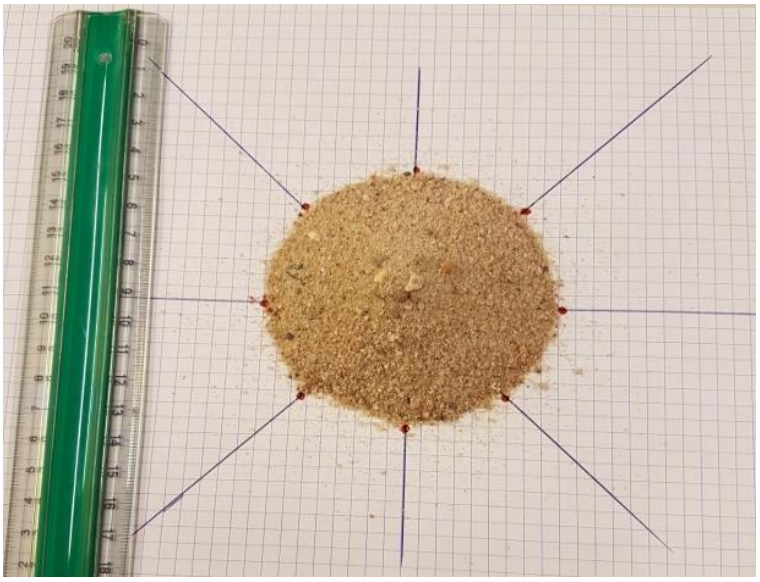

FIGURE A-6: ANGLE OF REPOSE MEASUREMENT

Five tests are performed per soil sample. For each test, the width is determined in four different directions, subsequently these results are averaged. This procedure is chosen to average out the inconsistency due to arbitrary grain orientation.

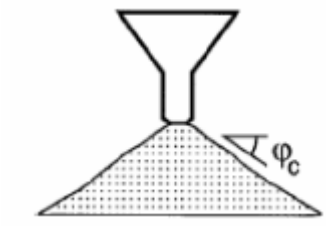

FIGURE A-7: GRAPHICAL REPRESENTATION ANGLE OF REPOSE

FIGURE A-8: ANGLE OF REPOSE MEASUREMENT OF HEIGHT

A.2.2. Parameter results

TABLE A-1: TESTS RESULTS ANGLE OF REPOSE

φ_c [°]	1	2	3	4	5	Average
Drente formation	31.0	31.8	30.9	30.4	31.2	31.1
Sterksel formation	32.1	33.4	32.9	33.5	31.9	32.8

A.3. MINIMUM AND MAXIMUM VOID RATIO

The different void ratios are determined in accordance with the Japanese standard (JGS). The different void ratios which have to be determined are: $e_{c0} = e_{max}$, $e_{d0} = e_{min}$ and $e_{i0} = 1.15*e_{max}$. The '0' in the subscript refers to a reference state of approximately zero effective stresses.

A.3.1. Test procedure

The maximum void ratio is determined by slowly building up the sand sample in the mould using a funnel. During this process, it is important to keep a minimal distance between the opening of the funnel and the sand surface. This way, the compaction of the sand will be as limited as possible or even non-existent.

The sample made to determine the minimum void ratio is prepared in five layers. Each layer was compacted using a 60g stick to tap the mould.

After preparing both samples the void ratios can be calculated using the weight of the samples and equation 46 to 49.

$$e = \frac{V_{voids}}{V_{solids}} \tag{46}$$

$$V_{solids} = \frac{M_{sample}}{\rho_{solids}} \tag{47}$$

$$V_{voids} = V_{sample} - V_{solids} \tag{48}$$

$$\rho_{solids} = \frac{2{,}65kg}{cm^3} \tag{49}$$

A.3.2. Parameter results

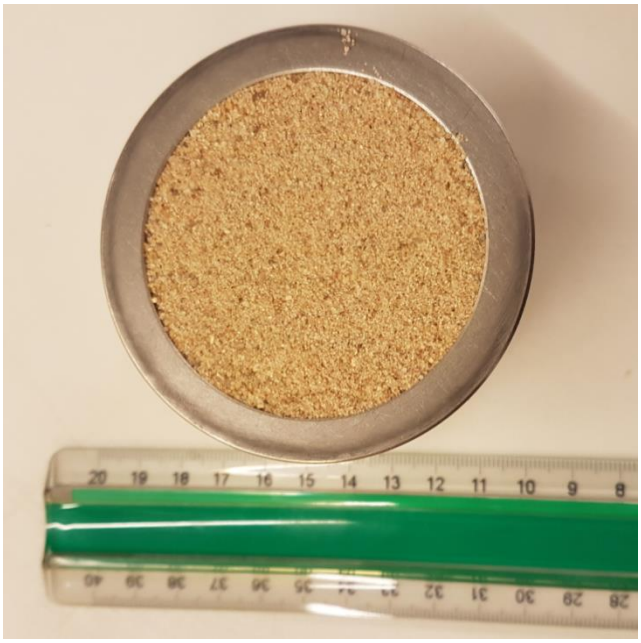

Figure A-9: FILLED TESTING MOLD JAPANESE STANDARD TEST

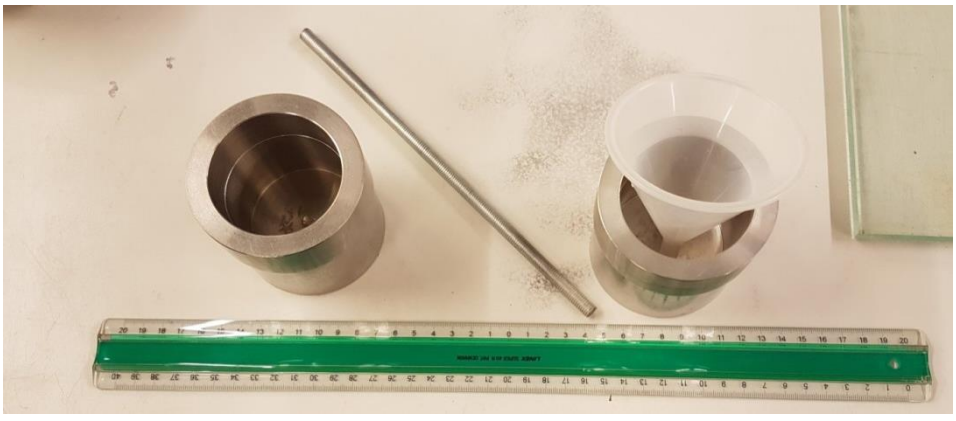

FIGURE A-10: TESTING EQUIPMENT MINIMUM AND MAXIMUM VOID RATIO JAPANESE STANDARD

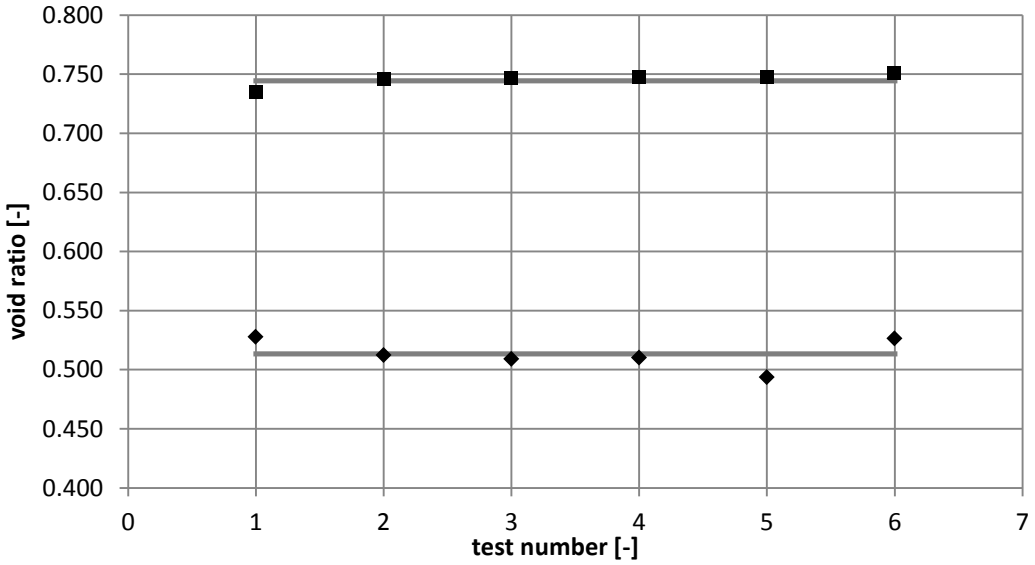

FIGURE A-11: E_{MIN} (♦) AND E_{MAX} (■) OF DRENTE FORMATION SAND, AVERAGE AS DASHED LINE

TABLE A-2: E_{MIN}, E_{MAX} AND E_I OF DRENTE FORMATION SAND

$e_{d0,DR}$	*0.513*
$e_{c0,DR}$	*0.744*
$e_{i0,DR}$	*0.857*

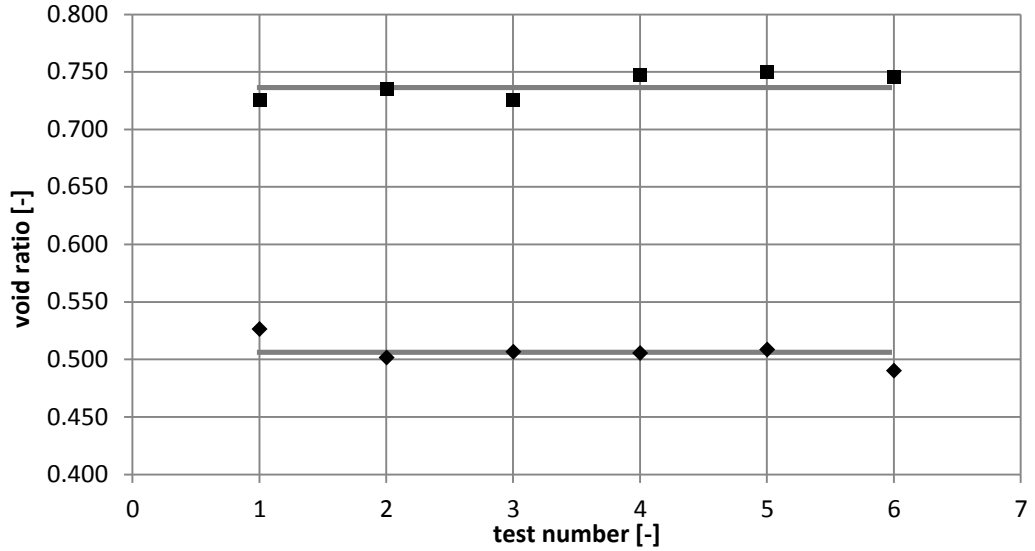

FIGURE A-12: E_{MIN} (♦) AND E_{MAX} (■) OF STERKSEL FORMATION SAND, AVERAGE AS DASHED LINE

TABLE A-3: E_{MIN}, E_{MAX} AND E_I OF STERKSEL FORMATION SAND

$e_{d0,ST}$	*0.506*
$e_{c0,ST}$	*0.736*
$e_{i0,ST}$	*0.849*

A.4. OEDOMETER

With help of oedometer tests, the stiffness parameters h_s and n can be determined. Please refer to equation 50 (Bauer, 1996).

$$\frac{e_i}{e_{i0}} = \frac{e_c}{e_{c0}} = \frac{e_d}{e_{d0}} = \mathrm{e}^{\left(-\frac{3p_s}{h_s}\right)^n} \tag{50}$$

A.4.1. Test procedure

The oedometer tests are performed at three different densities, very loose, very dense and medium dense in dry conditions. Before starting the tests, the oedometer set up is calibrated and the arm factor is determined. For the oedometer used, the arm factor is equal to 11.16. Using this factor the loading scheme and resulting oedometric pressures are displayed in Table A-4.

TABLE A-4: LOADING SCHEME OEDOMETER TESTS

Weight increment [kg]	Cumulative weight [kg]	Load [N]	sig'$_{oedometer}$ [kPa]
0.25	0.25	2.5	8.8
0.5	0.75	7.4	26.5
1	1.75	17.2	61.7
5	6.75	66.3	238.1
10	16.75	164.3	590.7
20	36.75	360.5	1296.1
20	56.75	556.7	2001.4
10	66.75	654.8	2354.1
10	76.75	752.9	2706.8
10	86.75	851.0	3059.5
10	96.75	949.1	3412.1

FIGURE A-13: OEDOMETER SET-UP

FIGURE A-14: CLOSE UP INSTALLED OEDOMETER MOULD

A.4.2. Test Results

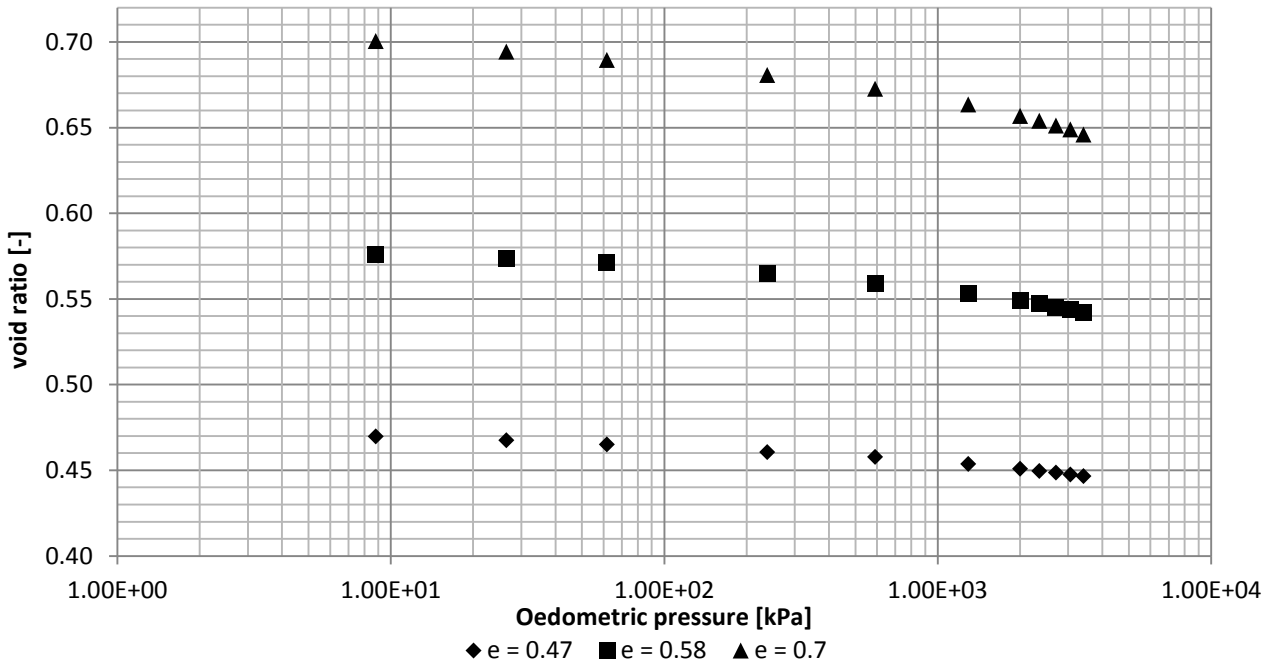

FIGURE A-15: OEDOMETER TESTS ON DRENTE FORMATION SAND FOR DENSE (E_0=0.47), MEDIUM DENSE (E_0=0.58) AND LOOSE (E=0.7) PACKING

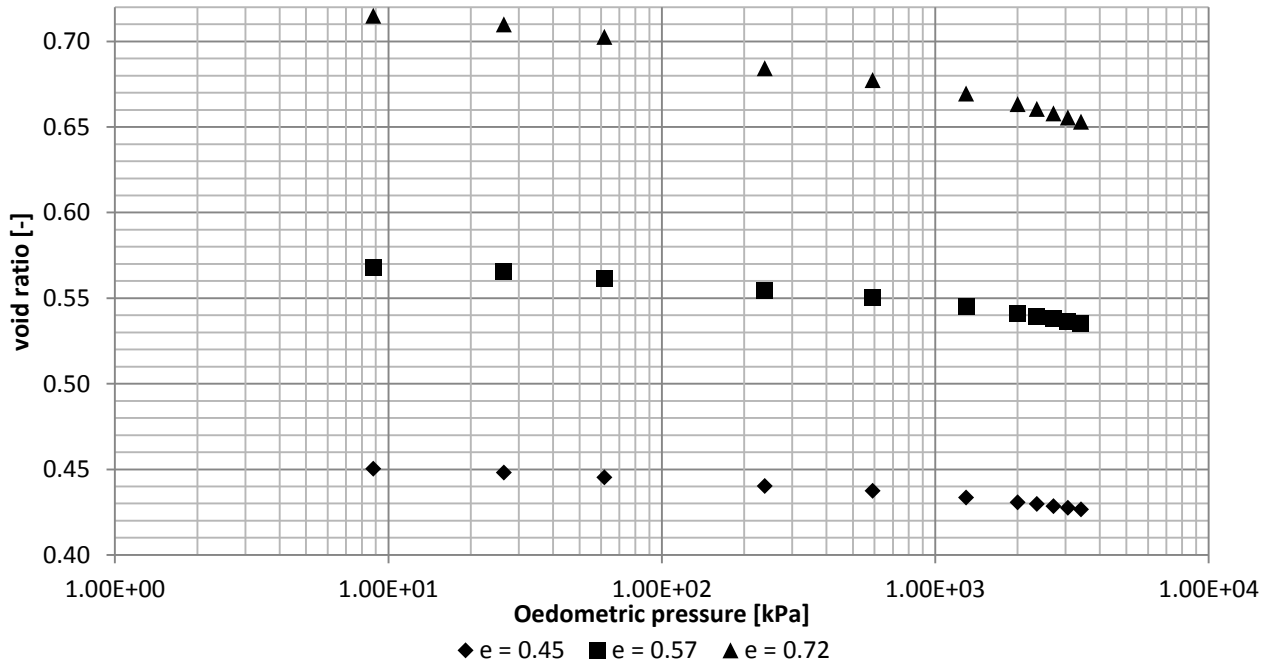

FIGURE A-16: OEDOMETER TESTS ON STERKSEL FORMATION SAND FOR DENSE (E_0=0.47), MEDIUM DENSE (E_0=0.58) AND LOOSE (E=0.7) PACKING

A.4.3. Parameter results

In the Figures below, the parameters h_s and n are determined and fitted using the formula of Herle and Gudehus (1999). The black dotted line uses the formula directly. For the grey line, the void ratio is calculated fitting the curve on the data points varying h_s and n. Table A-5 summarises the results of h_s and n for both Drente and Sterksel.

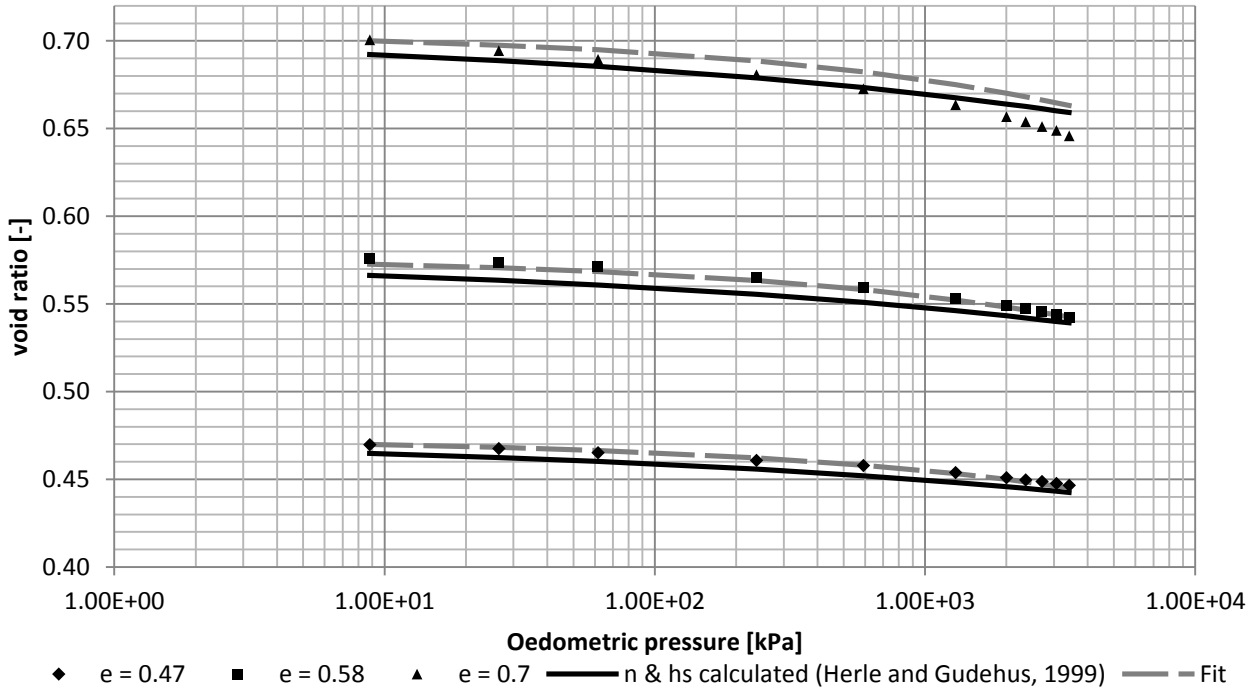

FIGURE A-17: OEDOMETRIC RESPONSE DRENTE IN ACCORDANCE WITH HERLE AND GUDEHUS (1999) AND FIT

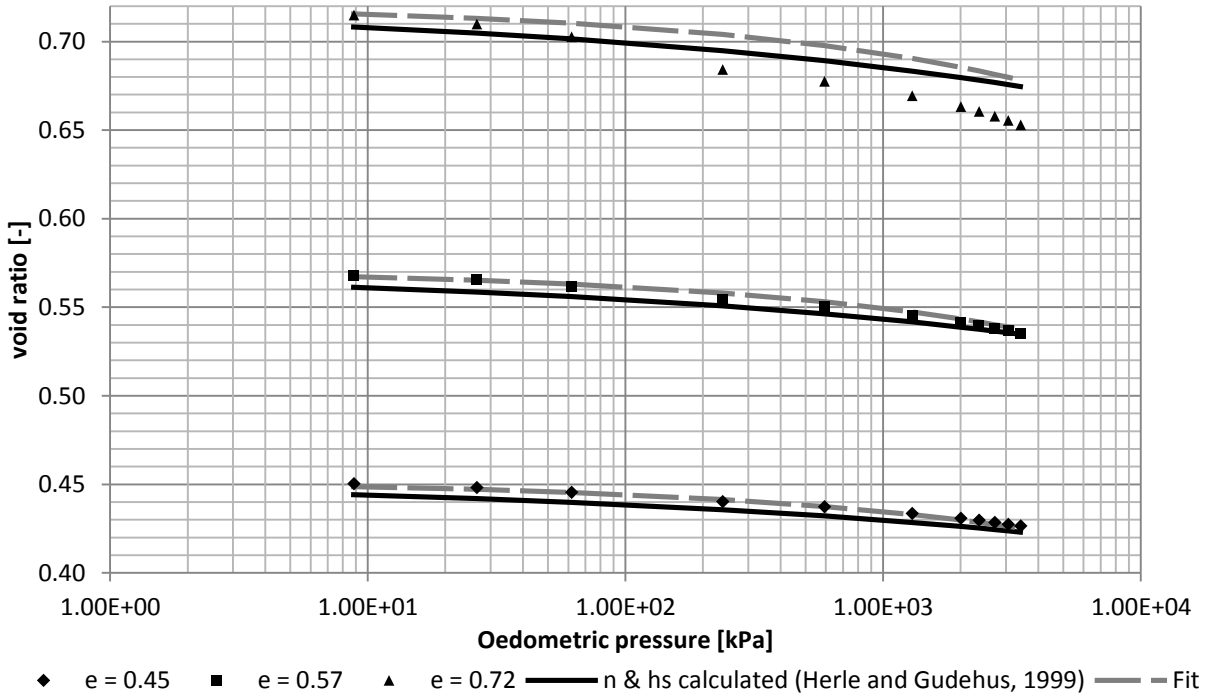

FIGURE A-18: OEDOMETRIC RESPONSE STERKSEL IN ACCORDANCE WITH HERLE AND GUDEHUS (1999) AND FIT

TABLE A-5: STIFFNESS PARAMETERS H_S AND N BASED ON FIT

Geological formation	h_s **[GPa]**	n **[-]**
Drente (B320 – M13)	11	0.4
Sterksel (B320 – M16)	14	0.36

A.4.4. Comparison Plaxis Soil Testing Facility (STF)

To check if the results of the oedometer test are modelled correctly within the hypoplastic formulation, the Plaxis STF is used. In this feature, element tests are numerically approximated using a single soil element. The continuum formulation of the constitutive model is used as a basis for this behaviour. The results for the different void ratios are displayed in Figures A-19 to A-24. As shown in these figures, the theoretically determined h_s and n values do not fit the test result when implemented in the hypoplastic formulation. To overcome this issue, for each void ratio the best fit is created in the STF. Next, an average fit over the three different void ratios is made per soil to determine the overall best fitting h_s and n parameters.

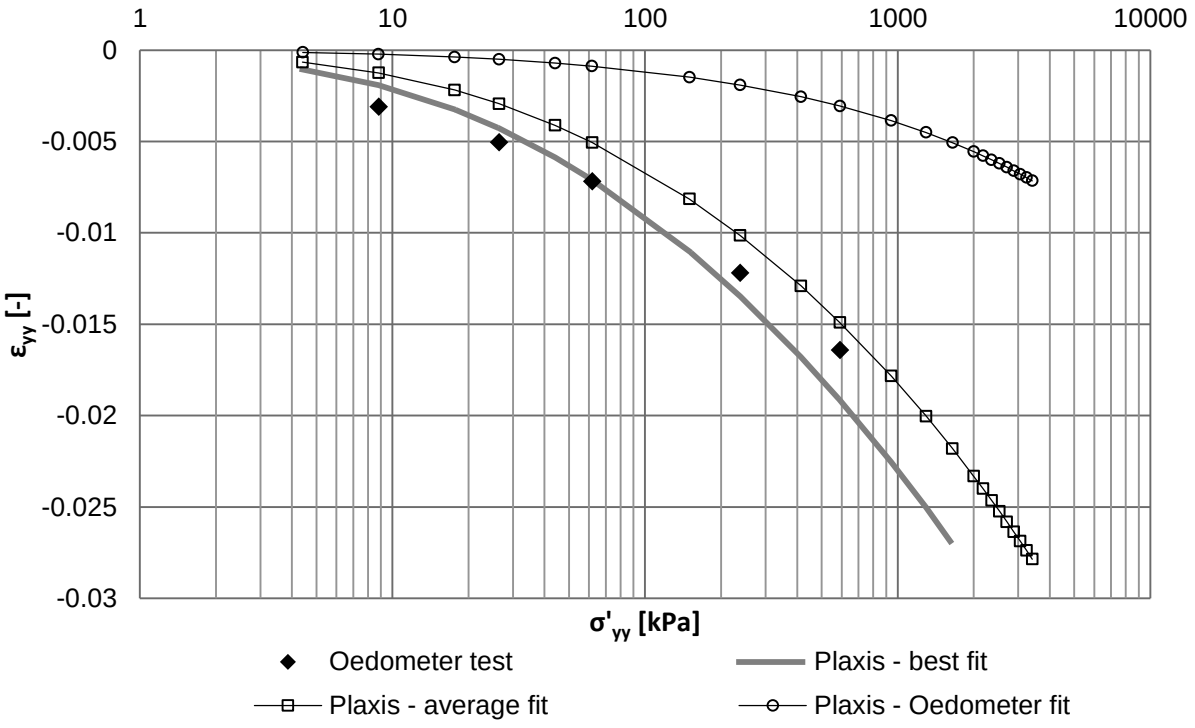

FIGURE A-19: OEDOMETRIC RESPONSE SAMPLE DRENTE , E = 0.47

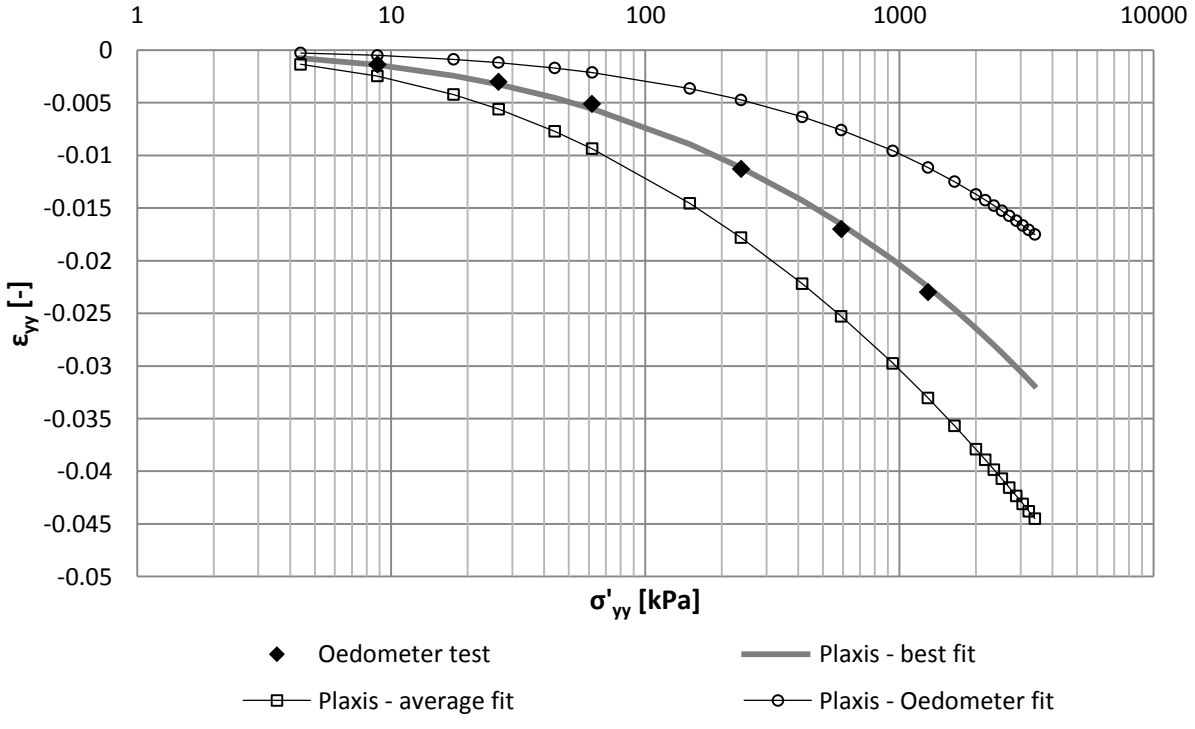

FIGURE A-20: OEDOMETRIC RESPONSE SAMPLE DRENTE, E=0.58

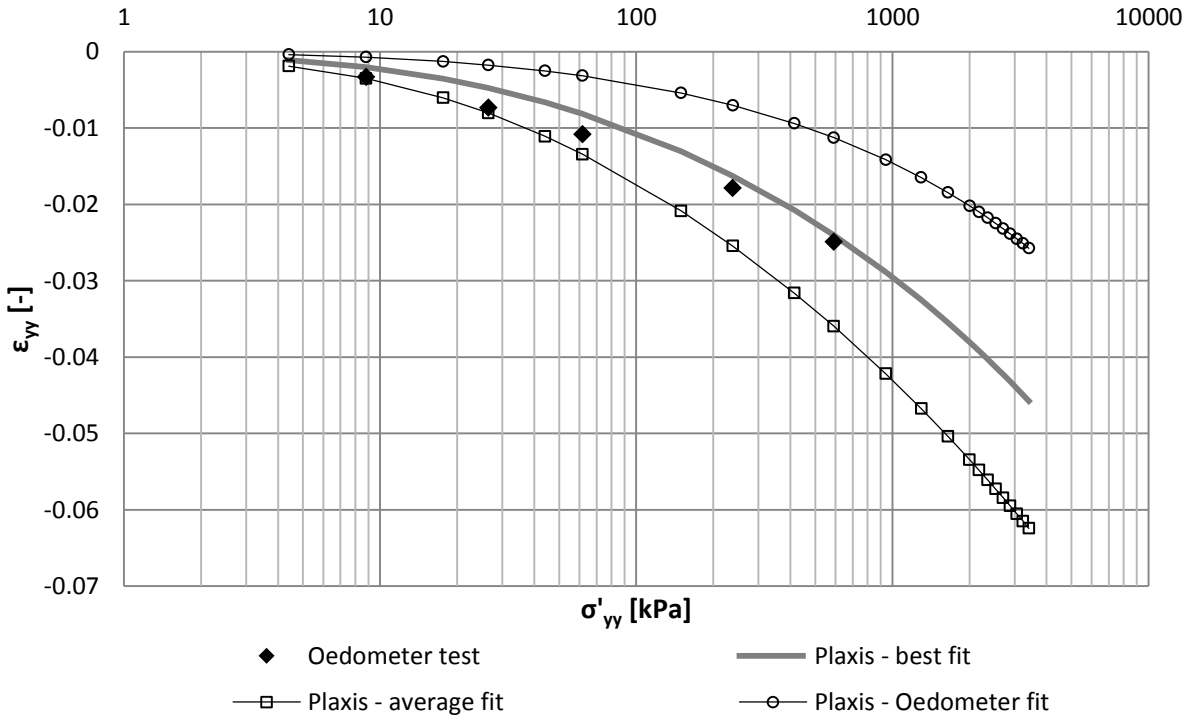

FIGURE A-21: OEDOMETRIC RESPONSE SAMPLE DRENTE, E=0.71

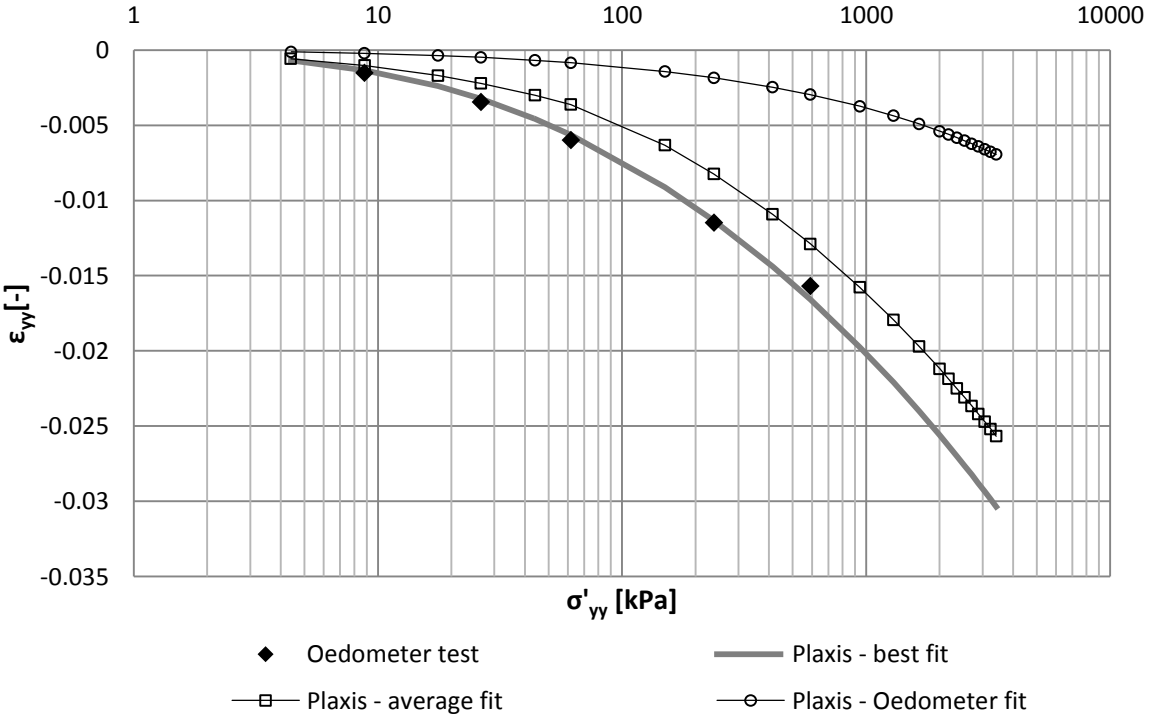

FIGURE A-22: OEDOMETRIC RESPONSE SAMPLE STERKSEL, E=0.45

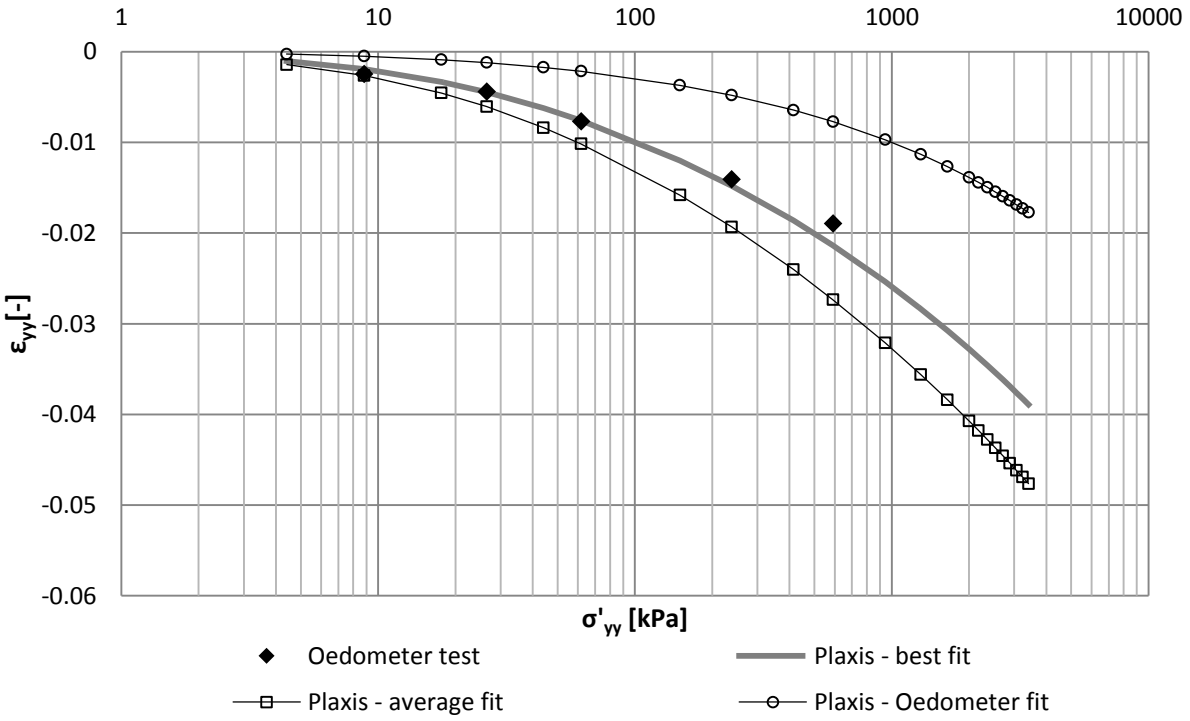

FIGURE A-23: OEDOMETRIC RESPONSE SAMPLE STERKSEL, E=0.57

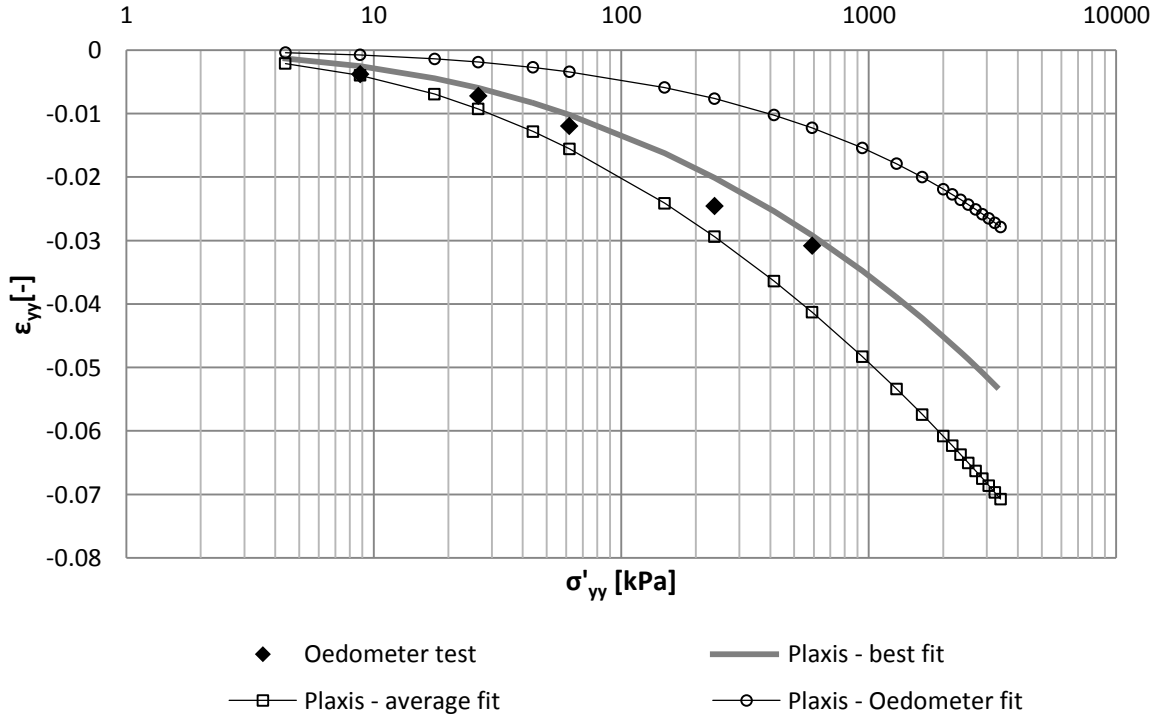

FIGURE A-24: OEDOMETRIC RESPONSE SAMPLE STERKSEL, E=0.72

As shown in the Figures A-19 to A-24, the void ratios for the densest sample have a lower *e* than e_{min} which seems wrong. However, the JGS method (JGS) to determine e_{min} uses a relative light tapping stick and a heavy mould and is only an approximation. Therefore, it is possible to get a lower void ratio in the, lighter, oedometer mould. As this is theoretically speaking impossible, it is unknown how the continuum formulation exactly handles this.

Another important thing to notice is the difference between h_s and *n* determined using Plaxis. They differ significantly from the theoretical values gained from the formula of Herle and Gudehus (1999). Table A-6 and A-7 display the differences.

TABLE A-6: COMPARISON H_S: PLAXIS STF AND THEORY

h_s [GPa]	Plaxis – Average fit	Theoretical fit
Drente (B320-13)	13	11
Sterksel (B320-16)	10	14

TABLE A-7: COMPARISON N: PLAXIS STF AND THEORY

n [-]	Plaxis – Average fit	Theoretical fit
Drente (B320-13)	0.27	0.4
Sterksel (B320-16)	0.26	0.36

As Plaxis will be used to model the pile response, the values determined with the STF will be used for further numerical modelling.

TABLE A-8: CHOSEN H_S AND *N*

	h_s [GPa]	*n* [-]
Drente (B320-13)	13	0.27
Sterksel (B320-16)	10	0.26

A.5. DIRECT SHEAR TEST

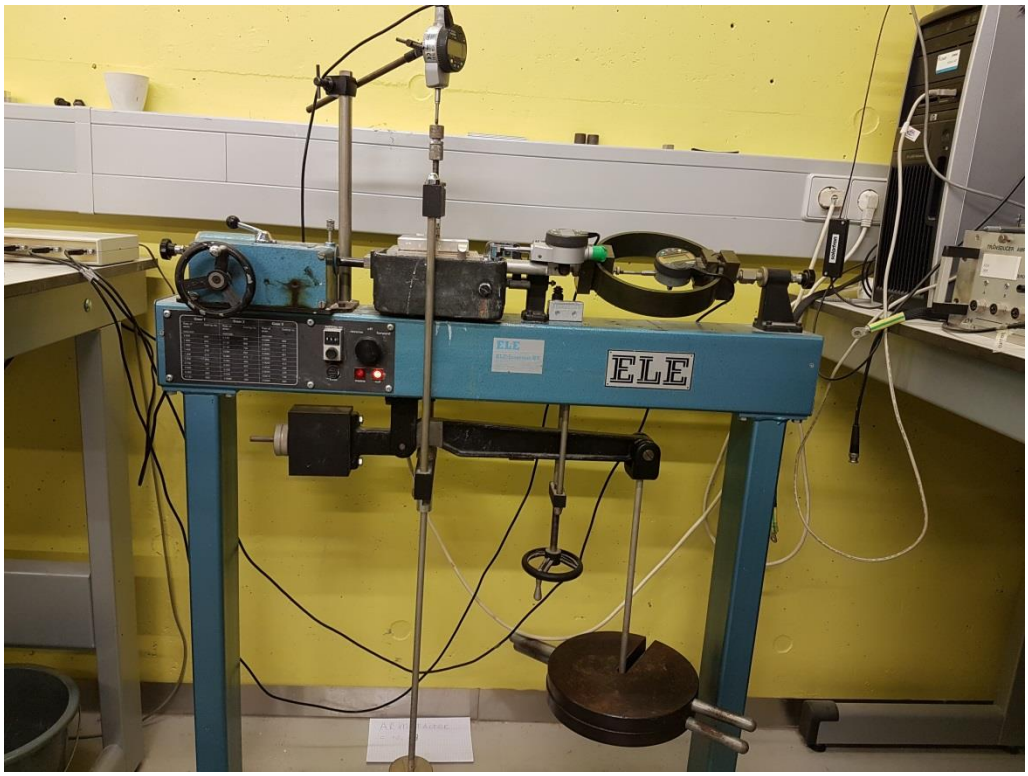

FIGURE A-25: PHOTOGRAPH DIRECT SHEAR APPARATUS, SIDE VIEW

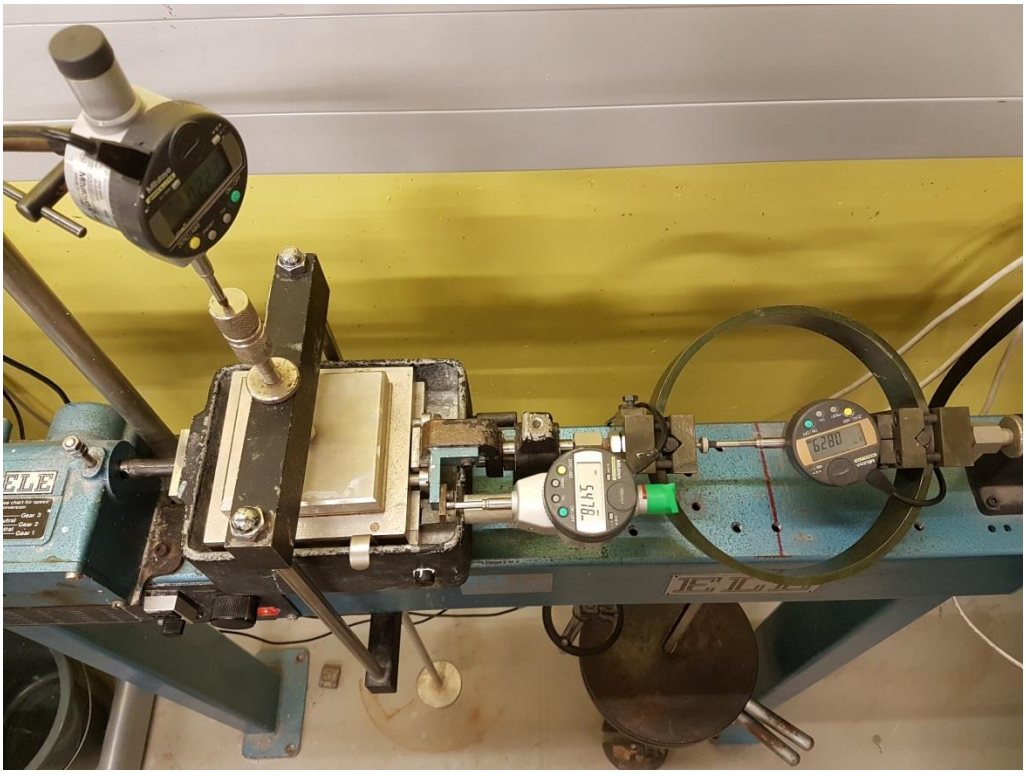

FIGURE A-26: PHOTOGRAPH DIRECT SHEAR APPARATUS, TOP VIEW

The pyknotropy exponent α is preferably determined using a triaxial setup (Herle and Gudehus, 1999). However, as it was impossible to perform triaxial tests, direct shear tests are done to approximate α. This parameter relates the peak friction angle φ_p to the dilatancy rate v_p. Both parameters can be determined from a triaxial test as well as from a direct shear test. The direct shear tests are performed in dry conditions since drained behaviour can be assumed

A.5.1. Test procedure

Direct shear tests are performed at two different relative densities. For determining α, dilative behaviour needs to occur, hence 80% and 90% relative density are arbitrarily chosen. For both relative densities, the direct shear tests are performed at different stress levels. This ensures deviations as a result of heterogeneity are minimized. Normal stresses σ_{yy} were taken at 100 kPa, 200 kPa and 300 kPa, since these are realistic stress levels.

Before performing the test, the arm factor is determined at 10.28. During testing it is important to watch the top cap displacement. When it tilts, the vertical displacement becomes inaccurate. This can result into continuing vertical displacement of the top cap after full dilation, see Figure A-27 and unrealistic dilation rates can occur.

FIGURE A-27: TOP CAP TILTING DURING LOADING

A.5.2. Test Results

From the results of the shear box tests both a σ_{yy},ε_{yy}-diagram and a ε_v,ε_{yy}-diagram are plotted. From these graphs, respectively the peak friction angle φ_p and the dilantancy rate v_p can be determined. Next, these parameters are used to calculate α using equation 51.

$$\alpha = \frac{\ln\left[6\dfrac{\left(2+K_p\right)^2 + a^2K_p\left(K_p - 1 - \tan \mathrm{v}_p\right)}{a\left(2+K_p\right)\left(5K_p-2\right)\sqrt{4+2\left(1+\tan \mathrm{v}_p\right)^2}}\right]}{\ln\left(\dfrac{e-e_d}{e_c-e_d}\right)} \tag{51}$$

$$a = \frac{\sqrt{3}(3-\sin\varphi_c)}{2\sqrt{2}\sin\varphi_c} \tag{52}$$

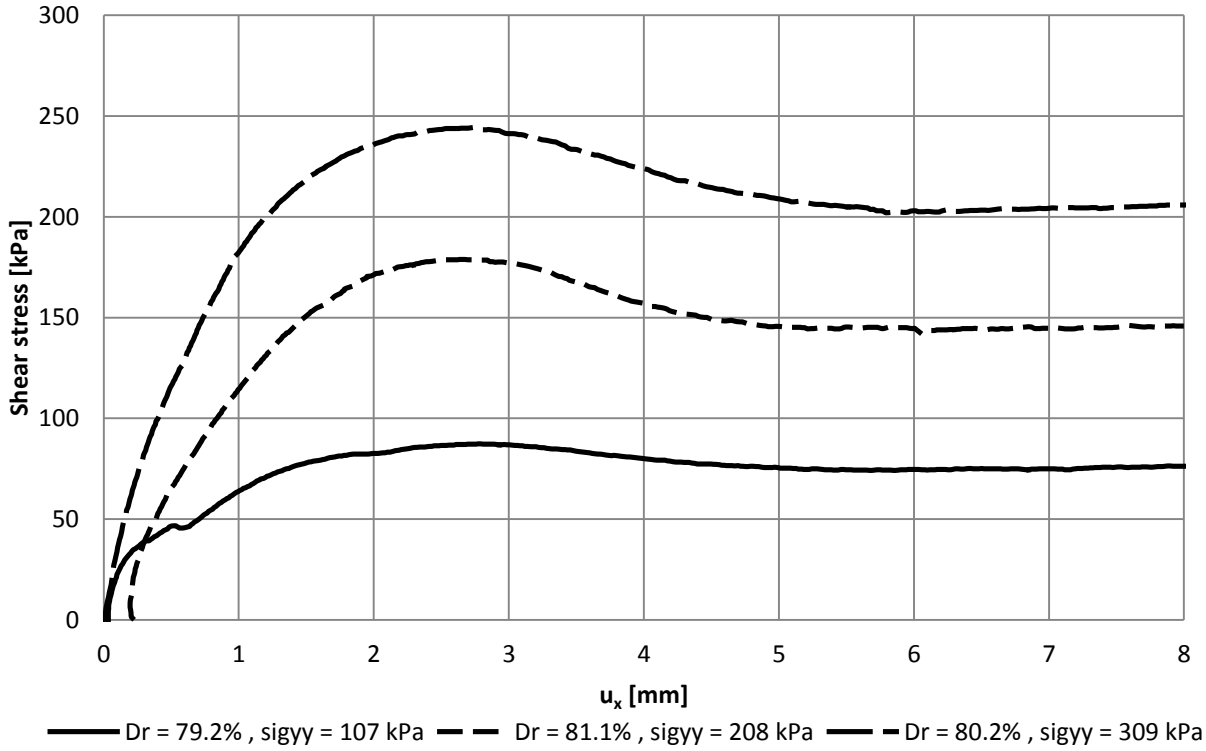

FIGURE A-28: SHEAR STRESS, SAMPLE DRENTE: D_R=80%, σ_{YY} =100, 200 & 300 KPA

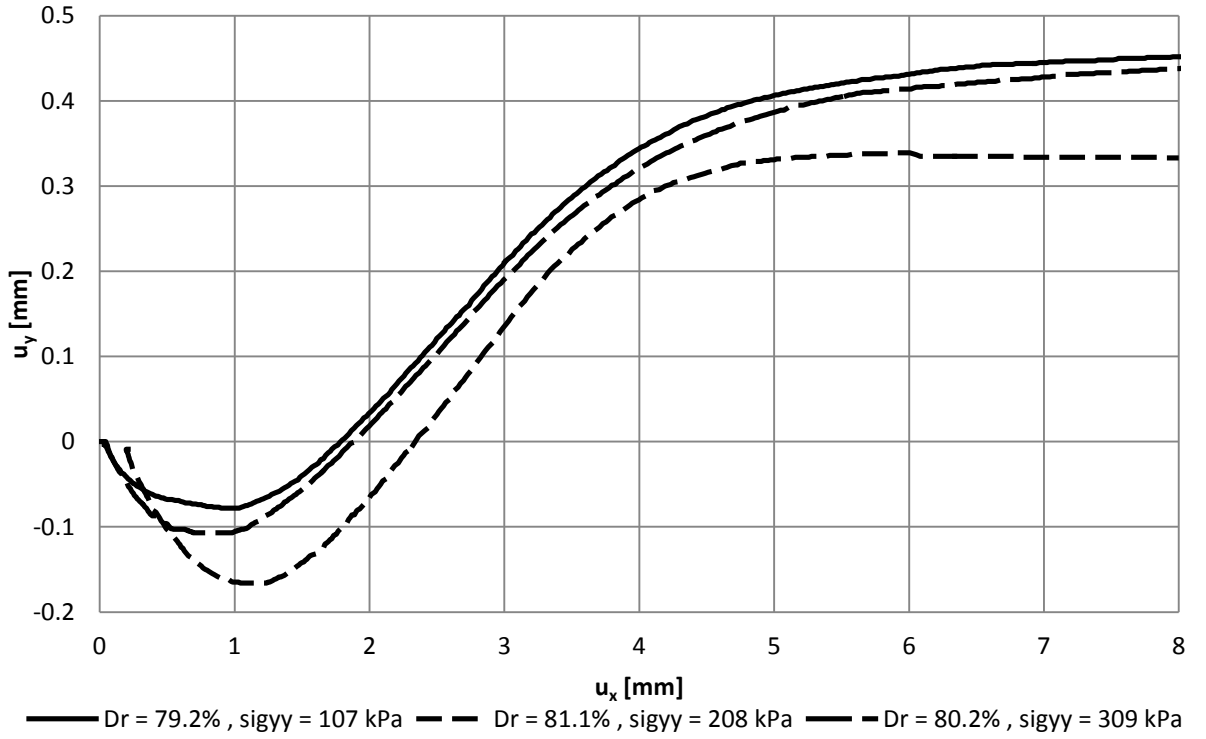

FIGURE A-29: DISPLACEMENTS, SAMPLE DRENTE: D_R=80%, σ_{YY} =100, 200 & 300 KPA

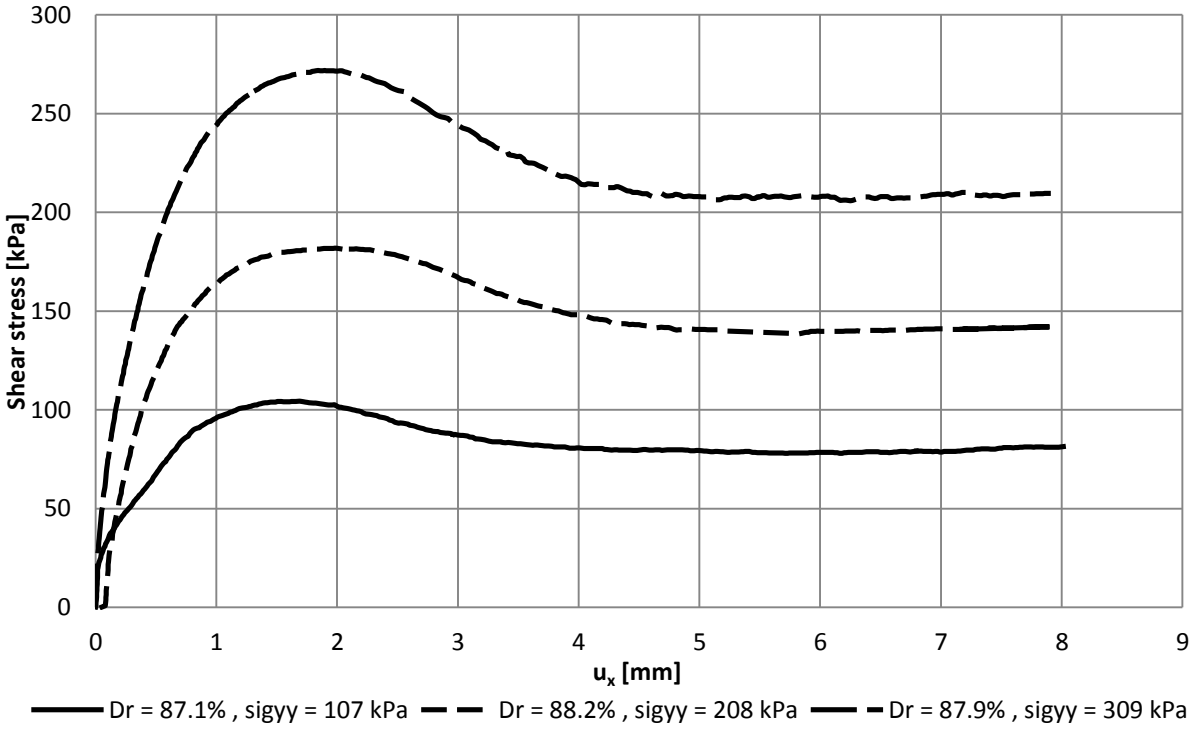

FIGURE A-30: SHEAR STRESS, SAMPLE DRENTE: D_R=90%, σ_{YY} =100, 200 & 300 KPA

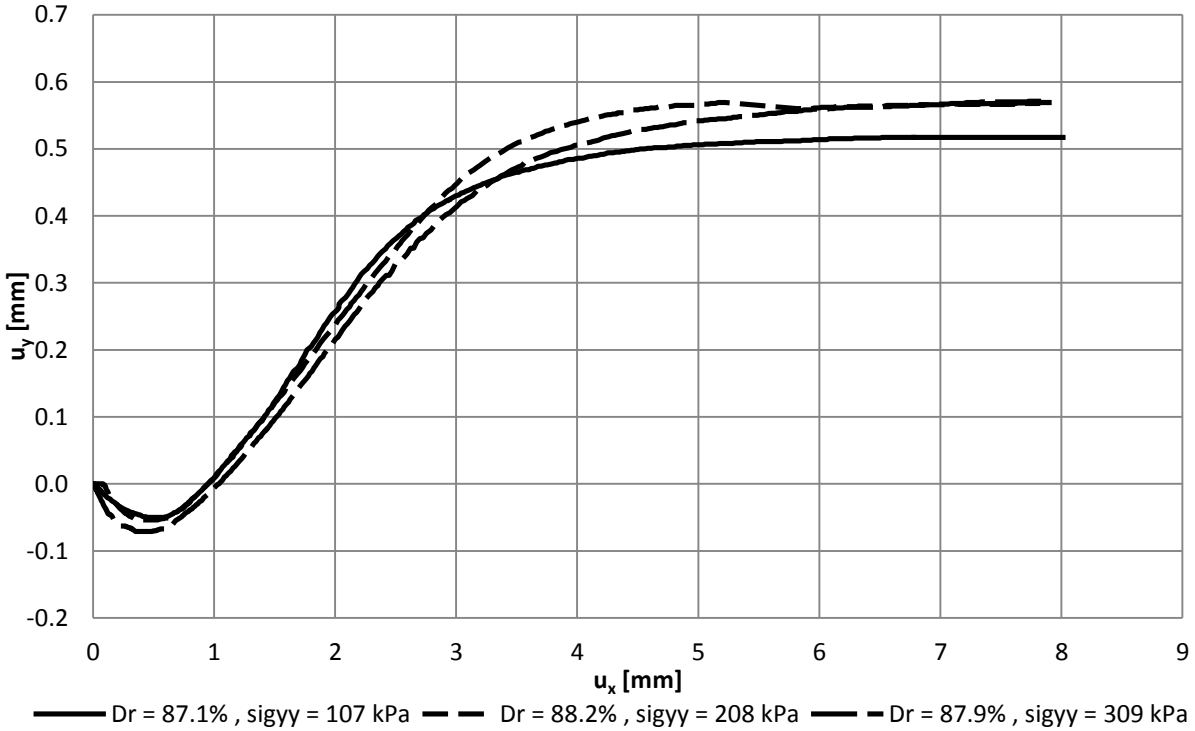

FIGURE A-31: DISPLACEMENTS, SAMPLE DRENTE: D_R=90%, σ_{YY} =100, 200 & 300 KPA

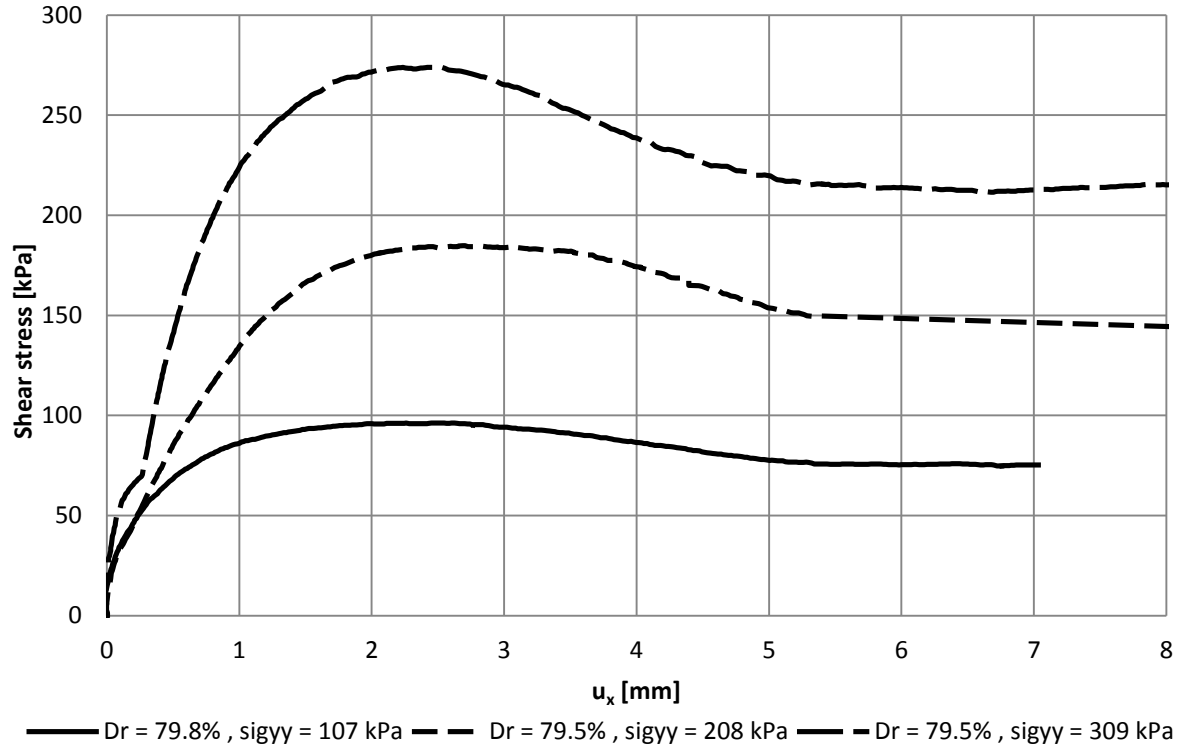

FIGURE A-32: SHEAR STRESS, SAMPLE STERKSEL: D_R=80%, σ_{YY} =100, 200 & 300 KPA

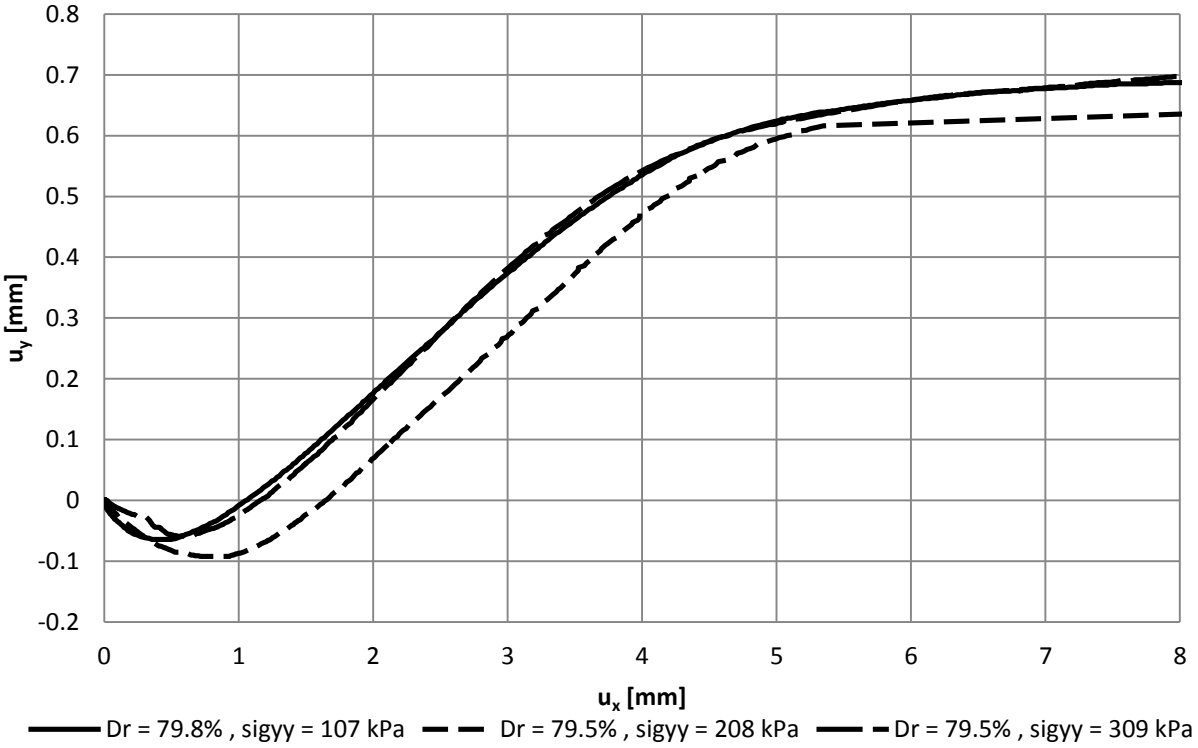

FIGURE A-33: DISPLACEMENTS, SAMPLE STERKSEL: D_R=80%, σ_{YY} =100, 200 & 300 KPA

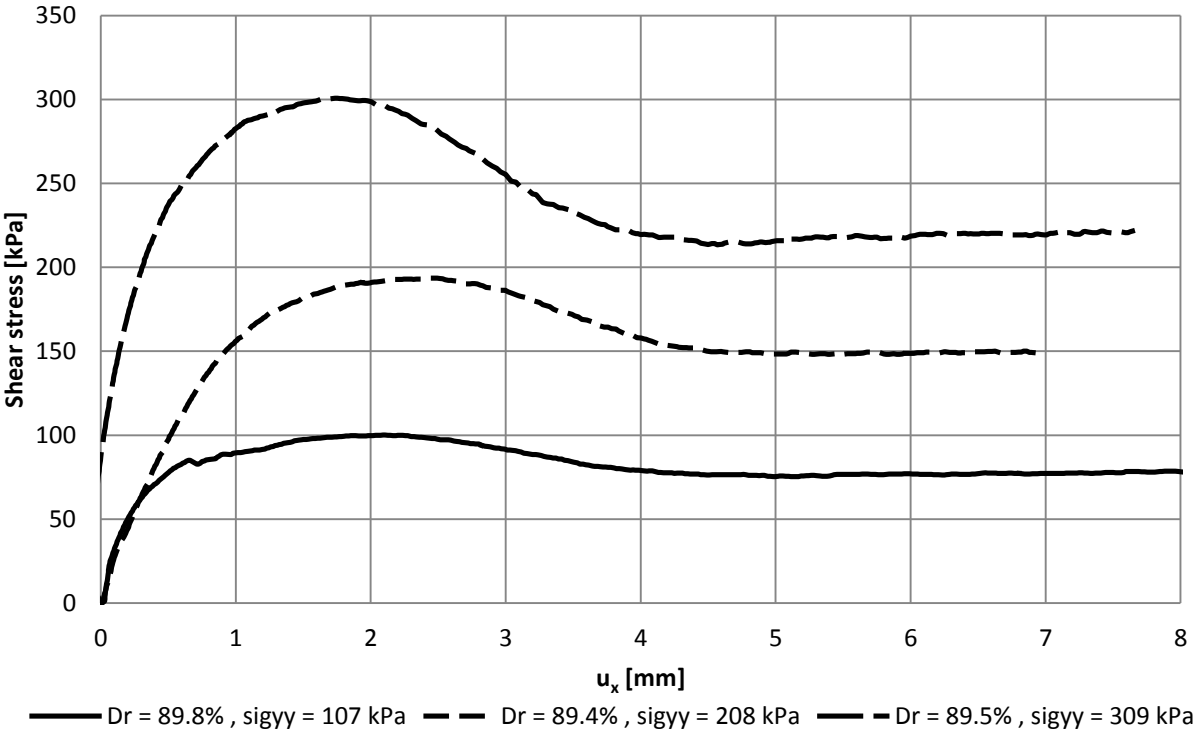

FIGURE A-34: SHEAR STRESS, SAMPLE STERKSEL: D_R=90%, σ_{YY} =100, 200 & 300 KPA

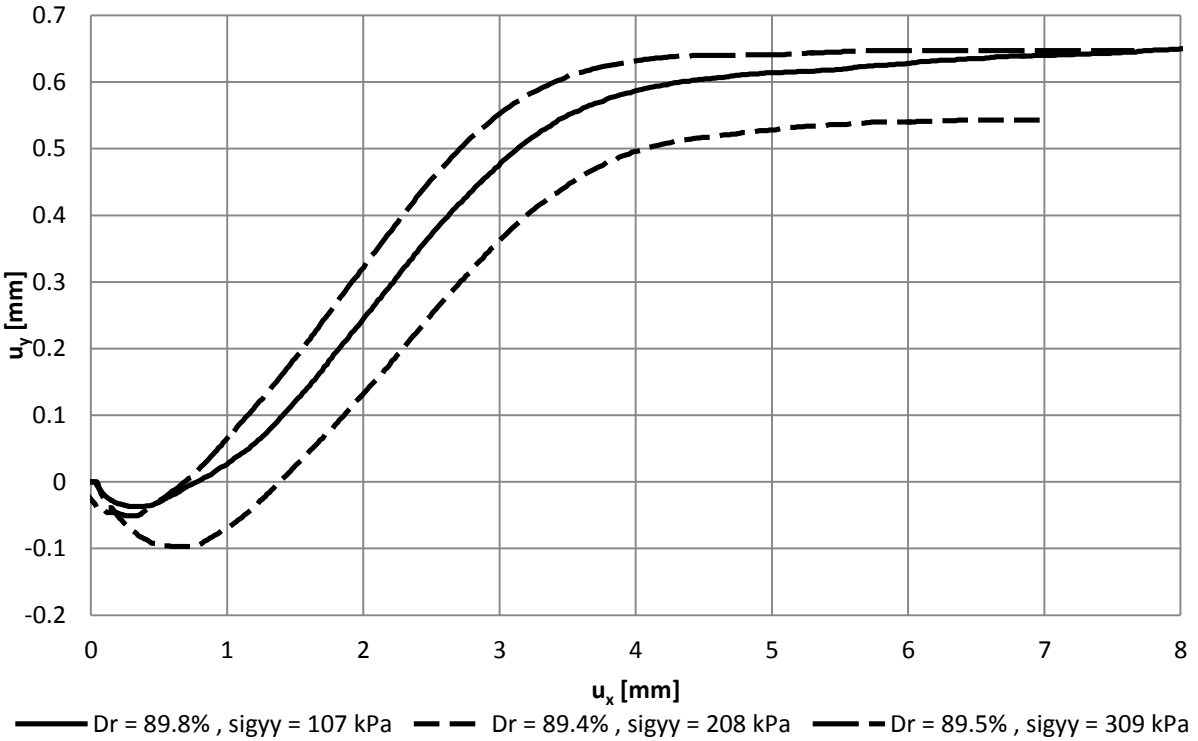

FIGURE A-35: DISPLACEMENTS, SAMPLE STERKSEL: D_R=90%, σ_{YY} =100, 200 & 300 KPA

A.5.3. Parameter results

From the graphs in the previous subsection, v_p and φ_p are determined. Using equation 51, α is calculated. This is presented in Table A-9 and A-10. The average value for the Drente and Sterksel formation respectively are 0.151 and 0.158.

TABLE A-9: CALCULATION α PARAMETER DRENTE

D_R [%]	80%	80%	80%	90%	90%	90%
σ_{yy} [kPa]	100	200	300	100	200	300
v_p [°]	42.1	38.2	38.2	30.4	34.2	30.0
φ_p [°]	44.3	41.2	41.4	39.2	40.7	38.3
α [-]	0.152	0.145	0.147	0.150	0.158	0.154

TABLE A-10: CALCULATION α PARAMETER STERKSEL

D_R [%]	80%	80%	80%	90%	90%	90%
σ_{yy} [kPa]	100	200	300	100	200	300
v_p [°]	33.3	34.4	36.2	39.9	38.1	41.9
φ_p [°]	42.0	41.7	41.6	43.1	43.0	44.3
α [-]	0.157	0.172	0.190	0.144	0.135	0.150

A.5.4. Comparison Plaxis Soil Testing Facility (STF)

Implementing the above found parameters into the STF of Plaxis. It can be checked if α found in the previous subsection matches the result based on the complete constitutive model. It should be noted that the STF can only simulate a direct simple shear tests, showing a different mobilization of shear stresses compared to the direct shear (DS) test. In terms of the $\tau - \varepsilon_1$ development, this translates into a longer mobilization from peak to residual shear stress. Since the peak and residual shear stress should have similar values, they are used to check whether α is approximately right.

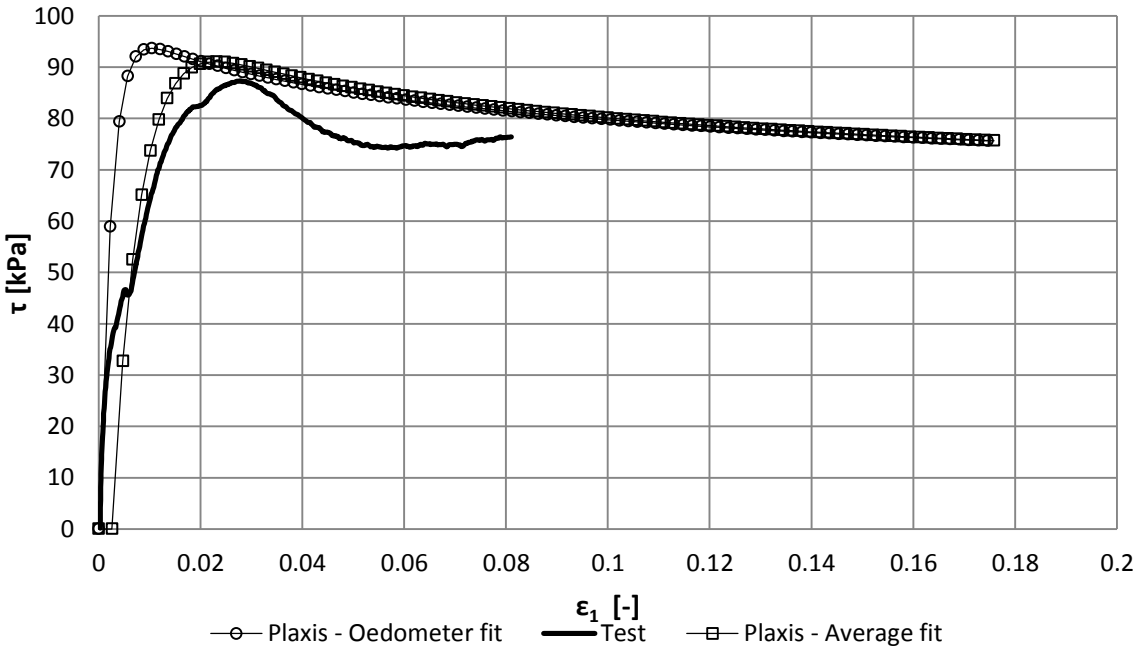

FIGURE A-36: COMPARISON STF – DS TEST: DRENTE D_R=80%, σ_{YY}=100 KPA

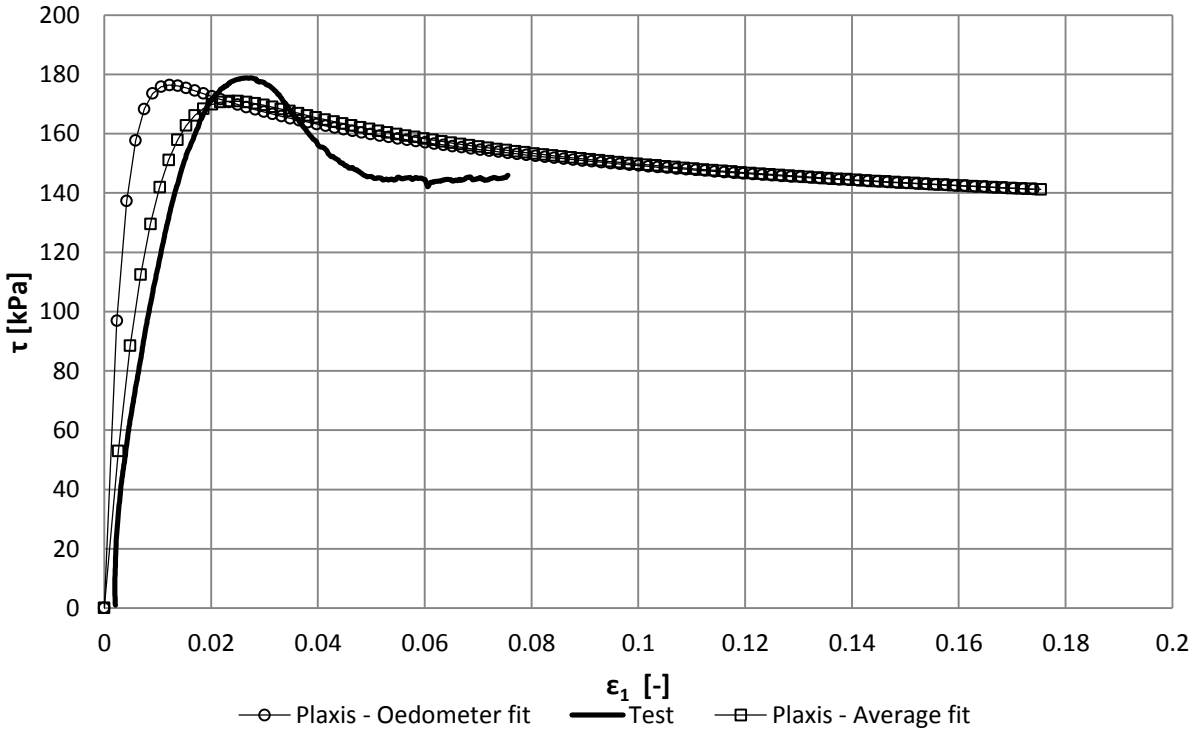

FIGURE A-37: COMPARISON STF – DS TEST: DRENTE, D_R=80%, σ_{YY}=200 KPA

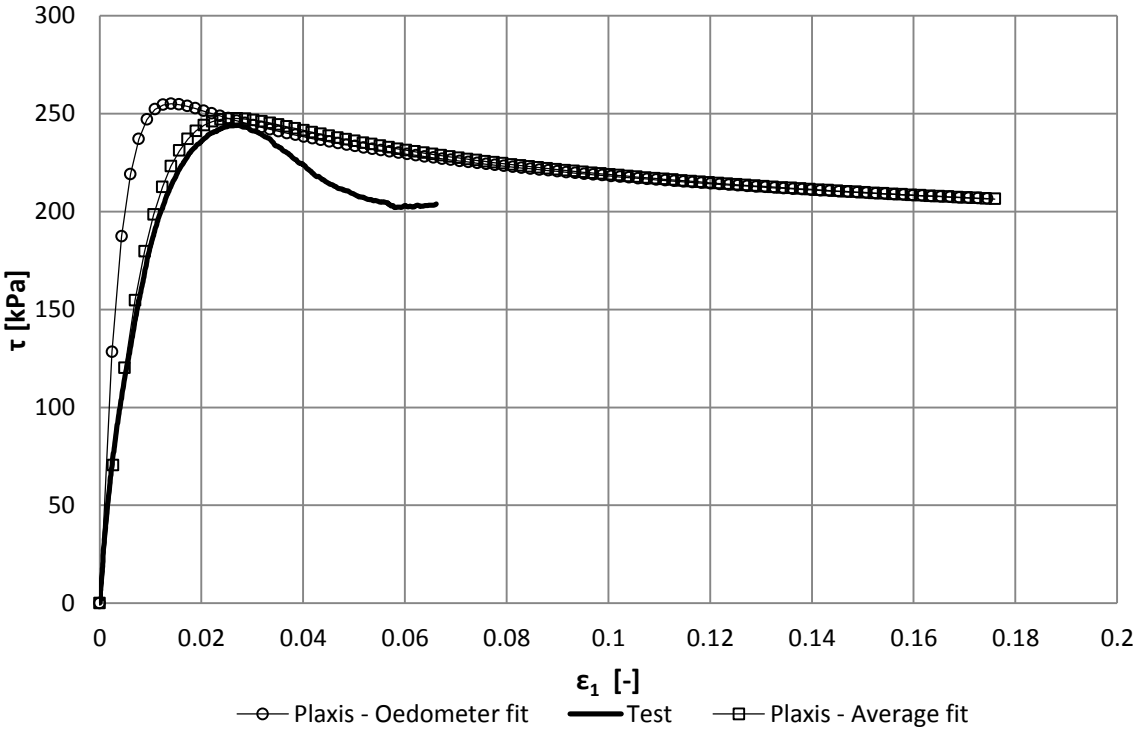

FIGURE A-38: COMPARISON STF – DS TEST: DRENTE, D_R=80%, σ_{YY}=300 KPA

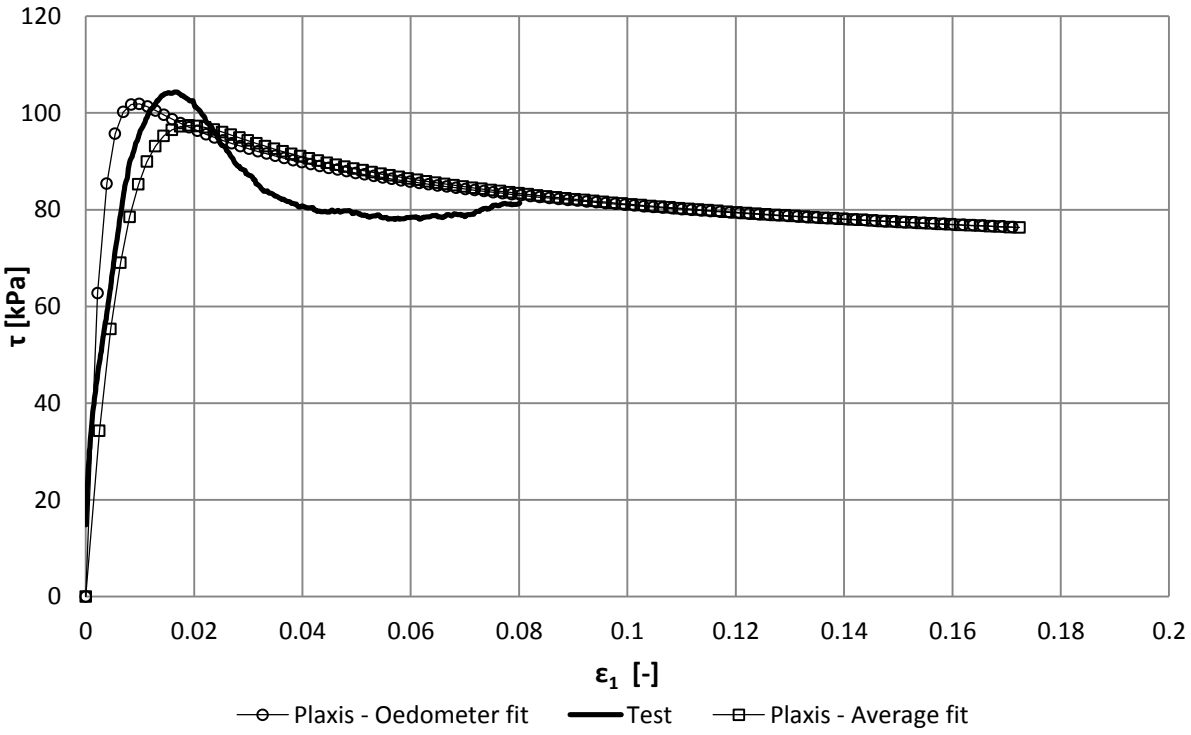

FIGURE A-39: COMPARISON STF – DS TEST: DRENTE, D_R=90%, σ_{YY}=100 KPA

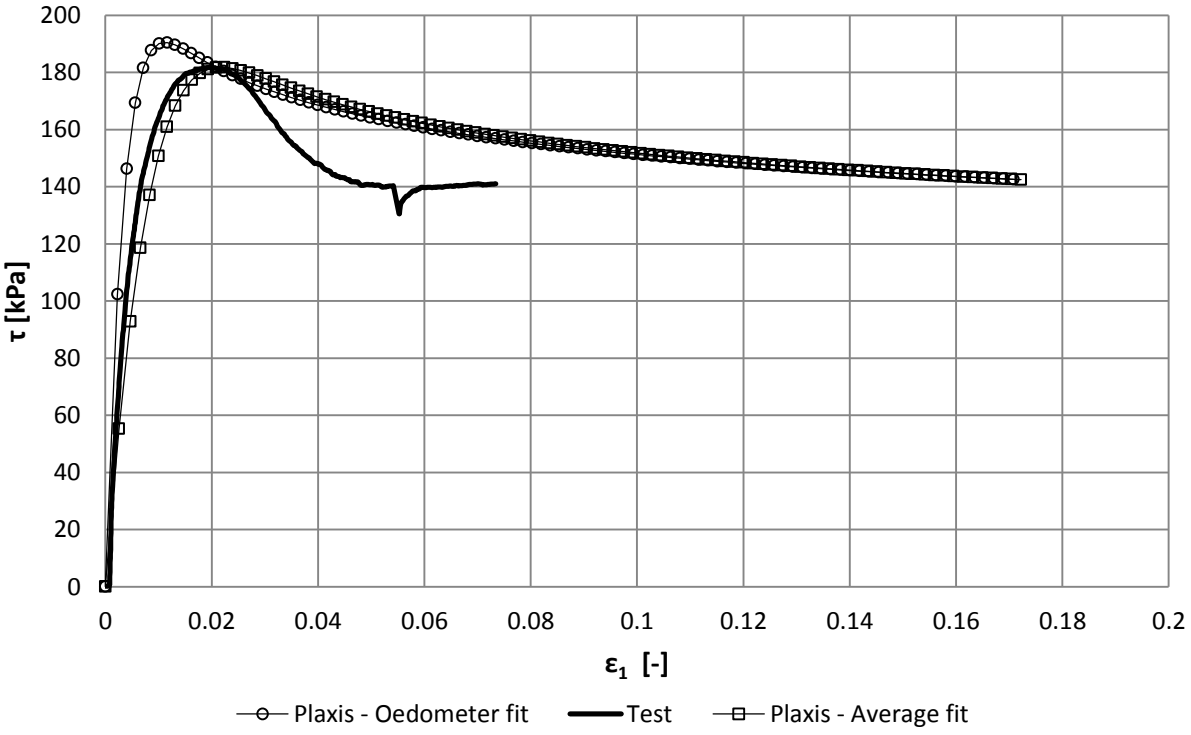

FIGURE A-40: COMPARISON STF – DS TEST: DRENTE, D_R=90%, σ_{YY}=200 KPA

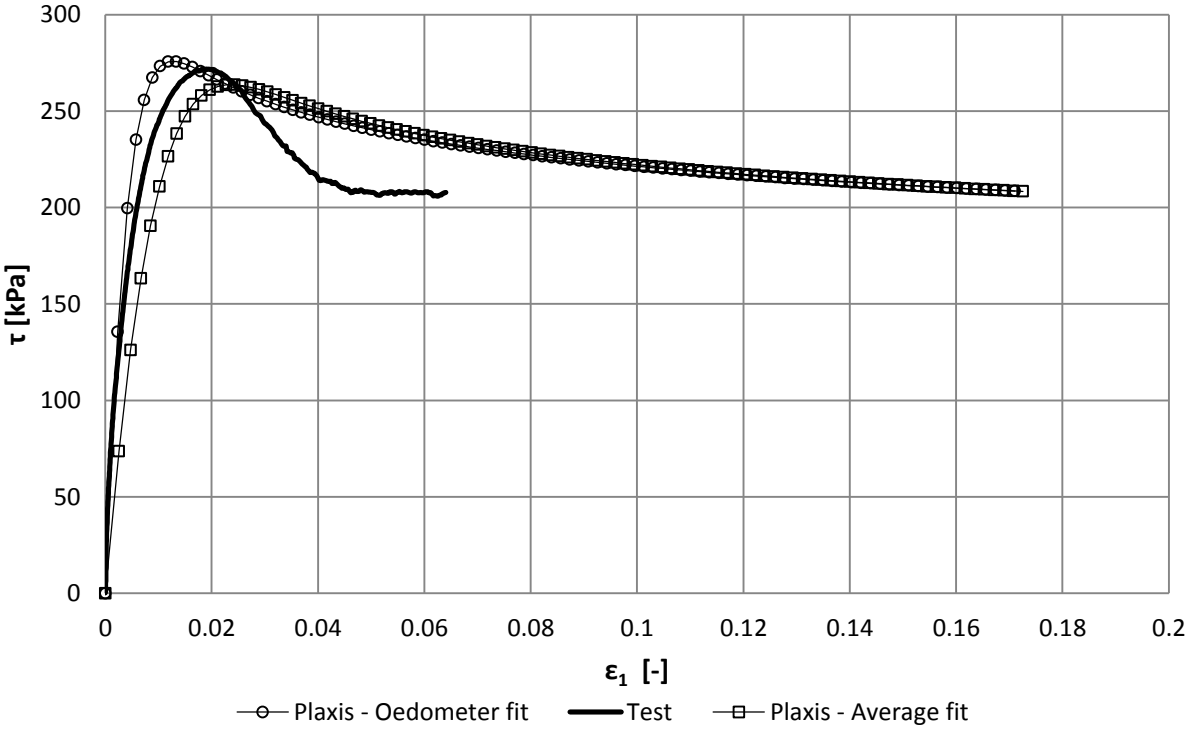

FIGURE A-41: COMPARISON STF – DS TEST: DRENTE, D_R=90%, σ_{YY}=300 KPA

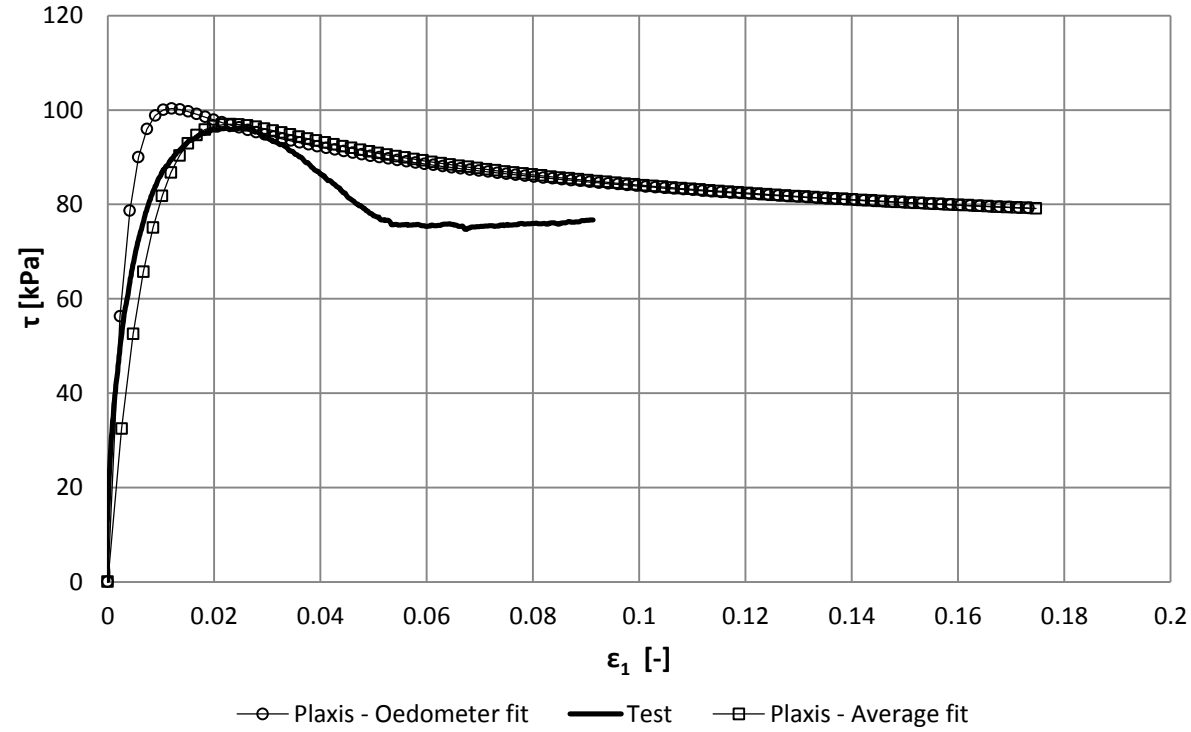

FIGURE A-42: COMPARISON STF – DS TEST: STERKSEL, D_R=80%, σ_{YY}=100 KPA

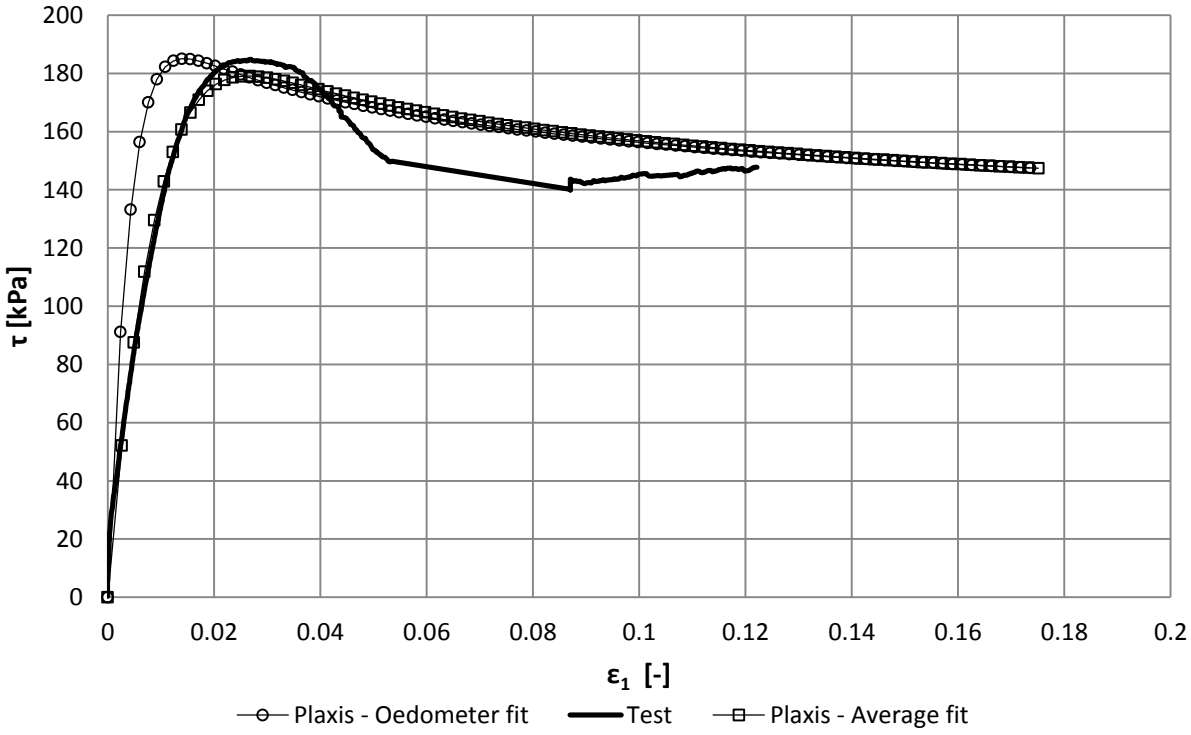

FIGURE A-43: COMPARISON STF – DS TEST: STERKSEL, D_R=80%, σ_{YY}=200 KPA

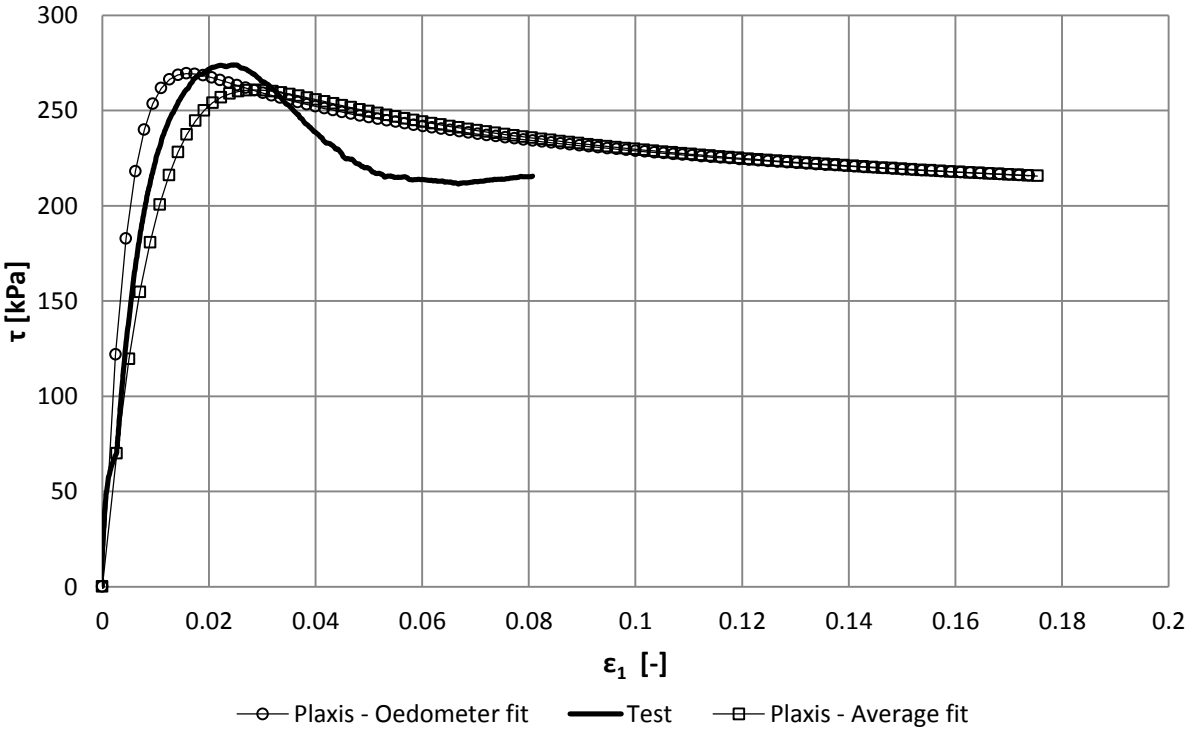

FIGURE A-44: COMPARISON STF – DS TEST: STERKSEL, D_R=80%, σ_{YY}=300 KPA

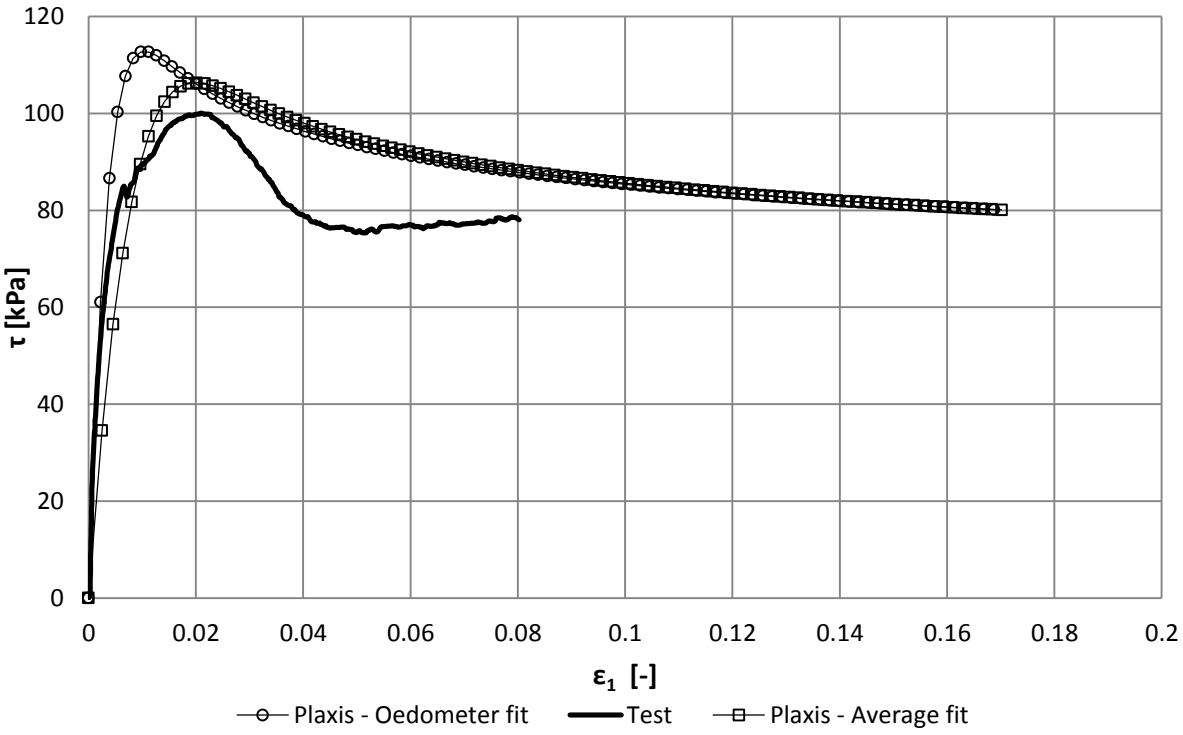

FIGURE A-45: COMPARISON STF – DS TEST: STERKSEL, D_R=90%, σ_{YY}=100 KPA

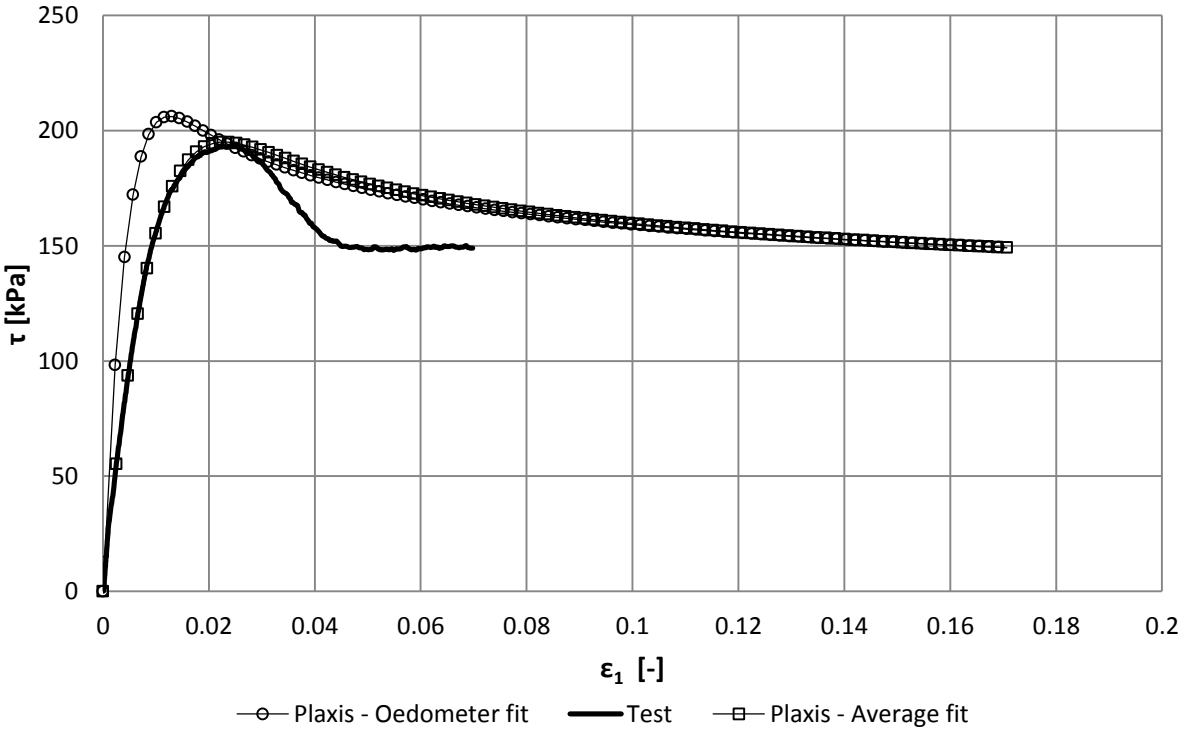

FIGURE A-46: COMPARISON STF – DS TEST: STERKSEL, D_R=90%, σ_{YY}=200 KPA

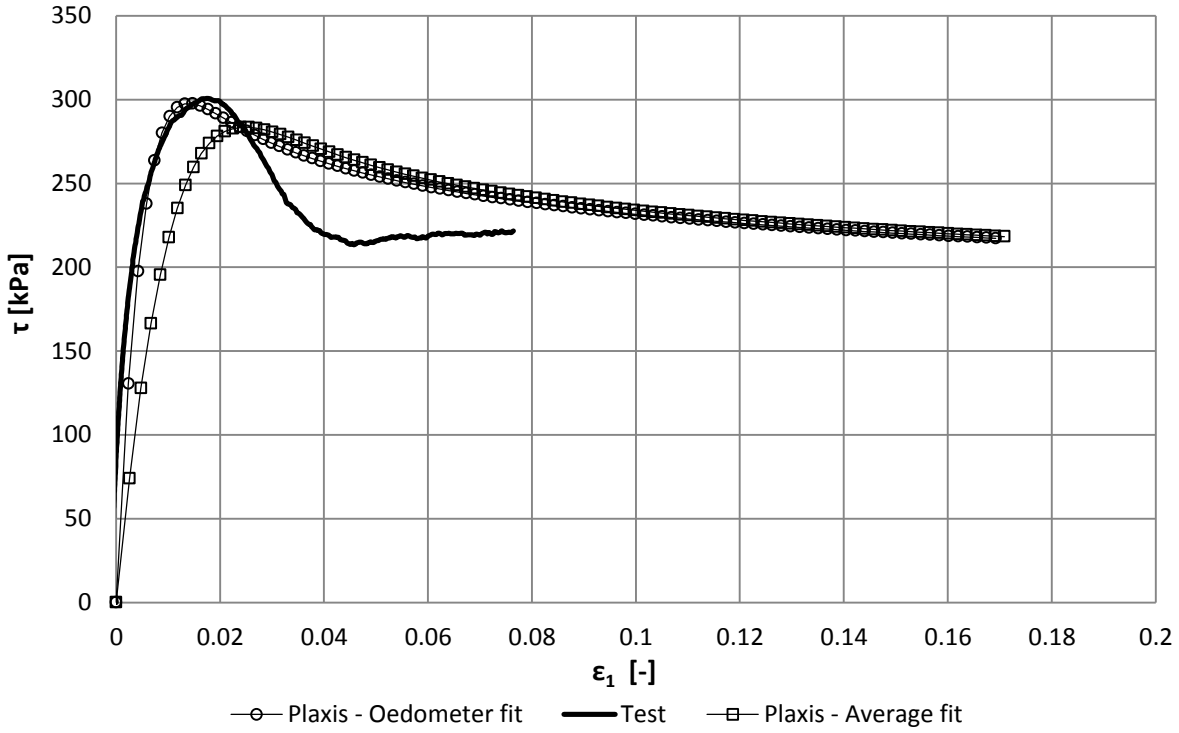

FIGURE A-47: COMPARISON STF – DS TEST: STERKSEL, D_R=90%, σ_{YY}=300 KPA

Both the Oedometer fit and the average fit of Plaxis give results which are in the order of magnitude of the direct shear tests. Therefore, α determined in the previous subsection can be considered a valid approximation.

A.6. CONCLUSION HYPOPLASTICITY PARAMETERS

Both soils have comparable HP parameters. This is presented in Table A.11.

TABLE A-11: HYPOPLASTIC PARAMETERS FORMATION DRENTE & STERKSEL

	φ_c [°]	h_s [GPa]	n [-]	e_{d0} [-]	e_{c0} [-]	e_{i0} [-]	α [-]	β [-]
Drente	31.1	13	0.27	0.51	0.74	0.86	0.151	1
Sterksel	32.8	10	0.26	0.51	0.74	0.85	0.157	1

Last, it is important to notice β is set to 1. This can actually vary (Herle and Gudehus, 1999), but as the influence of this parameter is small it is not calculated it is simply chosen to be 1.

B. NUMERICAL MODELLING RESULTS

B.1. MOBILISATION PRINCIPLE EFFECTIVE STRESSES (FINE MESH, NO INTERFACE)

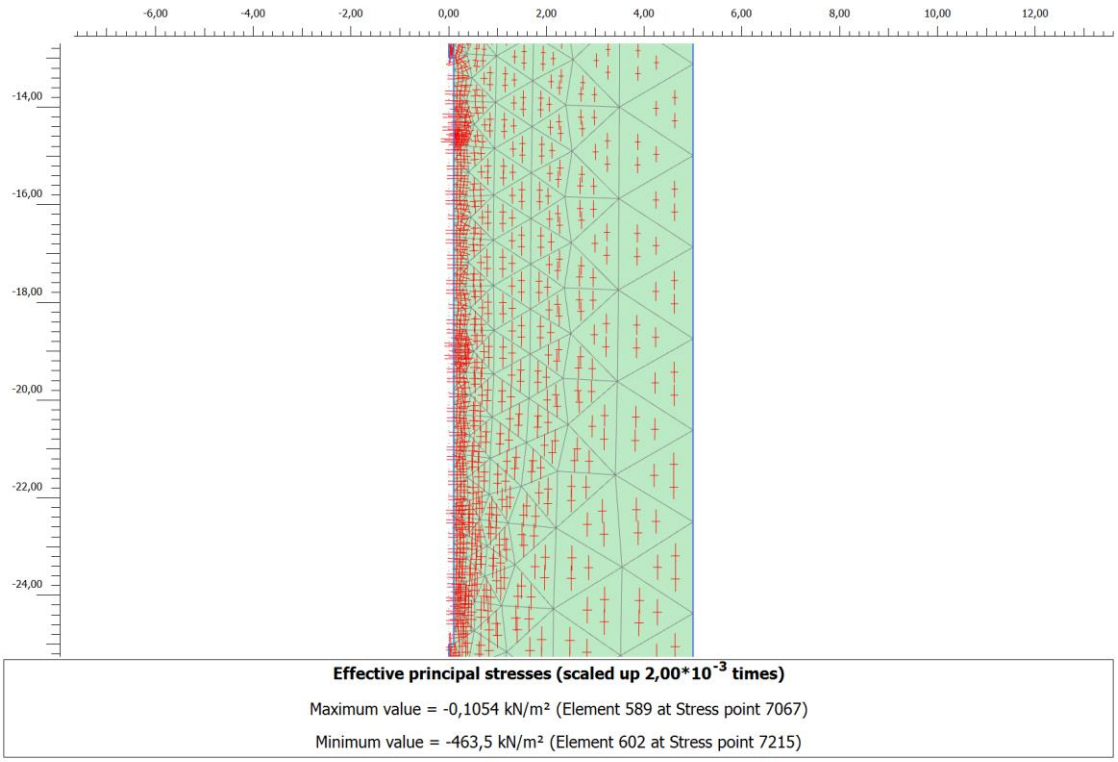

FIGURE B-1: PRINCIPAL STRESS DIRECTIONS: PRESSURISATION 500 KPA

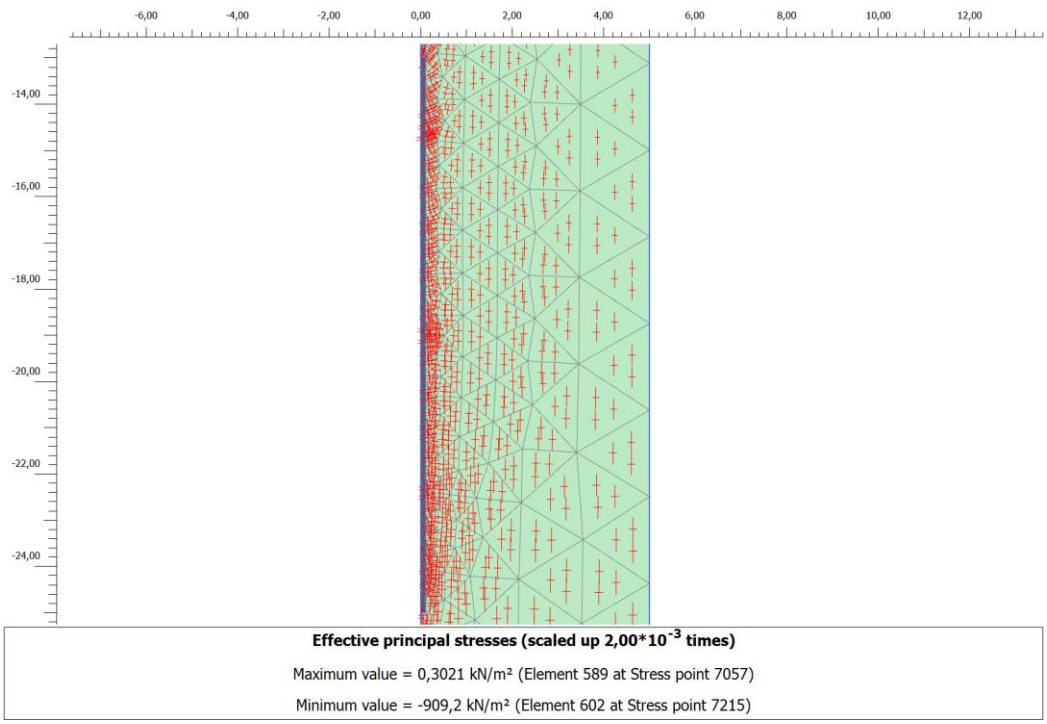

FIGURE B-2: PRINCIPAL STRESS DIRECTIONS: 10% F_P

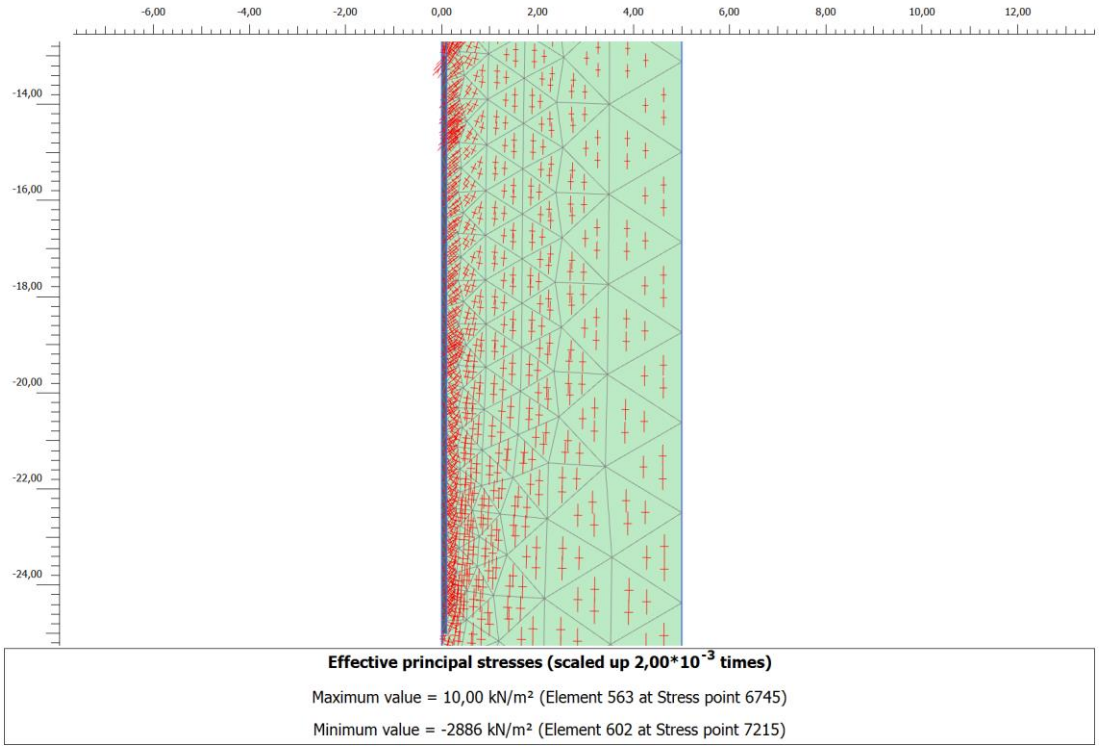

FIGURE B-3: PRINCIPAL STRESS DIRECTIONS: 40% F_P

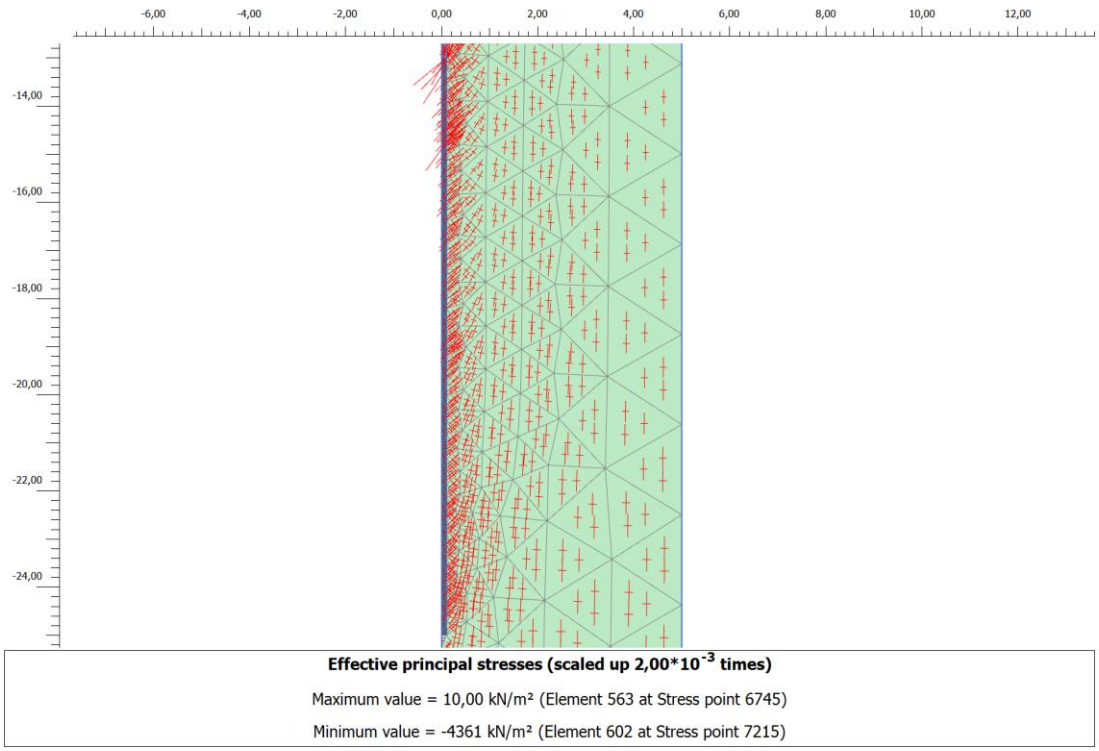

FIGURE B-4: PRINCIPAL STRESS DIRECTIONS: 70% F_P

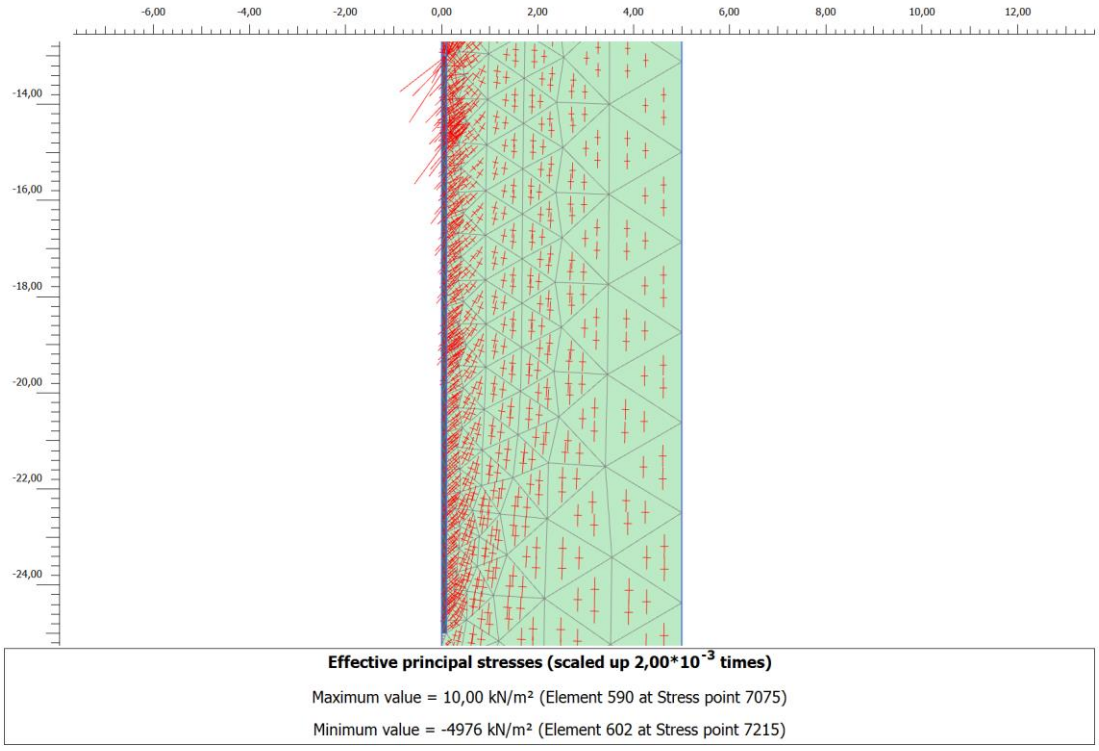

FIGURE B-5: PRINCIPAL STRESS DIRECTIONS: 90% F_P

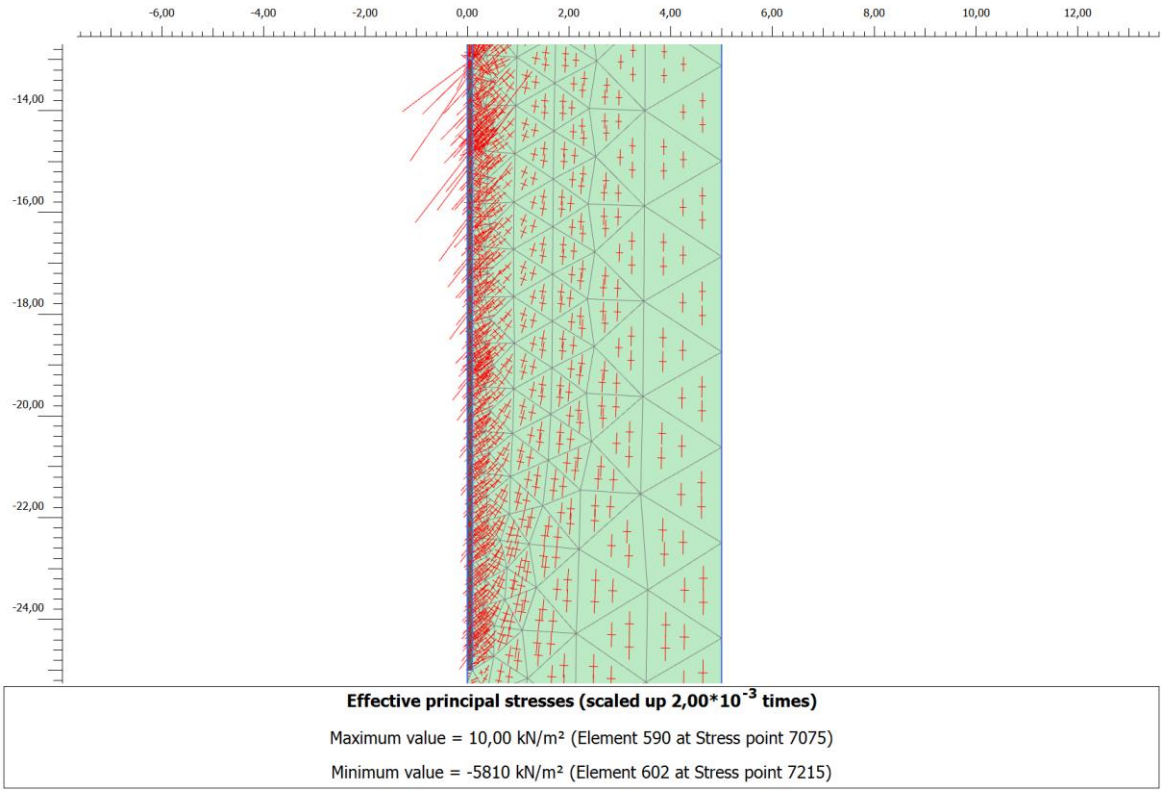

FIGURE B-6: PRINCIPAL STRESS DIRECTIONS: 120% F_P

B.2. Mobilised shear stresses: cross section next to micropile (fine mesh, no interface)

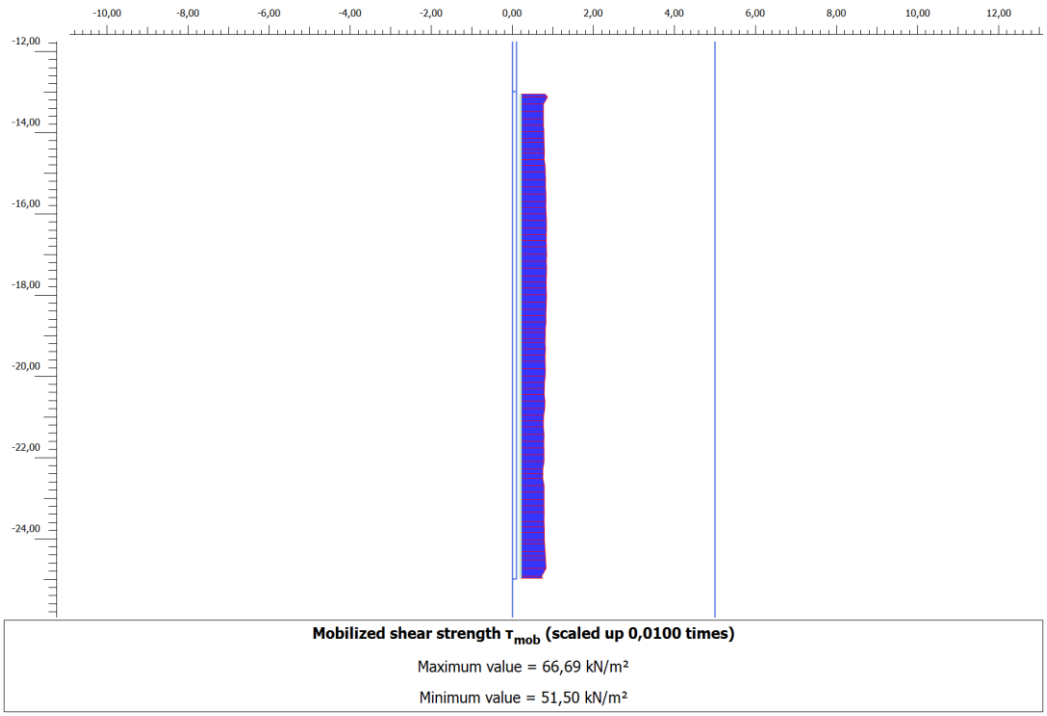

FIGURE B-7: MOBILISED SHEAR STRESS: 10% F_P

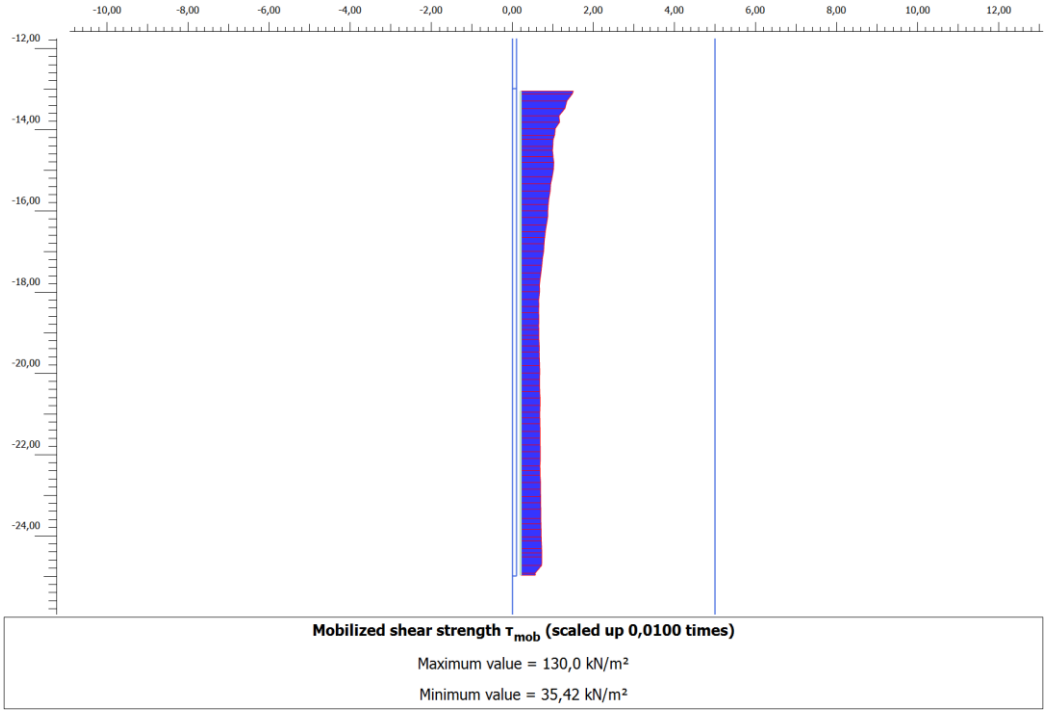

FIGURE B-8: MOBILISED SHEAR STRESS: 40% F_P

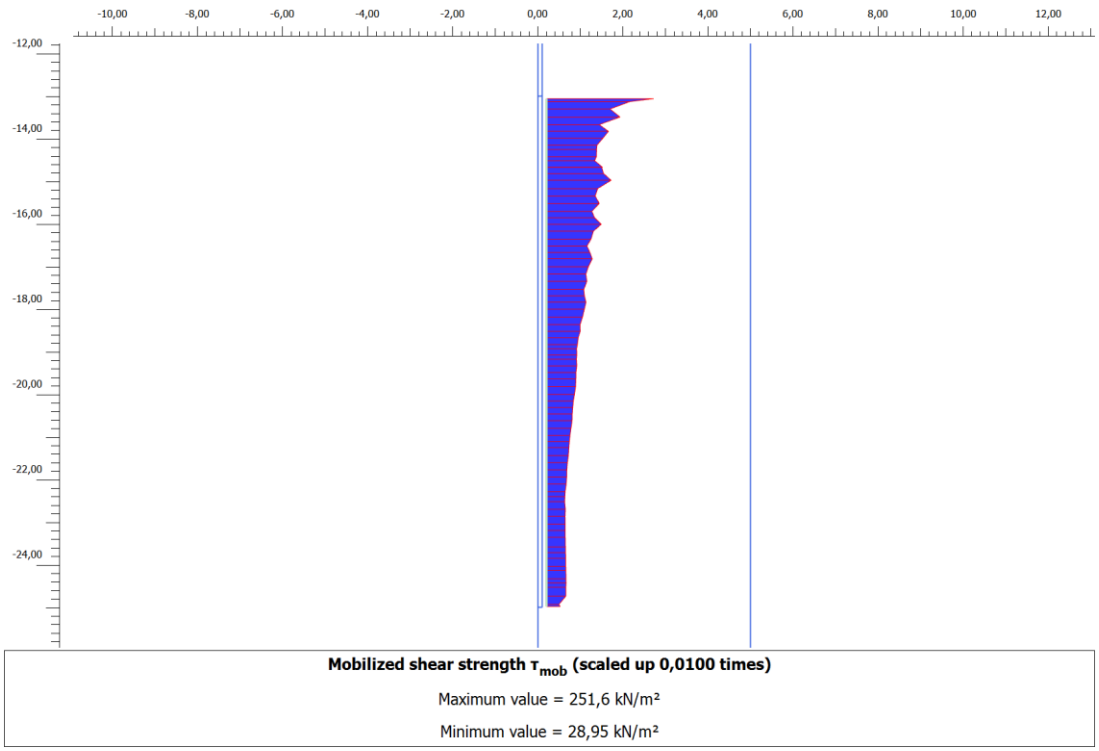

FIGURE B-9: MOBILISED SHEAR STRESS: 70% F_P

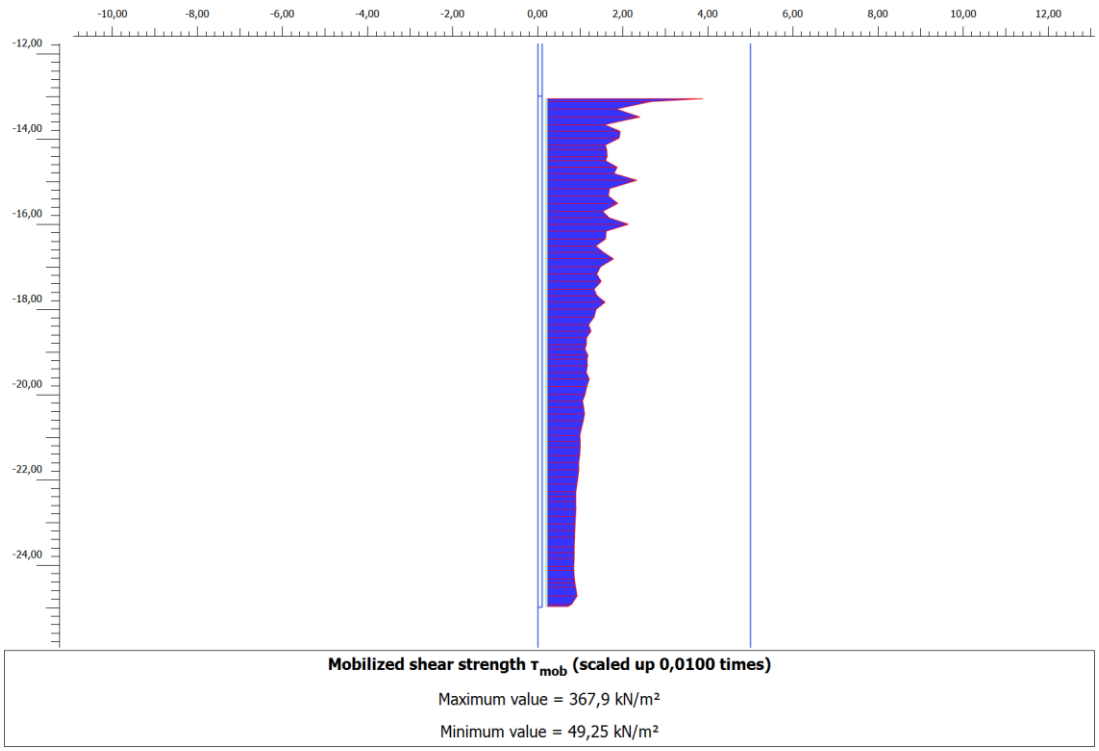

FIGURE B-10: MOBILISED SHEAR STRESS: 90% F_P

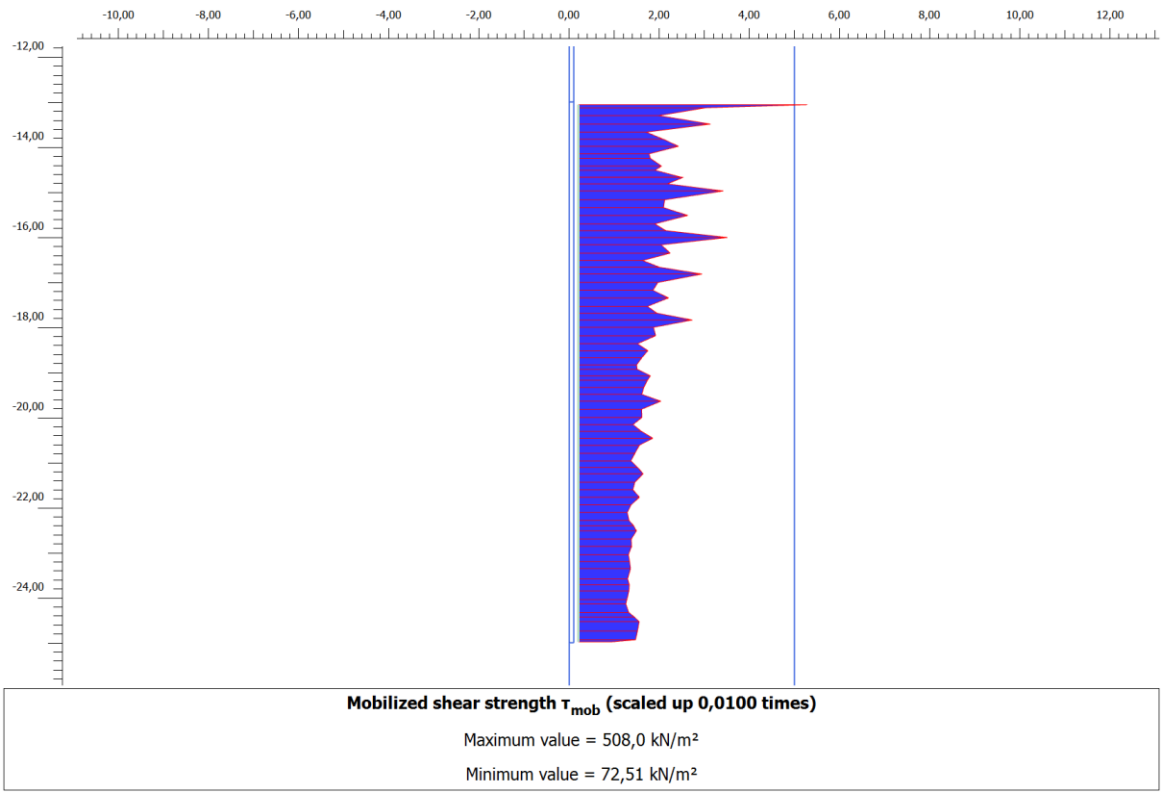

FIGURE B-11: MOBILISED SHEAR STRESS: 120% F_P

B.3. INACCURACIES WITH INTERFACE (NOT ACTIVATED)

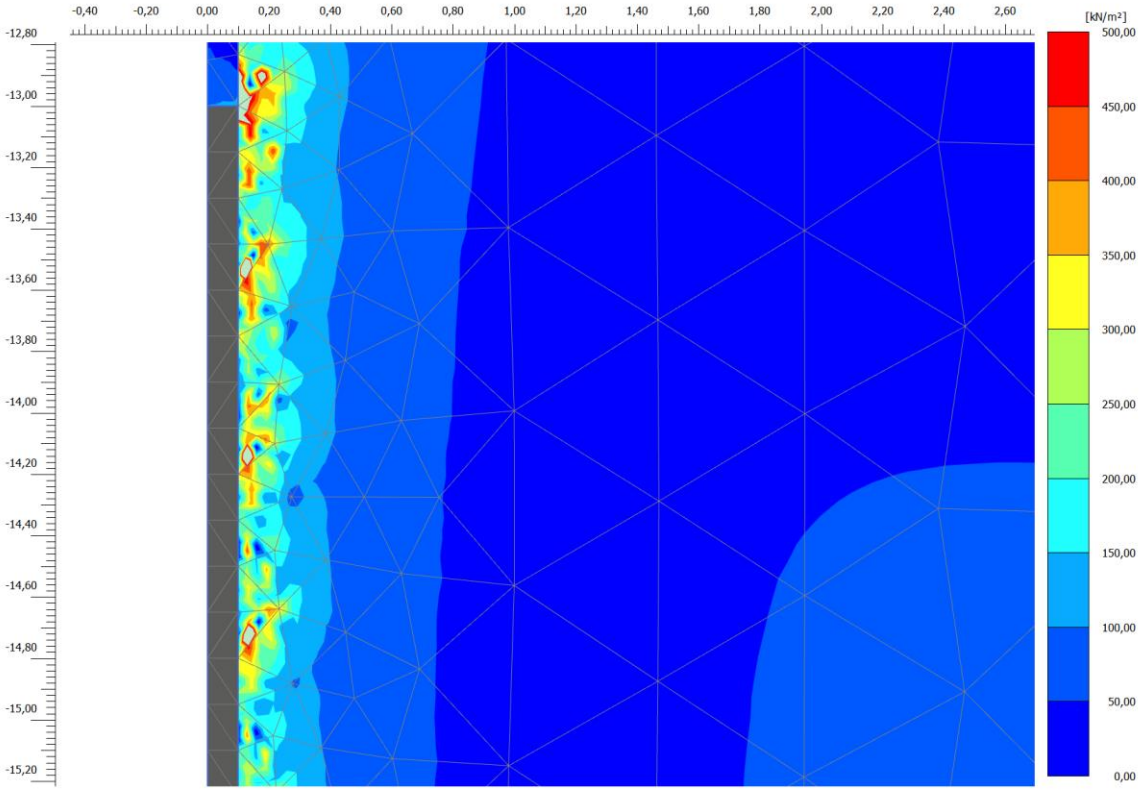

FIGURE B-12: INACCURACIES MOBILISED SHEAR STRESS, MODEL WITH INTERFACE (NOT ACTIVATED), 120% F_p

B.4. INACCURACIES WITH INTERFACE (ACTIVATED)

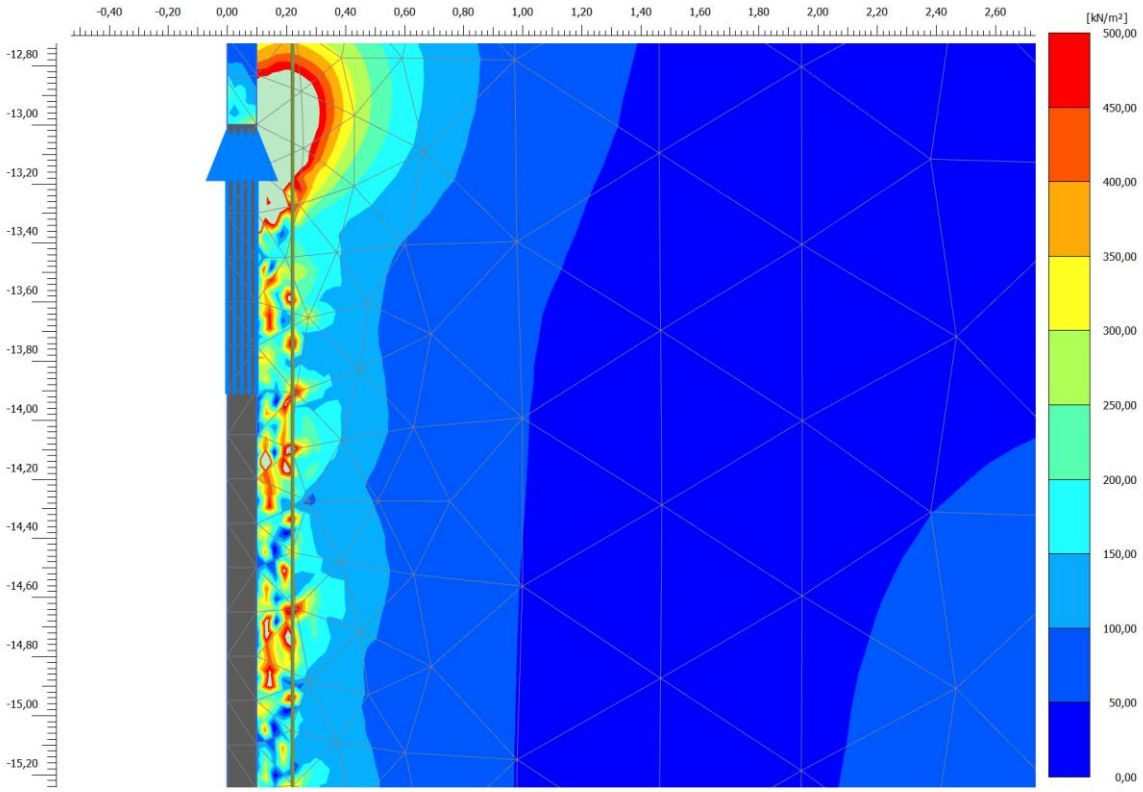

FIGURE B-13: INACCURACIES MOBILISED SHEAR STRESS, MODEL WITH INTERFACE (ACTIVATED), 120% F_P

B.5. INACCURACIES WITH REDUCED MICROPILE STIFFNESS

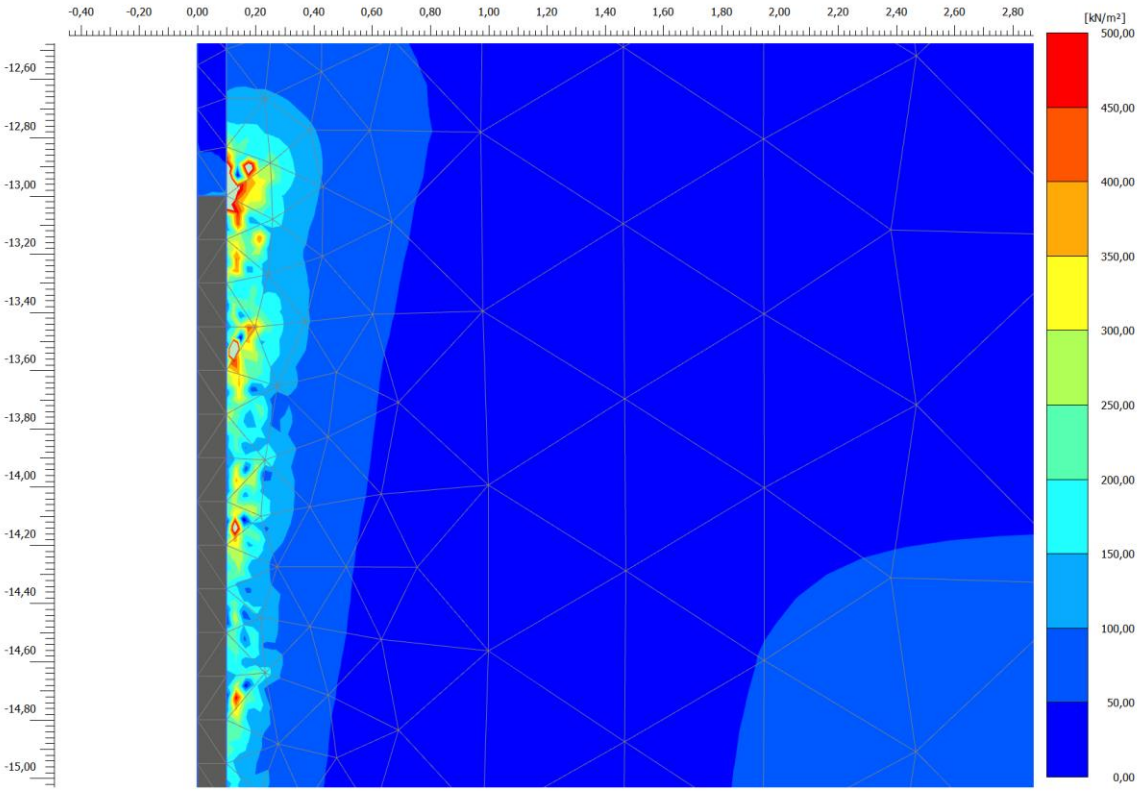

FIGURE B-14: INACCURACIES MOBILISED SHEAR STRESS, REDUCED STIFFNESS MICROPILE, 40% F_P

C. SMALL SCALE PHYSICAL MODELLING RESULTS

C.1. MOBILISED SHEAR STRESS DEVELOPMENT

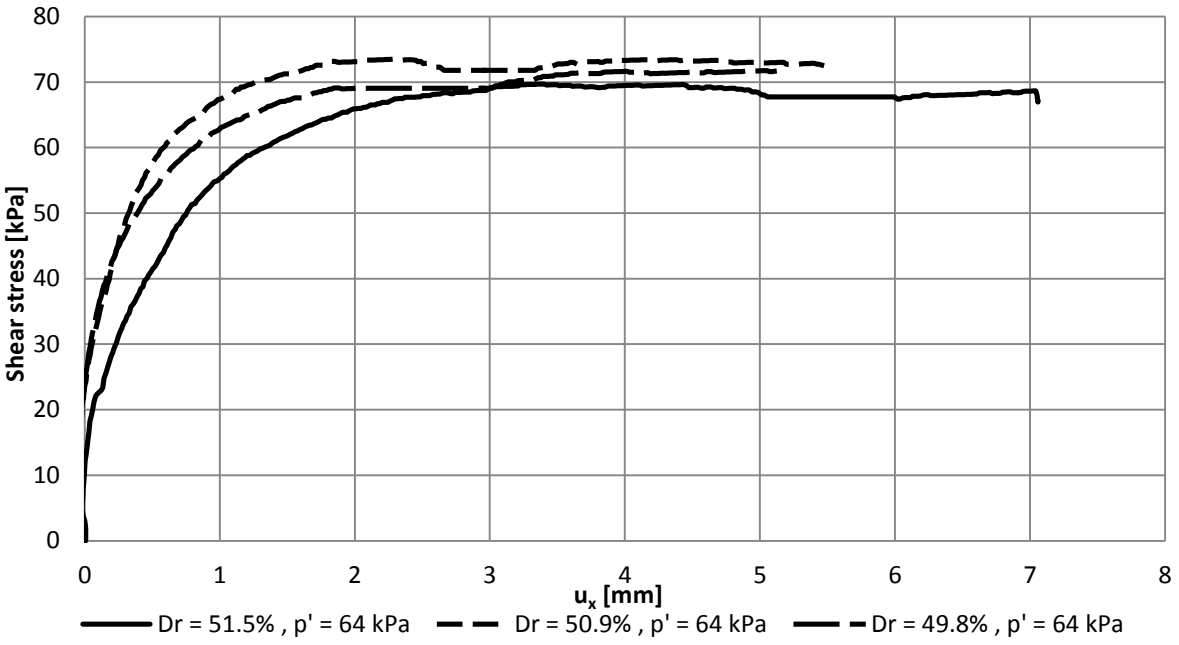

FIGURE C-1: MOBILISED SHEAR STRESS $D_R \approx 50\%$, P'=64KPA

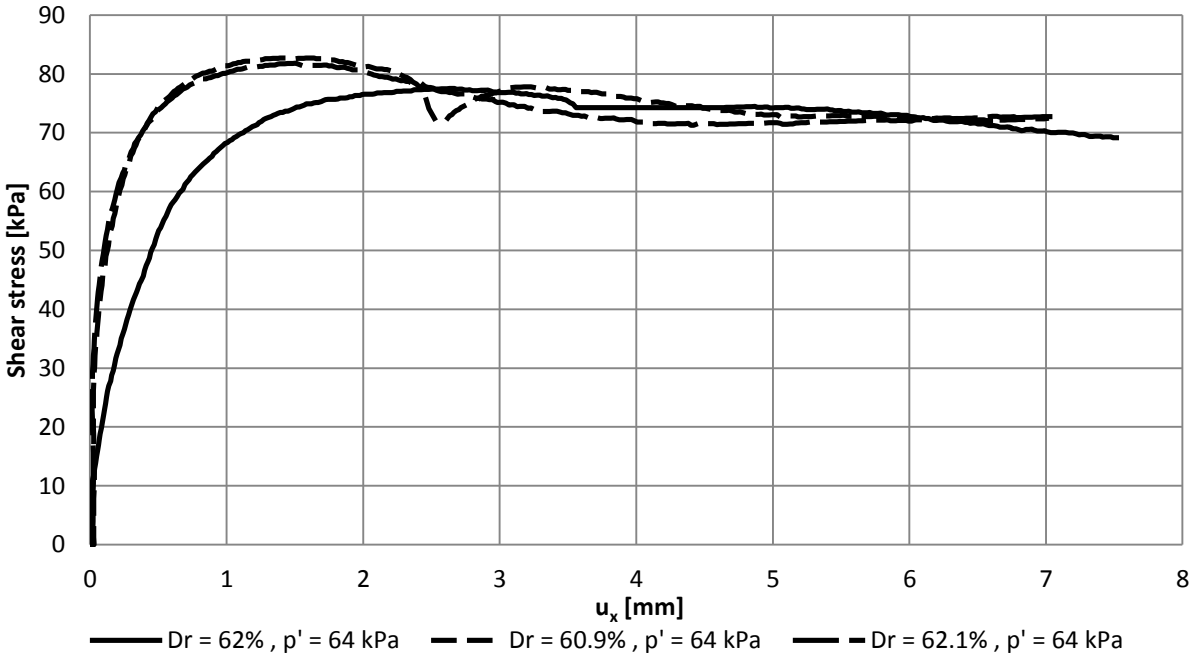

FIGURE C-2: MOBILISED SHEAR STRESS $D_R \approx 60\%$, P'=64 KPA

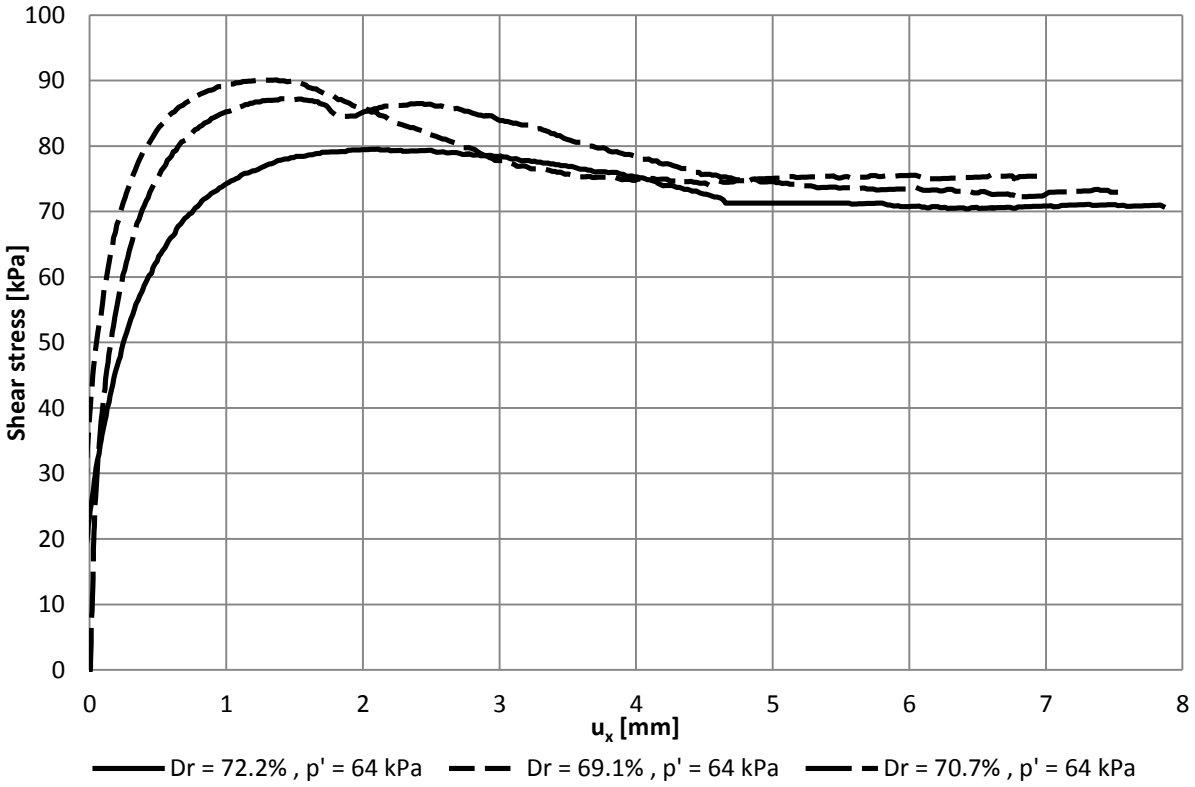

FIGURE C-3: : MOBILISED SHEAR STRESS D_R≈70%, P'=64 KPA

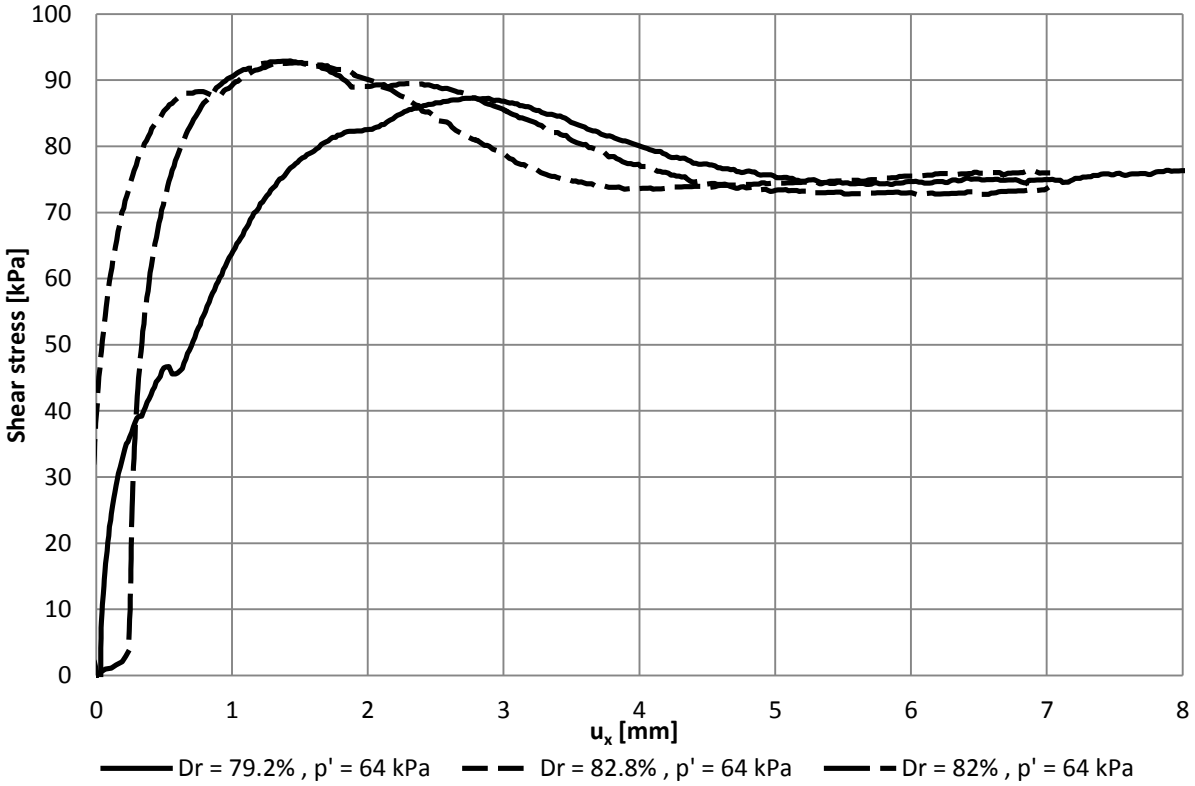

FIGURE C-4: MOBILISED SHEAR STRESS D_R≈80%, P'=64 KPA

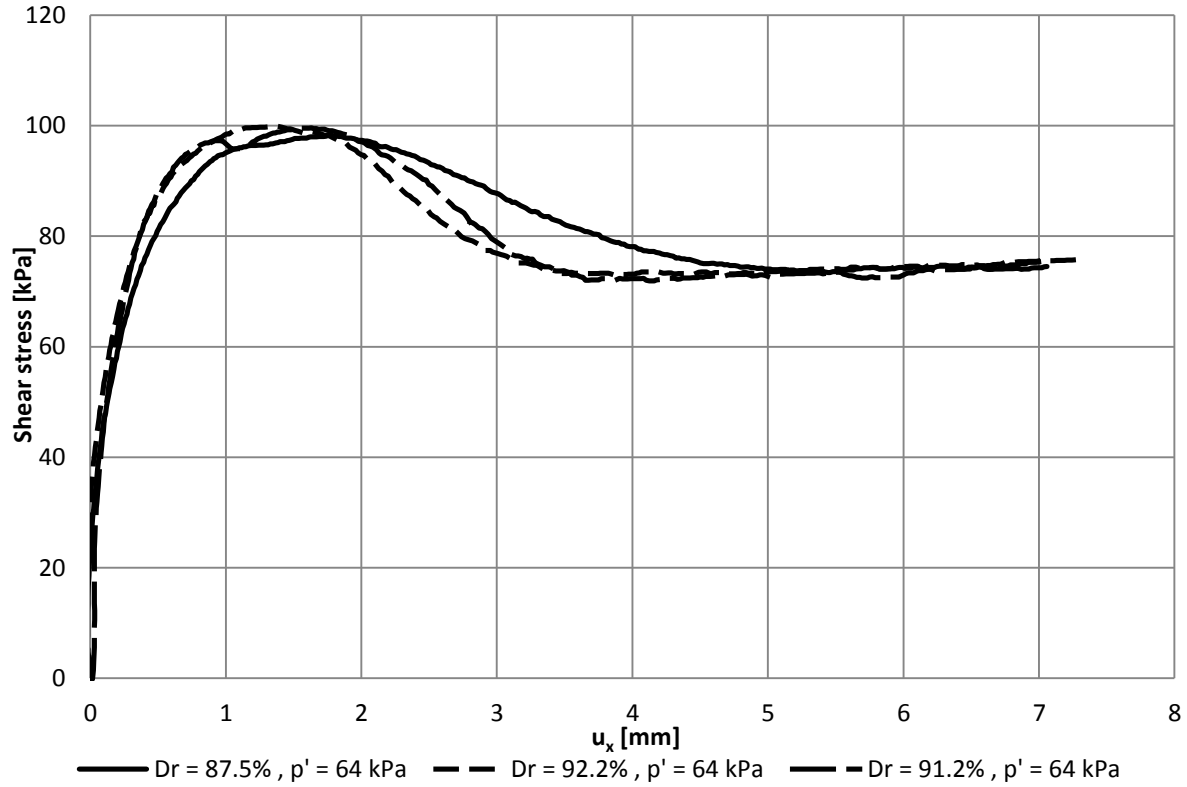

FIGURE C-5: MOBILISED SHEAR STRESS D_R≈90%, P'=64 KPA

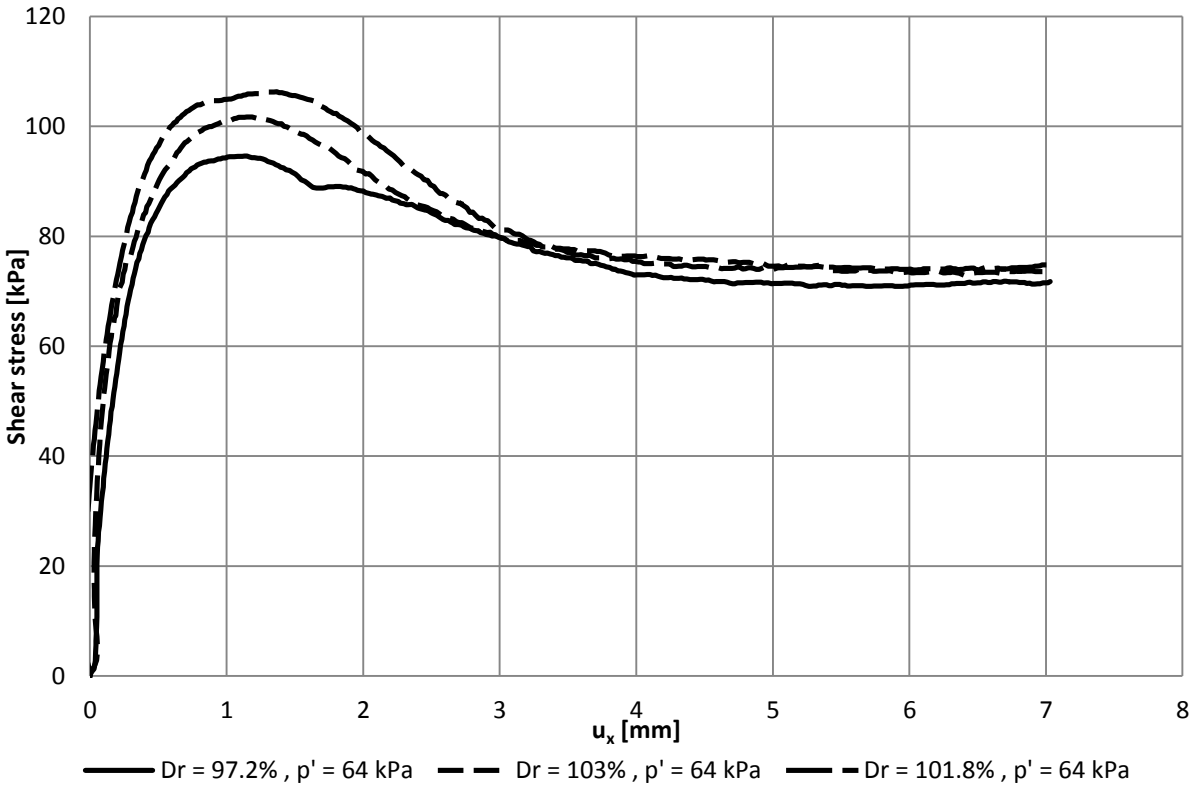

FIGURE C-6: MOBILISED SHEAR STRESS D_R≈100%, P'=64 KPA

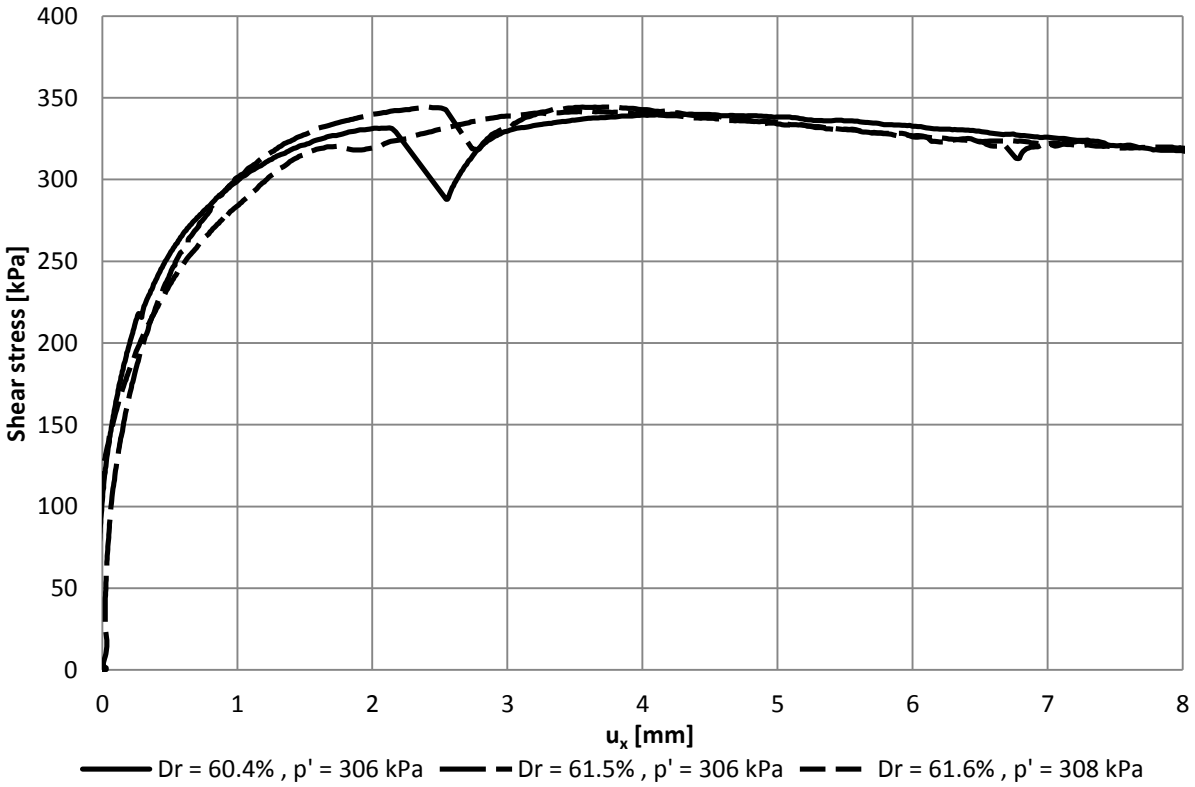

FIGURE C-7: MOBILISED SHEAR STRESS $D_R \approx 60\%$, P'=306 KPA

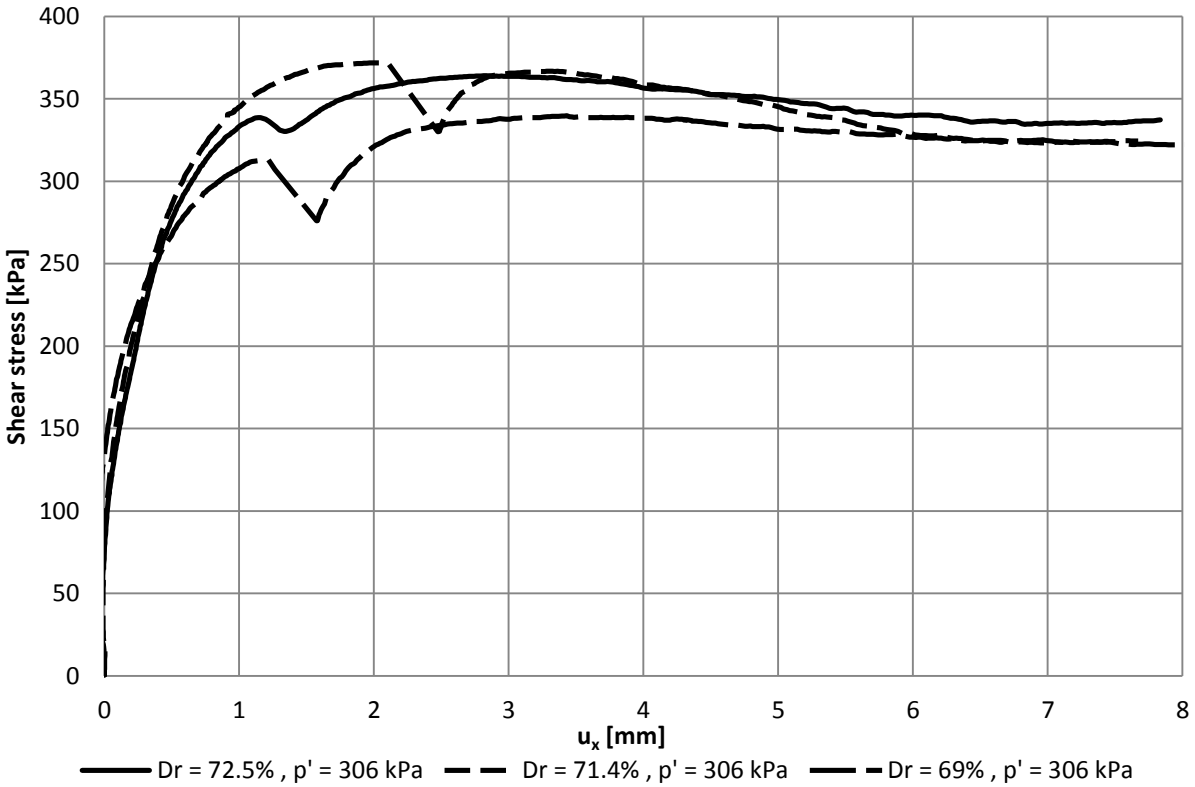

FIGURE C-8: MOBILISED SHEAR STRESS $D_R \approx 70\%$, P'=306 KPA

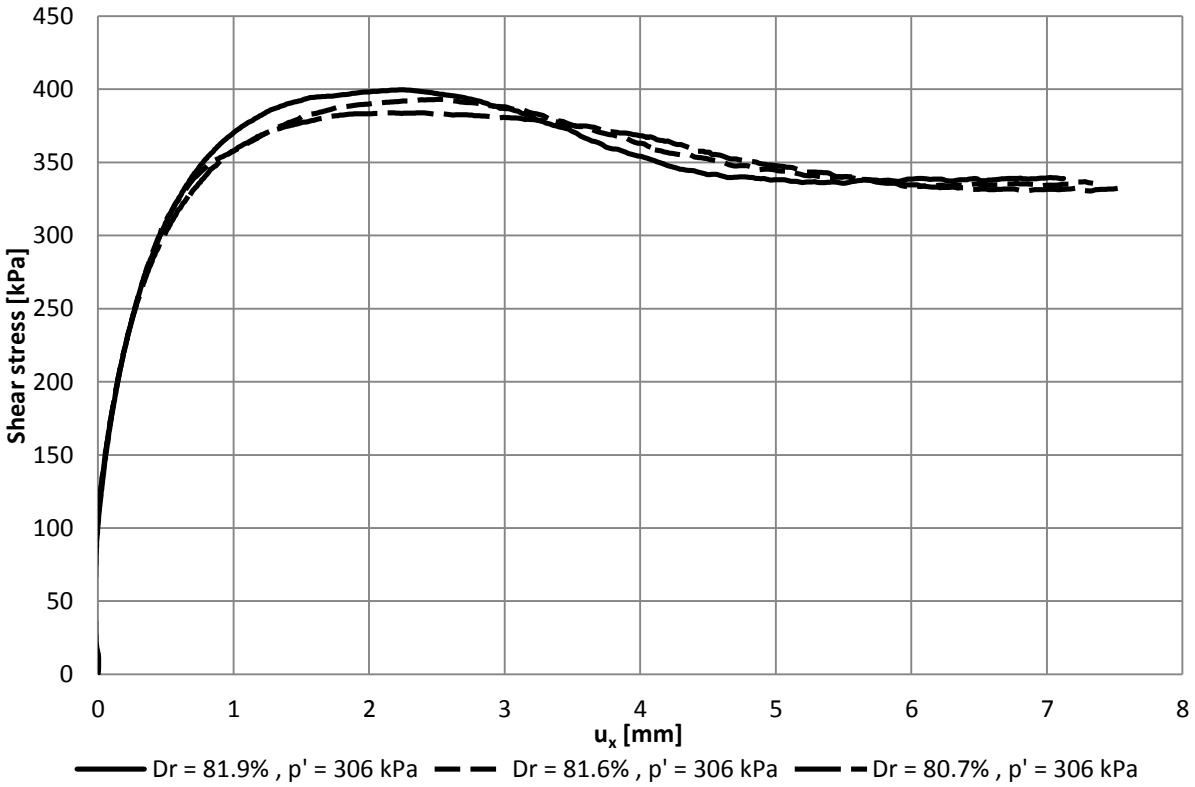

FIGURE C-9: MOBILISED SHEAR STRESS D_R≈80%, P'=306 KPA

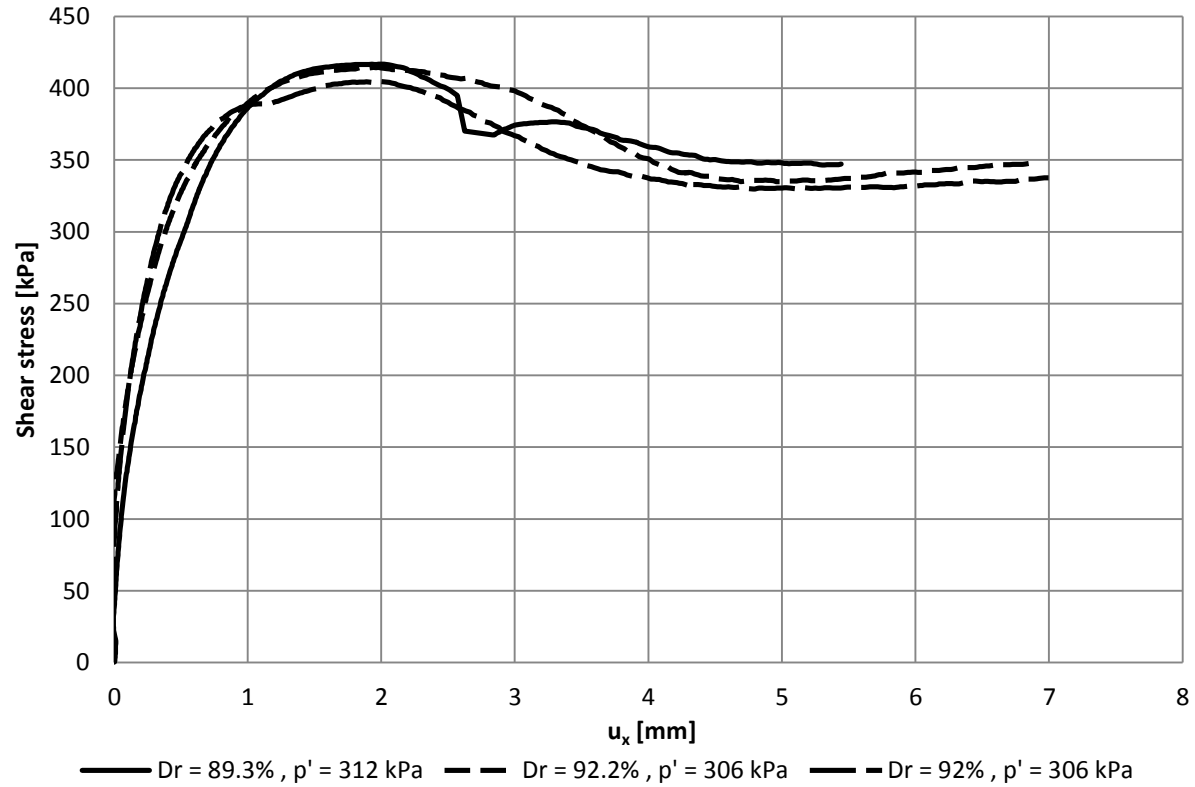

FIGURE C-10: MOBILISED SHEAR STRESS D_R≈90%, P'=306 KPA

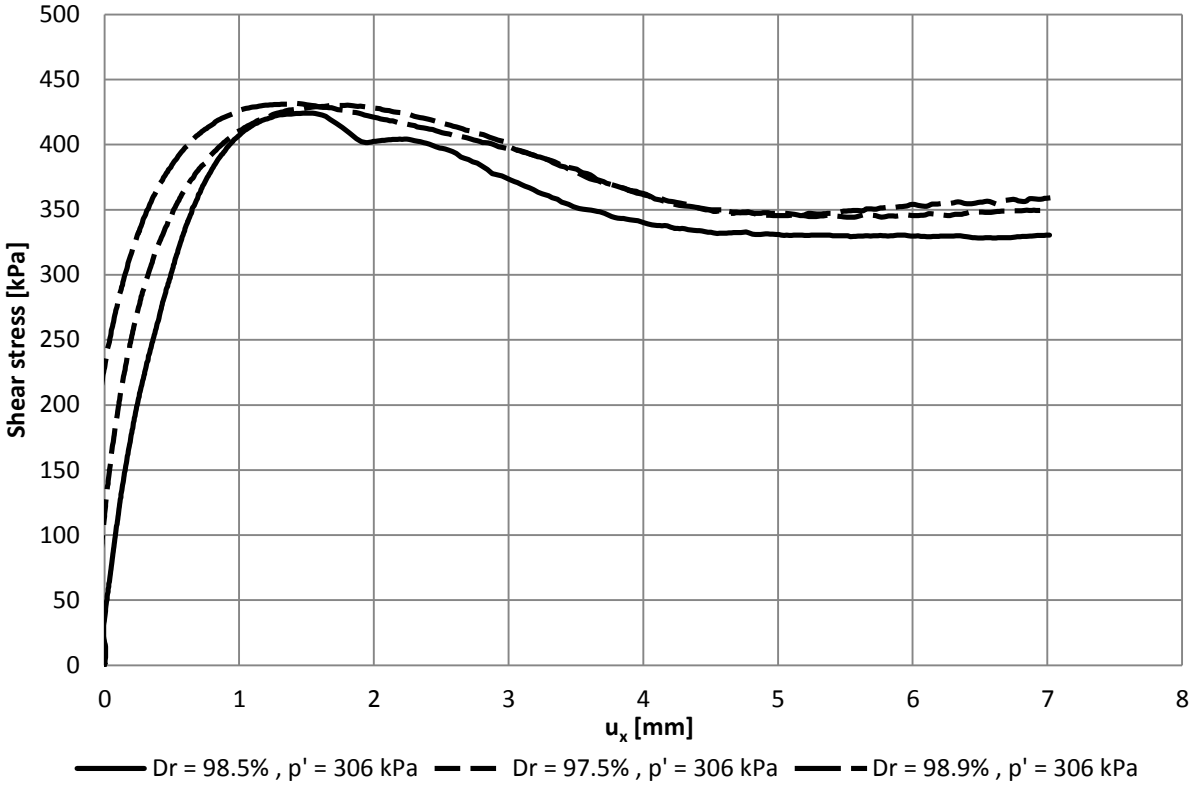

FIGURE C-11: MOBILISED SHEAR STRESS $D_R \approx 100\%$, P'=306 KPA

C.2. PEAK – RESIDUAL SHEAR STRESS

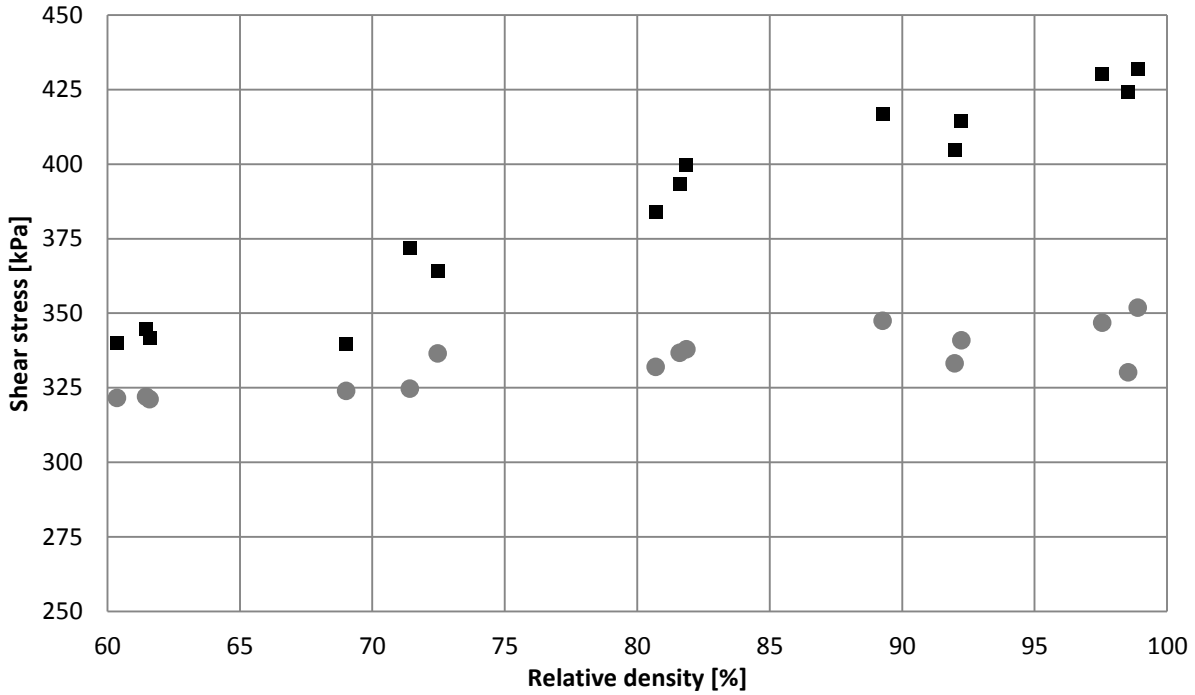

FIGURE C-12: T_{PEAK} (=■) AND $T_{RESIDUAL}$ (=●) WITH VARYING D_R, P'= 306 KPA

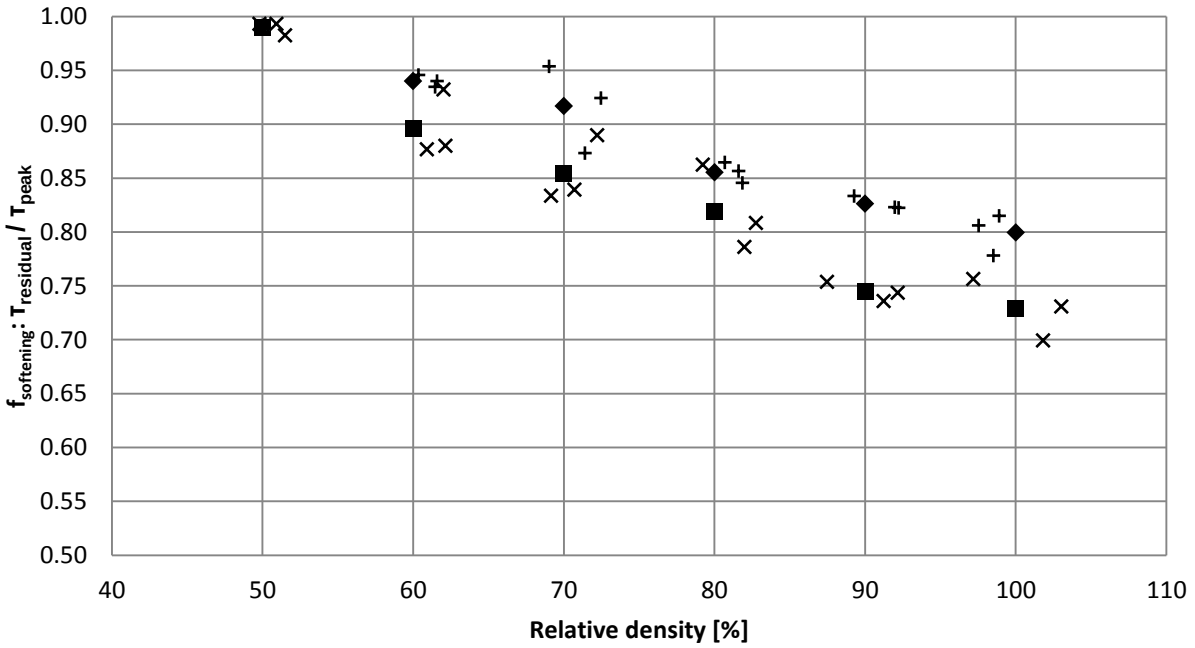

FIGURE C-13 RATIO BETWEEN T_{PEAK} AND $T_{RESIDUAL}$, P'=107 KPA (AVERAGE=■, TEST=X) & P'=306 KPA (AVERAGE=♦, TEST=+)

C.3. DISPLACEMENTS PEAK AND RESIDUAL

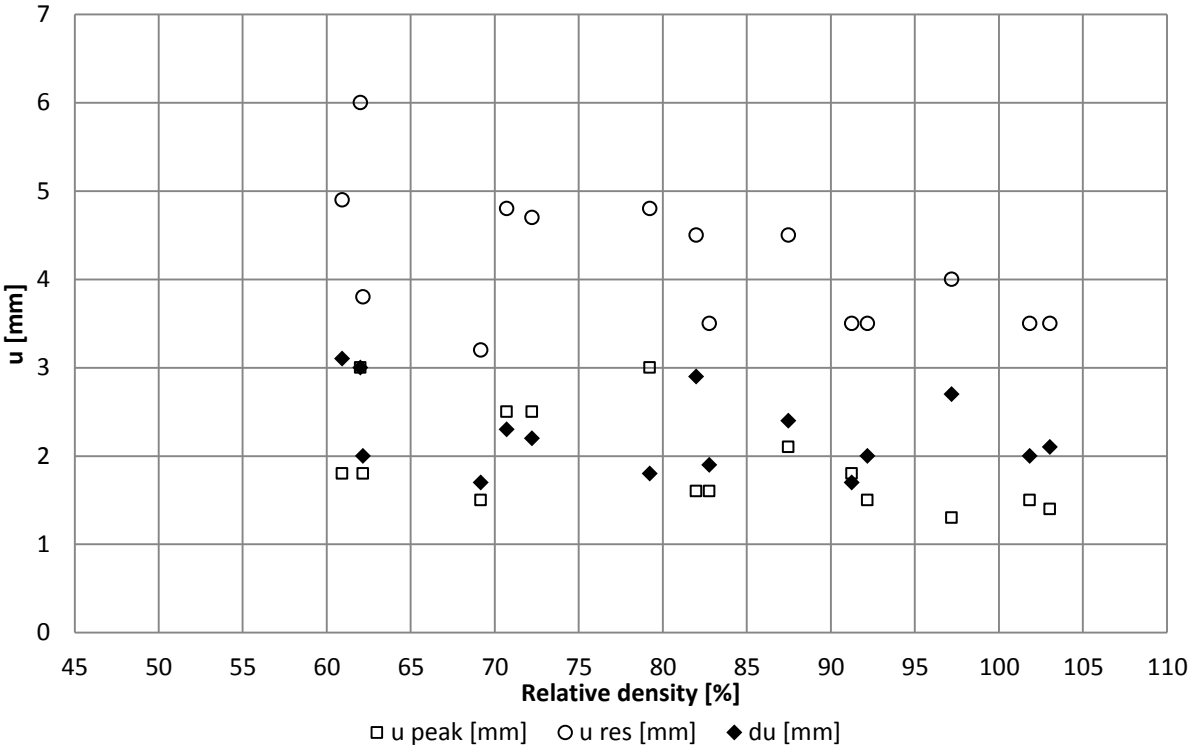

FIGURE C-15: DISPLACEMENT TO T_{PEAK} (□) AND $T_{RESIDUAL}$(○) AND THE DIFFERENCE OF BOTH, DU (♦) AT P'=306 KPA

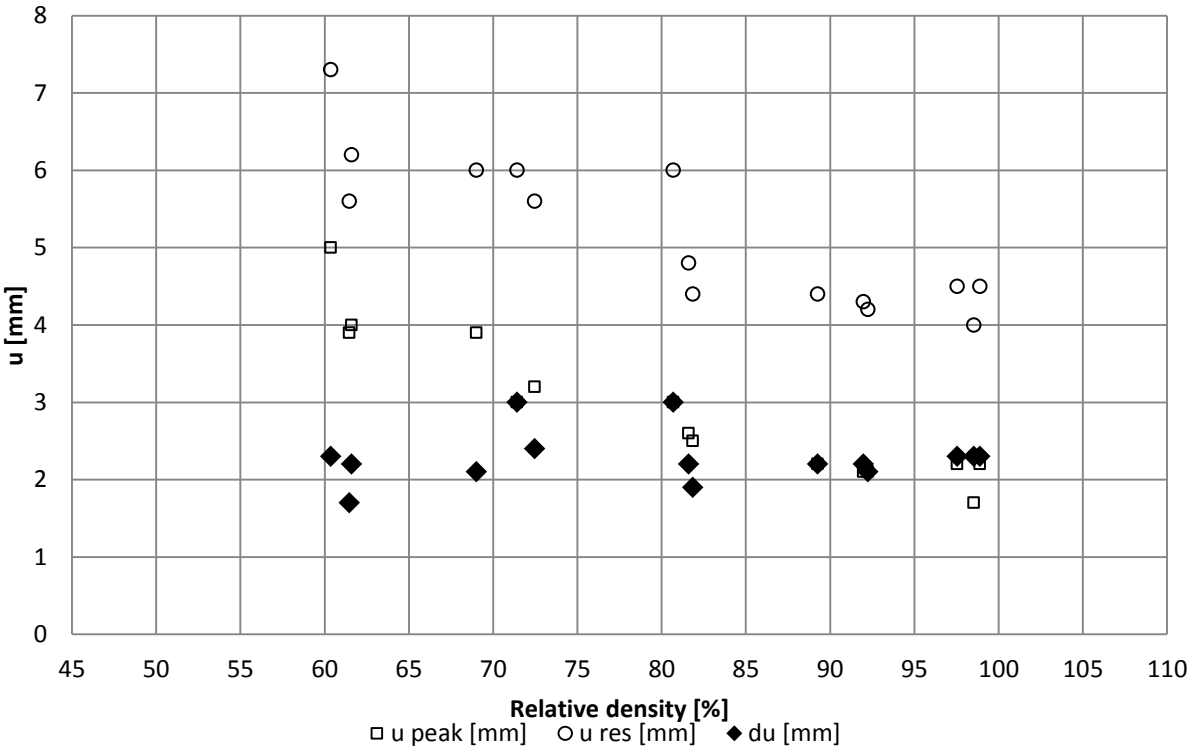

FIGURE C-14: DISPLACEMENT TO T_{PEAK} (□) AND $T_{RESIDUAL}$(○) AND THE DIFFERENCE OF BOTH, DU (♦) AT P'=306 KPA

D. LARGE SCALE TESTING

FIGURE D-1: LARGE SCALE TEST SET-UP, FRONT VIEW

FIGURE D-2: LARGE SCALE SET-UP, SIDE VIEW

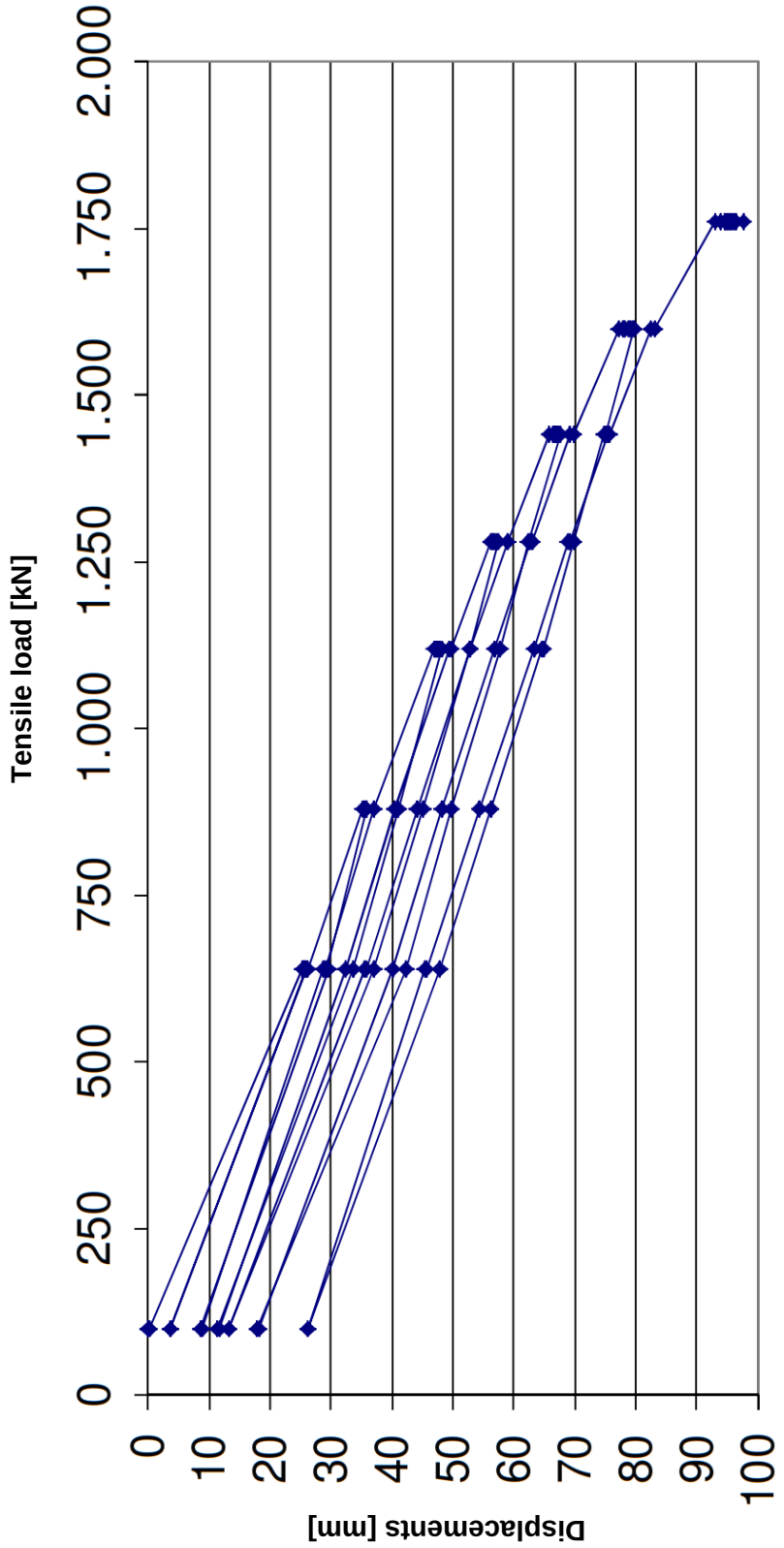

FIGURE D-3: FAILURE TEST ON PILE 2 IN ACCORDANCE WITH CUR236

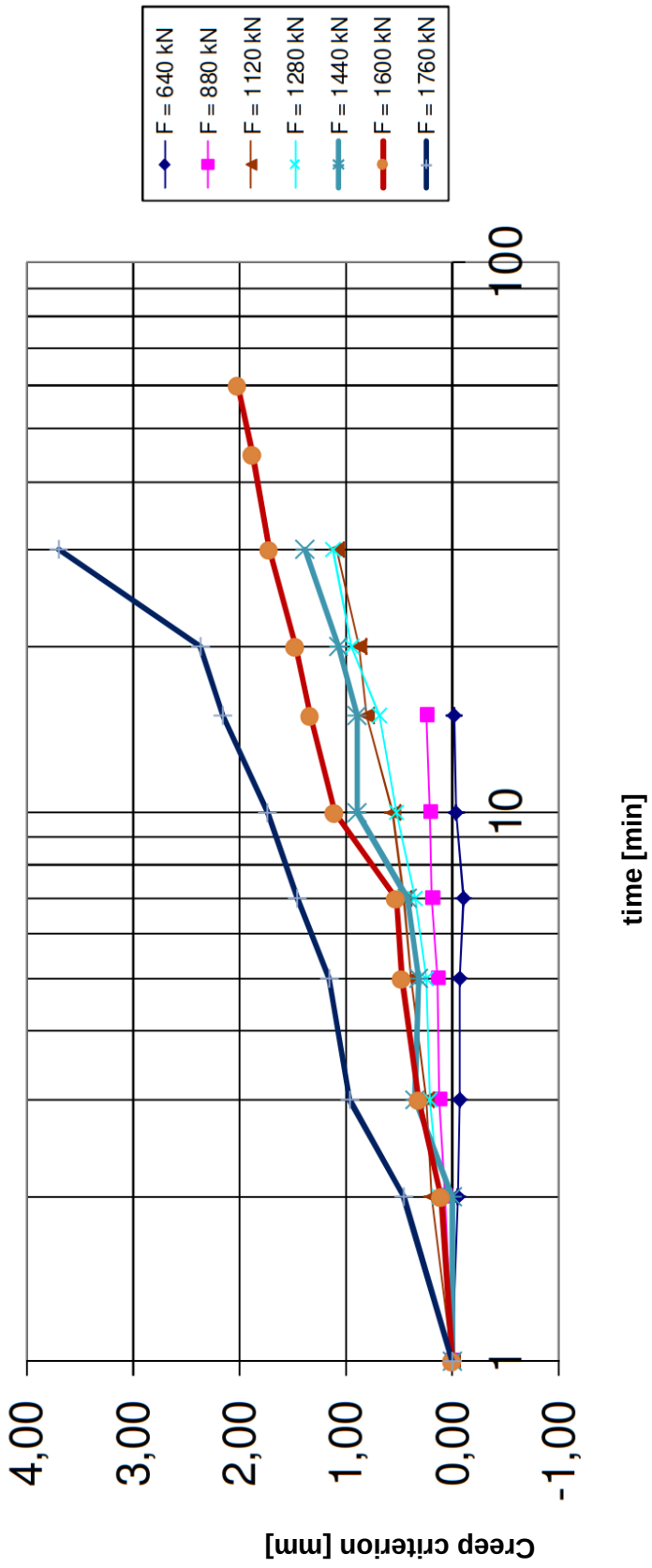

FIGURE D-4: CREEP CRITERION DURING FAILURE TEST PILE 2

TABLE D-1: SOFTENING TEST PILE 2

t [min]	F [kN]	u [m]
1	1803	1.22534
2	1801	1.22535
3	1797.9	1.22538
4	1795.5	1.22537
5	1794	1.22537
6	1791.7	1.22539
7	1790	1.22538
8	1789.2	1.2254
9	1788.2	1.22538
10	1786.9	1.22538
11	1785.5	1.22539
12	1784.6	1.22539
13	1783.9	1.22537
14	1782.6	1.2254
15	1782.4	1.22539
16	1781.9	1.22542
17	1781.2	1.22543
18	1779.9	1.22542
19	1779.7	1.22541
20	1779.2	1.22542
21	1778.5	1.22541
22	1777.6	1.22538
23	1777.2	1.22541
24	1776.7	1.2254
25	1776.5	1.22541